CHARACTERISATION OF A REACTIVE CRYSTALLIZATION

Meifen Jiang

A thesis submitted for the degree of Doctor of Philosophy

Chemical Engineering

School of Engineering and Physical Sciences

Heriot-Watt University

April 2019

Abstract

Pharmaceutical synthesis involves work up, reaction, crystallization, filtration and further downstream processes. This thesis project focuses on a reactive crystallization in order to gain scientific understanding of how reaction kinetics and parameters could affect targeted crystal specifications. Paracetamol synthesis is chosen as the model reactive crystallization process because it is significant in pharmaceutical industry and can be operated under simple conditions with 4-aminophenol and acetic anhydride as reactants. To maximize yield, the solubility for crystallization was optimized first, from which suitable reagent concentrations were determined. As in a single process, solubility for crystallization in the reactive crystallization of paracetamol was controlled by the solvent compositions that were directly produced in the reaction step.

The effects of reaction temperature and water content on reaction kinetics and mechanism as well as product quality were jointly investigated for the first time. Higher reaction rate constants for paracetamol synthesis were obtained for higher temperatures. Form I crystals with high purity were obtained with the presence of water, and 4'-acetoxyacetanilide without water. It has demonstrated that the reagents and solvents from the reaction step are the means for controlling and delivering required crystal properties in an oscillatory baffled reactor (OBR).

Finally, the reactive seeded cooling crystallization of paracetamol was carried out in a continuous oscillatory baffled reactor (COBR) based on the learnings from its batch counterpart. Effects of mixing intensity on crystal properties were discussed, crystals size reduced with the increase of oscillatory Reynolds number (R_{eo}). The seeding strategy was investigated at a fixed seed size and various seed masses, smooth and encrustation free runs were undertaken with the crystallization path close to the solubility curve. Both temporal and spatial steady states in concentration and size were attained by analysing the concentrations and crystal sizes at two locations along the COBR. Particle products of polymorphic form I were continuously generated with an average purity of 99.96 %.

Acknowledgements

I would like to take this opportunity to thank those people who have helped me during this PhD research.

Firstly, my thanks go to my supervisor, Professor Xiong-Wei Ni, for providing the opportunity to work on this project, and also for his valuable guidance, continuous support and encouragement throughout the four year study. I would also like to thank Professor Gerard Markx and Mr Craig Bell, not only for providing me the chance to undertake a teaching role within the department, but for their kind advice on communication with students.

Many thanks to my colleagues, in particular, Juliet Adelakun and Arabella McLaughlin for all the useful discussions and advice during the project. Thanks to other members of the COBRA group: Guillermo Jimeno Millor, Ross Laska, Francisca Navarro Fuentes and Mohamed Chilmeran for their kind assistance on the research.

I am also grateful to the laboratory technicians at Heriot-Watt University, in particular Mr Richard Kinsella, Mr Douglas Wagener and Mr Andrew Haston for their efforts in constructing and maintaining apparatus in the laboratory. Thanks to Mr Cameron Smith, Mr Stuart Grant, and Mrs Mary Pratt for their support in purchasing and delivering laboratory essentials.

I would like to thank the Doctoral Training Centre in Continuous Manufacturing and Crystallization (CMAC) as well as Heriot-Watt University for funding this research.

Finally, I thank my family for their continued love, support and encouragement throughout all of this PhD work.

ACADEMIC REGISTRY

Research Thesis Submission

Name*:*	Meifen Jiang		
School:	School of Engineering and Physical Sciences		
Version: *(i.e. First, Resubmission, Final)*	Final	Degree Sought:	Doctor of Philosophy in Chemical Engineering

Declaration

In accordance with the appropriate regulations I hereby submit my thesis and I declare that:

1) the thesis embodies the results of my own work and has been composed by myself
2) where appropriate, I have made acknowledgement of the work of others and have made reference to work carried out in collaboration with other persons
3) the thesis is the correct version of the thesis for submission and is the same version as any electronic versions submitted*.
4) my thesis for the award referred to, deposited in the Heriot-Watt University Library, should be made available for loan or photocopying and be available via the Institutional Repository, subject to such conditions as the Librarian may require
5) I understand that as a student of the University I am required to abide by the Regulations of the University and to conform to its discipline.
6) I confirm that the thesis has been verified against plagiarism via an approved plagiarism detection application e.g. Turnitin.

* *Please note that it is the responsibility of the candidate to ensure that the correct version of the thesis is submitted.*

Signature of Candidate*:*	Meifen Jiang	Date:	02/05/2019

Submission

Submitted By *(name in capitals):*	
Signature of Individual Submitting:	
Date Submitted:	

For Completion in the Student Service Centre (SSC)

Received in the SSC by *(name in capitals):*			
1.1 Method of Submission *(Handed in to SSC; posted through internal/external mail):*			
1.2 E-thesis Submitted (**mandatory for final theses)**			
Signature:		Date:	

Table of Contents

Lists of Tables

Lists of Figures

Nomenclature

Symbol	Definition	Units
a	Solute activity in supersaturated solution	
a*	Solute activity in saturated solution	
a_0	Standard activity	
A	Nucleation rate constant	# s^{-1} m^{-3}
A_1	Column cross sectional area	m^2
A_2	Baffle orifice area	m^2
A_s	Crystal surface area	m^2
b	Apparent nucleation order	
B	Kubota interpretation nucleation rate	m^{-3} s^{-1}
c	Actual concentration	kg m^{-3}
c_i	Solute concentration at the crystal-solution interface	kg m^{-3}
Δc	Concentration difference	kg m^{-3}
Δc_{max}	Maximum solution supersaturation	kg m^{-3}
c*	Equilibrium concentration	kg m^{-3}
C_A	Concentrations of 4-aminophenol at any time	g L^{-1}
C_{A0}	Concentrations of 4-aminophenol at time zero	g L^{-1}
C_D	Orifice discharge coefficient	
C_{seed}	Seed loading	%
d	Baffle orifice size	m
D	Coefficient of diffusion of the solute	m^2 s^{-1}
D	Diameter of column	mm
d_{32}	Sauter mean size diameter	m
D_b	Baffle diameter	m
D_c	Diameter of reactor column	m
f	Proportionality constant	
f	Linear frequency	Hz
F	Crystal shape factor constant	

F_{main}	Main flow rate	g min^{-1}
F_{seed}	Flow rate for seeding solution	g min^{-1}
G	Overall linear growth rate	m s^{-1}
ΔG	Overall free energy difference	J
$\Delta G'_{crit}$	Overall free energy required for heterogeneous nucleation	J
ΔG_{crit}	Overall free energy required for homogeneous nucleation	J
ΔG_s	Surface free energy	J
ΔG_v	Volume freee energy	J
g	Growth order	
ΔH	Heat of dissolution	J
J	Nucleation rate	kg m^{-3} min^{-1}
K	Boltzmann constant (the gas constant per molecule)	J K^{-1}
k	Nucleation constant	
k'_b	Mass nucleation rate constant	
k_b	Number nucleation rate constant	
k_m	coefficient of mass transfer	kg s^{-1} m^{-2}
k_d	coefficient of mass transfer	kg s^{-1} m^{-2}
k_r	coefficient of reaction rate	kg s^{-1} m^{-2}
k_G	Growth rate constant	m s^{-1}
K_G	Overall crystal growth coefficient	kg $m^{-2}s^{-1}$
K'_G	Overall mass transfer coefficient	kg $m^{-2}s^{-1}$
K_La	Volumetric mass transfer coefficient	h^{-1}
L	Baffle spacing	m
m	Mass of deposited solid	kg
N	Detected nuclei number	
N_b	Number of baffles per unit length	m^{-1}
N_m	Minimum detectable number of the nuclei	
N_s	Number of seed crystals	#
P/V	Power density	W m^{-3}
q	First-order reaction rate constant	min^{-1}

R	Universal gas constant	$J\ mol^{-1}\ K^{-1}$
r	Radius of nuclei	m
r_c	Critical cluster size	m
Re_n	Net flow Reynolds number	
Re_o	Oscillatory Reynolds number	
r_R	Generation rate of paracetamol	$g\ L^{-1}\ min^{-1}$
S	Supersaturation ratio	
S_{ip}	Ideal size of product crystals	µm
S_p	Actual products size	µm
S_s	Size of seed crystals	
St	Strouhal number	
T	Absolute temperature	K
t	Reaction time	min
T_0	Saturation temperature	K
T_b	Baffle thickness	m
T_n	Nucleation temperature	K
u	Mean velocity	$m\ s^{-1}$
v	Molecular volume	$m^3\ mol^{-1}$
V	Sample volume or working volume of a crystallizer	m^3
W_{seed}	Mass of seed crystal	g
W_{theo}	Mass of dissolved solute turned into crystals	g
w	Mass of crystalline deposited pur unit mass of solvent when the solutiono is cooled by 1 ºC	
x_0	Amplitude of oscillation from centre to peak	m

α	Crystal volume shape factor	
β	Crystal surface shape factor	
γ	Interfacial surface tension	$J\ m^{-2}$
γ_{cl}	Interfacial tensions between crystal and liquid	$J\ m^{-2}$
γ_{cs}	Interfacial tensions between crystalline and impurity solid surface	$J\ m^{-2}$

γ_{sl}	Interfacial tensions between the foreign solid surface and the liquid	J m^{-2}
δ	Volume free energy change of the transformation	J mol^{-1}
δ	Thickness of stragnant film	m
ΔT_{max}	Maximum supercooling	K
ε	Baffle free area ratio	
θ	Contact angle	
μ	Chemical potential	J mol^{-1}
μ	Dynamic viscosity of the fluid	Pa.s
ν	Kinetic viscosity of the fluid	m^2 s^{-1}
μ_0	Standard chemical potential	J mol^{-1}
μ_{solid}	Chemical potentials of the solute in the solid phase	J mol^{-1}
$\mu_{solution}$	Chemical potentials of the solute in the solution	J mol^{-1}
$\Delta\mu$	Difference in the chemical potentials	J mol^{-1}
λ	Cooling rate	^oC h^{-1}
ρ	Fluid density	kg m^{-3}
ρ_c	Crystal density	kg m^{-3}
ρ_s	Density of solid crystal	g ml^{-1}
σ	Relative supersaturation ratio	
φ	Correction factor	
ω	Angular frequency	rad s^{-1}
Ψ	Velocity ratio	

Abbreviations

^{1}H NMR	Proton Nuclear Magnetic Resonance spectroscopy
4-AP	4-Aminophenol
AA	Acetic anhydride
AC	Acetic acid
API	Active pharmaceutical ingredient
C1	Concentration of paracetamol in solution at sample point 1
C2	Concentration of paracetamol in solution at sample point 2

C3	Concentration of paracetamol in solution at sample point 3
COBR/COBC	Continuous oscillatory baffled reactor/crystallizer
DSC	Differential scanning calorimetry
FTIR	Fourier transform infra-red
HPLC	High performance liquid chromatography
LC-MS	Liquid chromatography–mass spectrometry
MSZW	Metastable zone width
OBR/OBC	Oscillatory baffled reactor
PAA	4-Acetoxyacetanilide
PARA	Paracetamol
PAT	Process analytical technologies
PVM	Process video microscope
RTD	Residence time distribution
STC	Stirred tank crystallizer
UV	Ultraviolet measurement
XRPD	X-ray powder diffraction

List of Publications and Presentations

Journal publications

1. M. Jiang and X. Ni, "Effects of water and temperature on reaction mechanism and crystal properties in a reactive crystallization of paracetamol", Chemical Engineering and Processing: Process Intensification, Vol. 131, 2018, p20-26. (Chapter 4)

2. M. Jiang and X. Ni, "Effects of solvents and impurity on crystallization kinetics and crystal properties in a reactive crystallization of paracetamol", submitted to Journal of Crystal Growth, Submitted. 2019. (Chapter 5)

3. M. Jiang and X. Ni, "Reactive crystallization of paracetamol in a continuous oscillatory baffled reactor", Organic Process Research & Development, Accepted. 2019. (Chapter 6)

Presentations

- M. Jiang and X. Ni. Characterisation of a Reactive Crystallization. The 4th Winter Process Chemistry Conference, (Poster) 12 – 14th December, 2016, Glasgow, UK.

- M. Jiang, X. W. Ni. Characterisation of a Reactive Crystallization. The 4th IMPEE Conference, (Oral presentation and poster) 3rd September, 2016, Heriot-Watt University, UK.

- M. Jiang, X. W. Ni. Characterisation of a Reactive Crystallization. The 48th British Association for Crystal Growth Conference, (Poster) 27-30th June, 2017, University of Manchester, UK.

Prize

1. Best Poster Presentation Award, The 4th IMPEE Conference, Heriot-Watt University, September, 2016

Chapter 1 - **Introduction**

1.1 Motivation of research

Pharmaceutical production involves synthesis, work up, crystallization, filtration and further downstream operations such as powder processing and formulation. Product specifications (crystal size distribution, polymorphic form, and morphology, etc.) are influenced by each of aforementioned processes, in particular, synthesis and crystallization. After synthesis, the raw product is required to be separated and purified via a recrystallization process[1, 2], however, the effect of reaction conditions on crystallization properties has rarely been examined. Lee et al. and Lee et al.[3, 4] researched the synthesis of acetaminophen (paracetamol) by reacting 4-animophenol with acetic anhydride. Kinetics of crystal growth and agglomeration were studied separately, the filtration property, flowability and dissolution rate for drug delivery of paracetamol crystals via three paths were compared. However, the kinetics of reaction process was not investigated which is also critical to the final properties of crystals. Another sample is the reactive crystallization of salicylic acid investigated by Caro et al.[5]. Their results showed that the mean size increased with decreasing both feeding rate and reactant concentrations. However, it was found that the crystallization kinetic parameter estimation was quite complex, as the objective function of hyper surface contained many different minima. Consequently their work failed to find a set of kinetic parameters that provides for a good description of all experimental data[5, 6]. In this PhD project, the effects of synthesis on crystallization kinetics and crystal morphologies will jointly be investigated, i.e. the reaction is linked with crystallization as a single process, this is new to previous separated studies of either reaction or recrystallization of paracetamol.

Traditional both synthesis and crystallization steps are carried out via batch operation, which has notably difficulties in scaling up and maintaining uniform mixing conditions [7-9] . This means that the products produced are often of a lower quality, leading to disconnected characterization and consumption of energy. Continuous oscillatory baffled reactor/crystallizer (COBR) has received increased attention since 1990s. It has attractive performances in producing and maintaining a consistent mixing environment for flow substances[10, 11]. For example, Lawton et al.[12, 13] compared a typical API cooling crystallization between a batch stirred tank crystalliser and a COBC,

operation efficiency was significantly improved from 9 h and 40 min to about 12 min with better crystal properties. Besides of cooling crystallization, anti-solvent crystallization[14] and co-crystallization [15] were also studied in COBR. The applications of COBR in continuous manufacturing and crystallization were reviewed by Zhang et al. [16], McGlone et al.[17] and Wang et al.[18]; different types of continuous crystallizers were compared and areas for further developments were highlighted including chemical compatibility research, encrustation mitigation, process analytical tools (PAT) and real-time feedback control [16-18]. However, there has been few study on continuous reactive crystallization in a COBR and there is no suitable seeded process for such reactive crystallization ever reported.

1.2 Objective of research

This PhD work addresses the challenges of combining synthesis and crystallization in a continuous process. This project will focus on the characterization of a synthesis crystallization in order to gain scientific understanding of how reaction kinetics or conditions could affect targeted crystal specifications. Therefore, the strategical objectives of this PhD project consist of three parts:

- To characterize the chosen synthesis crystallization process and to obtain reaction kinetics and understand how parameters affecting kinetics;

- To study the subsequent crystallization process and comprehend nucleation and growth kinetics;

- To investigate and compare reaction and crystallization kinetics and establish how both kinetics could be employed to control solute properties and crystal specifications in a continuous oscillatory baffle reactor (COBR).

1.3 Structure of thesis

This thesis is divided into seven chapters. Following this introduction, a literature review on the prevalent theories relevant to synthesis and crystallization mechanisms of the selected model compound is outlined in Chapter 2. This chapter also provides the literature background for general theories of crystallization, as well as the investigations of batch and continuous oscillatory baffled reactors.

Chapter 3 presents the chemical screening results and solubility measurement. Both online and offline analytical tools are discussed for monitoring the reactive crystallization process, with calibration and testing results presented. Experimental procedures for different setups are given in Chapters 4 to 6.

Chapter 4 presents the reaction scheme and mechanism, and focuses on the effects of water and temperature on kinetics of paracetamol synthesis as well as on particle properties. Chapter 5 describes the reactive crystallization of paracetamol in an OBR. The effects of solvents and impurity on crystallization kinetics and performances are examined. Based on that, a reactive seeded cooling crystallization of paracetamol is investigated in a COBR in Chapter 6. Effects of seeding load and mixing intensity on crystallization kinetics and crystal properties are discussed. By analysing the concentrations and crystal sizes at two locations along the COBR, both temporal and spatial steady states in concentration and size are assessed.

Chapter 7 concludes the main findings from this work, and summarises the achievements of reactive crystallization of paracetamol in OBR and COBR. Recommendations for future work are also given in this chapter, followed by the appendixes and a list of references.

Chapter 2 – **Literature review**

The purpose of this chapter is to set the present research project in context of the previous studies relevant to paracetamol synthesis, crystallization sciences and process mechanisms, as well as oscillatory baffled mixing studies.

2.1 Paracetamol synthesis

A comprehensive list of potential reactions for reactive crystallization has been listed in the Appendix A. Both small and large molecule compounds were compared and presented, considering factors including safety, product solubility, operation difficulties and cost, etc. Paracetamol synthesis was chosen to be the model reaction for this project due to its significant usage in pharmaceutical industry and its simple operation requirements. Based on this project design, other reactions listed in the appendix can also be applied in the future. More details about API selection can be found in Chapter 3.

Paracetamol, which is also known as acetaminophen or p-hydroxyacetanilide, is one of the most widely used analgesic drug in the world today. It is white powder crystalline, and has a melting point ranging from 169-171 ºC[1].

2.1.1 Paracetamol synthesis route

Since firstly synthesized by Morse in 1878[19], paracetamol production method has been changed many times in order to enhance the productivity and product property. The procedures can be clarified into four groups according to their starting materials, i.e. paracetamol can be prepared from 4-hydroxyacetophenone[20-22], nitrobenzene[23-27], 4-nitrophenol[28-30], and 4-amniophenol[1, 2], each of which is discussed below. Thus the following section was structured according to the reaction starting materials in order to understand different synthesis mechanisms of paracetamol from various beginning materials.

2.1.1.1 From 4-hydroxyacetophenone

Paracetamol was prepared by Davenport and Hilton[20] in 1984 using a two-step process: firstly, a ketoxime（4-hydroxyacetophenone oxime) was obtained by reacting 4-hydroxyacetophenone with a hydroxylamine salt and a base, the ketoxime was then subjected to a Beckmann rearrangement with an acid catalyst such as hydrogen fluoride, trifluoroacetic acid, fuming sulfuric acid or thionyl chloride in liquid sulfur dioxide. The reaction proceeds as indicated in Figure 2.1. In this method, 4-hydroxyacetophenone oxime from step one must be collected from the aqueous solution by crystallization, followed by washing, drying, storage and handling prior to the Beckmann rearrangement. This adds to operating difficulties and costs. Moreover, the use of strong acid catalysts in step two requires necessary neutralization procedures and tedious work ups to recover paracetamol and catalyst from the crude reaction mixture.

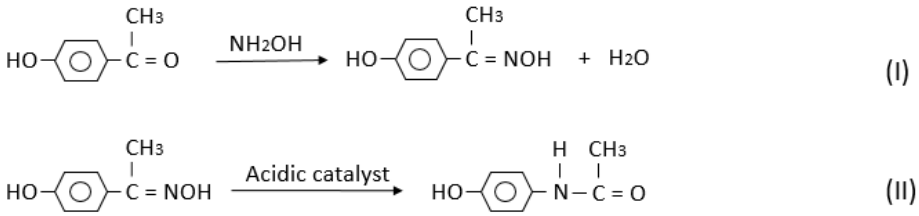

Figure 2.1 Schemes for two-step process of paracetamol synthesis[20]

Fritch et al.[21] provided an alternative method to the above process by using an alkyl ester of alkanoic acid (e.g. ethyl acetate) as the reaction solvent for the Beckman rearrangement and thionyl chloride or phosphorous oxytrichloride as catalyst to prepare paracetamol of high yield. This method allows 4-hydroxyacetophenone oxime to be extracted easily from the aqueous integrated solution in the first step and the mixture can then be treated directly with the catalyst after removal of water. The utilization of alkyl alkanoate ester and insoluble catalyst also provides an easy separation workup for paracetamol products and catalyst recycling.

In 2009, Ghiaci et al.[22] reported their paracetamol synthesis by liquid phase Beckmann rearrangement using new types of catalyst, which were generated by impregnation of silica with phosphoric acid at various ratios. Acetone, acetonitrile,

methanol and water were employed as reaction solvents. Results showed that the conversion of paracetamol was low in polar protic media, whereas in polar aprotic solvent, the conversion rose to 100% in acetone, since 4-hydroxyacetophenone has difficulties to contact with the catalyst in a polar protic solvent. Compared with traditional homogeneous acid catalysts, new types of solid acid catalysts are more active and selective for the synthesis of paracetamol, achieving good conversion of oximes in shorter reaction times.

2.1.1.2 From nitrobenzene

The reduction of nitrobenzene to phenylhydroxylamine followed by rearrangement to p-aminophenol without isolation of the intermediate product was studied by Bassford[23] in 1938 using zinc dust as the reduction agent. The process is shown in Figure 2.2 where nitrobenzene was added to a low percentage ammonium or alkaline earth salt solution. The mix was vigorously agitated and zinc hydroxide was formed on the addition of zinc dust. Nitrobenzene and water was removed by filtration, the filtrate and washings were acidified with any non-oxidizing mineral acid. The acid solution was heated to about 80-100 ºC and cooled and neutralized, after that p-aminophenol precipitated out of solution and was recovered by filtration.

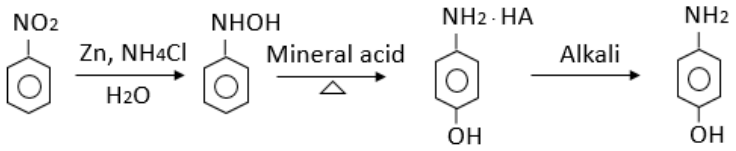

Figure 2.2 Scheme for the production of paracetamol by Bassford[23]

Henke and Vaughen[24] improved the above method in 1940 where p-aminophenol was produced directly by the catalytic hydrogenation of nitrobenzene in mineral acid solution. However, the disadvantages for this kind of reaction are that the reaction proceeds undesirably slowly and the use of high pressure equipment with high agitation is required. Because of these, the process was further improved by Louis[25] in 1956 where para-aminophenol was produced with carefully controlled proportions of

supported platinum catalyst and starting materials for the reduction part. This allowed the reaction to proceed smoothly with mild agitation and without undissolved nitrobenzene remaining in the acid reaction medium. Thus a separate phase of nitrobenzene was prevented from coating the catalyst or reducing its activity. However, one of the disadvantages for previous processes is that a feeding mechanism of high precision was needed to maintain the desirable degree of control. Any accidental variations of nitrobenzene would result in reaction rate fluctuations or products of low quality. Another disadvantage is the high costs of noble metal catalyst and their recovery.

Godfrey and De[26] suggested a more efficient and economical method in 1961 by the electronic reduction of nitrobenzene in sulfuric acid solution (Figure 2.3). The reduction medium was neutralized by calcium carbonate to a PH of 1.5-4.9. The precipitated sulphate was filtered off and the filtrate solvent was extracted with benzene. The aqueous phase was then directly acetylated without intermediate separation of p-aminophenol. The yield of paracetamol product was about 80 - 90 %.

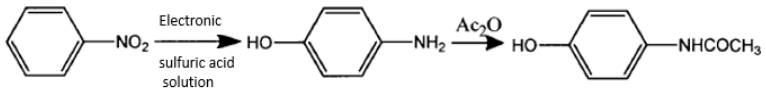

Figure 2.3 The electronic reduction of nitrobenzene to produce paracetamol[26]

A continuous catalyst recovery process was reported by Benner[31] in 1968. Nitrobenzene was hydrogenated in the presence of a dilute sulfuric acid solution, and all integrates were added in a reduction vessel. A settling chamber was connected to the overflow line to hold the level constant in the vessel. The catalyst suspended in nitrobenzene settled to the bottom of the chamber and could be pumped back to the reduction vessel for reuse, or to a metal refiner for recovery after filtration. Rylander et al.[32] disclosed an improved method in 1973. The platinum group metal catalyst was employed to carry out the selective hydrogenation of nitrobenzene and rearrangement in the presence of dimethyl sulfoxide (DMSO) and dilute sulfuric acid. A great product recovery was achieved by running the reaction until absorption of two molar equivalents of hydrogen per mole of nitrobenzene with even a slight addition of DMSO.

Another continuous process to prepare p-aminophenol in a 3-hydrogenator cascade system was reported by Caskey and Chapman[33] in 1986. The reacting mixture was charged to the first reactor at a temperature of 70- 100 ºC, which was consist of fresh nitrobenzene, concentrated sulfuric acid, water, platinum on carbon catalyst and a divalent sulphur compound such as diethyl sulphide. The hydrogenation was carried out once hydrogen was introduced into the same reactor. The overflows of the first reactor went to the next reactor which was also agitated under hydrogen pressure and temperature control. Separation of different phases proceeded in a decant tank which connected to the last hydrogenator. During reaction, the amount of by-product aniline was minimized in the presence of the sulfur compound, and the acid helped the phenylhydroxylamine to be rearranged to p-aminophenol, the conversion of nitrobenzene in the reactor system was typically about 80%.

A batch system which was optimized for the synthesis of p-aminophenol by catalystic hudrofenation of nitrobenzene in acid medium was studied by Rode et al.[27] in 1999. Parameters such as acid concentration, agitation speed, organic phase hold up and catalyst loading were found to have significant effects on reaction selectivity.

2.1.1.3 From p-nitrophenol

Morse [19] firstly reported a direct method in 1878 for the production of paracetamol by using tin and acetic acid on p-nitrophenol. Similar methods with various concentrated acetic acid were presented by Tingle and Williams in 1907[28]. A number of disadvantages existed in this kind of procedure: (1) it was hard to remove the tin and incomplete removal of tin salts can result in contamination of paracetamol products; (2) it was uneconomical to carry out this process with in excess amount of metal required for a chemical reduction with tin and a weak acid like acetic acid. Therefore, simpler and more efficient processes were required to produce paracetamol.

Morris[34] in 1963 developed a method of simultaneous reduction of p-nitrophenol and acylation of p-aminophenol without prior isolation. Using acetic acid as the solvent, p-nitrophenol was reduced with gaseous hydrogen over a bed of palladium catalyst, and 1-1.2 equivalent of acetic anhydride was added at the same time to produce acetylaminophenol. This method could be operated continuously when all the starting

materials: hydrogen, nitrophenol, acetic acid and acetic anhydride were subjected concurrently or counter-currently in the presence of catalyst. The paracetamol was produced with a yield of 75-100 % and of excellent quality.

This method was then improved by Duesel and Godfrey[29] in 1967. Acetic anhydride together with the acetylation medium was used as the reaction solvent. Distilled water was added to make the reaction product and catalyst filtration was easily handled. The paracetamol product isolated from the reaction medium was found suitably pure for direct pharmaceutical application without need for further purification. The reaction could be carried out at a temperature ranging from 70 -100 °C, the yield was 88 – 90 %.

Ruopp and Thorn[35] reported a process in 1981 for the direct preparation of paracetamol from p-nitrophenol. They found out that borate ion, such as boric acid, could prevent the production of undesirable side products and discoloration effects during the hydrolysis of p-chloronitrobenzene and hydrogenation of 4-nitrophenol procedures. This allowed the production of aminophenol by subjecting the nitrophenol directly to hydrogenation without prior separation and purification steps. The boric acid was added to p-nitophenol before the hydrogenation and acetylation, or to the p-chlorotrobenzene before or during the subsequent hydrolysis. The p-nitrophenol containing hydrolysate was then applied directly to the acetylation to produce high purified paracetamol, using palladium-on-carbon as the hydrogenation catalyst.

Generally, there are various catalysts being applied to hydrogenate p-nitrophenol to prepare p-aminophenol: strong acid, such as sulfuric, hydrochloric and phosphoric acids[36, 37]; metal material, e.g. aluminium, platinum, palladium or noble metal and their oxides[31, 34, 36, 38, 39]; and molybdenum sulfide or platinum sulfide-on-carbon[40], etc. The p-aminophenol obtained from all these methods required substantial purification steps before employed to produce paracetamol, paracetamol product so produced was of an acceptable purity [41-44].

Besides all the investigations on catalytic hydrogenation methods, reaction kinetics had also been studied. Ness and Warner[30] in 1987 hydrogenated p-nitrophenol to p-aminophenol and concurrently acetylated the p-aminophenol to paracetamol under

controlled conditions to achieve acetic anhydride with no excess when the hydrogenation reaction was completed. Compared to previous researches, this method effectively shortened the reaction time and produced paracetamol of improved quality. Vaidya et al. [45] studied the intrinsic kinetics of catalytic hydrogenation of p-nitrophenol to p-aminophenol and found that the solvent polarity could increase the hydrogenation rate and catalytic activity.

2.1.1.4 From 4-aminophenol

For the one-step process, paracetamol was prepared by reacting acetylation of 4-aminophenol with a small stoichiometric excess of acetic anhydride in an aqueous medium at a high temperature (see Figure 2.4). A crude aqueous reaction mixture was produced and followed by a crystallization step to recover paracetamol product. As mainly applied for pharmaceutical purposes, the crystallization process must carefully be controlled to obtain crystals with desired properties (high purity, good morphology, narrow particle size distribution, steady polymorphic form, less agglomerates, etc.) using series of process analytical tools. It indicated that a high grade of the starting material p-aminophenol was essential to produce a pharmaceutical grade of paracetamol.

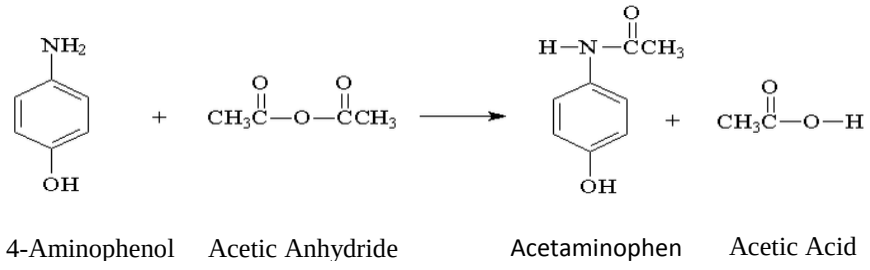

Figure 2.4 Synthesis of paracetamol

Young[1] in 1963 discovered a simpler method to prepare a relatively pure paracetamol without the need of highly pure p-aminophenol nor a catalyst or blanket gas. In this process, p-aminophenol was mixed with water and acetic anhydride, wherein the amount of water delivered a weight ratio to p-aminophenol at least about 0.5 to 1. The reaction was carried out rapidly at a temperature of 70 or 85 ºC with agitation. Raw

paracetamol product was separated by cooling, and then purified further by dissolving and crystallising in an aqueous solution of ammonium hydroxide. Solid absorbent such as carbon black could be added to the solution. White crystalline paracetamol of good physical properties was obtained after filtration with a yield of 94%.

Baron et al. in 1975[2] also provided a methodology for the preparation of paracetamol in pure form where 4-aminophenol was dissolved in hot acetic acid, treated with carbon, filtered and the filtrate was further treated with acetic anhydride at 85 ºC. The advantage for this method was that the colour forming bodies were efficiently removed from the starting material by the carbon treatment, and no neutralization was needed. This was not expected in Young's research[1], however, the yield of the first crop crystals was quite low due to the limited solubility of p-aminophenol in aqueous solution. Paracetamol of higher purity was finally separated by cooling crystallization. To increase the yield, the mother liquor was recycled after the separation of paracetamol product.

Huber [46] in 1981 developed a stepwise reaction scheme in which the hydrogenation of p-nitrophenol was interrupted, acetylation of p-aminophenol accomplished and followed by at least one further hydrogenation step, each of which was proceeded by another acetylation step. The pH was kept below about 7.0. There was no excess acetic anhydride or strong acid required in this method. However, it was difficult to control the correct percentage of the initial reduction reaction before the initiation of the acetylation reaction on a commercial scale.

Another direct synthesis of paracetamol from hydroquinone has been development by Joncour et al. in 2014[47]. Paracetamol was generated in acetic acid using ammonium acetate as the mediating agent at elevated temperatures (230 ºC, 15 hours). Excellent selectivity (> 95 %) and high yield were obtained in the absence of metallic catalysts. However, due to the demanding operational conditions, this route was not chosen for paracetamol reactive crystallization in this project.

Although staring with different materials, all these above methods combining with the recrystallization process can produce paracetamol with good qualities. However, paracetamol synthesis using 4-aminophenol requires simple conditions, has less overall process time and generates no gas. Moreover, opportunities for impurities, which are

resulted from previous reactions, to pass over to the final step can significantly be reduced. Therefore, the route for producing paracetamol via 4-aminophemol was chosen in this work.

2.1.2 Reactors

The reactors for paracetamol synthesis vary from one method to another, depending highly on the operation conditions. The most common reactor is the jacketed reaction vessel as used by Ruopp and Thorn[35], in which the reaction temperature was easily controlled. A Parr shaker was employed in Freifelder's research (cited by Morris[34]), the reaction was carried out at room temperature and an ice bath was utilized to cool down the mixing slurry after the reaction completed. A stirred autoclave was applied in the study of Davenport and Hilton[20] to meet different arrangements of pressure and temperature. Ghiaci et al.[22] carried out experiments in a 50 ml round-bottom flask with a reflux condenser, a thermos-stated bath was used to control the reaction temperature.

It has been known that the hydrogenation and acetylation processes in batch reactors are not overly efficient, even for the single step reactions. The temperature is difficult to control because of the continuously changing heat released from the reactions. For instance, the single step operation suggested by Morris[34] could easily be adapted to a continuous process, however, the scale of any fixed bed reactor and conversion of p-nitrophenol would be highly depended on the cooling efficiency due to the highly exothermic reaction. In that case, Foster et al. [48] suggested a process for producing paracetamol on a continuous basis in a stirred tank reactor, by catalytically hydrogenating p-nitrophenol and concurrently acylating p-aminophenol with acetic anhydride. Compared to batch operation, the continuous process provides a high purity product by minimizing the concentration of reaction by-products and is easier to operate with a constant heat release.

2.1.3 Summary

Paracetamol can be prepared from 4-hydroxyacetophenone[20-22], nitrobenzene[23-27], 4-nitrophenol[28-30] and 4-amniophenol[1, 2]. The one step acylation of p-aminophenol

has been attracting more attention due to its simple conditions with zero-gas involved. In general, most of the synthesis operations were limited by a following recrystallization process to obtain desired crystal size distributions and morphologies. Moreover, operations in batch platforms would also lead to problems in scaling up and solvent shift efficiency. In this PhD research, paracetamol is produced by acylating p-aminophenol with anhydride in the presence of distilled water and a seeded cooling crystallization process is directly followed without prior separation. The reactive crystallization is firstly investigated in a batch oscillatory baffled system, and then adapted to a continuous OBR to fulfil the objectives of this research project. All these will be discussed in the next section.

2.2 Paracetamol crystallization

In pharmaceutical industries, crystallization is a key unit operation with approximately 90% of small molecule active pharmaceutical ingredient (API) manufacturing processes containing a crystallization step[49]. It is an important purification process by forming a highly pure crystalline solid throughout a solid-liquid separation[50]. It is also a particle formation process by which molecules in solution are transformed into a solid phase of regular lattice structure under different controls [50, 51].

Solution crystallization can generally be described in two stages: nucleation and crystal growth. The degree of nucleation and crystal growth determines important product properties, such as crystal size and size distribution [52]. Furthermore, the growth rate affects the purity of crystalline products as fast growth may lead to liquid inclusions. The prerequisite for crystallization to occur is a supersaturated solution which is not at equilibrium. Crystallization occurs when the solution system strives to reach equilibrium and supersaturation that strongly depends on the liquid-liquid and/or solid-liquid mixing state. Therefore, desired and reproducible product qualities are associated with the good control of three steps in a crystallization process[53, 54]:

i. Achievement of supersaturation

ii. Formation of crystal nuclei (nucleation)

iii. Subsequent crystal growth

2.2.1 Supersaturation

In a crystallization process, supersaturation provides the required driving force for nucleation and crystal growth, both of which accelerate as the level of supersaturation increases. It is therefore desirable to minimize the extent of nucleation process and maximize the crystal growth so that most of the material dissolved in the solution can accumulate on the surfaces of a small number of crystals in order to obtain the required crystal size distribution. This can be achieved by controlling the level of supersaturation during the crystallization process[55].

Supersaturation is a relationship of solution concentration as a function of temperature, which is closely linked with the solubility of a compound[56]. Thermodynamically, if a solution comprising a given solute is in equilibrium, the chemical potentials of the solute in the solution, $\mu_{solution}$, and the solute in the solid phase, μ_{solid},, must be equal[57], as shown below:

$$\Delta\mu = \mu_{solution} - \mu_{solid} = 0 \qquad (2\text{-}1)$$

where $\Delta\mu$ is the difference in the chemical potentials (J mol^{-1}). A typical solubility profile, as established by the three distinct regions: undersaturated, metastable and supersaturated, are presented in Figure 2.5.

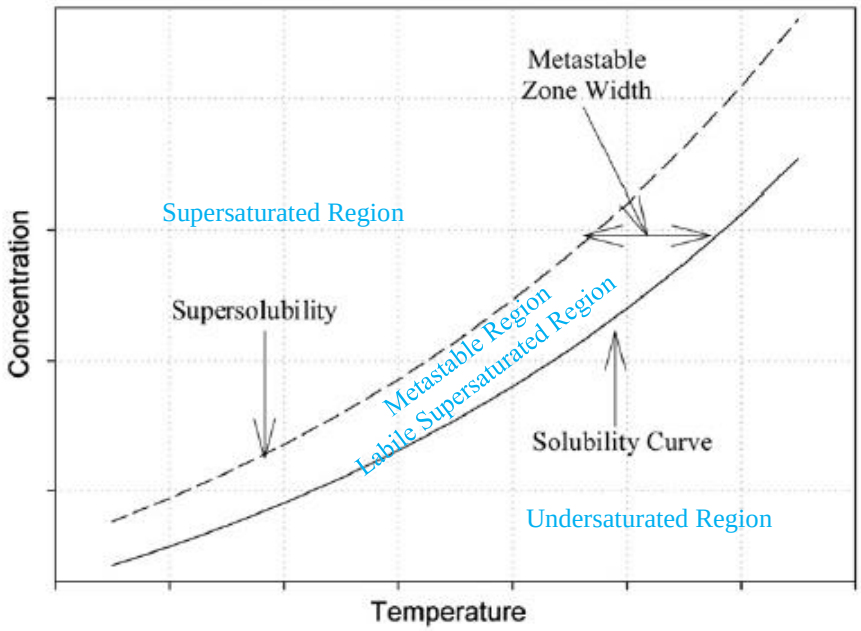

Figure 2.5 General schematic of a model solubility profile[58]

Understanding the phase equilibria is crucial to crystallization. Solution will nucleate spontaneously in labile region, and crystal will dissolve in undersaturated region. While in metastable region, crystals will grow[59]. In undersaturated region, $\mu_{solution} < \mu_{solid}$, which leads to the value of $\Delta\mu$ negative. This means that solid crystals will dissolve and no nucleation occurs. When the solution is cooled/evaporated/added with an anti-solvent, it crosses the solubility curve (see Figure 2.5) and enters the metastable region, where the value of $\Delta\mu$ is positive[12, 60]. This indicates that the solute in the solution state predominates, which is a prerequisite for crystallization[57]. However, supersaturation in solution alone is insufficient for nucleation to occur. Seeding would however be necessary to induce nucleation since spontaneous crystallization is rather unwanted. A certain level of supersaturation, also known as the supersolubility (see Figure 2.5), is required for the creation of new solid interfaces. The region between the supersolubility and the solubility curve is known as the metastable zone (MSZ) which is considered ideal for crystal growth[58]. The solution must only be seeded at certain levels of supersaturation, ideally within the MSZ. This can ensure that the seeds, which are the source of crystal nuclei, restrain from dissolving, so that the solution is not too undersaturated[61]. A typical pathway of a seeded crystallization process is presented in Figure 2.6 below by the dotted line.

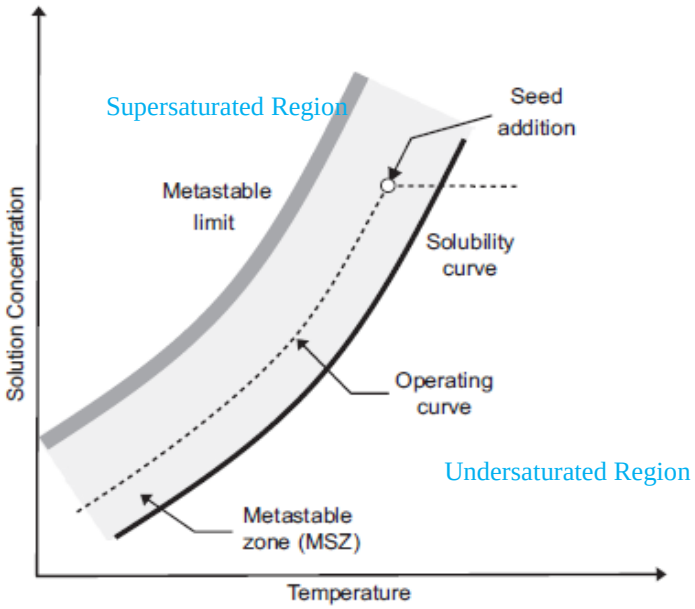

Figure 2.6 General schematic of a seeded crystallization process[62]

It can be seen in Figure 2.6 that as an undersaturated solution is cooled (dashed line), it crosses its solubility curve and enters the MSZ, within which an optimal seeding point is located. Specific supersaturation requirements can be met for seeding to be effective, thus allowing a better controlled nucleation process to take place. Otherwise, as a result of increasing the rate of supersaturation by further cooling/evaporating/anti-solvent addition, the solution will pass the MSZ limit and move into the supersaturated region.

The chemical potential, μ (J mol^{-1}), can be expressed by means of the standard potential, μ_0 (J mol^{-1}), and the standard activity, a_0, as shown below:

$$\mu = \mu_0 + RT\ln a_0 \qquad (2\text{-}2)$$

Where R is the universal gas constant (8.314 J mol^{-1} K^{-1}) and T the absolute temperature (K).

The fundamental dimensionless driving force can be obtained by substituting the above into Eq. (2-2) [63], the following can be derived:

$$\frac{\Delta\mu}{RT} = \ln\frac{a}{a^*} = \ln S \tag{2-3}$$

where S is the fundamental supersaturation in the system, a and a* are activity in supersaturated solution and solute activity in saturated solution, respectively. For practical purposes, it is difficult to obtain the real value of activity in solution system. Generally, the driving force $\ln\left(\frac{a}{a^*}\right)$ or supersaturation ratio (a/a*) is usually converted in terms of concentration with the assumption that its activity is independent of concentration, i.e. the solution activity coefficient of a supersaturation solution is equal to that of a saturated solution [61, 64, 65], so that:

$$\ln S = \ln\frac{c}{c^*} \tag{2-4}$$

Where c is the actual concentration (kg m^{-3}), and c* is the equilibrium concentration (kg m^{-3}).The supersaturation of a system can be expressed in different ways, among which the most common ones are the concentration driving force, Δc, the supersaturation ratio, S, and the relative supersaturation ratio, σ. These expressions are defined as[51]:

$$\Delta c = c - c^* \tag{2-5}$$

$$\sigma = \frac{c-c^*}{c^*} \tag{2-6}$$

$$S = \frac{c}{c^*} \tag{2-7}$$

Considerable confusion can be caused if the units of concentration are not clearly defined for Δc. The temperature must be specified for analysing supersaturation. In this PhD work, the supersaturation ratio S is chosen to be the main expression for crystallization driving force.

2.2.2 Types of crystallization

Achievement of supersaturation may occur by (see Figure 2.7):

- Cooling – reduce the temperature to reduce solubility
- Evaporation – reduce the solution volume
- Anti-solvent - addition of precipitant or diluent to reduce solubility
- Chemical reaction

Supersaturation is usually generated by these four main methods – any single one or a combination, in series or parallel as shown in Figure 2.7. Therefore, there are a number of ways to crystallize fine chemicals or active pharmaceutical ingredients (APIs) from their solutions [66-70].

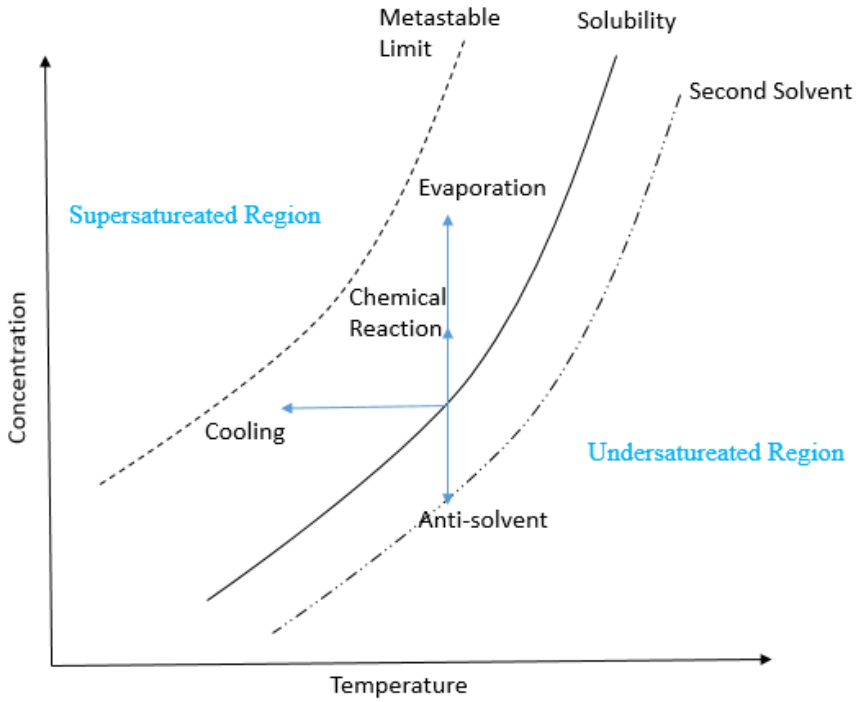

Figure 2.7 Diagram of crystallization methods

2.2.2.1 Cooling crystallization

Cooling crystallization is the most common technique in industrial applications. In cooling crystallization, supersaturation is generated due to the reduction in solubility with temperature, the solvent capacity of the system remaining approximately constant[59, 71]. Figure 2.7 shows a schematic diagram describing a typical cooling crystallization process. When a solution is cooled at a constant concentration of dissolved crystals, supersaturation will increase. Nucleation can occur once the solution moves into the metastable zone with seeding, or crystallization will take place spontaneously once the solution is moved to the labile supersaturated region with further cooling[12, 65]. The rate of supersaturation generation is dependent on cooling rate, thus theoretically cooling crystallization allows both nucleation and growth rate of crystals to be controlled. To achieve that, various online, in-situ process analytical technologies (PATs) are employed in the increasing number of crystallization operations [55, 72-76]. For instance, an integrated array of PATs, focused beam reflectance measurement, particle vision microscopy, Raman spectroscopy and in-house development crystallization process informatics system software (CryPRINS) were used in the research of Powell et al.[77] to monitor the periodic steady-state flow crystallization of paracetamol.

Natural cooling is the simplest method to cool a solution, which is determined by the heat transfer capacity of the crystallizer. However, natural cooling will lead to various supersaturations that may be detrimental to the process as there is no control on the cooling process. It has the potential to decrease the temperature rapidly to pass through the metastable zone and reach the uncontrolled nucleation region without seeding. This is a major problem to cause oiling out, agglomeration, a wide crystal size distribution and occlusion of solvent and impurities. Another problem of uncontrolled cooling is the accumulation of crystals scaling on the cooling surface caused by low temperatures at the wall, leading to non-uniformity in products[78].

Mullin and Nyvlt [51, 79] derived cooling strategies to match the cooling rate with the increasing surface area, which were very useful to control supersaturation. They prescribed cooling rates much slower at the outset than natural cooling in order to maintain supersaturation in or close to the growth region when the crystal surface area for growth was low. This method can reduce encrustation by limiting temperature differences across the jacket.

Seeding is a key variable in the control of cooling crystallization. The ideal seeding point is when the solution first crosses the solubility curve. However, the solution temperature can be affected by several factors, including the actual concentration of the material to be crystallized, mixing intensities as well as the impurities affecting the solubility. There are two cases if not seeding properly. Generally, if the seed is added at a temperature too far above the solubility temperature, the seed may totally be dissolved in the solution, which makes no contribution to the crystallization, resulting in uncontrolled nucleation; if on the other hand the seed is added at a temperature too far below the solubility temperature, the product may have already nucleated. In either case, the increase in nucleation could result in a decrease in impurity rejection and/or a change in particle size distribution and other physical attributes[78]. More discussions about seeding will be presented in the following section 2.2.3.3.

2.2.2.2 Evaporation crystallization

In evaporation crystallization, supersaturation is produced by the loss of solvent accompanied by a subsequent reduction of solvent capacity with time, assuming the process is an isothermal operation with the solubility of a solute in solvent remaining almost constant[70]. A schematic sketch of an evaporation crystallization process is illustrated in Figure 2.8.

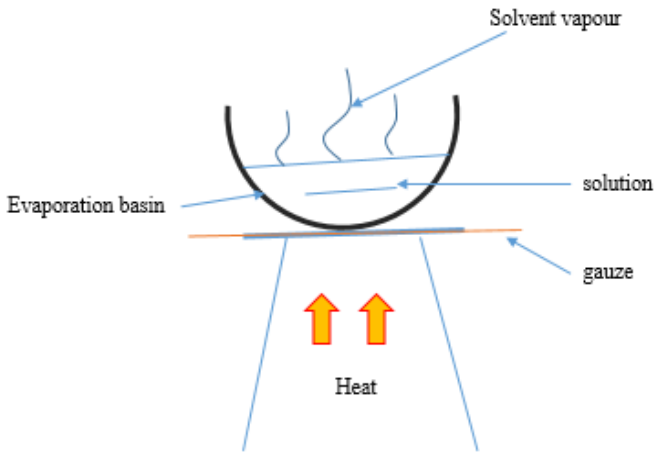

Figure 2.8 Schematic of evaporation crystallization

It is difficult to determine when exactly the solution crosses the saturation line as the concentration increases, seeds are then suggested to be added as slurry in the evaporation solvent[78]. In addition, uncontrolled nucleation takes place in evaporation crystallization due to localized supersaturation at the liquid-vapour-solid interfaces. Therefore, although widely practiced for production of industrial chemicals, evaporation crystallization is rarely used in pharmaceutical operations as it is often not applicable or achievable to control the conditions for crystallization [78, 80].

2.2.2.3 Anti-solvent crystallization

In anti-solvent crystallization, supersaturation is generated by the addition of an anti-solvent to reduce the solute solubility and consequently the solvent capacity of the system increases with time[70]. Figure 2.7 compares the different routes of cooling and anti-solvent crystallization processes. Instead of cooling the system, anti-solvent (e.g., water) is added to the solvent (e.g., acetone) at a constant temperature[81].

The polymorph of crystals generated through anti-solvent addition is difficult to manipulate as it creates extremely high supersaturation levels in a short period of time[82]. Thus anti-solvent crystallization often yields small crystals with a narrow size distribution because of the high rate of crystallization. The control of both supersaturation and crystal growth can be achieved by controlling the anti-solvent addition rate, and considering the effects of various process parameters on size, number, shape, degree of agglomeration and polymorphic form of product crystals, including the type of anti-solvent, feed concentration, solution concentration, anti-solvent addition rate and agitation intensity[83].

Mitchell et al.[84] studied the anti-solvent crystallization of paracetamol in ethanol-water solutions. The primary nucleation kinetics was estimated from metastable zone width and induction times. The effects of solvent composition on the nucleation rates were investigated. Kachrimanis and Malamataris[85] examined the effects of polymer on properties of paracetamol crystals during an anti-solvent crystallization (ethanol/water system). Crystal yield, micromeritic and compression behaviour could be improved in the presence of polymers. Granberg et al.[86] studied the influence of solvent

composition on the crystallization of paracetamol in acetone-water mixtures, the growth kinetics of paracetamol in different solvent compositions were investigated[87].

Image analysis or photographic methods are very useful in determining the presence of nucleation conditions[88, 89]. Brown and Ni[81] studied the anti-solvent crystallization (acetone/water system) of paracetamol in an oscillatory baffled crystallizer (OBC) where a laser illuminated video imaging system was used to determine the instantaneous and overall average crystal growth rate. The video imaging results showed a high degree of agreement compared with those of the standard sampling techniques.

2.2.2.4 Reactive crystallization

Reactive crystallization is characterized when the supersaturation of a crystallizing solute is created by chemical reaction, i.e. supersaturation occurs as a consequence of the production of a desired component[70]. The solubility and solvent capacity may remain constant, and both the reaction and crystallization steps may be treated as occurring in series.

In reactive crystallization processes, the solubility of the formed compound is normally low or very low. The reaction can be very fast compared to both the mass transfer rate and the growth rate of the crystals, e.g. precipitations, thereby a region with high supersaturation and subsequent rapid nucleation and growth will form around the feed point of reactants[90]. For this type of processes, it is difficult to control particle properties in the precipitation part because there is usually no practical method to slow down the reaction process. Therefore, successful operation depends on a careful balance between the addition rate of the reagents, local supersaturation, global supersaturation, mass transfer and crystal growth surface area[78]. Moreover, mixing condition in the crystallizer has a significant influence on the final product characteristics, while interactions are complex as nucleation and growth kinetics in reaction crystallization are poorly understood[5, 6]. The lack of mathematical optimization studies on reactive crystallization could also be attributed to the difficulty in modelling the mixing kinetics[91].

Reactive crystallizations are commonly used in production of some inorganic compounds like calcium carbonate and barium sulphate, but are also extensively used in production of pharmaceuticals and organic fine chemicals. A common procedure is to feed one reactant into an agitated solution of the other reactant. Generally, the crystal size is found to decrease with increasing feed rate in single-feed semi-batch experiments[92]. For instance, Slund and Rasmuson [93] studied semi-batch precipitation of benzoic acid in a stirred tank reactor and found that the influences of agitation rate, agitator type and feed point location could well be correlated by the estimated feed point energy dissipation rate. Larger crystals were produced with a decreased feed rate and decreased reactant concentrations.

Ståhl et al.[6] estimated the kinetics of the reactive crystallization of benzoic acid by mixing hydrochloric acid and sodium benzoate solutions in a T-mixer. After examining the optimization process and evaluating the model and kinetics, it was concluded that care must be exercised in both the design of the model and the determination of kinetics. Similarly, a reactive crystallization of salicylic acid was investigated by Caro et al.[5]. Dilute hydrochloric acid was added to an aqueous solution of sodium salicylate in a semi-batch reactive crystallization process. Results showed that the mean size increased with decreasing feeding rate and reactant concentrations. There was also a decrease in mean size with increasing feed pipe diameter. However, the crystallization kinetic parameter estimation was found to be quite complex, as the objective function of hyper surface contained many different minima. Consequently their work failed to find a set of kinetic parameters that provides for a good description of all experimental data[5, 6].

However, Utomo et al.[94] proposed that a controlled supersaturation at the addition of the reagents required an initial charge of seed to prevent uncontrolled nucleation, leading to the creation of an excess number of particles. Ammonium phosphates were produced in their research by reacting ammonia and phosphoric acid in a jacketed semi-batch reactive crystalliser equipped with a dual feed system and a turbine type agitator. Effects of various parameters (seed crystals, feeding system, feed flow rate, initial supersaturation, feeding time and mixing intensity) on the reactive crystallization supersaturation, crystal yield, crystal shape and final crystal size distribution (CSD) were studied to understand the kinetics. Wang and Ward[95] studied the seeding policy and the operation of a batch reactive crystallization process of L-glutamic acid. The result showed

that seeding could almost entirely be used to suppress nucleation, and late-growth trajectories would generate smaller final nucleated mass fraction, which was supported by rigorous simulation and optimization. In the study of Alatalo et al.[96], glutamic acid was precipitated by adding sulphuric acid to a mono sodium glutamate solution in a reactive semi-batch crystallization process. In order to investigate the feedback control, they built up a closed-loop control process to manipulate the driving force of reactive crystallization using the feed rate of acid. This allowed the glutamate ion concentration to be adjusted according to time dependent pre-fined set point trajectories, which led to the control of both the polymorphic form and the crystal size distribution.

Compared with the precipitations described above, reactive crystallization involves a chemical synthesis firstly that produces a new solute totally dissolved in the reaction/crystallization solution. A supersaturation can then be generated through either cooling down the solution or by the addition of anti-solvent, thus crystallization takes place subsequently after the reaction step[97]. In other words, the reaction conditions would affect the solution properties and concentrations that have further impact on the following crystallization step. Characterization of this type is the aim of this PhD work, more literature review is given in this section.

Caldeira and Ni[97] mixed water and vanillin in a fed batch oscillatory baffled reactor at 60 ºC. The mixture and sodium hydrogen sulphite were then charged into the continuous oscillatory baffled reactor (COBR) which was at the same temperature. Vanisal sodium crystals were produced by the synthesis reaction and followed by a cooling process. Another example was the reactive crystallization of acetylsalicylic acid[97], acetic anhydride and salicylic acid were mixed at 90 ºC while the concentrate sulphuric acid was pumped into the COBR at room temperature. The chemical reaction took place at 60°C with good mixing of all reactants at laminar flow conditions. The crystals of acetylsalicylic acid were then obtained by a cooling crystallization process afterwards.

Ni and Mackley[7] studied the irreversible reaction between sodium hydroxide and ethyl acetate in both a pulsatile flow and a stirred tank reactor. The conductivity drop during the reaction was observed and the kinetics of the reaction were investigated according to the conductivity change of sodium hydroxide. The synthesis and crystallization of poly(ethylene glycol)-poly(caprolactone) diblock copolymers (PEG-

PCL) was studied by He et al.[98]. Mutual influences between PEG and PCL crystallization were examined by altering the relative block length. The result showed microphase separation occurred because the PCL and PEG blocks liked to crystallize themselves in all the copolymers; and the crystallization temperature and time depended on the relative block length.

Lee et al. and Lee et al.[3, 4] researched the synthesis of paracetamol by reacting 4-animophenol with acetic anhydride. Paracetamol particles were produced from three different crystallization paths with various modes of agitation and additions of sodium hydroxide. The concentration of paracetamol, temperature and pH value throughout reaction and crystallization were monitored by process analytical tools. Crystallization kinetics and crystals agglomeration were studied, whereas the filtration property, flowability and dissolution rate from different methods were compared. However, the effects of reaction conditions and kinetics on crystal properties have not been investigated.

In this PhD project, the focus is on the reactive crystallization of paracetamol in order to understand if the reaction kinetics could be manipulated to influence crystallization kinetics and crystal specifications.

2.2.3 Crystal nucleation

It has been known that supersaturation alone is not sufficient to cause crystallization[51, 60]. Crystals can develop only when a number of solid bodies, nuclei or seeds exist in the solution. Nucleation can take place spontaneously (homogeneous nucleation) or be induced artificially (heterogeneous or secondary nucleation). There are a number of mechanisms for nucleation once the solution is supersaturated. The scheme is displayed in Figure 2.9. Primary nucleation is reserved for the cases that do not contain crystalline matter. On the contrary, secondary nucleation refers to the behaviour that nuclei generated in the presence of crystals in a supersaturated system.

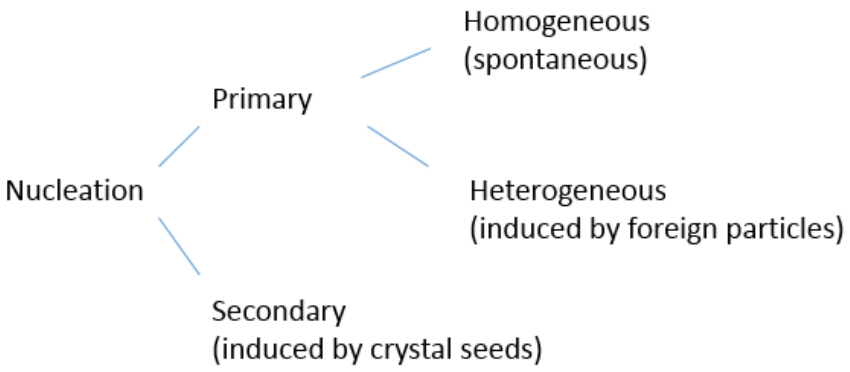

Figure 2.9 Nucleation mechanisms[51]

2.2.3.1 Homogeneous nucleation

The formation of a stable crystal nucleus within a homogeneous fluid is not known for certain. According to the classical nucleation theory, in a saturated solution clusters of solute molecules are constantly forming and dissolving as a reversible process. Once supersaturation is achieved, the formation of nucleus becomes more possible. However, this consolidation of solute molecules to create tangible solid surfaces has an energy barrier. The probability of forming a stable cluster or nucleus is determined by the energy of its formation and growth.[60]

The overall free energy difference, ΔG (J), between a small particle of solute and the solute in solution is defined as the summation of the surface free energy, ΔG_s (J) and the volume freee energy, ΔG_v (J) [51] as:

$$\Delta G = \Delta G_s + \Delta G_v \tag{2-8}$$

$$\Delta G_s = 4\pi r^2 \gamma \tag{2-9}$$

$$\Delta G_v = -\frac{4\pi r^3 \delta}{3v} \tag{2-10}$$

where r is the radius of nuclei (m); v the molecular volume (m^3 mol^{-1}); γ the interfacial surface tension (J m^{-2}); and δ the volume free energy change of the transformation (J mol^{-1}).

The two terms ΔG_s and ΔG_v have opposite signs and rely differently upon r, thus the sum ΔG will pass through a maximum value, ΔG_{crit} (Figure 2.10). The critical free energy difference, ΔG_{crit} (J), corresponds to the critical nucleus redues, r_c (m), which is the minimum size of radius for a cluster to retain stable.

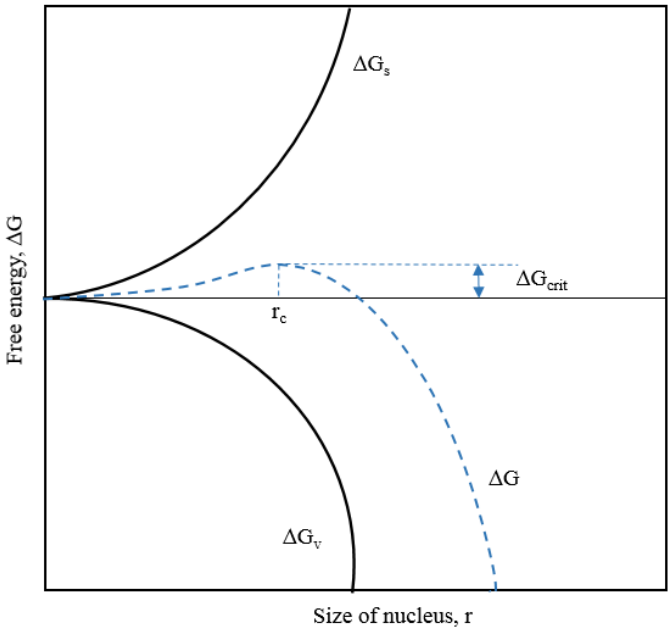

Figure 2.10 Free energy diagram for nucleation[51]

For a spherical cluster, $\frac{d\Delta G}{d\,r} = 0$, by substituting Eq.(2-9) and Eq.(2-10) into Eq.(2-8) and differentiating for r, the critical cluster size is determined as:

$$r_c = \frac{2\gamma\, v}{\delta} \tag{2-11}$$

According to the basic Gibbs-Thomson Relationship, for a non-electrolyte it can be written as:

$$\ln S = \frac{2\gamma v}{KTr} \tag{2-12}$$

where K is the Boltzmann constant, (the gas constant per molecule, $K=1.3805 \times 10^{-23}$ J K^{-1}). So

$$\delta = KT \ln S \tag{2-13}$$

It can be seen that the r_c is a function of the chemical potential difference, combining Eq. (2-11) and (2-13) we get:

$$r_c = \frac{2\gamma v}{KT \ln S} \tag{2-14}$$

The critical free energy is then determined by:

$$\Delta G_{crit} = \frac{16\pi\gamma^3 v^2}{3\,\delta^2} = \frac{16\pi\gamma^3 v^2}{3\,K^2T^2(\ln S)^2} \tag{2-15}$$

Eqs. (2.14) and (2.15) show that the size of critical nucleus is dependent on supersaturation, $r_c \propto (\ln S)^{-1}$, whereas the critical free energy difference is also a function of the supersaturation, $\Delta G_{crit} \propto (\ln S)^{-2}$. These relationships are shown in Figure 2.11, where it can be seen that both r_c and ΔG_{crit} decrease when supersaturation increases.

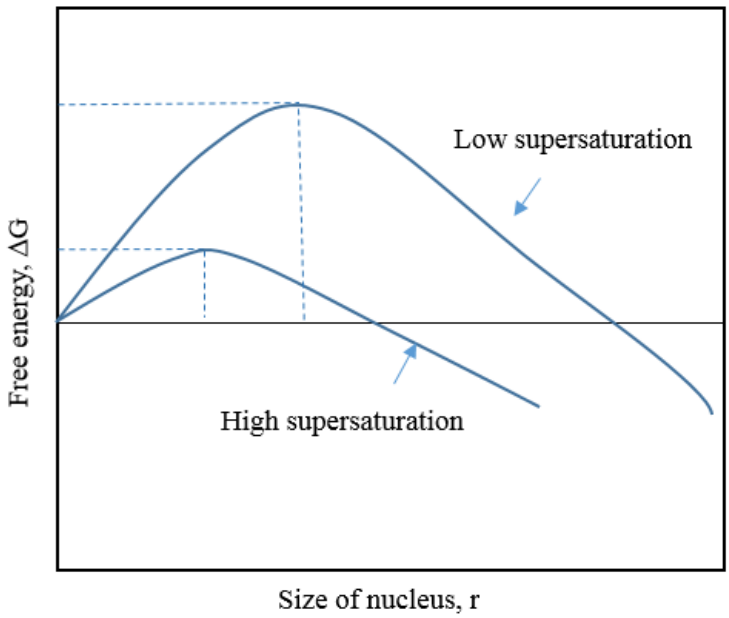

Figure 2.11 Effect of supersaturation on nucleation free energy and critical nucleus size

The nucleation rate, J (kg m^{-3} min^{-1}), effected by free energy, is illustrated as:

$$J = Ae^{\frac{-\Delta G}{kT}} \tag{2-16}$$

where A is the rate constant, # s^{-1} m^{-3}. Combining Eq. (2.15), it indicates that the rate of nucleation is governed by temperature, T; degree of supersaturation, S; and the interfacial tension, γ. Figure 2.12 plots the nucleation rate with respect to supersaturation. It can be seen that the rate of nucleation rapidly increases till the critical level of supersaturation is exceeded.

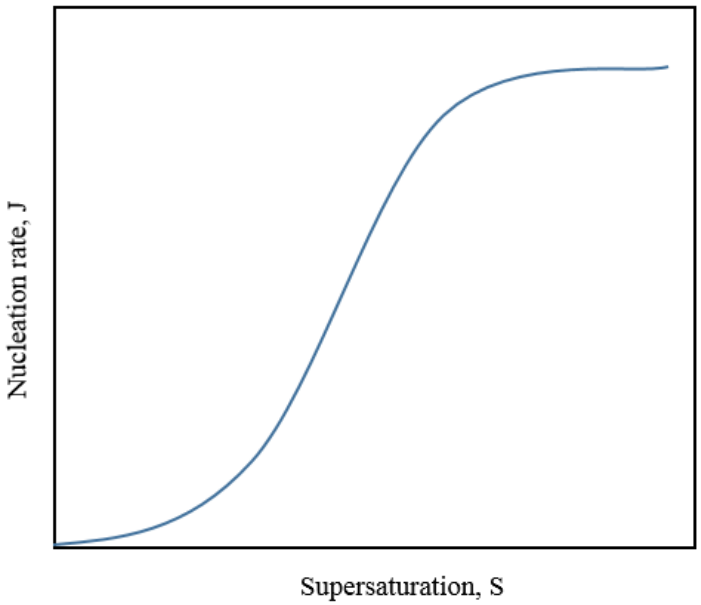

Figure 2.12 Nucleation rate as a function of supersaturation[60]

2.2.3.2 Heterogeneous nucleation

It is generally accepted that homogeneous nucleation is rarely seen in crystallization applications. It is virtually impossible to prepare a solution completely free of foreign bodies, such as atmospheric dust or remnants of a previous batch. Heterogeneous nucleation, with the presence of foreign bodies, can occur at a lower degree of supersaturation than that required for the spontaneous nucleation in a 'clean' system. This leads to higher nucleation temperatures and nucleation rates. Solid impurities can induce opportunities for absorption of solute molecules, reducing the energy barrier associated with the formation of a critical nucleus. Therefore, the overall free energy required for heterogeneous nucleation $\Delta G'_{crit}$ (J) must be less than that for homogeneous nucleation, ΔG_{crit} (J), as shown in Eq. (2.17):

$$\Delta G'_{crit} = \emptyset \Delta G_{crit} \tag{2-17}$$

where $\emptyset$ is the correction factor and $0 < \emptyset < 1$.

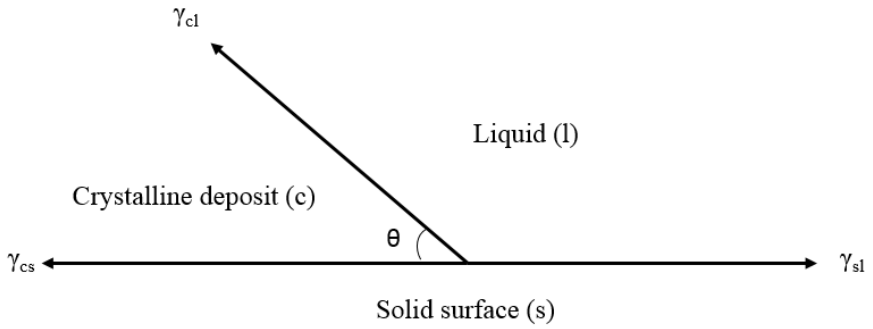

Figure 2.13 Interfacial tensions at the boundaries in heterogeneous nucleation[51]

It has been mentioned earlier that interfacial tension, γ, is one of the vital factors for controlling nucleation process. Mullin[51] presented an interfacial energy diagram for three phases (two solids, one liquid) that involved in nucleation (Figure 2.13). The contact angle θ is the angle between the foreign solid and the surface of crystalline deposit. The value of θ can be predicted by resolving the three forces in Figure 2.13 as:

$$\cos\theta = \frac{\gamma_{sl}-\gamma_{cs}}{\gamma_{cl}} \tag{2-18}$$

where γ_{sl}, γ_{cs}, and γ_{cl} stand for the interfacial tensions between the foreign solid surface and the liquid, between the growing crystalline and the impurity solid surface, and between crystal and liquid.

Based on that, Volmer[99] defined the value of ∅ as:

$$\emptyset = \frac{(2+\cos\theta)(1-\cos\theta)^2}{4} \tag{2-19}$$

If there is completely no correlation between crystal structure and solid impurity surface, θ = 180°, then ∅ equals to 1, this illustrates that the overall free energy for nucleation is the same as that for homogeneous nucleation, i.e. no heterogeneous nucleation takes place. If there is partial affinity between crystal and solid of impurity, then 0° < θ < 180°. In this case ∅ is less than 1 and $\Delta G'_{crit}$ is less than $\Delta G_{crit.}$ Thus heterogeneous nucleation will take place due to reduced critical free energy.

2.2.3.3 Secondary nucleation

If the contact angle θ equals 0°, $\Delta G'_{crit}$ will be zero, nucleation will take place at much lower supersaturation than that of primary nucleation. This is called secondary nucleation. A few mechanisms for secondary nucleation have been studied by many researchers. Contact nucleation and seeding nucleation are the two main types.

Collisions in solution system can cause breakages at the point of contact, inducing contact nucleation when a single crystal is split into fine particles in the supersaturated solution and becomes secondary nuclei. The collisions can be caused by the contacts between crystals and crystallizer walls/agitator/impellor or other crystals. Agitating speed is directly proportional to the properties of crystal products [51, 100].

Beside of mixing in solution, fluid flow is also responsible for secondary nucleation[101, 102]. Micro-crystalline dust could be swept into supersaturated regions by the solution flowing past by seed crystals. Alternatively, crystals adhere to the surface could be shed off and induced into the solution by fluid flow, causing secondary nucleation. Therefore, secondary nucleation relies not only on supersaturation control, but also the hydrodynamics in crystallizers. It is generally agreed that a good understanding of secondary nucleation is very important to control over nucleation process in industry to prevent rapid nucleation which would cause deviation from targeted crystal properties.

As a result, adding seeds in supersaturated solutions is widely employed in crystallizations to dominate nucleation mechanism and control particle growth under reproducible conditions[103]. Furthermore, inoculation of seeds could efficiently avoid encrustations, control polymorphic crystal form and the specifications of final products such as crystal morphology and size distributions [104]. In general, the seeding efficacy is dependent on several questions involving how to prepare seeds, seeds quality, seeding method, seeding temperature, seeding load, seed size and etc.[103].

- How to prepare seeds

It is essential to have consistent and well defined seeds from suitable preparation methods for high quality crystallization products. Sometimes seeds can simply be induced to the system by scraping the surface of the crystallizer[105], or can crystallize from an unseeded fast cooling process[106]. Normally, seeds are prepared via procedures including milling, washing and sieving[107]. To find out the effects of seeds preparation on products properties, seeded crystallizations of potassium dichromate in water were carried out by Aamir et al. [107] using seeds prepared by three different methods: crystalline-sieved, milled-washed-sieved and milled-sieved. The experimental measured size distributions of products were compared with simulation results from a population balance model. A good agreement was shown when the seeds of good quality with no fines, while over-prediction of crystal size distribution appeared when the seeds contained fine particles or dusts. Growth kinetics were different as a result of different surface properties between the milled and crystallised seeds. The kink densities in the milled seeds could be optimized by washing process smoothening the fractured faces and edges[108].

- How to seed

Seeding for crystallization involves introducing solute crystals to solution by either single crystal or a certain mass of dry crystals, or a slurry that contains particular amount of crystals[109]. For dry addition, attention has to be given to make sure that the seeds are uniformly dispersed in the solution instead of attaching on the wall of the crystallizer. Otherwise, particle clumping or aggregation is likely to happen as a result of powder adhesion[108]. Slurry seeding can disperse dry seeds in a certain volume of liquid before their addition into any crystallization system, especially for continuous crystallizers. This also helps to smoothen any fractured edges of the seed particles via growth and Ostwald ripening[108].

Novel designs of continuous seeding with freshly prepared seed suspension have been developed in recent years[108]. Seed crystals could continuously be prepared in a separate nucleation unit by precipitation, antisolvent or quench crystallization method[110, 111]. The slurry was then fed into a concentrated solution where supersaturation was created by the temperature trajectory along the crystallizer.

In the research of Ferguson and co-workers[112], seed slurry was generated in a plug flow device by a single addition anti-solvent (ethanol/water system), and used to seed the equivalent batch cooling crystallization of benzoic acid. The final crystal properties were controlled by variation of the seeding properties and unequal flowrates of feed/anti-solvent.

- Seeding temperature/ Seeding load

As mentioned in section 2.2.2.1, seeds should be introduced in the solution at specific conditions of supersaturation to make sure the seeding to be effective[62, 113], ideally within the metastable zone with as shown in Figure 2.2 previously. The seeding point lies between the solubility curve and the metastable limit line beyond which spontaneous nucleation would occur. If seeds are added in the under-saturated region, seeds would be dissolved reducing the seeding effective. Conversely, if seeds are added in the supersaturated region, primary nucleation has already taken place, reducing the effectiveness of seeding. The seeding point varies from compound to compound based on different experimental conditions.

Al-Zoubi and Malamataris[105] studied the influences of seeding temperature, initial concentration and cooling temperature on the transformation of paracetamol from monoclinic to orthorhombic nucleation in ethanoic solution. While monoclinic nucleation occurred at high initial concentrations, low seeding temperatures and long seeding times, orthorhombic form increased the yield by increasing initial concentrations, reproducible production of pure orthorhombic form was achieved at medium initial concentrations, higher cooling temperatures and agitation rates[114].

Mohammad et al.[115] studied the crystallization of carbamazepine-saccharin co-crystal where crystallization temperature increased with the increases of seeding temperature and seeding load, and nucleation time decreased with seeding load. This was as expected because higher seeding load resulted in more surface area for expediting nucleation process.

- Seed size

Generally, besides of nucleation induction, both seed load and seed size contribute to the necessary surface area for crystal growth. The questions of 'how much seed mass to add?' and 'what size is the seed?' really depend on the specifications of final crystal particles. If large particles are required, less seeds enable fewer particles to grow bigger at a certain amount of crystallizing material. On the other hand, if small particles are needed, more seeds are then added therefore the growth is spreading across a greater number of crystals, resulting in smaller amount of growth for each particle[109]. For an unagglomerated growth only model, the relationship between products size and seed size can be illustrated by Eq. (2-20) as below.

$$\frac{W_f}{W_{seed}} = \frac{FN_s\rho_s S_{ip}^3}{FN_s\rho_s S_s^3} = \left(\frac{S_{ip}}{S_s}\right)^3 \tag{2-20}$$

where Ns is the number of seed crystals which is assumed to be conserved, F is the crystal shape factor, L_s is the seed size (μm) and L_{ip} the size of the ideal product crystals (μm), ρ_s is the density of solid crystal (g ml^{-1}). The final mass of crystals produced, W_f (g), is the sum of the seed mass, W_{seed} (g), and the theoretical yield, W_{theo} (g).

According to Eq. (2-20), the ratio of the actual number of product particles, N_p, to the ideal number of total crystals (the number of seed particles), N_s, can be expressed as:

$$\frac{N_p}{N_s} = \left(\frac{W_f}{W_{seed}}\right)\left(\frac{S_s}{S_p}\right)^3 \tag{2-21}$$

The value of N_p/N_s can be employed to analyse the degree of agglomeration. If agglomeration occurs, the number of crystals at the end of the process will be smaller than the initial seeding number ($0<N_p/N_s<1$). On the other hand, if nucleation and growth are the dominate mechanisms, the value of N_p/N_s will be larger than 1. This principle was utilized by Warstat and Ulrich[116] where the effects of seed mass, cooling profile, seed size, supersaturation and seed quality on the specifications of product crystals were examined thoroughly. It was found that increasing seed mass decreased the mean size of products as well as the dependence on the cooling procedure. The ratio of N_p/N_s decreased with seeding mass but increased with seed size. Nucleation happened at a high level of supersaturation, while breeding effects were found to be dominate for milled seed crystals that had a wide size distribution. The value of N_p/N_s was close to 1 for crystallized and

suspension seeds, which indicated that the number of product crystals was close to that of seed crystals and the process was dominated by the growth of seeds.

For seeding kinetics study, Frawley et al.[117] investigated the secondary nucleation kinetics of paracetamol in ethanol solutions in a seeded cooling crystallization process. A numerical model was developed to examine the effects of supersaturation, temperature, agitation and seed surface area on crystallization kinetics. The secondary nucleation rate was found to increase with seed surface area, supersaturation and agitation rate. The model simulation, which utilised the population balance equation and the method of moments, showed a good agreement with experimental data. Similarly, a direct estimation model was established by Long et al.[118] to simultaneously examine the growth kinetic parameters of mass deposition rate and growth order. Based on a series of isothermal batch crystallization operations of mono-ammonium phosphate, it was found that both parameters decreased with the seeding mass. This finding could help to control the seeding crystallization kinetics for generating desirable crystal products.

Actually, instead of seeding, gassing is an innovative technology to induce nucleation in cooling crystallization, which was recently discussed by Kleetz et al.[119]. It was found out that both gassing and seeding crystallization could provide more specified products with increased production capacity compared to the unseeded operation. Gassing crystallization was estimated to be a competitive alternative to seeding with less effort in process design to ensure constant performance.

2.2.3.4 Nucleation kinetics

In crystallization, nucleation plays a decisive role in determining the crystal structure and size distribution. Much of the literature has been focused on nucleation for the obvious reason that the number and size of nuclei initially formed can dominate the remainder of the operation[78]. Hence, understanding of the fundamentals of nucleation is important to achieve control over these properties[120, 121].

The Nývlt equation [122-125] is the classical approach for nucleation kinetics estimation, which usually gives a good fit to experimentally measured MSZW. It is assumed that the nucleation rate J at the beginning of nucleation was related to the

maximum solution supersaturation Δc_{max} as well as the cooling rate λ. This was expressed according to Eq. (2-22) and Eq. (2-23):

$$J=k\,\Delta C_{max}^{b} = k\,(\frac{dc}{dT}\Delta T_{max})^{b} \tag{2-22}$$

$$J = (\frac{dc}{dT})\,\lambda \tag{2-23}$$

where ΔT_{max} is the maximum supercooling between the saturation temperature T_0 and nucleation temperature T_n, c is the mole fraction solubility of solute at temperature T, b and k denote the apparent nucleation order and nucleation constant, respectively, and λ is the cooling rate. Eliminating the nucleation rate J in equations Eq. (2-22) and (2-23), then taking logarithms on both sides, we obtain Eq. (2-24):

$$\ln(\Delta T_{max}) = \frac{1}{b}\ln\lambda - \frac{1}{b}\ln k + \frac{1-b}{b}\ln(\frac{dc}{dT}) \tag{2-24}$$

Therefore, a linear relationship between $\ln \Delta T_{max}$ and $\ln \lambda$ can be predicted. This enables the analysis of nucleation kinetics combined with experimental work. The mass nucleation rate constant, k_b', is determined by the intercept, then converted to a number based rate constant by the following [125]:

$$k_b = \frac{k_b'}{\alpha\rho_c r^3} \tag{2-25}$$

Where k_b is the number nucleation rate constant, α volume shape factor, ρ_c the crystal density and r the average nuclei size (m).

However, the limitation of the Nývlt approach[126, 127] is that crystal growth had not been taken into account, and the derivation was based on the assumption that the solubility coefficient dc/dT did not depend on the saturation temperature T_0. This results in unclear physical nature of the nucleation order and nucleation constant. Recently, a self-constant Nývlt-like equation was proposed by Sangwal[126, 128, 129] and declared that an expression relating dimensionless maximum supercooling ($\Delta T_{max}/T_0$) with the

cooling rate λ was expected to describe the experimental ΔT_{max} data better than the original Nývlt equation. Then Eq. (2-24) was modified to Eq. (2-26):

$$\ln\left(\frac{\Delta T_{max}}{T_0}\right) = \frac{1}{b}\ln\lambda - \frac{1}{b}[\ln k + (2b-1)\ln T_0] + \frac{1-b}{b}\ln\left(\frac{dc}{TdT}\right) \quad (2\text{-}26)$$

It is assumed in the Sangwal's equation that the nucleation rate J was related to the maximum supersaturation ratio S_{max} by a powder-law expression, and based on the theory of regular solutions for temperature and solubility, the relative supersaturation ($S=c_2/c_1$) was described as a function of MSZW by Eq. (2-27)[126]:

$$J = k\ln S_{max}^{b} = k\left(\ln\frac{C_2}{C_1}\right)^{b} = k\left(\frac{\Delta H}{RT_1}\frac{\Delta T_{max}}{T_2}\right)^{b} \quad (2\text{-}27)$$

where c_1 and c_2 are solution concentrations at temperature T_1 and T_2, respectively, and $\Delta T= T_2-T_1$, ΔH is the heat of dissolution and R is the gas constant. Eq. (2-28) indicates that the nucleation rate is related to the generation rate of supersaturation, where f is the proportionality constant.

$$J = f\frac{\Delta C}{C_1\Delta t} = f\frac{\Delta C}{C_1\Delta T}\frac{\Delta T}{\Delta t} = f\frac{\Delta H}{RT_1T_2}\lambda \quad (2\text{-}28)$$

When T_1 attains the value of nucleation temperature T_n, the saturation temperature T_2 is replaced by the initial saturated temperature T_0. The combination of Eq. (2-27) and (2-28) gives:

$$\ln\left(\frac{\Delta T_{max}}{T_0}\right) = \frac{1}{b}\ln\lambda + \frac{1-b}{b}\ln\left(\frac{\Delta H}{RT_n}\right) + \frac{1}{b}\left(\ln\frac{f}{k}\right) - \frac{1}{b}\ln T_0 \quad (2\text{-}29)$$

This deviation predicts a linear relationship between ln ($\Delta T_{max}/T_0$) and ln λ, enables the determinations of nucleation order from slope 1/b. The main advantage for Eq. (2-29) compared with Eq. (2-24) is that the effect of initial saturation temperature T_0 on dc/dT is now included. However, it remains difficult to identify the influences of some physical factors, such as impurities and secondary nucleation.

Another approach was suggested by Kubota[130] to account for the dependence of the measured MSZW for a given system on the detection technique that was employed to indicate the first nucleation events, which was not considered by Nývlt. The Kubota interpretation equated the nucleation rate, B (m^{-3} s^{-1}), to the rate of the change of a detected nuclei density, $\frac{N}{V}$ (# m^{-3}) , with time[125]:

$$B = \frac{d(\frac{N}{V})}{dt} \tag{2-30}$$

$$\ln \Delta T_{max} = \frac{1}{b+1} \ln \left[\left(\frac{N_m}{V k_b'} \right) (b+1) \right] + \frac{1}{b+1} \ln \lambda \tag{2-31}$$

A plot of $\ln \Delta T_{max}$ versus ln λ would yield a straight line, with a gradient equal to $\frac{1}{b+1}$, shown in Eq. (2-31), where b is the nucleation order, $\frac{N_m}{V}$ the minimum detectable number density of the nuclei and is apparatus dependent. The mass nucleation rate constant, k_b', was then determined by the intercept similar to the Nývlt approach.

Besides the above theoretical interpretations on nucleation process, there are also some other kinetic studies, [120, 126-128] such as classical 3D nucleation theory approach and progressive 3D nucleation and etc. These are not discussed here, as these can be considered as the variants from the basic interpretations.

2.2.4 Crystal growth

Once a nucleus of a crystal has been established, it will continue to increase in size until the rate of growth units joining the crystal surface has exceeded that of the crystalline entities in supersaturated solution[63]. The analysis and development of industrial crystallization processes require knowledge of growth kinetics, a number of crystal growth theories have been developed and are reviewed in the literature [60, 131-134], e.g. the surface energy theory, absorption layer theory, kinematic theory and the diffusion-reaction theory. Most of the theories have not been able to predict or describe the growth of crystals as a function of important independent variables because of the complex parameters that cannot be evaluated experimentally[134, 135]. Generally, the diffusion

model is commonly applied to many crystallization processes for analysing mass transfer and similar kinetics. As a result, diffusion theory will be discussed in this section.

It was originally proposed by Noyes and Whitney[136] that the deposition of crystal on surface was essentially a diffusion process. Reversely, crystallization can be a dissolution process and the rates of both are determined by the concentrations on crystals surface and in the bulk of the solution. It was presented in Eq. (2-32) for crystallization process.

$$\frac{\mathrm{dm}}{\mathrm{dt}} = \mathrm{k_m A_s}(\mathrm{c} - \mathrm{c}^*) \tag{2-32}$$

Where m (kg) is the mass of solid deposited in time t (s); k_m the coefficient of mass transfer (kg s^{-1} m^{-2}); A_s the surface area of the crystal (m^2).

By assuming that there would be a thin stagnant film of liquid adjacent to the crystal surface, through which the solute molecules would diffuse, Nernst[137] proposed:

$$\frac{\mathrm{dm}}{\mathrm{dt}} = \frac{\mathrm{D}}{\delta}\mathrm{A}(\mathrm{c} - \mathrm{c}^*) \tag{2-33}$$

Where D is the coefficient of diffusion of the solute (kg m^{-1} s^{-1}) and δ is the thickness of stragnant film (m).

The value of δ would depend on the relative velocity between liquid and crystals, i.e. the degree of agitation in the system. Up to 150 μm of film thicknesses had been measured for stationary crystals in stagnant solution, while these valves were found to drop rapidly to virtually zero in vigorously agitated systems. As a result, this could lead to an infinite growth rate in the well mixed system, which obviously suggests that the concept of film diffusion alone is not sufficient to explain the mechanism of crystal growth. Furthermore, substances generally dissolve faster than they crystallize at the same temperature and composition. Thus crystallization is not necessarily the reverse of dissolution, or else they would be at the same rate[51].

As a response to these issues, a considerable modification by Berthoud[138] and Valeton [139] (all cited by Mullin [51]) was made to the diffusion theory. They suggested that there were two stages in the mass deposition process as shown in Figure 2.14.

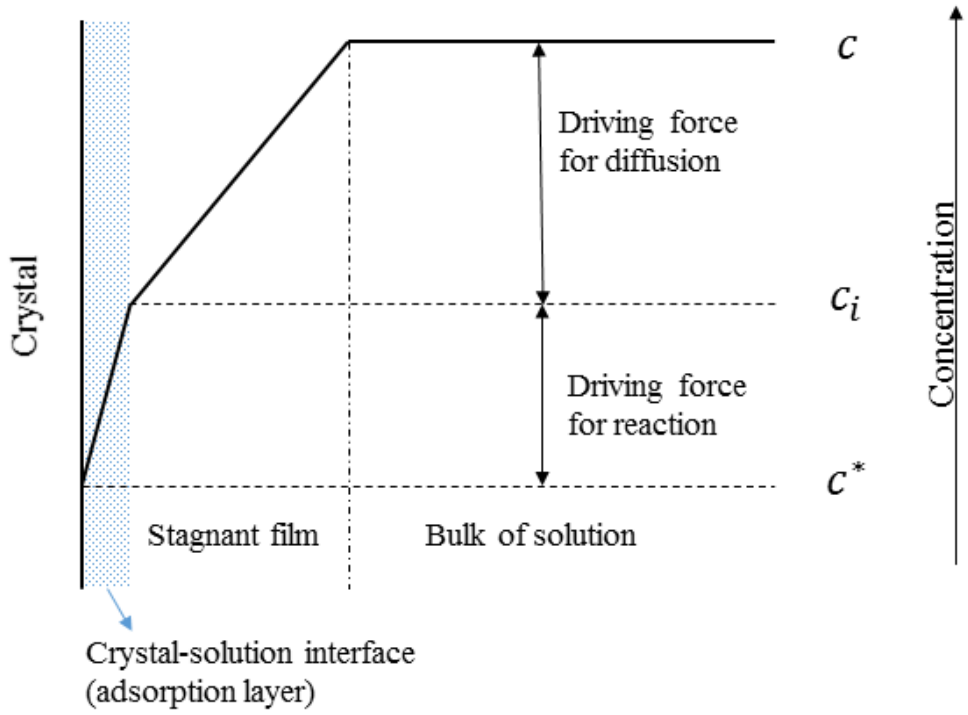

Figure 2.14 Concentration driving forces for the diffusion-reaction model[51]

Firstly, solute molecules were transported from the bulk of the fluid to the crystal surface, then followed by a first order 'reaction' when the solute molecules arranged themselves into the crystal lattice. The two steps were represented by equations:

$$\frac{\mathrm{dm}}{\mathrm{dt}} = \mathrm{k_d A(c - c_i)} \qquad \text{Diffusion} \qquad (2\text{-}34)$$

and

$$\frac{\mathrm{dm}}{\mathrm{dt}} = \mathrm{k_r A(c_i - c^*)} \qquad \text{Reaction} \qquad (2\text{-}35)$$

where k_d is the coefficient of mass transfer, kg s^{-1} m^{-2}; k_r the coefficient of reaction rate, kg s^{-1} m^{-2}; and c_i the solute concentration at the crystal-solution interface. Both stages

were taking place under the effect of different concentration driving forces as can be seen in Figure 2.14. However, the interfacial concentrations are difficult to measure in practice. Therefore, the term c_i is eliminated by considering an overall concentration driving force, $(c - c^*)$:

$$\frac{dm}{dt} = K_G A(c - c^*)^g \tag{2-36}$$

where k_G is the overall crystal growth coefficient, kg s^{-1} m^{-2}; and g is the order of overall growth process. If the surface reaction is a first order, i.e. g=1, the interfacial concentration c_i can be eliminated from Eq. (2-34) and (2-35), so that

$$\frac{dm}{dt} = \frac{A(c-c^*)}{\frac{1}{k_d}+\frac{1}{k_r}} \tag{2-37}$$

or

$$\frac{1}{K_G} = \frac{1}{k_d} + \frac{1}{k_r} \tag{2-38}$$

For extremely rapid reaction, the value of k_r is large, $K_G=k_d$ and the crystallization process is controlled by the diffusion process. Similarly, for large k_d, i.e. the diffusional operation is fast, $K_G=k_r$ and the process is controlled by the surface integration. Generally, the diffusional step is considered to be linearly depended on the concentration driving force, but the assumption of a first order surface reaction is not confirmed[51]. The rate equations can be expressed as

$$R_G = \frac{1}{A} \cdot \frac{dm}{dt} = k_r(c - c_i) \qquad \text{(Diffusion)} \tag{2-39}$$

$$= k_d(c - c^*)^r \qquad \text{(Reaction)} \tag{2-40}$$

$$= K_G(c - c^*)^g \qquad \text{(Overall)} \tag{2-41}$$

2.2.4.1 Growth kinetics

Fundamental studies have been focused on single crystal growth mechanisms, individual surface growth rates have been evaluated [140-142]. Various experimental measurements and estimations have been employed to determine overall mass transfer rates under controlled conditions, in turn, to obtain size-dependent growth rate [3, 65, 84, 86, 88, 143, 144]. There is however no generally accepted method for expressing the growth rate of crystallization, because of the highly dependence on supersaturation, solvent compositions, morphology, size, temperature and etc., the most convenient and useful method is to measure crystal growth rates in terms of mass deposited per unit time per unit area of crystal surface, instead of individual face growth rates[51]. The overall linear growth rate, G (m s^{-1}), can be illustrated as

$$G = K_G \frac{\beta}{3\alpha\rho_c} \Delta c^{\,g} \tag{2-42}$$

where $K'_{G,}$ ρ_c and g are the overall mass transfer coefficient (kg m^{-2} s^{-1}), crystal density (kg m^{-3}) and growth order, respectively. The growth rate is related to the level of supersaturation in terms of concentration difference as $\Delta c=(c-c^{\star})$, where c is the concentration in solution (kg $_{solute}$ $kg^{-1}{}_{solvent}$) and c* refers to solubility at the same temperature (kg $_{solute}$ $kg^{-1}{}_{solvent}$).

In this PhD work, the dimensionless supersaturation, S ($=\frac{c}{c^*}$), was applied to the evaluations of overall linear growth rates (Eq. 2-43), which indicated various supersaturation levels in different solvent conditions.

$$G = K_G \frac{\beta}{3\alpha\rho_c} (\ln S)^{\,g} \tag{2-43}$$

Similar equation as Eq. (2-41) was employed by Mohana and Myerson[134] and Granberg et al.[86] to establish and analyze the influence of the solvent composition on the average crystal growth rates.

2.3 Oscillatory flow devices

2.3.1 Introduction

Oscillatory flow was firstly investigated for applications in chemical engineering in the 1980s[145], based on the study of Van Dijick in 1935[146] on the oscillatory flow in a pulsed sieve plate column. Bellhouse[145] reported the study of oscillatory flow in furrowed channels in membrane filtration. Sobey et al.[147, 148] characterized the vortex mixing for this type of set up in 1980, while Knott and Mackley in the same year reported that mixing could be enhanced with vortex formation if sharp edges were presented in the flow. In 1987 Mackley[149] proposed the first conception of oscillatory baffled reactor in the form of a cylindrical tube with periodically spaced orifice baffles and a high mixing performance was achieved by the vortices generated via fluid oscillation. Brunold et al.[150] demonstrated the generation and cessation of large scale eddy mixing produced in shape edges in oscillatory flow, assessed this mixing by flow patterns and energy losses. Dickens et al.[151] reported that efficient radial and axial eddy mixing was achieved in a near plug flow operation. A large amount of research work has been carried out since then on mixing [152-155], heat transfer[156-158], mass transfer[159-161], scale up correlations[9, 162, 163] and residence time distribution[164-166]. In recent years, the research and development of OBR has subsequently paved the way for industrial applications in biological processes [167-169] and crystallization process [8, 65, 97, 113, 170, 171], the latter of which is relevant to this work.

2.3.2 Fluid mechanics

In an OBR, the fluid moving through baffles forms vortices or eddies[172] as shown in Figure 2.15. On the upstroke, vortices form behind the baffles providing axial and radial currents, while on the downward stroke, eddies formed by the upstroke are forced into the central portion of the column, creating significant radial motion, while new vortices are simultaneously generated behind the opposing baffle. The constant generation of eddies due to oscillations of fluid leads to a complex series of flow patterns which results in highly efficient axial and radial mixing. The mixing intensity is controlled by the oscillation frequencies and amplitudes. There are two methods for achieving oscillatory motions, the typical setup for each method will be discussed in Chapter 5 & 6.

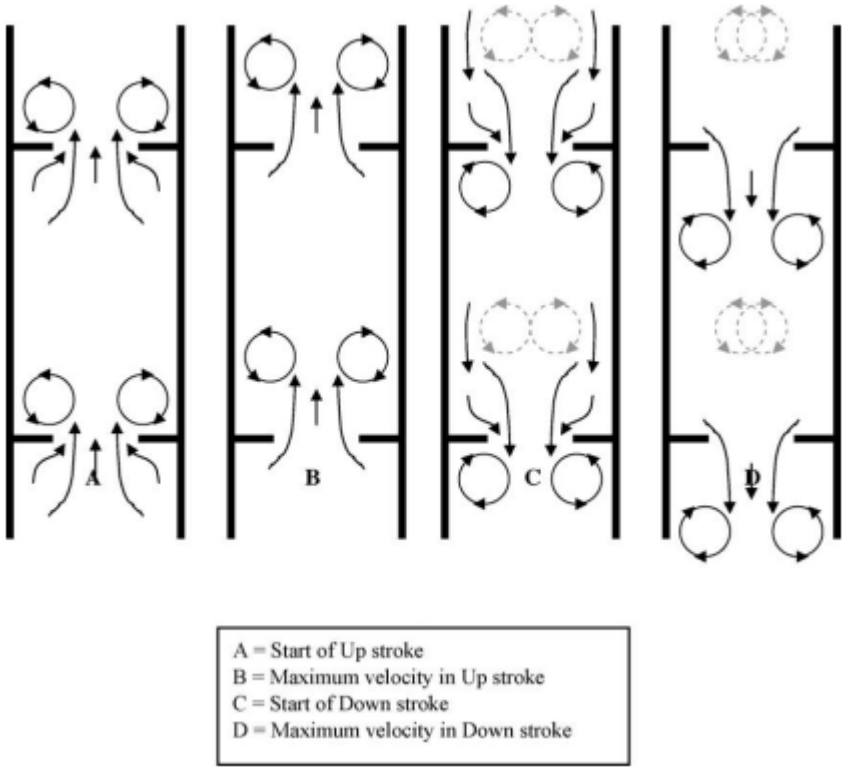

Figure 2.15 Formation of eddies in an OBR [172]

It has generally been agreed that the mixing performance of oscillatory baffled reactor can be characterised by two dimensionless groups: the oscillatory Reynolds number (Re_0) and the Strouhal number (St) which are defined by Eq. (2-44) and (2-45).

$$Re_0 = \frac{x_0 \omega D}{\nu} \tag{2-44}$$

$$St = \frac{D}{4\pi x_0} \tag{2-45}$$

where x_0 is the amplitude of oscillation from centre to peak (m); $\omega(= 2\pi f)$ the angular frequency (rad s^{-1}); f the linear frequency (Hz); D diameter of the column (m); and ν kinematic viscosity of the fluid (m^2 s^{-1}).

The oscillatory Reynolds number measures the intensity of oscillation and the Strouhal number represents the ratio of column diameter to amplitude of oscillation that

determines the length of eddy propagation showing how effectively the system is at generating vortices[165].

It was reported that the flow mixing density was low at $Re_0 < 250$, vortices exhibited essentially 2D axi-symmetry. In the region of 100 a potential separating current was noted[164]. In contrast, when Re_0 was above 250, the symmetry was broken, the flow showed 3D turbulence and a well-mixed flow scheme developed progressively. The transition of turbulent flow started at around $Re_0 = 2100$[166].

In a continuous OBR, a net flow Reynolds number is relevant as:

$$Re_n = \frac{\rho u D}{\mu} \tag{2-46}$$

where ρ is the fluid density (kg m^{-3}) and u is the mean velocity (m s^{-1}), μ dynamic viscosity of the fluid (Pa.s). To maximize the mixing effect, the value of Re_0 should be higher than Re_n. Eq. (2-47) as defined by a velocity ratio, Ψ, as[156]:

$$\Psi = \frac{Re_0}{Re_n} \tag{2-47}$$

It is recommended that for oscillatory flow operation, $Re_0 \geq 100$, $St \leq 0.5$, $Re_n \geq 50$ and velocity ratio Ψ in the range of 2 - 10[17].

2.3.3 Reactor Geometry

In order to optimize the mixing conditions in terms of heat and mass transfer in an OBR, it is important to understand the reactor geometry that controls the vortex generation including baffle type, baffle thickness, T_b (m), baffle orifice size, d (m), baffle diameter, D_b (m), and baffle spacing, L (m). Figure 2.16 illustrates a typical configuration of an OBR with a diameter of D_c (m).

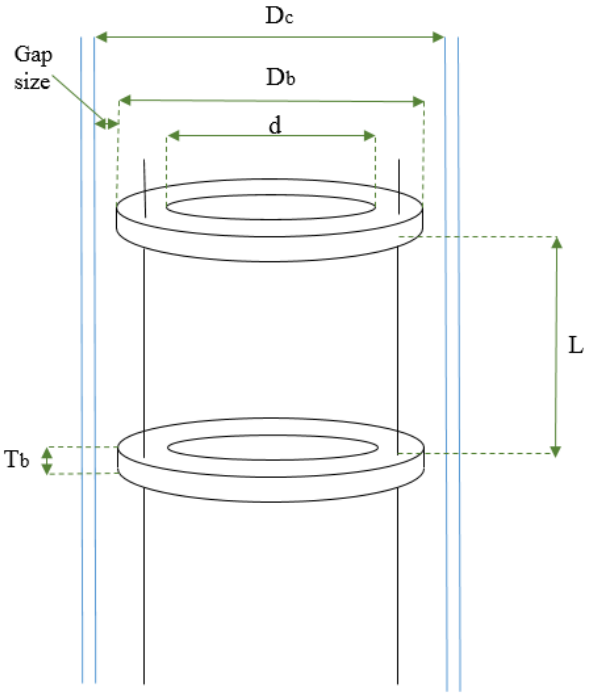

Figure 2.16 Typical OBR baffle scheme

Baffle spacing of 1.5 times the column diameter was suggested by Zhang et al. [155] for generating the optimal mixing conditions in an oil-water system, while Ni and Gao[160] in 1996 reported an optimal baffle spacing of 1.8 times Dc in a mass transfer study involving air and water for a better vortex generation. Gough et al. [153] in 1997 stated that better mixing can be generated using a baffle spacing of up to 2 times the column diameter and an oscillation amplitude of one quarter the baffle spacing..

By performing a thorough investigation, a baffle thickness of 2-3 mm and the baffle free area of 20-22 % were identified to provide the highest mass transfer rate[173, 174]. The baffle free area ratio, ε, was defined as the baffle orifice area divided by the tube cross sectional area, as shown in Eq. (2-48).

$$\varepsilon = \frac{A_2}{A_1} \tag{2-48}$$

where A_1 is the column cross sectional area, m^2 and A_2 is the baffle orifice area, m^2.

The gap size between the outer diameter of the baffle and the wall of the column plays an important role in mixing time. Ni and Stevenson[154] reported that the larger the gap size, the longer time the system took to achieve good mixing and thus the lesser efficient of the OBR system.

OBRs with four types of baffles (helical, integral, single orifice and multi-orifice) were investigated by Ahmed et al.[175] on their performances in two phase flows. The multi-orifice was highly recommended for gas-liquid systems, as it showed the most significant enhancement in the volumetric mass transfer coefficient. In the contrast, the helically baffled design was not recommended for gas-liquid mass transfer applications. Similarly, baffle designs on radial/axial fluid stretching and mixing were investigated [176], the disc-donut baffles could be useful for multiphase applications due to significant shear strain rates and axial dispersion. On the other hand, the helical blade designs were suggested for decreasing axial dispersion, while maintaining significant levels of shear strain.

2.3.4 Mass and heat transfer studies

Mass transfer of oxygen into water was reported for oscillatory flow in a baffled tube by Hewgill et al. (1993)[159], a six-fold increase in k_La was measured as compared with those for a bubble column. Ni et al. (1995)[152] showed a 75% increase in k_La for air-yeast system. Much higher production rate of pullulan was also presented by Gaidhani et al.[161]. In ozone-water mass transfer study, Al-Abduly and co-workers [177] reported 5 and 3 times more efficient for the OBR than the baffled (no oscillation) and bubble columns respectively. The enhancement was due to the uniform bubble size distributions and smaller mean size, prolonged bubble residence times and gas hold up[178] and enhanced breakage rate[179, 180].

In terms of heat transfer, Mackley et al.[157] found that the presence of baffles and oscillations significantly enhanced heat transfer in continuous systems. The heat transfer rate was strongly depended on oscillation intensity including frequency and amplitude. A correlation was proposed by Mackley and Stonestreet in 1995 [156] to predict the Nusselt number (Nu) within the range of $100 \leqslant Re_n \leqslant 1200$, $0 < Re_o \leqslant 800$, which was fitted to the experimental data (Eq. (2-49)). A 30 times improvement in Nusselt

number could be attained at specific conditions for continuous operations[156]. Stephens and Mackley[158] reported that both pulsing fluid and oscillating baffle batch systems were energy efficient and better heat transfer, comparing to a stirred tank system with similar energy input.

$$\mathrm{Nu} = 0.0035\mathrm{Re_n^{1.3}Pr^{\frac{1}{3}}} + 0.3[\frac{\mathrm{Re_0^{2.2}}}{(\mathrm{Re_n}+800)^{1.25}}] \quad (2\text{-}49)$$

Recently, Law et al.[181] developed a new method (Eq. (2-50))for predicting heat transfer in OBR with the most comprehensive experimental work to date and covering a wider range of operating conditions ($200 \leqslant R_{en} \leqslant 1300$, $0 < R_{eo} \leqslant 8700$). Moreover, the Prandtl number (Pr) at a range of 4.4 - 73 was also included. The accuracy was within 30 %, which was more accurate than the previous correlations.

$$\mathrm{Nu} = 0.022\mathrm{Re_n^{0.7}Pr^{0.3}Re_0^{0.44}} \qquad (0 < \mathrm{Re_0} \leq 1300) \quad (2\text{-}50)$$

$$\mathrm{Nu} = 0.52\mathrm{Re_n^{0.7}Pr^{0.3}} \qquad (\mathrm{Re_0} > 1300) \quad (2\text{-}51)$$

2.3.5 Residence time distribution (RTD)

Residence time distribution (RTD) is a tool for assessing reactor performances and have extensively been used in the research and development of oscillatory baffled reactors. Mackley and Ni (1991) [163] reported the near to plug flow RTD by manipulating different oscillatory parameters. Ni and Pereira[175] and Reis and coworkers[176] investigated the effects of oscillatory amplitude and frequency on RTD. Stonestreet and Veeken[166] showed that RTD was dependent on both net and imposed oscillatory flows, a velocity ratio, Ψ, was employed to determine where the system could be operated close to a plug flow, the optimum RTD was achieved in the range of $1.8 \leqslant \Psi \leqslant 2.0$.

Whereas most of the previous studies were carried out based on a single phase liquid flow[165], residence time distribution of liquid and solid phase in a continuous oscillatory baffled crystallizer was studied by Kacker et al.[182] via a heterogeneous tracer system (melamine-water). They found that mixing intensity at 2 mm and 2 Hz was

sufficient to obtain plug flow like mixing of suspending all four slurry concentrations tested (Figure 2.17).

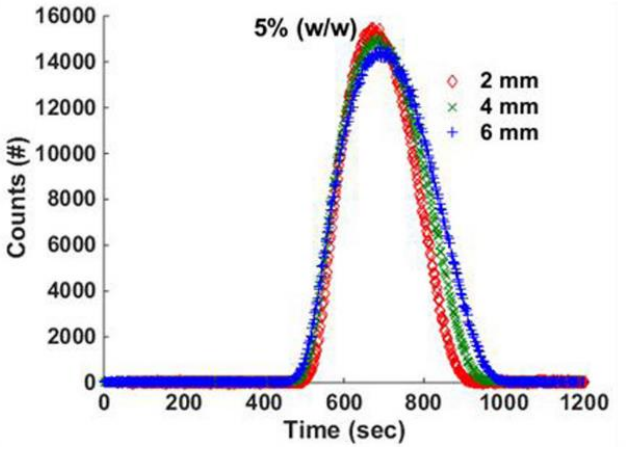

Figure 2.17 Particle counts distribution, measured by FBRM at the exit of DN15 crystalliser (f = 2 Hz, flow rate = 100 ml min^{-1})[181]

In this work, a COBR will be used for both reaction and crystallization of paracetamol.

2.3.6 Power density

In order to compare mixing efficiency or reactor performance among different devices, power density (power dissipation per unit volume) is used as the common basis [156, 164, 183].The power density for an OBR is defined by Eq. (2-49):

$$\frac{P}{V} = \frac{2N_b\rho(1-\varepsilon^2)}{3\pi C_D^2\varepsilon^2} x_0^3\omega^3 \qquad (2\text{-}52)$$

where P/V is the power density (W m^{-3}); ρ the fluid density (kg m^{-3}); N_b the number of baffles per unit length (m^{-1}); C_D the orifice discharge coefficient (usually taken as 0.7)[184, 185]; ε the fractional free area of baffles; $x_0$the amplitude of oscillation from centre to peak (m); and ω is the angular frequency (rad s^{-1}). Although there have been two different models for estimating power dissipation rate in OBR, the recent CFD work by Jimeno Miller et al.[186] (2018) showed that both the quasi-steady model and the eddy

enhancement model give similar power density estimations and can be used interchangeably. For this reason, only one power density equation above is presented in this work.

OBR mixing was more energy efficient than a STR[7], the power densities in two OBRs of different scales was constant[187]. In cooling crystallisation of L-glutamic acid, the MSZW in an OBR was more constant and narrower than that in a STR within the same power dissipation range, metastable form of crystals was not obtained in the OBR due to stronger mixing[188]. Thus, compared with STRs, the better mixing conditions in OBRs can achieve a narrower MSZW and a stable solid form that is more suitable for secondary processes.

2.3.7 Crystallization in COBR

Batch crystallization is the most common used method in pharmaceutical industry, while some of the crystallization operations are well understood[189, 190], there are however significant issues with batch-to-batch variability, large footprints and wastes. Consistent mixing environment for flow substances in COBR [10, 11] enables uniform suspension of solids in solution, better heat and mass transfer, more operational flexibility and more sites for implementing online process analytical technologies (PAT) [17], together with its linear scale-up correlation. These are the essential requirements for crystallisation, which has attracted increased research work in continuous crystallisation in COBR. Lawton et al.[12] compared a typical cooling crystallization of pharmaceutical API in a batch STR and a COBR, uniform crystal size was obtained with faster filtration rate in the latter, in addition, a 9 h and 40 mins batch operation was completed in about 12 mins in the COBR.

Once steady state has been achieved, continuous processing generates products with little variation[191]. Briggs et al.[192] successfully carried out a seeded cooling crystallization of β-L-glutamic acid in a 25 m long COBC, the steady state was achieved constantly after 2 residence times and remained for at least 10 hours producing desirable polymorph and purity. Besides of cooling crystallization, anti-solvent crystallization[14, 193] and co-crystals production[15] were also undertaken. Brown et al.[14] achieved both temporal and spatial steady states for solute concentrations; spatial steady states for

crystal size in the anti-solvent crystallization of salicylic acid in a COBR, however, the temporal steady state for crystal size was hard to attain due to the unstable flow rates. In the study of a spherical crystallization of benzoic acid by Pena et al.[193], using a spatially distributed solvent, anti-solvent and binder addition strategy, the steady state for total counts was observed after four residence times. However, the individual mechanism for each step was not attainable due to the back mixing of the system. α-Lipoic acid: nicotinamide co-crystals were generated continuously by Zhao et al.[15] in a 24 m jacketed glass COBC (diameter 16 mm) for 2-3 hours at a flow rate of 70 ml min^{-1}.

Applications of COBR in continuous manufacturing and crystallization were reviewed by Zhang et al. [16], McGlone et al.[17] and Wang et al.[18], different types of continuous crystallizers were compared and areas for further development were highlighted including chemical compatibility, encrustation mitigation, PAT, and real-time feedback control [16-18]. A system-based workflow for pharmaceuticals was developed by Brown et al.[194] where case studies were presented to demonstrate how to define the methodology, make key decisions and observe outputs at each stage, thus to avoid risks from decisions made on any aspect of the process. This workflow was successfully applied to a seeded continuous cooling crystallization and met the specific targeted crystal size.

2.4 Summary

Very little work on reactive crystallization of paracetamol can be seen in the literature review, this is the gap and also the focus of this PhD work. Since reaction conditions affect solution properties and concentrations that have further impact on the following crystallization, it is therefore essential to understand the reaction mechanism and kinetics, as well as parameters influencing reaction kinetics; investigate how reaction conditions affect nucleation and growth kinetics in the subsequent crystallization process.

Chapter 3 – **Experimental setup and methods**

This chapter presents the screening work for the targeted compound of investigation, and properties of reagents involved in this research. Solubility measurement procedures are outlined, and analytical methods for determinations of reaction and crystallization kinetics are also described in this chapter. Crystallisers and the associated operating procedures used in each aspect of this PhD programs are given separately in later chapters.

3.1 Chemical screening

A comprehensive list of potential recipes (Table A.1 and Table A.2 in the Appendix) has been established in order to identify the most suitable pharmaceutical compounds generated via reactive crystallization methodology, balancing different factors including suitability, safety, usage, cost and operating difficulties. Among the list, aspirin, paracetamol, benzoic acid and L-glutamic acid are the potential small molecule compounds, while clorprenaline succinate, phenytoin-Zn, sulfadiazine-Zn and piperazine ferulate are examples of larger molecules. Over 90% of the active pharmaceutical ingredients (API) in pharmaceutical industry are crystals of small organic molecules[195]; and more than 80% of all traded drugs have a molecular weight below 450 g mol^{-1}[196]. This is why small molecules are the focus of this work. In addition, larger molecular compounds are less likely to crystallize than smaller ones[197], as more complex reactions and long reaction times are often required in different synthesis steps. As a result, the target is on small molecule compounds. Paracetamol was finally selected as the final candidate compound due to its:

- significant application in pharmaceutical industry;
- simple operation requirements for synthesis
- suitable solubility data for cooling crystallization
- dependence of polymorphic forms on operation conditions

Starting materials for paracetamol synthesis include 4-aminophenol, water and acetic anhydride, whereas paracetamol and acetic acid are reaction products. Basic information of physical properties of these chemicals are listed in Table 3.1.

Table 3.1 Characteristics and physical properties of reagents used throughout experiments

Reagent	Molecular Weight	Molecular Formula	Structure Formula	Product Information	Purity Grade
4-Aminophenmol	109.13g mol^{-1}	C_6H_7NO	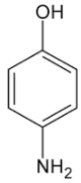	CAS No:123-30-8 Density: 1.13 g cm^{-3} Melting point:187.5 ºC Boiling point:284 ºC	≥ 99%
Acetic Anhydride	102.09 g mol^{-1}	$C_4H_6O_3$	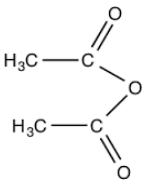	CAS No:108-24-7 Density:1.08 g cm^{-3} Melting point:-73.1 ºC Boiling point:139.7 ºC	≥ 99%
Acetic acid	60.05 g mol^{-1}	$C_2H_4O_2$	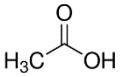	CAS No: 64-19-7 Density:1.05 g cm^{-3} Melting point:16.6 ºC Boiling point:118.1 ºC	-
Paracetamol	151.16 g mol^{-1}	$C_8H_9NO_2$	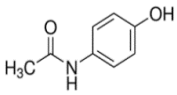	CAS No:103-90-2 Density:1.263 g cm^{-3} Melting point:169 ºC Boiling point:420 ºC	98.0-102.0%
Water	18.02 g mol^{-1}	H_2O	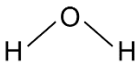	CAS No:7732-18-5 Density:1.0 g cm^{-3} Melting point:0 ºC Boiling point:100 ºC	Resistivity of 18.2 MΩ cm at 25°C

3.2 Solubility measurement

As introduced in section 2.1.1.4, paracetamol is produced with acetic acid as a side product, which is also the solvent for the following crystallization process. The solubility of paracetamol in various mixtures of acetic acid and water at different temperatures was thus studied. The following procedures were operated by referencing previous studies on paracetamol solubility measurements[3, 4].

About 10 mg of paracetamol was weighed in a 10 mL scintillation vial. The mixture solutions of water and acetic acid with different ratios (acetic acid: water = 0:10, 3:7, 5:5, 7:3, 8:2 and 10:0) were titrated carefully into the vial by a micropipette with intermittent shaking until all solids had been dissolved. The solubility values at five different temperatures of 20 ºC, 35 ºC, 50 ºC, 65 ºC, and 75 ºC were determined in a water bath, and each measurement was repeated three times. From that the solubility of paracetamol in various solvents was calculated by dividing the weight of paracetamol solid over the total weight of solvents added to the vial. The results for paracetamol solubility are listed in Table B.1 in Appendix and applied to all the following chapters.

3.3 Characterisation methods

In order to extract the kinetics for this reactive crystallization process, concentrations of at least one species, either a reactant or a product, must be followed and recorded during the process. There are a number of process analytical tools as listed in Table 3.2 that would allow such data to be generated. In the following sections, the validity of each tool was examined in details.

Table 3.2 Process analytical tools for the synthesis crystallization

Analytical tools		Function
FTIR	(online)	To measure the solute concentration profile as a function of time
UV-vis	(offline)	To monitor concentration profiles of a reactant as a function of time
HPLC	(offline)	To quantify concentration of a reactant remained in a sample
Microscope	(offline)	To check products purity To display crystal size and shape
XRD	(offline)	To evaluate crystal polymorph
Mastersizer	(offline)	To confirm crystal size distribution
PVM	(online)	To monitor crystal shape and size profiles along time
DSC	(offline)	To check purity of products

3.3.1 FTIR measurement

Fourier transform infrared analysis (FTIR) is commonly used to determine the concentration of solute in pharmaceutical fields [198, 199]. The working principle is that an infrared spectrum represents a fingerprint of a sample with absorption peaks corresponding to the frequencies of vibrations between the covalent bonds of the atoms making up the material. According to the peak interpretation list from Joseph et al.[200], there are three functional group peaks for the paracetamol product (See Table 3.3).

Table 3.3 Peak interpretation list for paracetamol

Range (cm^{-1})	**Group and Class**	**Assignment and Remarks**
1630-1680 (vs)	C=O in secondary amides	C=O stretch (Amide I band)
1475-1565 (vs)	NH in secondary amides	NH deformation (Amide II bond)
1485-1515 (m)	Benzene ring in aromatic compounds	Ring stretch, sharp band

Hojjati and Rohani[201] measured the concentration of paracetamol in isopropanol solutions using an in-situ FTIR device, the wavenumbers ranging 1200-1285 cm^{-1} and 1490-1725 cm^{-1} were associated with the absorption spectrum of paracetamol. Fujiwara et al.[202] found very challenging to obtain an accurate concentration measurement of paracetamol in water, because of the low solubility and the noise imbedded in the FTIR spectra. They chose peaks at wavenumbers of 1250, 1514 and 1575 cm^{-1} for their calibration model. Mitchell et al. and Ó'Ciardhá et al.[84, 143] studied the growth kinetics of paracetamol in ethanol solutions in cooling crystallization; indicated that the peak of 1517 cm^{-1} was sensitive to the changes of concentration and temperature (Figure 3.1).

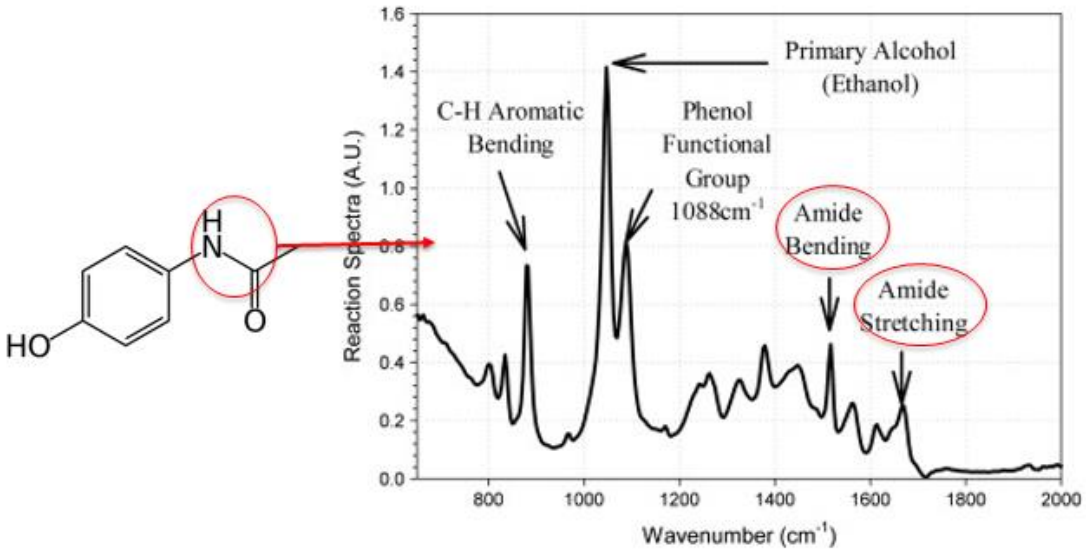

Figure 3.1 FTIR spectrum for paracetamol and ethanol solution system

In this project, both paracetamol and 4-aminophenol are measured in solid state by an offline FTIR; and their spectrums are compared in Figure 3.2. There are two peaks in paracetamol at 1670 and 1540 cm^{-1} as circled in Figure 3.2 denoting the C=O bond stretching and NH deformation, which are different from those of 4-aminophenol. When both paracetamol and 4-aminophenol in the solution of dimethyl sulfoxide (DMSO), peaks for paracetamol at the wavenumbers of 1670 and 1540 cm^{-1} (as circled in Figure 3.3) are distinct from the spectra of 4-aminophenol, while both compounds have a sharp peak at 1514 cm^{-1}, indicating the benzene ring stretch.

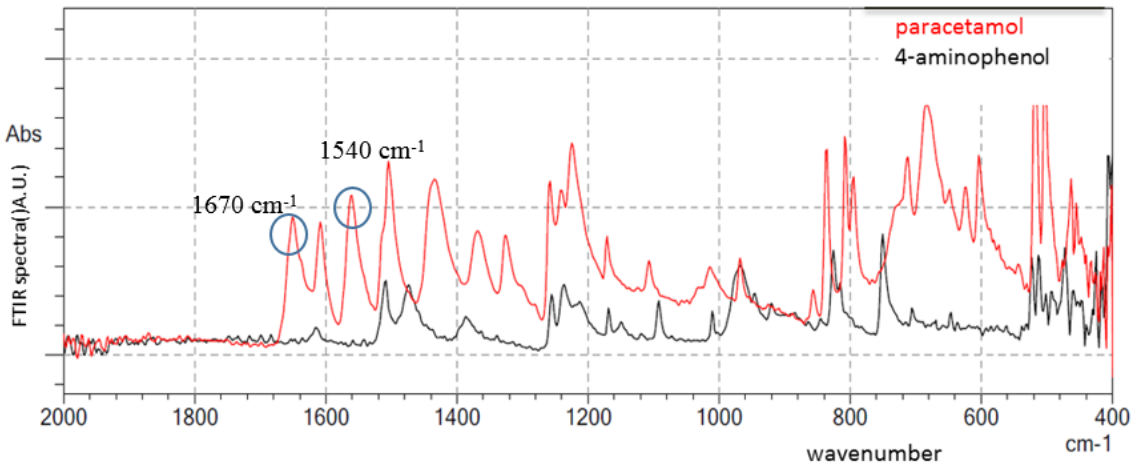

Figure 3.2 FTIR spectrums for paracetamol and 4-aminophenol in solid state

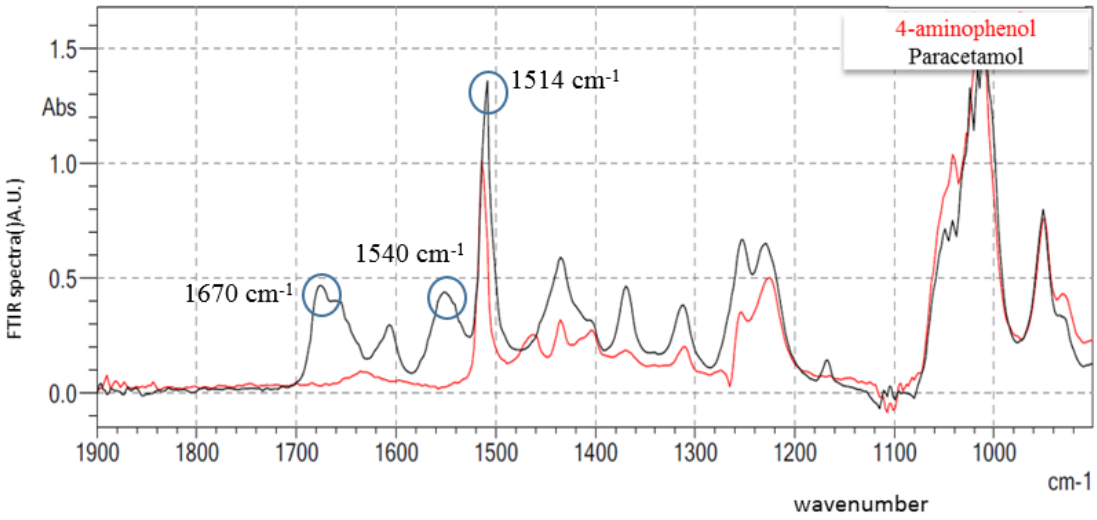

Figure 3.3 FTIR spectrums for paracetamol and 4-aminophenol in DMSO solvent

Peak at 1540 cm^{-1} is chosen to identify paracetamol products, as Peak at 1670 cm^{-1} is not suitable because it will be mixed up with peaks of water and acetic acid, as shown in Figure 3.4, which were confirmed by similar results in other solvent systems. As seen from Figure 3.4, the chosen peak is very small which leads to difficulties in measurement. Solvents such as ethanol, acetone, IPA and water were used in order to increase the peak height due to the increase of the solubility.

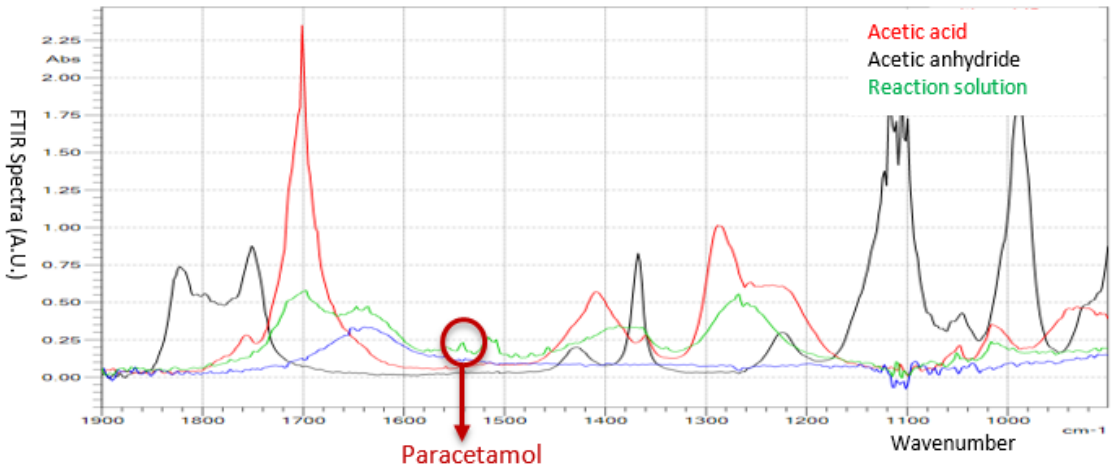

Figure 3.4 FTIR spectrum for acetic acid and acetic anhydride compared with that of reaction solution

When both 4-aminophenol and paracetamol are in either acetic acid or aqueous acetic acid solution that is the solvent used in this work, it is again difficult to identify the paracetamol peak from the mixture of reaction solutions, as shown in Figure 3.5. The only peak of NH bond at 1540 cm^{-1} is identifiable but is too small to be measured accurately. Consequently, the FTIR is not suitable for monitoring concentrations of paracetamol during the synthesis when acetic acid is involved.

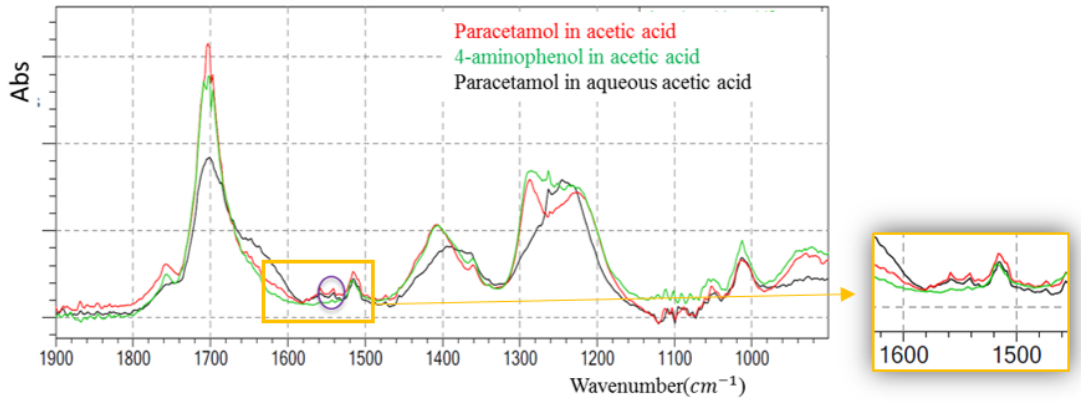

Figure 3.5 FTIR spectrums for paracetamol and 4-aminophenol dissolved in reaction solutions

3.3.2 UV-vis spectroscopy

Ultraviolet-visible (UV-vis) spectroscopy was employed to identify the product (paracetamol) and for quantitative analysis. The work principle for UV-vis is based on the interaction of light with materials. A distinct spectrum will be produced when a chemical compound absorbs ultraviolet radiations. For paracetamol the UV spectrum peaks at the wavelength of 243 nm, increases with increasing paracetamol concentrations, as shown in Figure 3.6. However, one of the limitations for the UV equipment is that the samples (0.300 ml) taken from reaction need to be diluted 100,000 times which leads to a lot of human errors. To investigate the viability of the UV tool, a series of paracetamol solution samples were prepared with known concentrations. A linear relationship between the height of paracetamol absorption peak and its concentration is obtained.

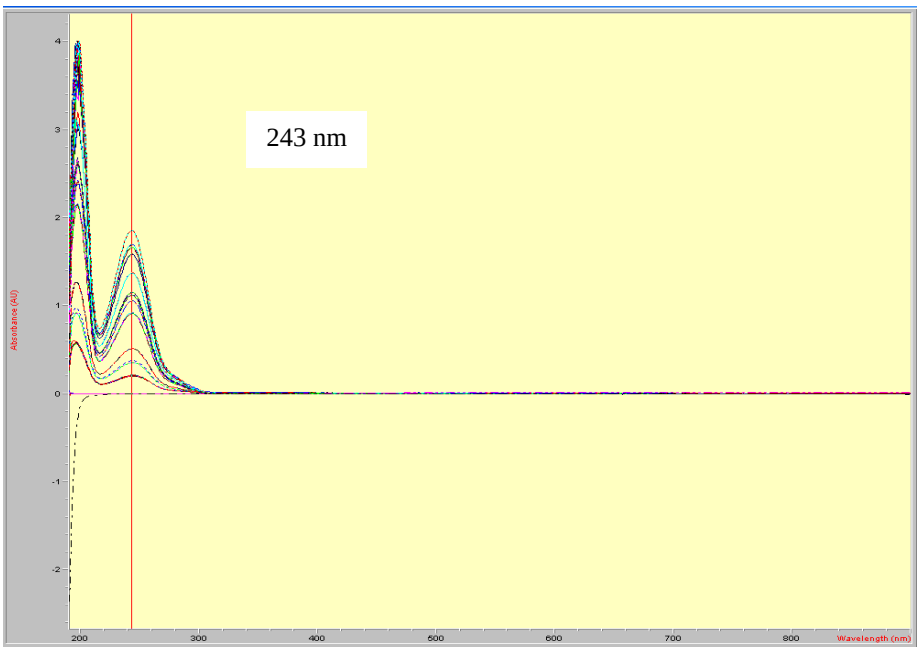

Figure 3.6 UV measurement for reaction samples

The concentration of paracetamol was then analysed by a UV-vis spectrophotometer (Hewlett-Packard Model 8453, wavelength range: 190 - 1100 nm) based on the characteristic UV absorbance peak at 243 nm. The calibration experiments were carried out from six known concentrations of 0, 0.3, 0.5, 0.7, 1.0, 1.3 g L^{-1}. Figure 3.7 shows the linear relationship of the absorbance value, A, as a function of the concentration, C, as: A = - 0.0015 + 0.686 C (g L^{-1}), with a correlation coefficient of 0.9984. Based on this, the purity of the paracetamol products was calculated and then compared with that from the purchased paracetamol.

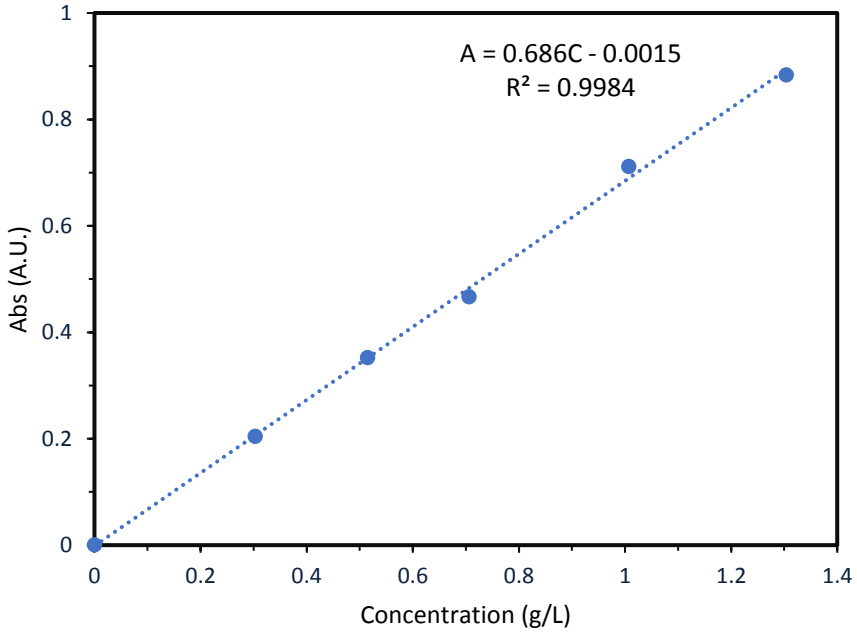

Figure 3.7 Calibration curve of paracetamol in methanol solution

3.3.3 HPLC measurement

High performance liquid chromatography (HPLC) is a technique in analytical chemistry to separate, identify and quantify the components in a mixture. The work principle is that a pressurized liquid solvent containing the sample mixture is pumped through a column filled with specific solid adsorbent materials. Different components will have different absorption rates resulting in the separation of components as they flow out the column. HPLC is mostly used in research such as separating the components of similar synthetic chemicals from each other or detecting a specific compound or impurities in medical drugs[203], so it is appropriate to consider the validity of this tool for this PhD work.

The HPLC in use is the Agilent1100 Series HPLC System and the chromatograph column was a reverse phase ZORBAX SB-C8 (4.6×150mm; 5µm packing). The UV detector was set at 243 nm and the mobile phase running throughout the system was a mixture of methanol and water with a ratio of 1:3.

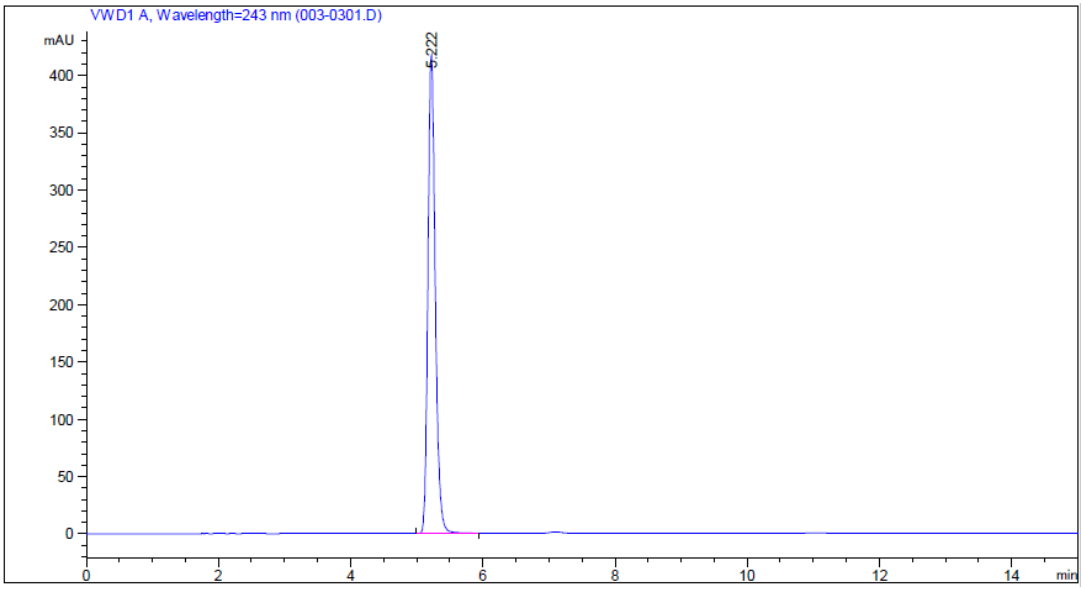

Figure 3.8 Paracetamol standard solution of paracetamol measured by HPLC

Figure 3.8 shows that the peak of paracetamol appears after 5 minutes at a flowrate of 0.8 ml min^{-1}, the peak is clean and sharp, indicating that the compounds in the mixture were well separated in the column and the viability of this tool is high. Subsequently a calibration curve was developed by injecting different but known concentrations of paracetamol solution into the column and was shown in Figure 3.9. A good linear relationship between the peak areas and concentration of paracetamol, i.e. Concentration = (Peak Area – 3.8927) ÷24833, confirms the validity and viability of this tool.

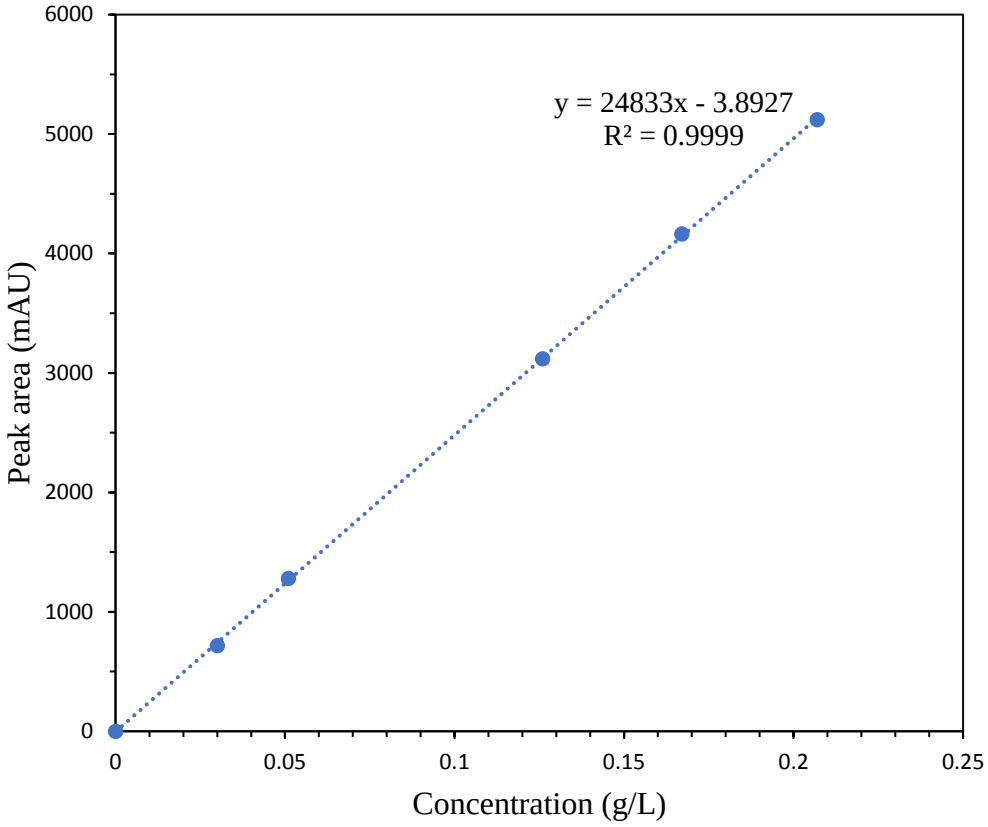

Figure 3.9 HPLC calibration curve for paracetamol

Calibration curves in Figures 3.7 and 3.9 indicate that both UV and HPLC are the adequate methods to quantify paracetamol concentrations for offline samples. However, compared with UV, HPLC can separate different components and identify impurities in mixed solutions. In this project, UV measurement was used for reaction kinetics analysis in chapter 4, whereas HPLC were applied for the determination of solute concentrations from OBR and COBR in chapter 5 & 6, as well as for analysis of products purity.

3.3.4 Mastersizer measurement

Mastersizer 3000 was used to analyze particles size distributions. The work principle is based on laser diffraction. When the beam of laser light is scattered by a group of particles, the angle of scattering light is related to particle size, i.e. the larger the particle size, the smaller the angle of light scattering. The angular scattering intensity is then analyzed to calculate the size of particles which are reported as a volume equivalent sphere diameter, as shown in Figure 3.10.

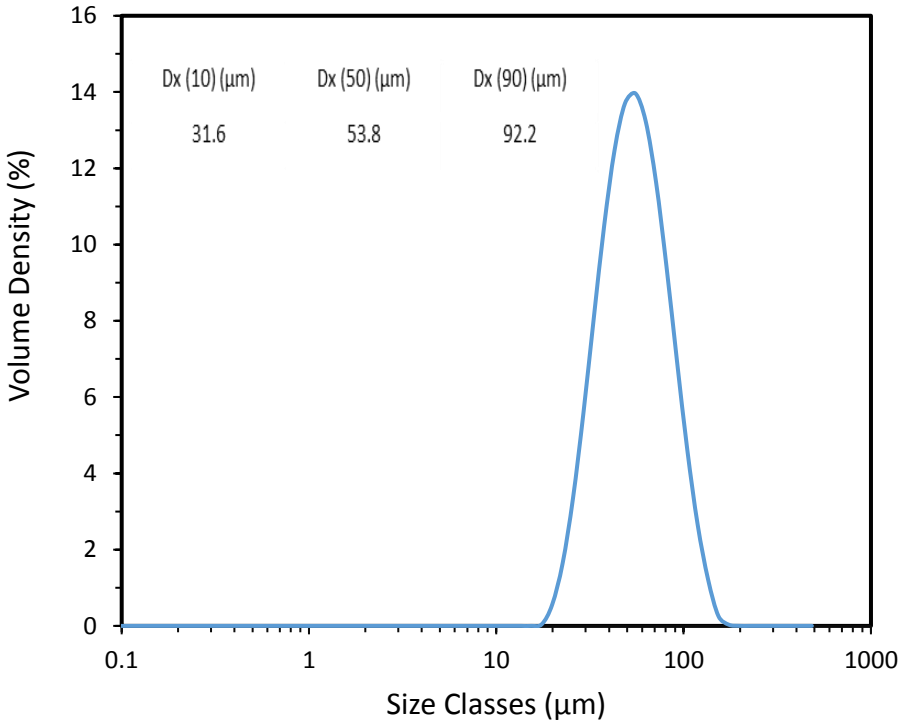

Figure 3.10 Crystal size distribution

3.3.5 Polymorphism analysis (X-ray powder diffraction measurement)

Paracetamol has three polymorphic forms: form I (monoclinic) is the commercially marketed product and used as high-dose tablets (300-500 mg), exhibiting poor compression ability[114], hence requiring binding agents in tableting process, which adds cost to its production. In the contrast, form II (orthorhombic) has much better compressibility than form I because of the sliding planes. Form III is very unstable and its crystal structure remains unknown, although Arthur[204] proposed a possible structure from powder diffraction measurement and theoretical predictions. Burley et al.[205] also claimed that the polymorphic form III of paracetamol was isolated using a specially designed methodology which is reproducible and reliable.

Form I is the thermodynamically stable form while form II is metastable under ambient conditions[206, 207]. There is enormous interest in the polymorphs of paracetamol in the literature, Boldyreva et al.[208] gave a good summary about the studies of the thermal properties of the polymorphs of paracetamol using DSC, X-ray diffraction, hot-stage microscopy and Roman spectropy, although the interpretations of

these observations were not always in a good agreement with each other. Méndez et al.[209] obtained paracetamol crystals from a methanol solution using a laminar-flow tubular crystallizer apparatus with different flowrates. The photomicrograph of samples taken at different times after nucleation showed clearly the presence of both form I and II. Mori et al.[210] described a new method for selective crystallization of the metastable form of paracetamol by applying ultrasonic irradiation at different frequencies in a supersaturated solution. In their research, plate-like (form I) crystals were crystallized by stirring while needle-like crystals (form II) crystallized by ultrasonic irradiation at a frequency of 28 kHz. In addition, paracetamol Form II crystals were generated reproducibly by Lee et al.[4] through cooling crystallization that was followed immediately after acetylation of 4-aminophenol coupled with neutralization of acetic acid.

X-ray powder diffraction is a rapid analytical technique to identify a crystalline and can provide information on unit cell dimensions. Figure 3.11 is the experimental powder X-ray diffraction for monoclinic paracetamol (form I) and orthorhombic paracetamol (form II) from Nichols and Frampton's work[211]. The XRD of paracetamol form II crystals from Lee's research[4] shows a high degree of agreement with the theoretical XRD pattern. XRPD pattern of plate-like crystals from Mori et al.[210] well matched with that of the Form I, likewise the XRPD pattern of needle-like crystals well with the form II; the plate shaped paracetamol crystals obtained in the research of Méndez et al.[209] were of form I and the needle shaped crystals of form II. The opposite outcomes from different researchers are probably influenced by operational conditions during both nucleation and growth processes [4, 51, 52].

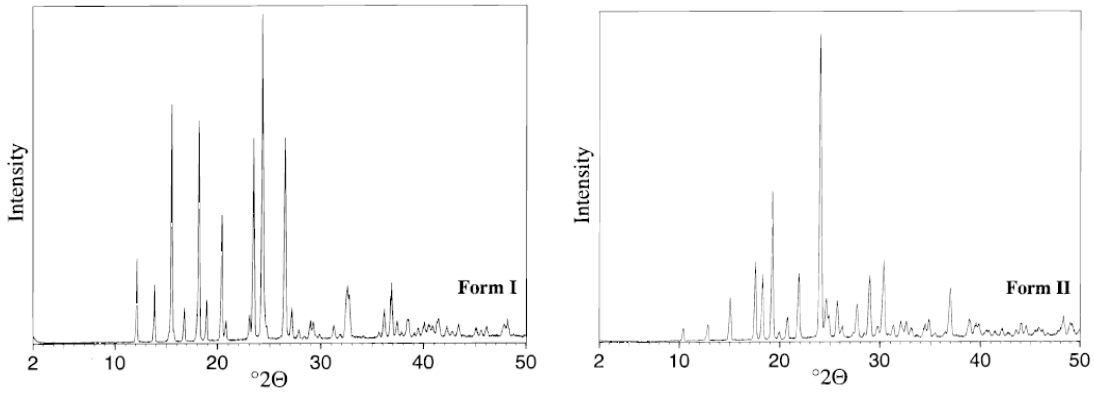

Figure 3.11 Experimental powder X-ray diffraction for monoclinic paracetamol (left) and orthorhombic paracetamol (right)[211]

3.3.6 Differential scanning calorimetry (DSC)

Thermal analysis is normally used to evaluate changes in thermodynamic properties that occur when the material is subjected to heat energy. Changes can be observed in the process of melting, dissolving, recrystallization and solid phase transformations indicated by endothermic or exothermic peaks. In this PhD work, a fine crystal product of a white colour was isolated after filtration, indicating good purity. The thermal analysis was carried out for the purchased paracetamol sample as well as for the crystals produced from the experiments.

The procedures are as follows: about 5 mg of a sample was weighted in a 10 µL aluminium pan and sealed before mounting it onto the analyser, an empty airtight sealed aluminium pan was used as reference. Each sample was subjected to a heat-cool-heat cycle, i.e. from 30 ºC to 230 ºC at a rate to 10 ºC min^{-1} with a holding time of 10 mins to ensure complete melting; then cooling from 230 ºC back to 30 ºC at the same rate with 20 mins holding time to make sure complete crystallization; the cycle was completed after a 2^{nd} thermal ramp up to 230 ºC.

Compared with the paracetamol from market with a purity of 98.0-101.0%, the experimental product has a very close melting point to the purchased one in the heating process. There is no extra peak in the DSC data, indicating that the purity of paracetamol produced in this work is as high as that of the purchased product.

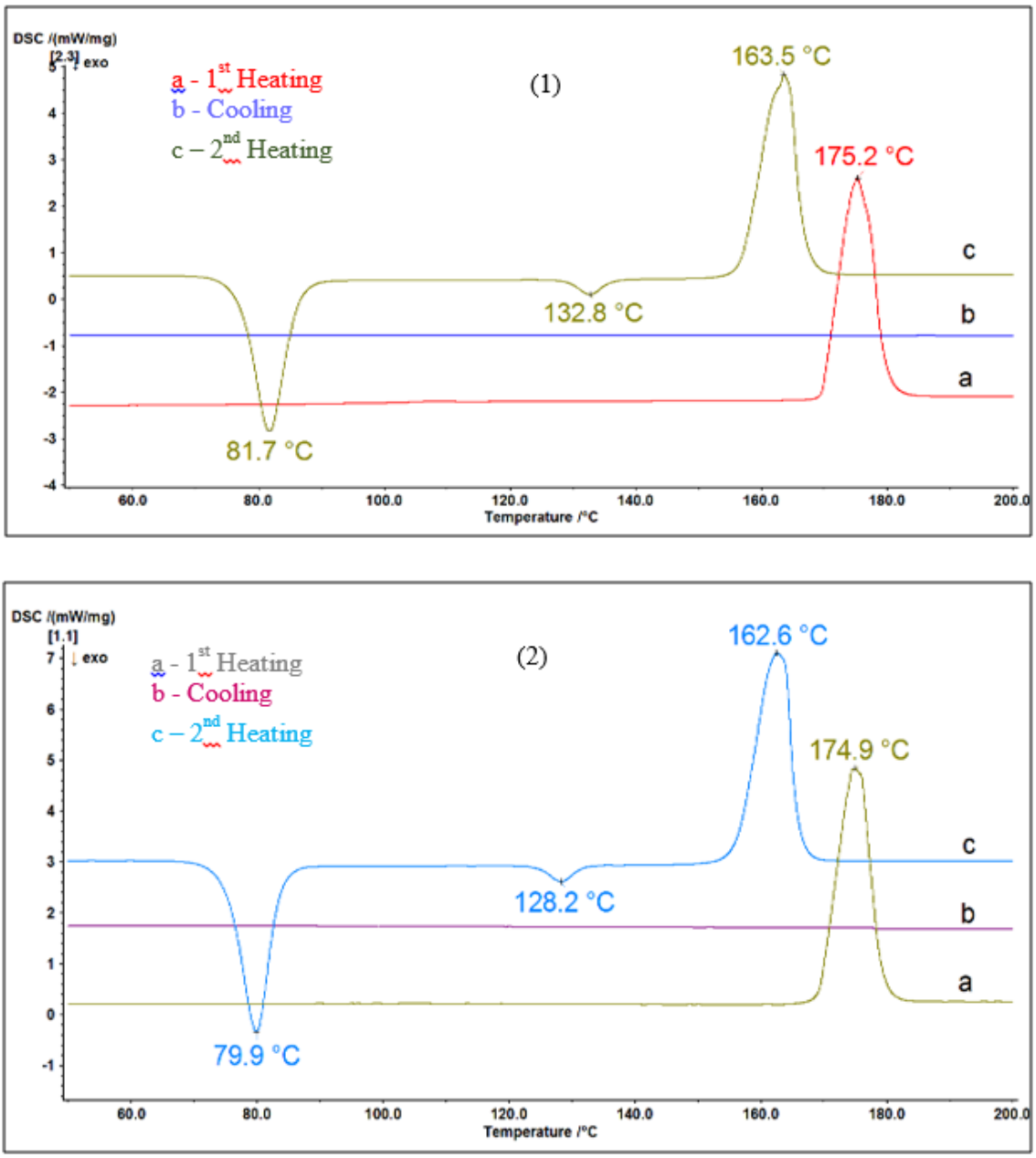

Figure 3.12 The DSC data of paracetamol, (1) Acetaminophen (Paracetamol) from Sigma Company, meets USP testing specifications, 98.0-101.0%; (2) Paracetamol from the reaction crystallization experiment

As shown in Figure 3.12 (1), during the first heating step, the purchased solid sample gave out a single sharp endothermic melting peak at 175.2 ºC, which showed a good agreement with the reported results of 172.3-176.3 ºC[212]. During the second heating, two exothermic peaks were seen at 81.7 and 132.8 ºC respectively, followed by the melting peak at 163.5 ºC. The first exothermic peak observed at 81.7 ºC suggests that the melt mass did not yet recrystallize into solid during the cooling process in the DSC

pan, instead remained glassy which was later recrystallized at 81.7 ºC in the following heating process[213]. The second exothermic peak at 132.8 ºC was believed to be a transition from form III to form II and this was agreed with literature data of 133 ºC[214]. The observed melting peak for form II was at 163.5 ºC, agreeing with the results of 160.1-164.3 ºC from Myrick et al.[212].

The very similar thermograms were obtained and shown in Figure 3.12 (2) for our experimental product, suggesting that the crystals produced by the reactive crystallization had the same polymorph, i.e. monoclinic (form I), as the bought paracetamol and subsequently transferred into Form II during the heating-cooling cycle.

All the melting points of 4 samples from the reactive crystallization at different reaction temperatures (section 4.3) displayed a perfect narrow range of melting points from 169.3 to 169.7 ºC (see Figure 3.13). This meets the requirement of a melting point ranging between 168 ºC and 172 ºC for pure paracetamol in literature[1, 21]. However, DSC data could not provide any quantitative analysis for the exact purity of each sample, HPLC is therefore employed to fulfil the task.

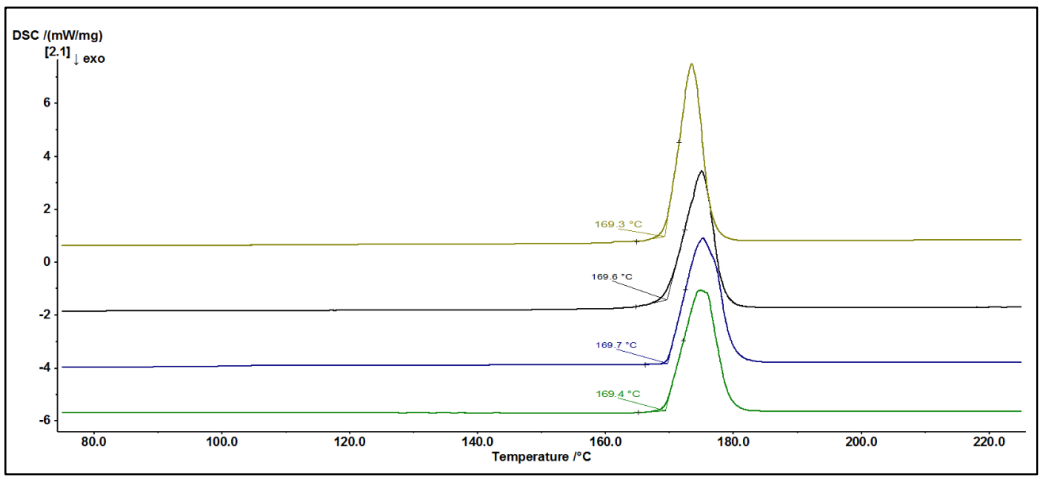

Figure 3.13 melting point of paracetamol products from the reactive crystallization

3.3.7 Particle video microscope (PVM)

In-situ crystal images, size distributions and counts were obtained by two PVM probes (Perdix Ltd) that are installed in the continuous oscillatory baffled crystalliser (see Figure 6.1 & 6.2). Although in-situ particle images from two positions along COBR can clearly be recorded (see Figure E.3 & E.4), the particles size information was not always accurate due to the blockages resulted from crystals adhere on the walls of camera as shown in Figure 3.14. Therefore, in Chapter 6, offline microscope and mastersizer were also employed, instead of PVM for crystal shape and size analysis.

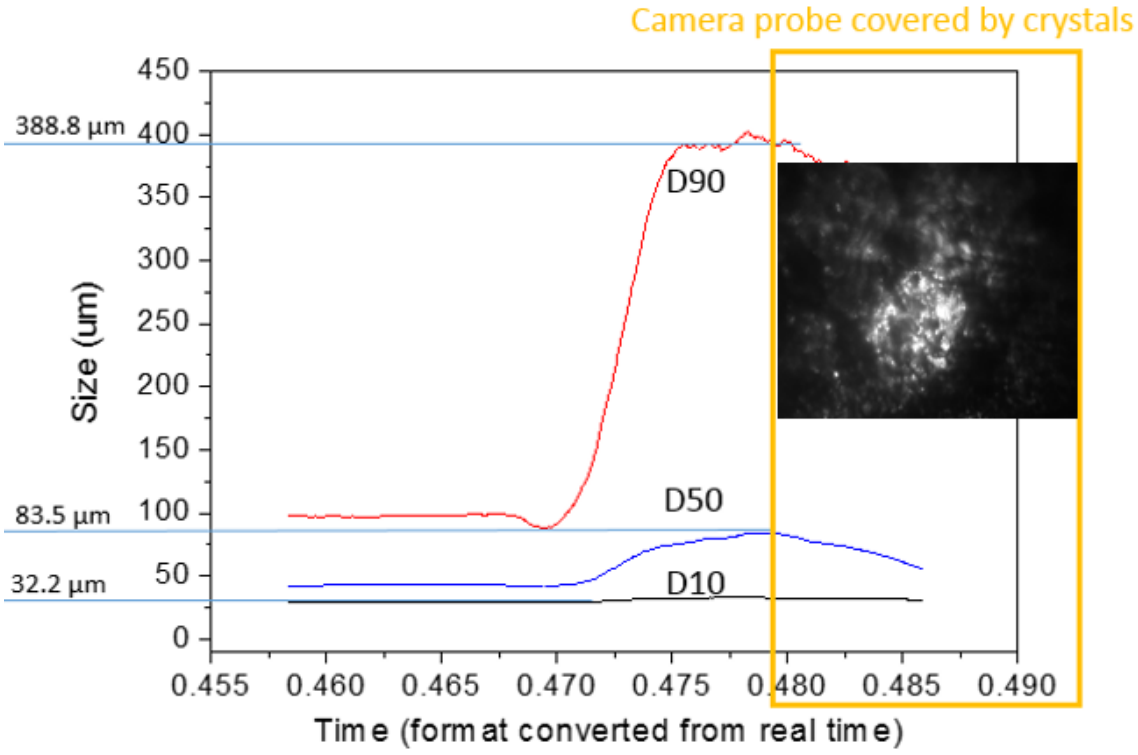

Figure 3.14 Particle size distribution results obtained from PVM with an image taken when camera probe was covered by crystals

Chapter 4– **Effects of water content and temperature on reaction kinetics**

This chapter presents the first set of experimental results on the investigation of the effects of water and temperature on reaction kinetics. The entire chapter was published in the journal of Chemical Engineering and Processing: Process Intensification, 2018, (131): 20-26.

4.1 Introduction

Paracetamol (Acetaminophen) is a widely used analgesic drug[215], traditionally manufactured by acetylating 4-aminophenol with a small stoichiometric excess of acetic anhydride in an aqueous medium [3, 4, 216]. Many variations in reaction synthesis route have since been implemented to enhance productivity and product properties, for instance, Baron et al.[2] dissolved 4-aminophenol in hot acetic acid, treated it with carbon, filtered it out, the filtrate was further treated with acetic anhydride at 85 °C; Young[1] added ammonium hydroxide to increase product purity; Ness and Warner[30] hydrogenated p-nitrophenol to p-aminophenol and concurrently acetylated the p-aminophenol to paracetamol; Caldeira[217] used phosphoric acid as the catalyst. Either a precipitation or crystallization step was then used to isolate paracetamol particles under limited control, affecting crystal properties [49-51, 195, 218, 219], i.e. two separate unit operations are the norm for reactive crystallization.

In this chapter, the reactive crystallization was treated as a single process for the purpose of continuous operation, solubility for crystallization was optimized as the first protocol, the concentrations of reactants that deliver the optimized solubility were retrospectively determined. By maintaining the targeted ratio of acetic acid to water in the reaction that optimizes the solubility, the effects of water and temperature on reaction kinetics, mechanism and crystal properties were jointly investigated; these are new from previous studies in this area. It is demonstrated that by manipulating reaction conditions, the control over crystal properties can be realized.

4.2 Chemicals and analytical methods

4-Aminophenol (Sigma Aldrich UK Ltd.; purity, ≥ 99 % HPLC grade; mp, 187.5 ºC; MW, 109.13 g mol^{-1}) was sourced in the form of light brown crystalline solid. Paracetamol (GlaxoSmithKline Pharmaceutical Company; purity, 99.8 %; mp, 169 ºC; MW, 151.16 g mol^{-1}) was purchased for the purpose of comparison with crystals produced. 4'-Acetoxyacetanilide (TCI AMERICA; purity, ≥99.0 % HPLC, Nitrogen; mp, 155 ºC; MW, 193.20 g mol^{-1}) was purchased for the identification and calibration of the intermediate product. Acetic anhydride (purity, 99+ % pure; density, 1.08 g cm^{-3}; MW, 102.09 g mol^{-1}) and methanol (purity, HPLC grade; density, 792 kg m^{-3}; MW, 32.04 g mol^{-1}) were also sourced. Distilled water (density, 1 g cm^{-3}; MW, 18.02 g mol^{-1}) was prepared in-house.

The purity of product particles was analyzed using the Agilent1100 Series HPLC System, and the chromatograph column was a reverse phase ZORBAX SB-C8 (4.6×150 mm; 5 µm packing), as mentioned previously in Chapter 3.3.3. The UV detector was set at 243 nm and the mobile phase running throughout the system was a mixture of methanol and water with a mass ratio of 1:3. The mass spectrometry measurement was carried out at the School of Chemistry, the University of Edinburgh. The concentration of paracetamol was analyzed by a UV-Vis spectrophotometer (Hewlett-Packard Model 8453) based on the characteristic UV absorbance peak at 243 nm, as described in Chapter 3.3.2.

The crystal size distributions were analyzed by a Mastersizer 3000™ (HYDRO, Malvern); the polymorphism of crystals by XRPD (Chemistry Department, Heriot-Watt University with the scanning range from 5 º to 85 º) and a Leica ATC 2000 Trinocular Microscope; the molecule structures of the products by the AV300 Proton Nuclear Magnetic Resonance spectroscopy (^{1}H NMR).

4.3 Experiments procedures

In the synthesis, paracetamol is produced with acetic acid as a side product, which is also the solvent for the following crystallization process. In order to maximize the solubility of paracetamol, a range of solubility were examined by mixing acetic acid with various

water contents at different temperatures. As mentioned in Chapter 3.2. 10 mg of paracetamol was firstly weighed in a 10 mL scintillation vial; the solutions of water and acetic acid with six different ratios (Acetic acid:Water = 0:10, 3:7, 5:5, 7:3, 8:2 and 10:0) were then carefully titrated into the vial by a micropipette with intermittent shaking until all solids had been dissolved. The solubility data at temperatures of 20, 35, 50, 65, and 75 °C were determined in a water bath, and each measurement was repeated three times. The solubilities of paracetamol in various solvents were calculated by dividing the weight of paracetamol solid over the total weight of solvents added to the vial, from which the amounts of reactants required to deliver such solubility in the said ratio of acetic acid to water were then back-calculated.

Once the ratio and the amounts of reactants have been determined, the reaction was then proceeded by charging 4-aminophenol (10 g or 0.09 mol), acetic anhydride (35 g or 0.34 mol) and different amounts of water into a pre-heated 250 ml jacked reactor at 50 °C and at 200 rpm.

Figure 4.1 shows the experimental set-up. A turbidity probe was fastened onto a thermocouple by means of a zipper, in this way, the probes remained stationary inside the beaker during the experimental cycles of cooling and heating. Both temperature and turbidity data were collected via a data acquisition system, i.e. NI Compact DAQ USB chassis (National Instruments Corp., NI cDAQ-9174), diagram details were given in the Appendix.

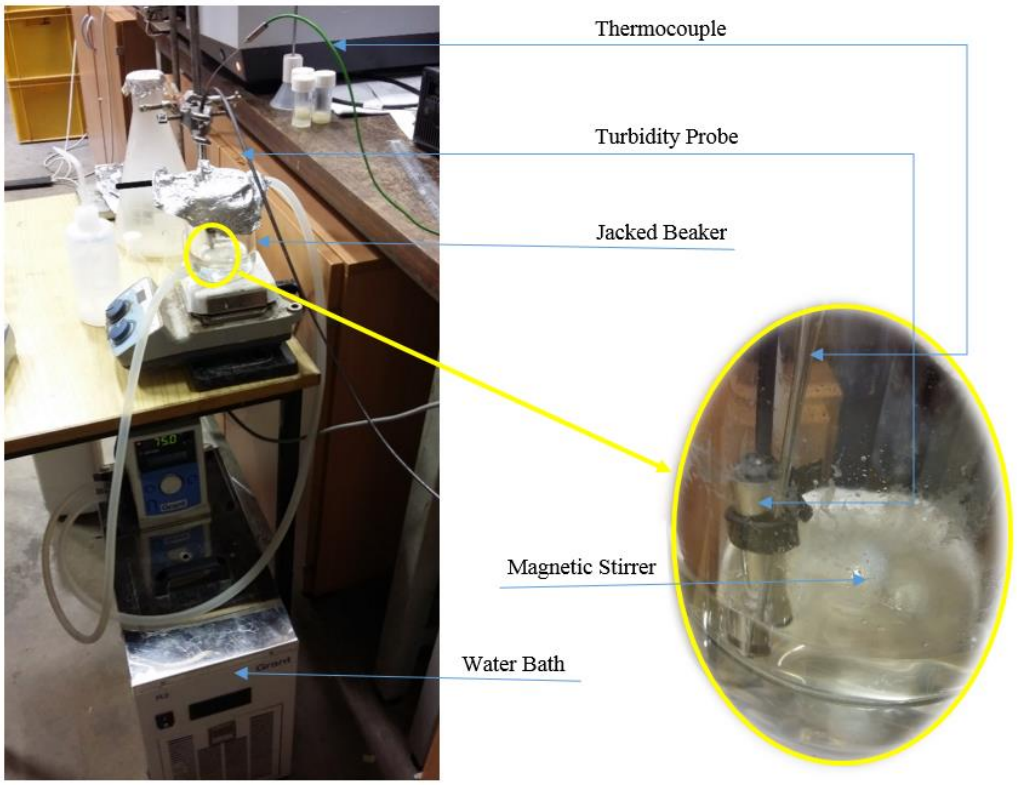

Figure 4.1 Set-up of a reactive crystallization of paracetamol for reaction kinetic study

The reactor was heated up to the constant desired temperature for the reaction to commence. 13 samples were taken at regular time intervals during the reaction process using a pipette with an accurate volume of 0.300 ml; quenched and diluted 10,000 times with the mobile phase solution (methanol: water = 1:3). The overall reaction time was about 60 min. The crystallization was thereafter immediately initiated by cooling the solution to 20 °C at a fixed cooling rate of 1.2 °C min^{-1}. A vacuum filtration was performed at the end of the crystallization at 20 ^{o}C and crystals were washed with distilled water and dried in an oven for 24 hours.

Some specific conditions are outlined below:

A) Water content effects – water contents of 0 g, 10 g (or 0.55 mol), and 20 g (or 1.11 mol) were used in reaction at a fixed operating condition of 70 °C and 200 rpm;

B) Temperature effects – this was investigated by performing the synthesis at four reaction temperatures (50 °C, 60 °C, 70 °C and 80 °C) at a fixed water content of 20 g (1.11 mol).

4.4 Optimization of solubility and determination of reactants contents

The reaction scheme for the reactive crystallization was shown in Figure 2.4 where acetic acid is the main solvent for paracetamol, the solubilities of paracetamol in the mixtures of acetic acid and water were measured (Appendix B)and shown in Figure 4.2. It is as expected that the solubility of paracetamol increases with temperature. Meanwhile, as the ratio of acetic acid to water increases, the capacity of paracetamol dissolution in the mixed solvent increases and reaches to a maximum value at Acid:H_2O = 7:3, and then declines with increasing acid contents.

In terms of the solubility of paracetamol in water, these range from about 0.009 to 0.049 g g^{-1} water for temperatures from 20 °C to 75 °C in this work and are comparable with literature data, e.g. from 0.010 to 0.035 g g^{-1} water for temperatures from 20 °C to 55 °C[124, 202]; 0.021 g ml^{-1} water at 30 °C[220]; of 0.017 g g^{-1} water[87]. Granberg and Rasmuson[87] also reported the solubility of paracetamol in acetic acid as 0.083 g g^{-1} at 30 °C, which is slightly higher than our data of 0.053 g g^{-1} acetic acid. Operational errors from the gravimetric method might be the main reason for the difference. For instance, in the research of Granberg and Rasmuson, the solubility of paracetamol was obtained by evaporating solvent of a saturated solution, errors might have resulted from the residual solvent tracked in the dried powders, leading to higher values. On the other hand, paracetamol solubility in this work was measured by adding drops of solvent to dissolve solute of a given mass, errors might have been caused by over-adding of solvent, leading to smaller values. All the measured solubility data and standard errors are shown in Appendix B.

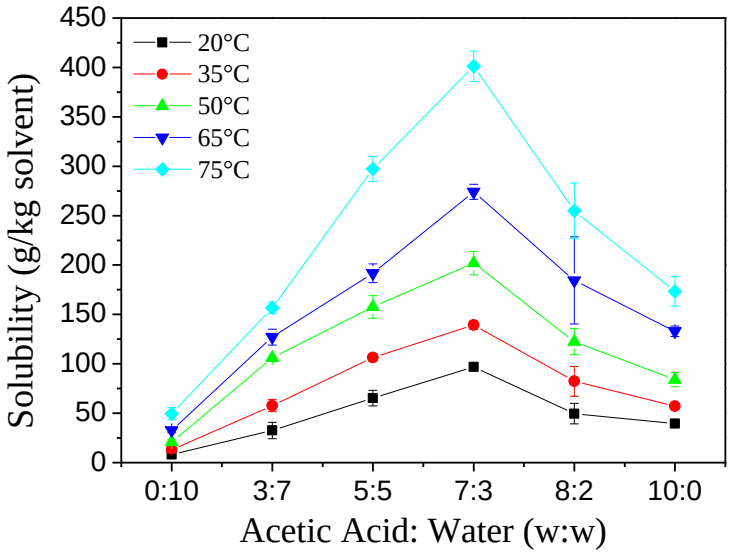

Figure 4.2. Solubility of paracetamol in different ratios of acetic acid to water

As shown in Figure 4.2, the highest solubility occurred when the mass ratio of acetic acid to water was at 7:3; the solubility increased from 96.83 to 401.23 g $kg^{-1}_{solvent}$ with the increasing reaction temperature from 20 °C to 75 °C, the latter was the reaction temperature. From the maximized solubility, the amounts of reactants were retrospectively calculated based on the reaction stoichiometry. In order to make up the desired ratio of 7:3 acetic acid to water, about 14.48 g (0.13 mol) 4-aminophenol should theoretically be reacting with an amount of acetic anhydride (36.55 g or 0.36 mol) in the 250 ml reactor at 75 °C, the extra acetic anhydride is then converted to acetic acid via a hydrolysis with water. In practice, however, the mass of crystals generated at the end of crystallization was so large that the mixing condition was adversely affected. On balance, the contents of 4-aminophenol and acetic anhydride were accordingly reduced by 30 % to 10 g (0.09 mol) and 35 g (0.34 mol) respectively; the temperature to 70 °C, this gives the best controls over both good supersaturation and better mixing.

4.5 Results and discussions

4.5.1 Effect of water content on reaction mechanism

Water in the paracetamol synthesis generally helps the hydrolysis of acetic anhydride, promoting the formation of paracetamol, however, there have been very few studies on

the effects of water on reaction kinetics and crystal properties. In this work, the effects of water content on reaction kinetics and mechanism were fully examined; 0 g, 10 g (0.55 mol) and 20 g (1.11 mol) distilled water were added into the synthesis, Figure 4.3 shows the profiles of concentrations of paracetamol with and without water. It is clear that the rising curve becomes steeper with water and the degree of steepness increases with the increasing amount of water. From the general reaction mechanism (nucleophilic addition-elimination) of paracetamol synthesis[219], on one hand, the lone pair of electrons on the amine of 4-aminophenol attacks the C=O bond of acetic anhydride to cause it polarized. Nitrogen has then a positive charge but regains electrons by losing a proton. The negative charge on the oxygen comes back in to reform the C=O bond. This leads to the other C-O bond to break and forms acetic acid as a by-product, while paracetamol is the product from the amide bond formation process (see Figure C.5 in Appendix). When water is added, the hydrolysis reaction between acetic anhydride and water generates H^+, these free hydrogen ions increase the reactivity in the solution, thus improve the reaction performance, as shown in Figure 4.3 that the more the added water, the quicker the level off becomes.

On the other hand, however, the acetic anhydride in excess in this work also leads to a reduction of paracetamol, with 4'-acetoxyacetanilide being detected in the solution. This can be postulated from the fact that the amount of diacetamate formed in the presence of the excess of acetic anhydride is very small and unstable in solution; is quickly hydrolyzed until an equilibrium has been reached. The fluctuations of the concentration of paracetamol near 10 minutes during the reaction in Figure 4.3 are the clear evidence.

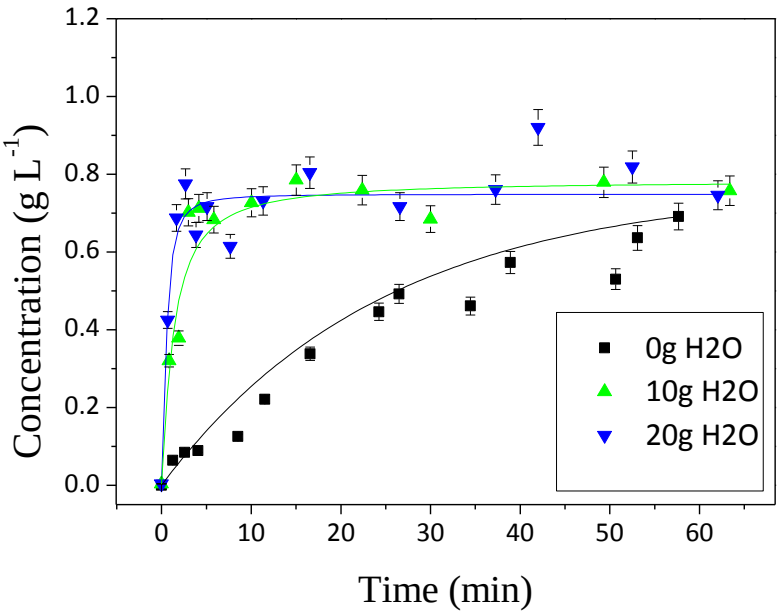

Figure 4.3. Concentration of paracetamol with different water contents (Temperature = 70 °C)

To understand better the reaction mechanism with the presence of water, the samples taken from the reacting solution were analyzed using the LC-MS, Figure 4.4 shows the chemical structures of paracetamol and diacetamate: the first peak at 3 min is the paracetamol molecular with a total density of 152.0647 g mol^{-1}, and the second peak at 4.7 min is a diacetamate of 194.0706 g mol^{-1}, the latter is also the molecular weight of 4'-acetoxyacetanilide. With this knowledge, the reaction scheme for paracetamol synthesis with and without water can now be illustrated in Figure 4.5. It can be seen that the synthesis of paracetamol (Reaction (1) in Figure 4.5) and the reaction between excess acetic anhydride and water (Reaction (2) in Figure 4.5) are the two main reactions. When water is absent in the system, diacetamate is formed as a side product (Side reaction in Figure 4.5). No reaction (2) occurs without water, excess acetic anhydride then over-reacts with primary product to form a byproduct. When water is added, the excess acetic anhydride is more likely to react with water, rather than to consume the –OH bonds of paracetamol molecules. As a result, acetic anhydride is consumed by reaction (2), which effectively keeps reaction (3) on the left hand side, thus less byproduct is formed. The acetic acid generated from reactions (1) and (2) together with water left in the system are the solvent for the follow-on cooling crystallization of paracetamol.

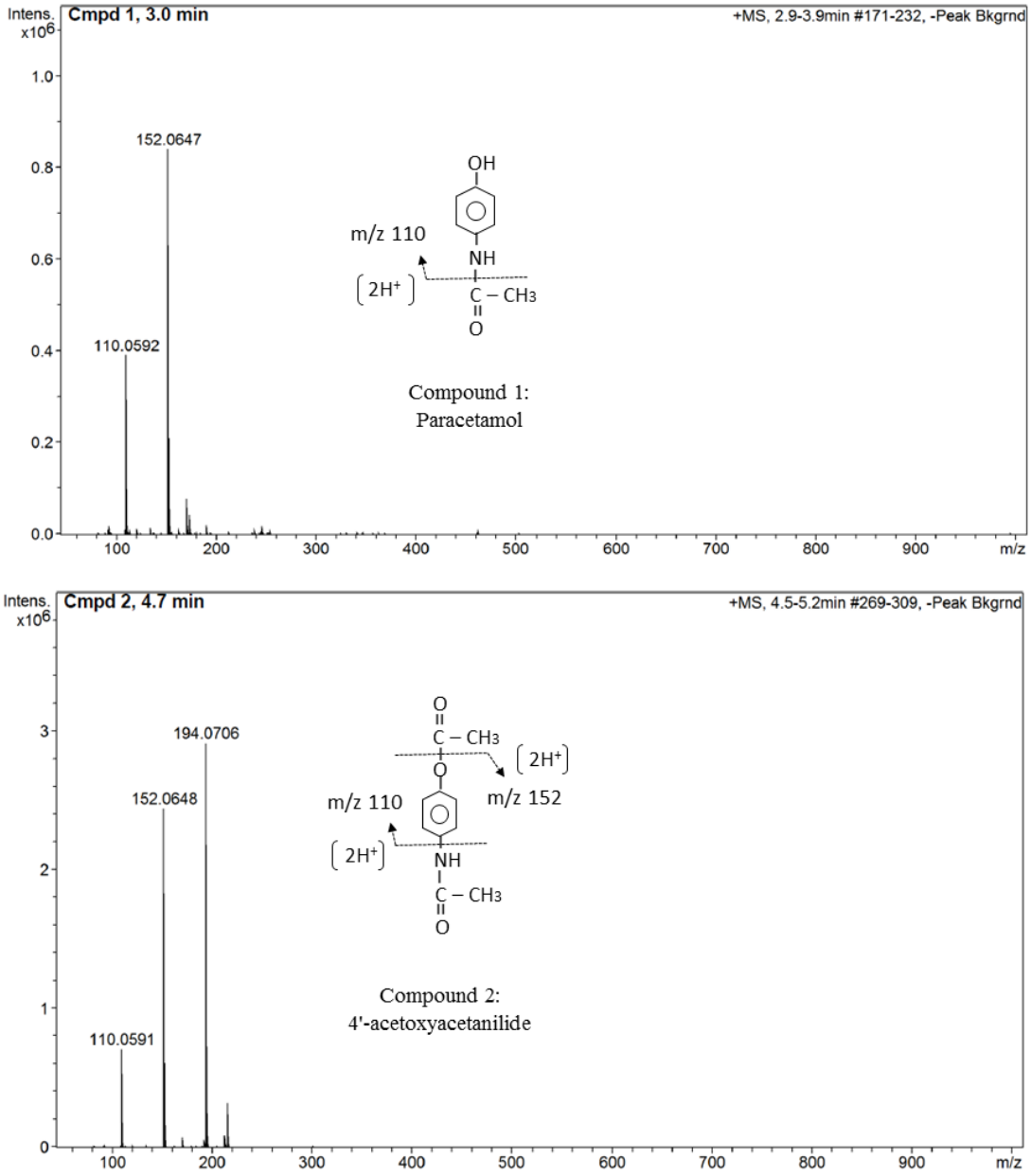

Figure 4.4 Sample analysis by LC-MS

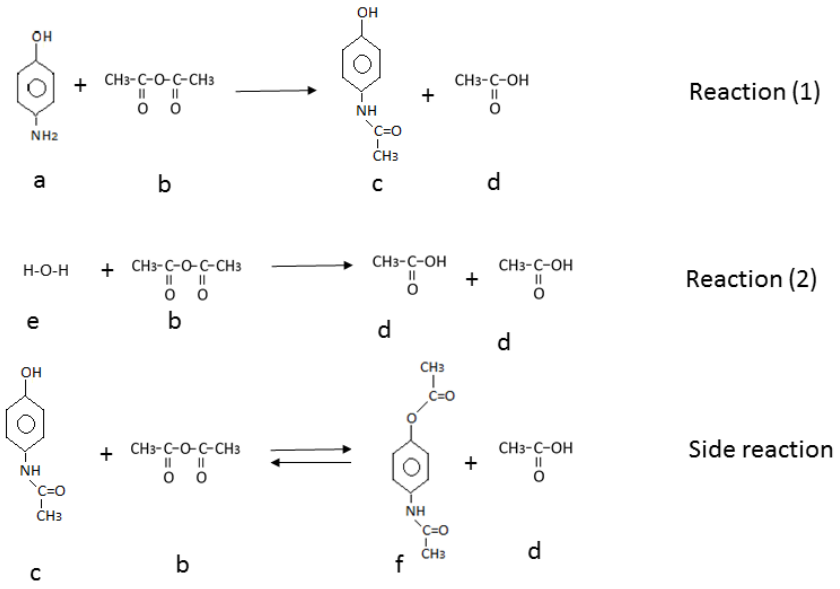

Figure 4.5 The reaction scheme for paracetamol synthesis with and without water (a, 4-aminophenol; b, acetic anhydride; c, paracetamol; d, acetic acid; e, water; f, 4'-acetoxyacetanilide)

4.5.2 Effect of temperature on reaction rate constant

From the reaction viewpoint, higher temperature leads to higher reaction rate. In the following experiments, reaction temperatures of 50 °C, 60 °C, 70 °C and 80 °C were studied at a fixed water content of 20 g (1.11 mol), Figure 4.6 shows the profiles of the concentrations of paracetamol as a function of time. It is seen that a common trend with an immediate increase in the concentration in the first five minutes of synthesis, then quick leveling off. As expected, higher concentrations of paracetamol were obtained for higher temperatures.

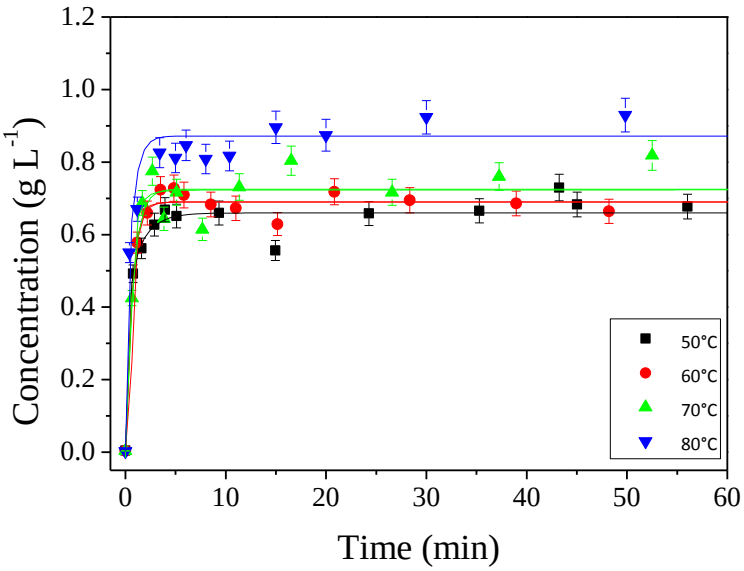

Figure 4.6 Concentration of paracetamol at different temperatures (water content = 20 g)

The data points in the first 5 minutes were then employed to extract the kinetics of the paracetamol synthesis. Because acetic anhydride was added in excess, a pseudo first-order reaction was found to be the main reaction kinetics. Although the reaction between acetic anhydride and water may also affect reactants, the overall kinetics is dominated by that of the slowest acylation step. Based on the limiting reagent of 4-aminophenol, it becomes:

$$r_R = -\frac{dC_A}{dt} = qC_A \qquad (4\text{-}1)$$

where r_R is the generation rate of paracetamol (g L^{-1} min^{-1}); C_A and C_{A0} are the concentrations of 4-aminophenol at any time and at t = 0 (g L^{-1}) and q is the reaction rate constant. By plotting $\ln\left(\frac{C_{A0}}{C_A}\right)$ vs time, a straight line fit was obtained that confirms the order of the reaction; the slope of the trend line is the rate constants, q; Table 4.1 summarizes the rate constants at various temperatures. Following the Arrhenius equation, the activation energy for this reaction was determined as 37.31 KJ mol^{-1}(see Appendix Figure C. 2).

Table 4.1 Influence of temperature on the rate constant of paracetamol synthesis

Temperature T (K)	Correlation coefficient	Rate constant, q (min^{-1})
323	0.7903	0.61
333	0.9733	0.94
343	0.9947	1.41
353	0.8645	1.99

Few literature has been found on the kinetics involving 4-aminophenol and excess acetic anhydride; one work close to our study involved almost equalmolar reactants and a 2nd order reaction kinetics was evaluated with a rate constant of 0.66 ml mg^{-1} min^{-1}[217]. It should be noticed that although the reaction between paracetamol and 4'-acetoxyacetanilide is affected by complex conditions (concentration, mixing, temperature, water content, PH and etc.), the reaction kinetics evaluated above is still applicable as the hydrolysis step has much faster kinetics and the overall kinetics is dominated by that of the slowest step. This is supported by the work of Lee et al.[3] and Srabovic et al.[219]. The reaction time in our work is approximately 10 minutes, which agrees with the literature results of from 3 to 15 minutes[1, 2, 217].

4.5.3 Effect of water content on supersaturation

The mixture of acetic acid and water is the solvent for crystallization after the reaction, different amounts of water used in the reaction step affect the solvent compositions as shown in Table 4.2, in turn the saturation and solubility. The degree of supersaturation is calculated for different water concentrations (see Figure 4.7), according to the solubility of paracetamol in these aqueous acetic acid solutions. It is seen in Figure 4.7 that less water leads to higher supersaturation, in turn smaller particle sizes. This is expected as higher supersaturation favours nucleation. The morphology of paracetamol crystals went through from needles to rod-like shape with the increase of water in the synthesis, the degree of the agglomerations seems to decrease with the increase of water content (Figure 4.8). The morphologies in our work are similar to these of previous studies by Sudha and Srinivasan [220]and Prasad et al.[221]. The exception is for the crystals on the top left of Figure 4.8, these were confirmed as 4'-acetoxyacetanilide particles of high purity by NMR. With excess acetic anhydride and in the absence of water in the reaction system,

the nucleophilic addition-elimination takes place on both –NH and –OH functional groups, 4'-acetoxyacetanilide cannot be hydrolyzed to form paracetamol, as shown in the reaction scheme above. In addition, the solubility of paracetamol is much higher than that of the side product [87, 221]. In summary, 4'-acetoxyacetanilide is the product from this reactive crystallization without water, while paracetamol with the presence of water. Both products are of high purities as there is no visible impurity peak shown in the NMR data (see Figure 4.13). In addition, 20 g of water content is the best condition for the desired crystal polymorph.

Table 4.2 Solvent compositions with different amount of water after reaction

Samples	**Water content**	**Solvent composition (mass ratio) (Acetic acid w%)**
S1	0 g (0 mol)	Acetic acid : Acetic anhydride = 2 : 9 (no water)
S2	5 g (0.28 mol)	Acetic acid : Water = 226 : 3 (98.69 w%)
S3	10 g (0.55 mol)	Acetic acid : Water = 13 : 2 (86.67 w%)
S4	20 g (1.11 mol)	Acetic acid: Water=7:3 (70 w %)

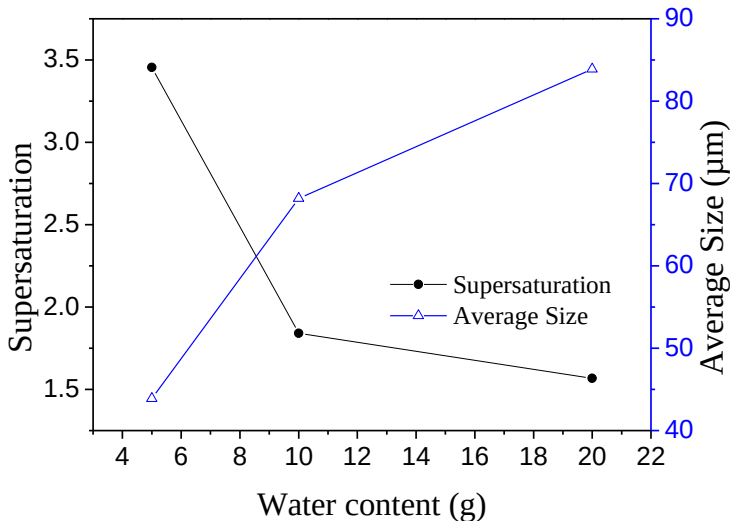

Figure 4.7 The supersaturation and crystal size as a function of water contents

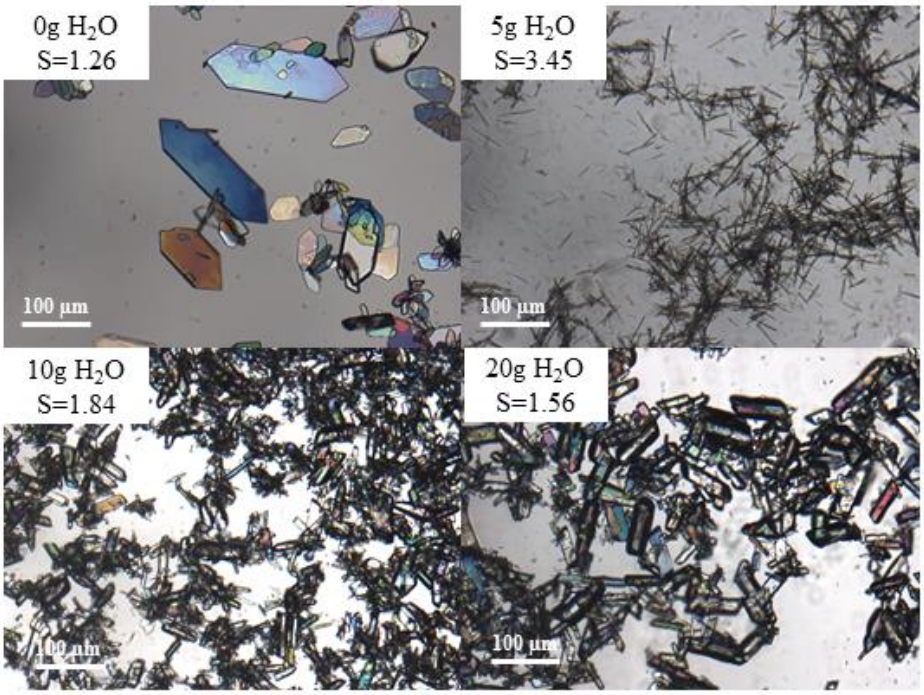

Figure 4.8 The effect of water content on crystals morphology

4.5.4 Effect of temperature on supersaturation

In continuous reactive crystallization, the temperature at the end of reaction will be the starting temperature of crystallization. For a constant temperature of 20 °C at the end of crystallization, the higher the reaction temperature, the larger the supercooling, in turn the supersaturation (see Figure 4.9), the smaller the crystal size. The morphology of crystal products at different temperatures is shown in Figure 4.10; no visible change in crystal shapes are seen, whereas the mean crystals sizes decreased when the temperature increased from 50 to 80 °C. To perform the reaction at lower temperatures while having little effect on product quality has both operational and environmental benefits. Generally, the crystals from the reaction temperature of 70 °C had uniform morphology and better size distribution.

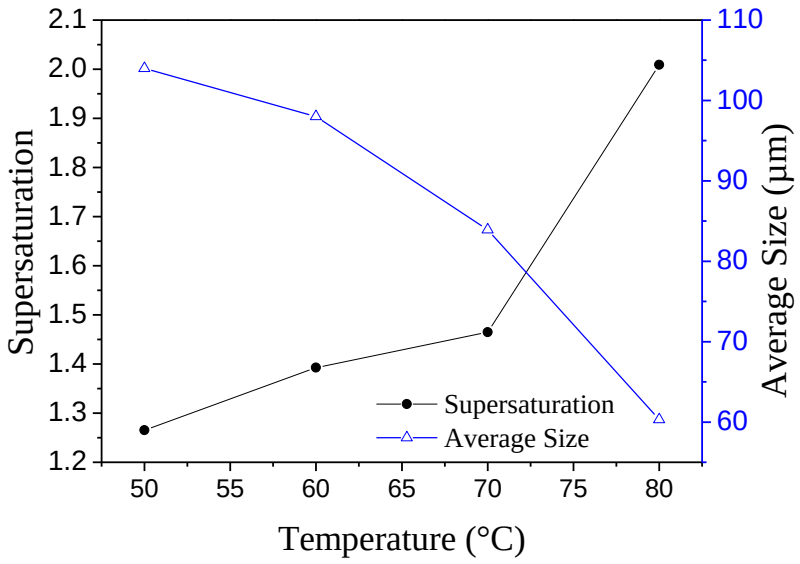

Figure 4.9 The supersaturation and crystal size as a function of reaction temperature

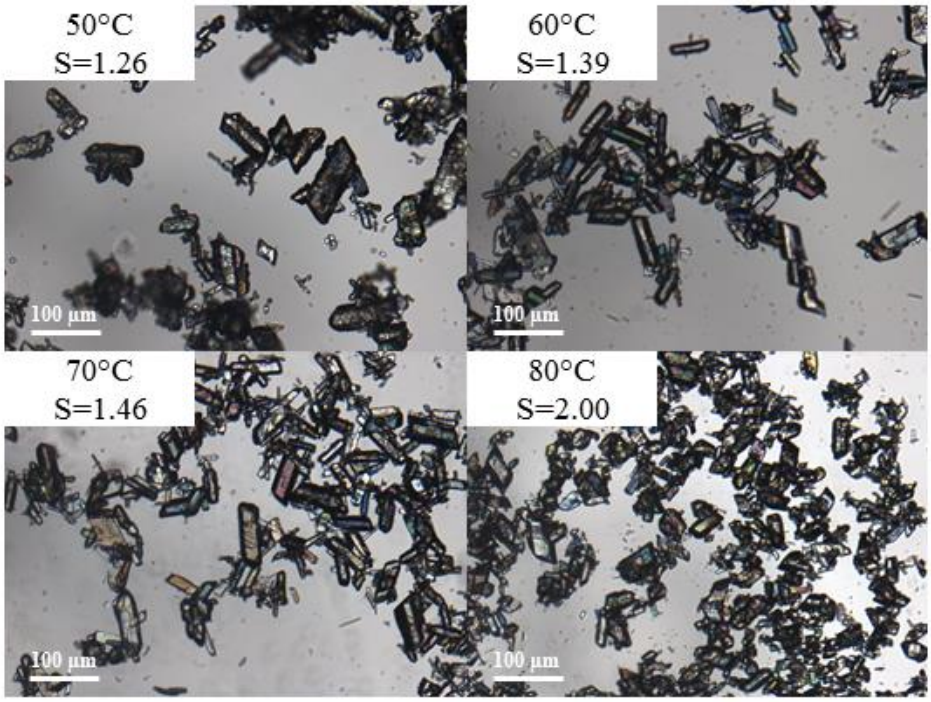

Figure 4.10 The effect of temperature on crystals morphology

4.5.5 Crystal properties

From a large number of experiments carried out, paracetamol alone was produced from reactions with 10 g and 20g of water at temperatures from 50 °C to 80 °C, whereas 4'-

acetoxyacetanilide was identified with 0 g and 5 g of water. Paracetamol particles with a high purity (~99 %) were made when enough water (≥ 10 g, or 0.55 mol) were present, while temperature had little effect on the product purity (see Figure C.6 & C.7 in Appendix).

In general, the variations in shapes among each solvent system are quite similar. Non-centrosymmetric growth and crystal shapes in Figure 4.8 and 4.10 agree with previous results predicted by steady–state morphologies [222, 223]. Sharp needle shaped crystals were observed for the reaction with less water concentration (5 g H_2O). Apart from the effect of high supersaturation, the presence of by-product is probably another reason for the development of needle-shaped crystals. Similar polymorphic forms were reported[224], involving aqueous solution containing 4'-acetoxyacetanilide.

All crystals with water are of form I, see the XRPD patterns in Figure 4.11 which are the same with these from Nichols and Frampton[211], while a different X-ray diffraction pattern is displayed for the crystals in absence of water; these hexagonal crystals are 4'-acetoxyacetanilide. This supports the NMR results (see Figure 4.13). The size distribution of paracetamol is shown in Figure 4.12 with D_{50} = 84.3 μm and is slightly broader when compared with the work of Fujiwara et al.[202] in a supersaturation-controlled seeded batch crystallization. Agglomerations occurring during the crystallization step could be the potential reason for this. It was found that there was less agglomerations for reactions with higher water contents, as the polarity of the solvent increases with the concentration of water. This agrees with previous study[225, 226] in that agglomerates became weaker in more polar solvents.

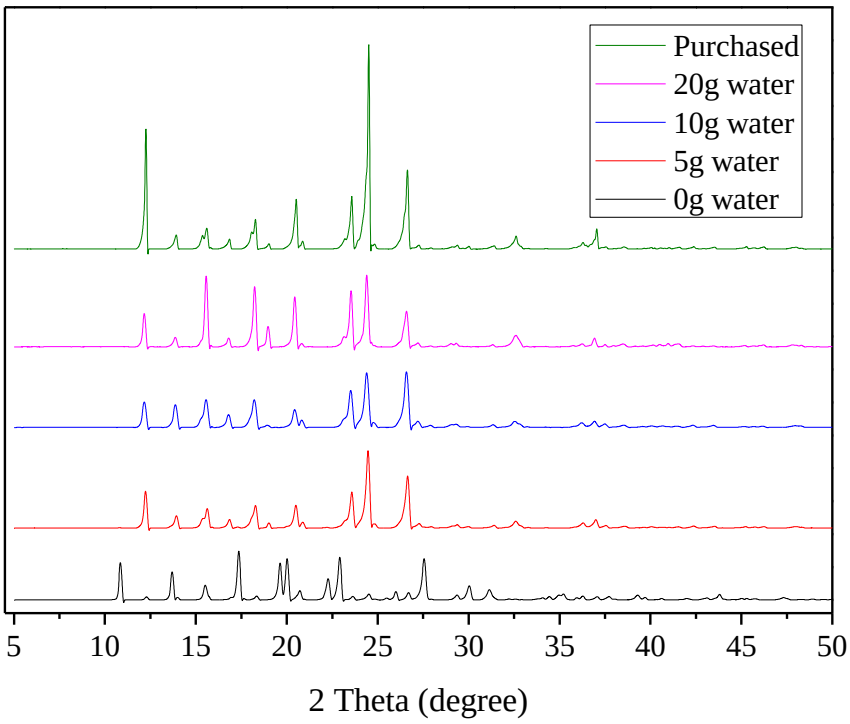

Figure 4.11 Powder X-ray diffractions for purchased and produced paracetamol with different water contents

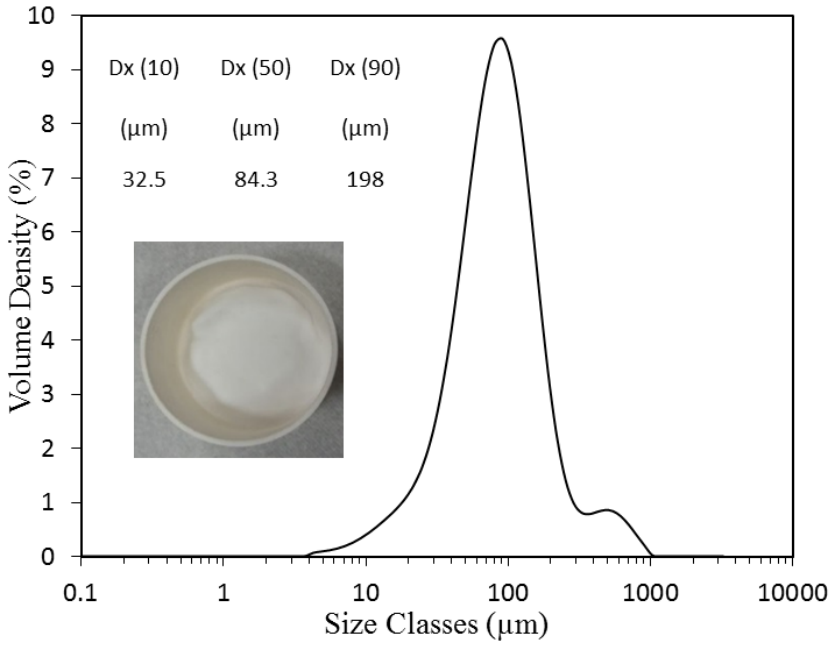

Figure 4.12 Crystal size distribution for paracetamol particles

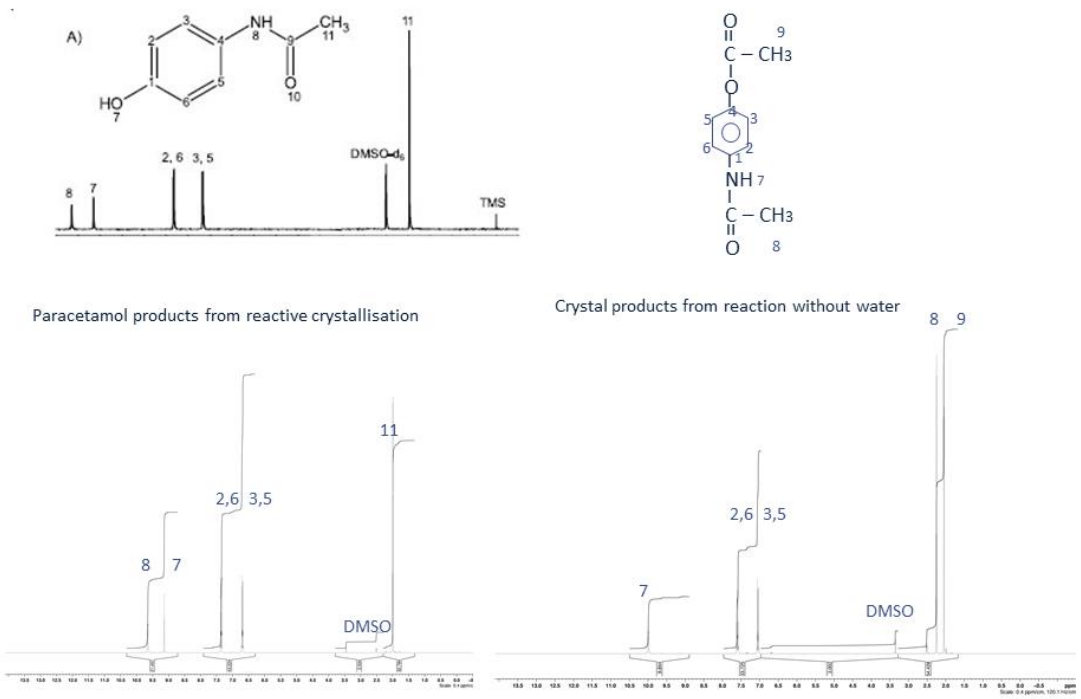

Figure 4.13 The NMR results for paracetamol product (left) and by-product from reaction without water (right)

4.6 Conclusions

In this work, the reactive crystallization of paracetamol was considered as a single process for the purpose of continuous operation. The solubility for crystallization was optimized first, from which suitable reagent concentrations were determined. The effects of reaction temperature and water content on reaction kinetics and mechanism as well as product quality were jointly investigated for the first time; Form I crystals with high purity were obtained with the presence of water, and 4'-acetoxyacetanilide without water. The understanding gained and the process conditions identified from this work are the basis for continuous operation, which is presented and discussed in Chapter 6.

Chapter 5 – **Effects of solvents and impurity on crystallization kinetics**

This chapter presents the second set of experimental results on the investigation of the effects of solvents and impurity on crystallisation kinetics. The entire chapter was submitted to the journal of Industrial Engineering and Chemistry Research.

5.1 Introduction

As stated previously, paracetamol can be manufactured by acetylating 4-aminophenol with a small stoichiometric excess of acetic anhydride in an aqueous medium[3, 4, 216], recrystallization step was thereafter added for the purpose of purification[1, 2, 30, 49-51, 195, 217-219]. Whilst significant progresses have been made to date, reaction and recrystallization have commonly been treated as two separate unit operations. Extensive work for recrystallization of paracetamol have been reported on cooling[58, 77, 84, 142, 143, 202, 209, 227, 228] and anti-solvent means[81, 85-89, 229-231]. In recent years, continuous crystallization has gained significant momentum as an attractive approach for the manufacture of fine chemicals and pharmaceuticals[17, 18], different reaction and crystallization conditions for paracetamol were reported[3], however, the effect of reaction conditions on crystallization kinetics has rarely been examined. In this work, the reactive crystallization of paracetamol was treated as a single process for the purpose of continuous operation, the stoichiometric proportions of reactants are determined based on the solvent compositions that deliver the optimized solubility for crystallization. By comparing nucleation and growth kinetics for different solvents directly resulted from the reaction, the effects of paracetamol synthesis on the following crystallization kinetics and crystal morphologies are jointly investigated, i.e. the reaction is linked with crystallization as a single process, these are new to previous separated studies of either reaction or recrystallization.

5.2 Kinetics

5.2.1 Nucleation kinetics

Nucleation kinetics were commonly estimated using the classical Nývlt equation [122-124] where the nucleation rate (J) is related to the maximum solution supersaturation

(Δc_{max}) and cooling rate (λ). The simplified Nývlt equation links the maximum supercooling (ΔT_{max}) with the cooling rate (λ) as:

$$\ln(\Delta T_{max}) = \frac{1}{b}\ln \lambda - \frac{1}{b}\ln k + \frac{1-b}{b}\ln(\frac{dC}{dT}) \quad (5\text{-}1)$$

where C is the mole fraction solubility of solute at a given temperature, b and k denote the apparent nucleation order and nucleation constant, respectively. It should be noted that the value of k depends on the formation of stable nuclei and the growth to visible entities, therefore the experimental method for measuring of MSZW can affect the nucleation orders. Both of the values for k and b are expected to be independent of the method used for nucleation rate measurement. Plotting ln (ΔT_{max}) vs ln λ displays a linear relationship, from which nucleation kinetics can be extracted. However, the limitation for the Nývlt approach[126, 127] is that the derivation was based on the assumption that the solubility coefficient (dc/dT) was independent of the saturation temperature T_0 (°C), leading to concentration-based units for the nucleation rate, in turn complicated units with non-sensical physical significance for the nucleation order and constant.

Recently, a self-consistent Nývlt equation by Sangwal[126, 128, 129] utilized a dimensionless maximum supercooling ($\Delta T_{max}/T_0$) with T_0 being the initial saturated temperature as:

$$\ln(\frac{\Delta T_{max}}{T_0}) = \frac{1}{b}\ln \lambda + \frac{1-b}{b}\ln(\frac{\Delta H}{RT_n}) + \frac{1}{b}(\ln \frac{f}{k}) - \frac{1}{b}\ln T_0 \quad (5\text{-}2)$$

where ΔH is the heat of dissolution (KJ mol^{-1}), R the gas constant (J $mol^{-1}K^{-1}$), T_n the nucleation temperature (K) and f the proportionality constant. A linear relationship between $\ln(\Delta T_{max}/T_0)$ and ln λ enables the determination of nucleation order from the slope 1/b. The main advantage of Eq. (5-2) over Eq. (5-1) is that the effect of saturation temperature T_0 on (dc/dT) is included. The Eq. (5-2) is used in this work.

5.2.2 Growth kinetics

As mentioned previously, crystal growth kinetics are important in the design and development of crystallization processes and many different theories have been employed

to facilitate crystal growth mechanisms[51, 132, 134], with fundamental studies on the evaluation of growth rates of individual surfaces[140-142, 232]. Various experimental measurements and estimations have also been utilized to determine overall mass transfer rates under controlled conditions, in turn size-dependent growth rate[3, 65, 84, 86, 88, 143, 144]. While there is no general accepted method for expressing the growth kinetics, crystal growth rate, G (m s^{-1}), in terms of mass deposited per unit time per unit area of crystal surface[51] is used in this work as:

$$G = K_G \frac{\beta}{3\alpha\rho_c} (\ln S)^g \tag{5-3}$$

where K_G, ρ and g are the overall mass transfer coefficient (kg m^{-2} s^{-1}), crystal density (kg m^{-3}) and growth order, respectively. The growth rate is related to the level of supersaturation in terms of a dimensionless concentration of S, where $S = \frac{c}{c^*}$, c is the concentration in solution (kg $_{solute}$ kg^{-1} $_{solvent}$) and c* refers to solubility at the same temperature (kg $_{solute}$ kg^{-1} $_{solvent}$).

5.3 Experimental section

5.3.1 Materials

The chemical compounds used to characterise the kinetics of the reactive crystallization in an OBR are the same as those for the investigation of reaction kinetics in Chapter 4.

5.3.2 Characterization

As described in Chapter 4, the concentration of paracetamol was analyzed using the Agilent 1100 Series HPLC System; crystal size distributions by a Mastersizer 3000™ (HYDRO, Malvern); morphologies of crystals by a Leica ATC 2000 Trinocular

Microscope, crystal surface properties by scanning electron microscope (SEM) and crystal polymorphs by Power X-Ray powder diffraction (XRPD).

5.3.3 Equipment

Reactive crystallization of paracetamol was performed in a jacketed oscillatory baffled reactor (OBR) with an internal diameter of 76 mm and a working volume of 1 L. A baffle string consists of 2 orifice baffles with orifice diameter and baffle space of 32 mm and 86 mm respectively, giving a baffle free area ratio of 0.21. A linear actuator connecting to the baffle string delivers different oscillation amplitudes and frequencies. The temperature within the OBR was controlled by a water bath (Grant Instruments GP 200/R2), enabling different linear cooling rates. The metastable zone width was determined from turbidity measurements using an online turbidity probe (METTLER TOLEDO). The schematic illustration of the OBR is shown in Figure 5.1.

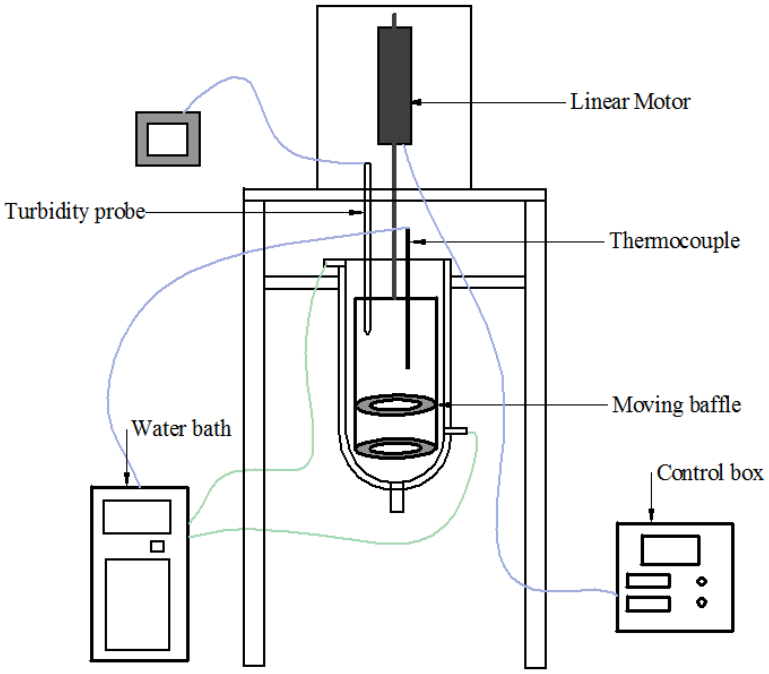

Figure 5.1 Schematic of OBR setup

5.4 Reagents, solvents and solubility

Paracetamol is produced by reacting 4-aminophenol and acetic anhydride with acetic acid as a side product when water reacts with acetic anhydride in excess, following the reaction scheme as shown in Figure 4.5. The same procedures as described in Chapter 4 were used here where different amounts of 4-aminophenol, acetic anhydride and water were charged into the preheated OBR at 50 °C under oscillation. The reaction was commenced when the OBR was further heated up and maintained at 75 °C. Samples were taken at regular time intervals using a pipette with an accurate volume of 0.300 ml; and were quenched and diluted 100 times with the mobile phase solution (methanol : water = 1:3). The overall reaction time was about 40 minutes; after which the crystallization was immediately initiated by cooling the solution to 20 °C at different cooling rates.

Figure 5.2A is the HPLC chromatogram for one of the samples where three peaks at retention time of 3.695, 5.193 and 11.286 min correspond to the solvent, paracetamol, and 4'-acetoxyacetanilide (PAA) respectively, from which concentrations of paracetamol and 4'-acetoxyacetanilide changing with time are obtained as shown in Figure 5.2B. It is seen that the concentration of paracetamol increases dramatically in the first 10 minutes and then stabilizes at an average value of 65.23 g L^{-1} before it falls, this is the initial concentration for crystallization. The solute concentration continues decreasing thereafter as more paracetamol particles are formed during crystallization. It is also seen that the generation of the impurity (PAA) via the side reaction (Figure 4.5) is continuous from the start, but at a much lower concentration than that of the target compound (Figure 5.2B). No visible impurity was observed on product crystals in both HPLC and NMR analysis, and a purity of 99 % was achieved.

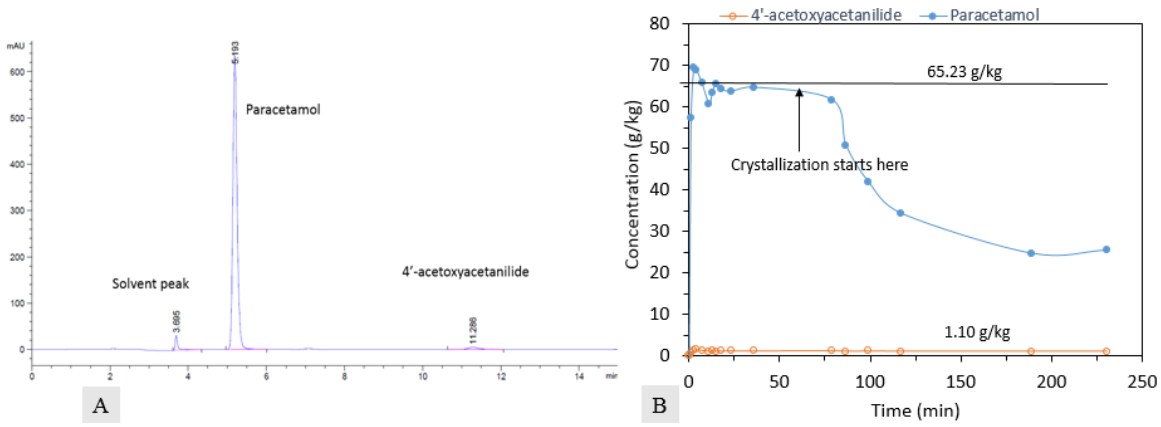

Figure 5.2 (A) HPLC chromatogram showing solvent, paracetamol and 4'-acetoxyacetanilide (PAA) peaks; (B) Concentrations of paracetamol and impurity (PAA) as a function of time

From the reaction scheme in Figure 4.5, the solvent for crystallization is a mixture of acetic acid and water that are directly generated from the reaction step, different ratios of which give different solubility as shown in Figure 4.2 with the highest at 7:3 (acetic acid : water). In this work, the effects of three acid to water ratios (1:9, 5:5 and 7:3) on crystallization kinetics and crystal properties were examined. The amounts of reactants (4-aminophenol and acetic anhydride) required to produce paracetamol in any of the above solvent ratios were back calculated according to the reaction stoichiometry and solubility profile (see Appendix D). This is how the reaction is linked with crystallization. Table 5.1 shows the various parameter settings for both reaction and crystallization conditions.

Table 5.1 Experimental conditions used for reactive crystallization of paracetamol

Acid : H_2O (w : w)	1:9				5:5			7:3		
AA : 4-AP (mol : mol)	1.8	2.0	2.3	2.7	1.8	2.0	2.3	1.8	2.3	2.7
Cooling rate (°C min^{-1})	0.8	0.8	0.4, 0.8, 1.2	0.8	0.8	0.4, 0.8, 1.2	0.8	0.4, 0.8, 1.2	0.8	0.8
Frequency (Hz)	1	1	0.5, 1.0, 2.0	1	1	0.5, 1.0, 2.0	1	0.5, 1.0, 2.0	1	1
Amplitude (mm)	44	44	44	44	44	44	44	44	44	44

5.5 Results and discussions

5.5.1 Effect of Solvent on Nucleation Kinetics

Figure 5.3 plots ln ($\Delta T_{max}/T_0$) vs ln λ from Eq. (5.2) for three solvent ratios of 1:9, 5:5 and 7:3, respectively. It can be seen that the metastable zone width (ΔT_{max}) increases for every solvent system as the cooling rate (λ) increases from 0.4 to 1.2 °C min^{-1}. At a given cooling rate, the lower the ratio of Acid: H_2O, the wider the MSZW, indicating that the MSZW can be controlled by the solvent compositions resulted from the reaction step. The influences of solvents on nucleation kinetics were investigated in recrystallization work[126, 233, 234]; the net effect of changing solvent led to an increase of solubility, in turn an increase of nucleation rate due to the decrease of interfacial tension between solute and solvent on specific faces[233-235]. Nucleation order (b) is highly dependent on the solubility of a solute in a given solvent[126]; and is 5.4, 15.5 and 14.1 in this work for the three solvents respectively, which are higher than 1.68 for paracetamol in ethanol by Mitchell and Frawley[58]; 1.29 – 6.23 for paracetamol in water by Nagy et al.[124] and 0.6 – 3.4 for paracetamol in methanol/water solutions by Ó'Ciardhá et al.[234]. Higher nucleation orders in this research are related to higher solubility of the solvents used, which leads to different levels of supersaturation. Moreover, agglomeration also contributes to high nucleation orders, the effect of which is still difficult to be separated using current PAT tools. In this work, agglomeration is mainly caused by high supersaturation. Once the nucleation has taken place, agglomerates are formed at a faster rate than that for nuclei to grow sufficiently large to be detectable, this gives a high nucleation order (between 8 and 20 according to crystallization theory). When supersaturation is relatively low, agglomeration is less apparent, leading to lower nucleation order, e.g. between 1.5 and 8. This explains the high nucleation orders from Figure 5.3.

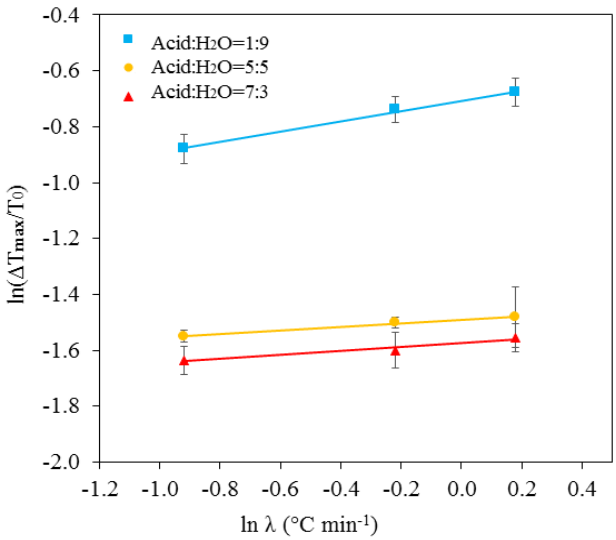

Figure 5.3 Plot of ln ($\Delta T_{max}/T_0$) vs ln λ for three solvent ratios

5.5.2 Effect of solvent on growth kinetics

In this work, the overall growth rate was determined by plotting crystals size as a function of time. Mastersizer was used for crystal size measurements for samples that were taken at regular time intervals once nucleation had been observed in the solution. By plotting the overall linear growth rate (G) against the supersaturation ($\frac{c}{c*}$) from Eq. (5-3), Figure 5.4 shows the increase of the growth rate with the supersaturation for each solvent composition. Our data are in the similar order of magnitude, but higher than others of recrystallization of paracetamol in various solutions [84, 86, 143, 236]. Reactive crystallization of paracetamol in a stirred tank with sodium hydroxide added after the reaction step gave the growth rates from 4.04 to 5.64 × 10^{-8} m s^{-1} using a sieving method[3], which are similar to our data (see Figure 5.4).

The growth orders (g) were extracted from the power law relationship displayed in Figure 5.4 as 4.27, 12.62, and 1.72 respectively for the three solvents. It is seen that there is no direct dependence of crystal growth order on the solvent composition. Ó'Ciardhá et al. [143] reported that solvent composition, solubility gradient and viscosity all contributed to crystal growth machanisms, where solvent ratio may decrease growth rate due to the selective absorption of solvent molecules, or enhance face growth rate by

causing a reduction in the interfacial tension[237-239], leading to an unclear role played by solvent in affecting crystal growth[142, 143]. It should be noted that levels of supersaturation in three solutions play an important role during crystallization. For the highest supersaturation in the 5:5 solvent ratio, micro nucleus were formed very fast and precipitated out of the solution quickly with agglomerations, leading to difficulties in sampling and size measurements. Aggolomerates seen in dry products can also lead to wider crystal size distributions. In this project, a high dispersion rate (2000 rpm) for particles suspension has been used in Mastersizer to reduce this type of errors caused by agglonerates.

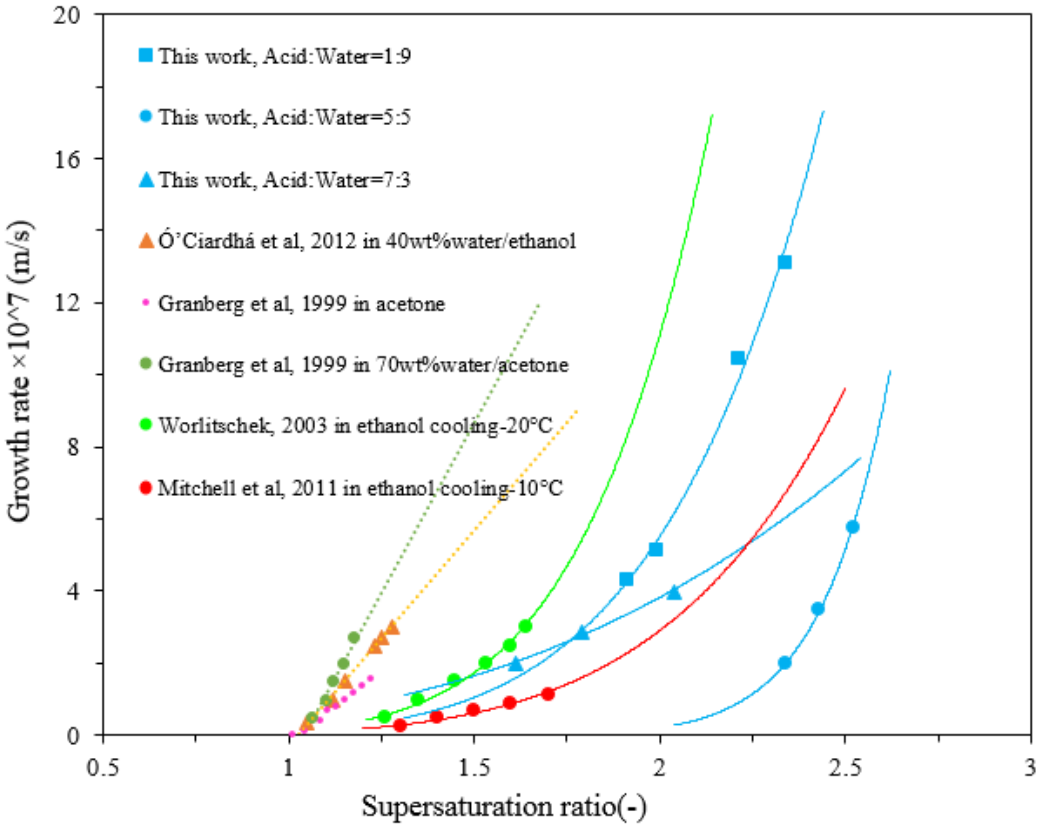

Figure 5.4 Comparison of growth rates between this work and previous researches

The main differences of this work with respect to past papers are that solvent compositions for crystallization in this work are directly produced from the reaction step, by varying the ratios of reactants (AA : 4-AP) at the start of the reaction, the control of supersaturation is achieved, connecting the reaction with the crystallization as a single process.

5.5.3 Effect of solvent on crystal shape

The effect of solvent ratios generated from the reaction on crystal shape is shown in Figure 5.5. The fairly high values of growth order imply that surface integration resistance is critical [51, 134, 240], rectangle column type of crystals is seen at the low ratio of Acid: H_2O. The columns become longer and thinner as the ratio increases. The crystal shape classification diagram by Li and Doherty [222] according to different functional groups of solvents also predicted the elongated shape for solvents of class 1 (involving acetic acid) and class 6 (water) with aspect ratios of crystals >3. However, higher aspect ratios of crystals in this work were generated in solvents of higher dispersive energies, e.g. water, this is different from the reported predictions and could be due to the increased concentrations of both paracetamol and impurity (PAA). From the SEM graphs (Figure 5.5), the lengths and diameters of over 30 crystals were measured microscopically, leading to the determination of the specific surface factors for crystals as 6.37, 5.31 and 4.75 for the three solvent systems respectively, which are comparable to 6.27~7.70 for rounded hexagonal crystals by Granberg and Rasmuson[144].

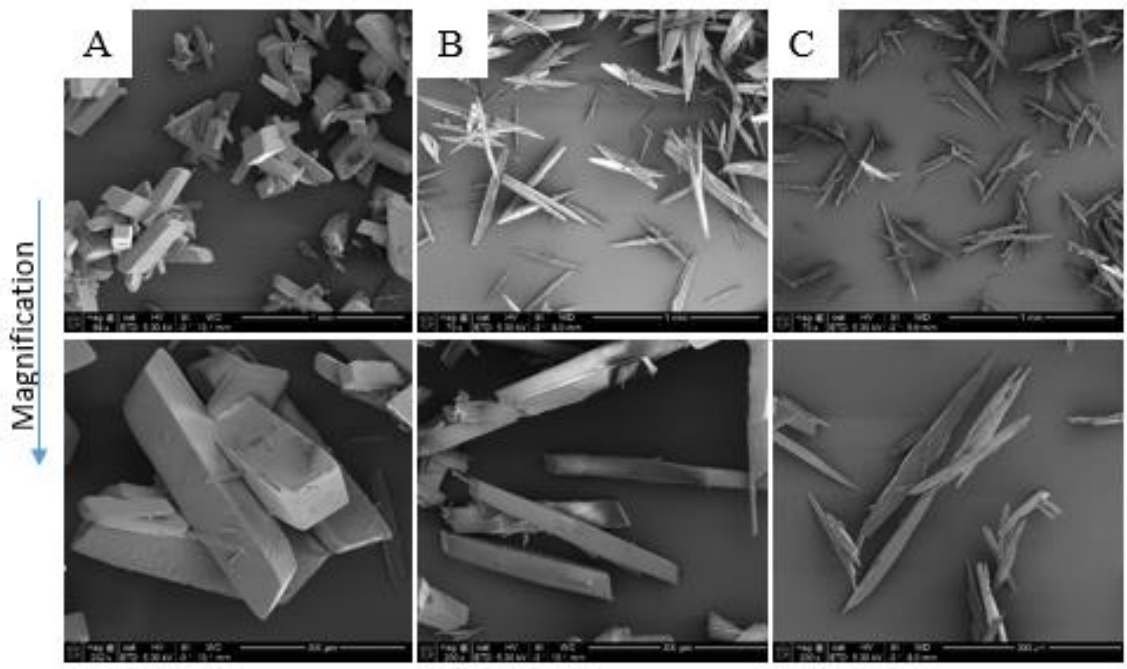

Figure 5.5 SEM measurements for paracetamol crystals in three solvents: (A) Acid: H_2O = 1:9, S = 1.99; (B) Acid: H_2O = 5:5, S = 2.34; (C) Acid: H_2O = 7:3, S = 2.04

5.5.4 Effect of impurity on crystal shape

In the reactive crystallization, the solubility for crystallization (Figure 4.2) is resulted from different solvent compositions that are formed by the reaction; the concentrations of paracetamol and 4'-acetoxyacetanilide (PAA) are also generated as given in Table 5.2. At a constant solvent composition, the increase of the reagent ratio of AA:4-AP decreases the concentrations of paracetamol and PAA, leading to different supersaturation for crystallization, in turn different crystal morphologies as seen in Figure 5.6, where smaller and finer crystals are expected when supersaturation increases. In this respect, the amount of impurity (PAA) is related to the supersaturation of paracetamol.

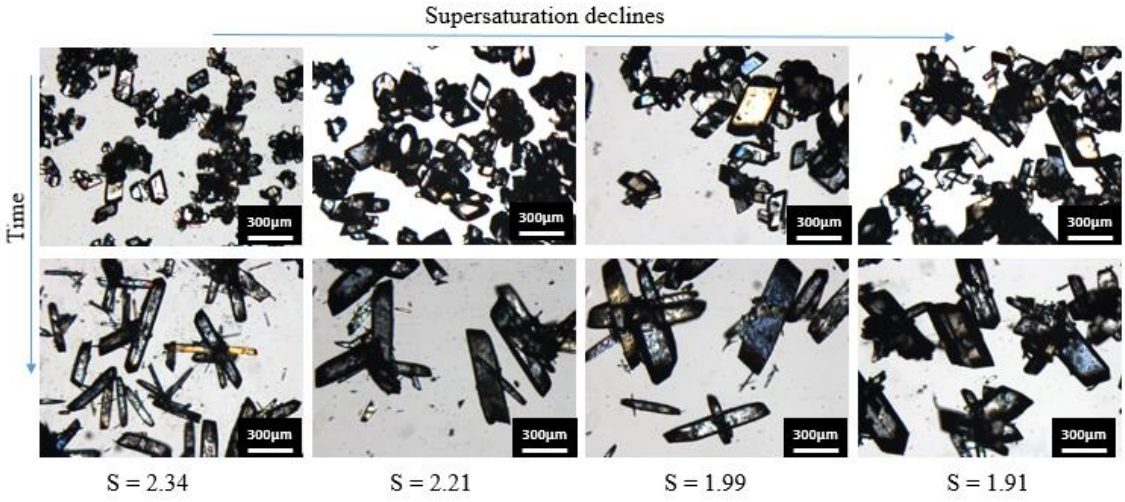

Figure 5.6 Microscope images of paracetamol crystals for different supersaturations at a fixed solvent ratio of Acid: H_2O = 1:9

The influence of PAA on paracetamol crystal growth and morphologies has been reported[141, 241], the growth rate of the [110] faces was significantly slowed down in the presence of PAA due to the largest degree of morphological instability, while the effect of PAA on other faces was less[223]. Crystal shapes changed from elongated to plate-like when the concentration of PAA decreased from 6.02 wt% to 0 wt%[221], which is similar to our data (Figure 5.6). As mentioned above, Figure 5.6 illustrates the effect of PAA on paracetamol crystal shapes for different supersaturation conditions. At the same solvent ratio, product crystals change from plate-like to elongated, indicating the

influence of PAA on crystal growth. PAA molecules can be adsorbed at particular positions on paracetamol crystals surfaces, resulting in crystal growth of specific facets. Therefore, the morphology of paracetamol particles from different solvent ratios and supersaturations was affected as shown in Appendix Figure D.9. This was confirmed by purity results in Figure 5.7.

Table 5.2 PARA and PAA concentrations in different solvent compositions by reaction

Acid : H_2O (w : w)	1:9				5:5			7:3		
AA : 4-AP (mol : mol)	1.8	2	2.3	2.7	1.8	2	2.3	1.8	2.3	2.7
PARA (mol kg^{-1})	0.599	0.514	0.441	0.375	2.029	1.96	1.803	2.382	2.214	2.004
PAA (mol kg^{-1})	0.006	0.006	0.005	0.005	0.158	0.093	0.052	0.233	0.137	0.105

Some agglomerations are observed (Figure 5.5), with a lesser degree for solvents of higher Acid: H_2O ratios. Different solvent systems have different polarities due to the interactions with H-bonding at crystal surfaces, e.g. polar solvents have stronger interactions, reducing the formation of crystalline bridges[225, 226]. For this work, the Acid: H_2O ratio of 1:9 has the highest polarity, but the degree of agglomeration is also high. This is opposite to previous work where agglomeration was found weaker for more polar solvents[225, 226]. This could attribute to the fact that the adhesion of the side product PAA in solution prevented the association of solvent molecules from depositing on crystal surfaces. Depending on the ratios of the starting materials, the concentrations of PAA increase with the increase of the ratios of Acid: H_2O as shown in Table 5.2.

5.5.5 Purity of crystal products

The purity of crystal products is plotted as a function of the reagent ratio in Figure 5.7. It is seen that the purities are generally high for all three solvents, with the highest purity of 99.84% at the Acid: H_2O ratio of 1:9 for all ratios of AA: 4-AP. Product purity increases with the ratio of the starting materials for the Acid: H_2O ratios of 5:5 and 7:3. At the same

ratio of AA: 4-AP, crystal purity decreases with the increase of the Acid: H_2O ratios from 1:9 to 7:3. This indicates that solvents and PAA molecules are more likely to be adsorbed onto crystal lattices at higher solubilities. This also agrees with the discussion for Table 5.2, as the concentration of PAA in solution increases with the concentration of paracetamol and the Acid: H_2O ratio. There are more chances for PAA molecules to get into paracetamol crystals lattice particularly for high Acid: H_2O ratios, thus leading to lower purities of paracetamol products. Figure 5.7 is a useful graph linking crystal purity (one of the crystal specifications) with the solvents for the crystallization and the starting materials for the reaction step. It is worth keeping in mind that all the product crystals in this work are monoclinic, which is polymorph Form I of paracetamol. This is consistent with previous published study on the reactive crystallization of paracetamol[242].

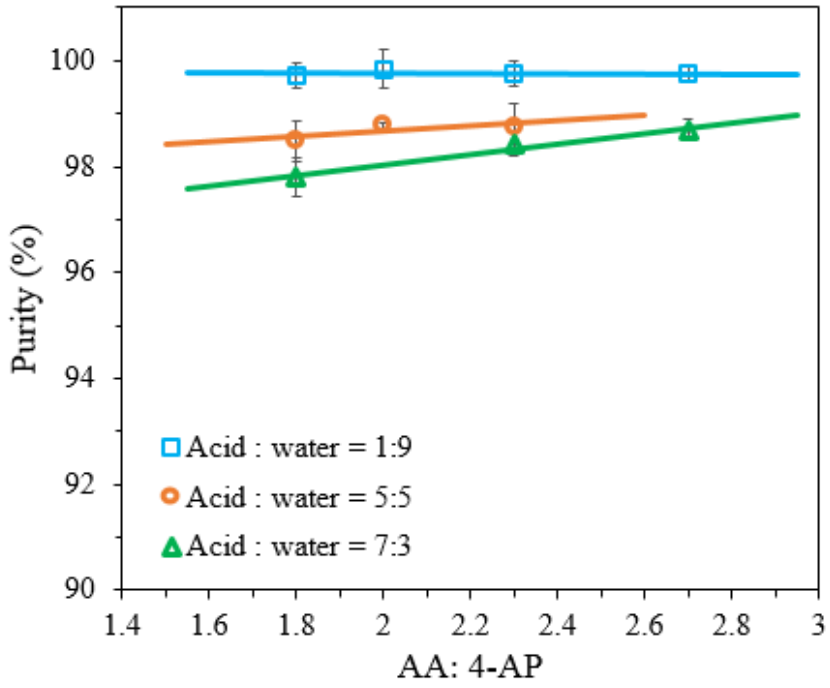

Figure 5.7 Crystal purity as a function of AA: 4-AP ratios for different solvents

5.6 Conclusions

When solvent compositions for crystallization are directly produced from the reaction, this enables the examination of the dependency of nucleation orders and growth rates on solvent compositions; a higher ratio of Acid:H_2O at the end of reaction leads to a higher nucleation order; growth rates are comparable with previous recrystallization data. Both

solvent compositions and reagent ratios are the means for influencing crystal morphology: crystals shapes change from column to needle-like with the increase of solvent compositions. At a fixed solvent, three reagent ratios of AA:4-AP at the start of reaction deliver three supersaturations for crystallization with different levels of impurity, affecting crystal morphology and causing agglomerations.

Chapter 6– **Application of reactive crystallization of paracetamol in a COBC**

The reactive crystallization of paracetamol in a COBR is reported in this chapter. Based on the kinetic and operational data obtained in batch crystallisers in Chapters 4 and 5, continuous synthesis and seeded cooling crystallisation are undertaken, investigations of seeding strategy, steady states of concentration and crystal sizes are presented. The entire chapter was accepted by the journal of Organic Process Research & Development.

6.1 Introduction

In industrial batch crystallization, we face the century old chemical engineering problem, i.e. mixing gets worse with increasing scales. What one has obtained in labs cannot be duplicated in production. The ability of providing a consistent mixing environment and superior heat/mass transfer for flow substances[10, 11] at all scales by continuous oscillatory baffled reactors/crystallizers (COBR/COBC) can bridge the gap, with an additional advantage of implementing online process analytical technologies (PAT)[17] anywhere along the length of COBR/COBC. This delivers consistent crystal properties and efficient process time, e.g. a 9 h and 40 min batch crystallization was achieved in 12 min in a COBC[12]. A seeded cooling crystallization of β-L-glutamic acid was successfully operated by Briggs et al.[192] in a DN15 (15 mm diameter) COBC. The steady state was achieved constantly after 2 residence times and remained for at least 10 hours, producing crystals of desirable polymorph and purity. In additional to cooling crystallization, anti-solvent[14] and co-crystal crystallization[15] were also carried out in COBC. However, few study has been published in continuous reactive seeded crystallization, which is the focus of this work.

Once again few literature can be seen for reactive crystallization of paracetamol in a continuous process, the closest one is the work by Agnew et al.[243, 244] who reported a selective access to produce metastable solid form of paracetamol in a COBR by adding metacetamol as a template molecule. In this work, paracetamol synthesis

followed by seeded cooling crystallization were, for the first time, investigated in a COBR under different operating conditions.

6.2 Experimental set up and procedures

6.2.1 Chemicals and analytical methods

6.2.1.1 Materials

The chemicals used in the reactive crystallizations of paracetamol in the COBR are the same as those presented in Chapter 4 and Chapter 5.

6.2.1.2 Characterization

The concentration of paracetamol from samples taken during reactive crystallization was also analyzed using the Agilent1100 Series HPLC System, with the same chromatograph column as in Chapter 5. Crystal size distributions, crystals morphologies and polymorphism were detected using suitable process analytical tools as mentioned previously.

6.2.2 Equipment

The reactive seeded cooling crystallization of paracetamol was performed in a DN15 (15 mm diameter) COBR horizontally orientated, Figure 6.1 shows the geometrical set-up. The DN15 COBR consisted of 11 jacketed baffled straight tubes and 6 non-jacketed bends wrapped with thermos-sleeves to reduce heat loss. The total length and the volume of the COBR were 9.5 m and 1.68 L respectively. A linear motor with a control box was utilized to provide oscillation at various frequencies and amplitudes.

Peristaltic pumps (Watson Marlow 520S) were used to feed reactants and seeds from their respective stirred tanks. Water was circulated through the jackets of the COBR at preset temperatures by 3 water baths (GP 200) in order to establish three temperature zones (showing as different colours and line widths in Figure 6.2) for reaction and crystallization. Six thermocouples (T1 – T6 in Figure 6.2) were employed to record the

temperature profiles of the operation. The temperature of seed suspension was controlled and maintained by a separate water bath to achieve the required supersaturation. The tubing connecting the seed suspension with the COBR was properly insulated to ensure the correct seeding temperature. During operation, samples were taken at 3 sample points (see Figure 6.2) at regular times where sample point 1 was located at the end of reaction to monitor and confirm the completion of the reaction, points 2 and 3 were located in the crystallization section for the characterization of crystals.

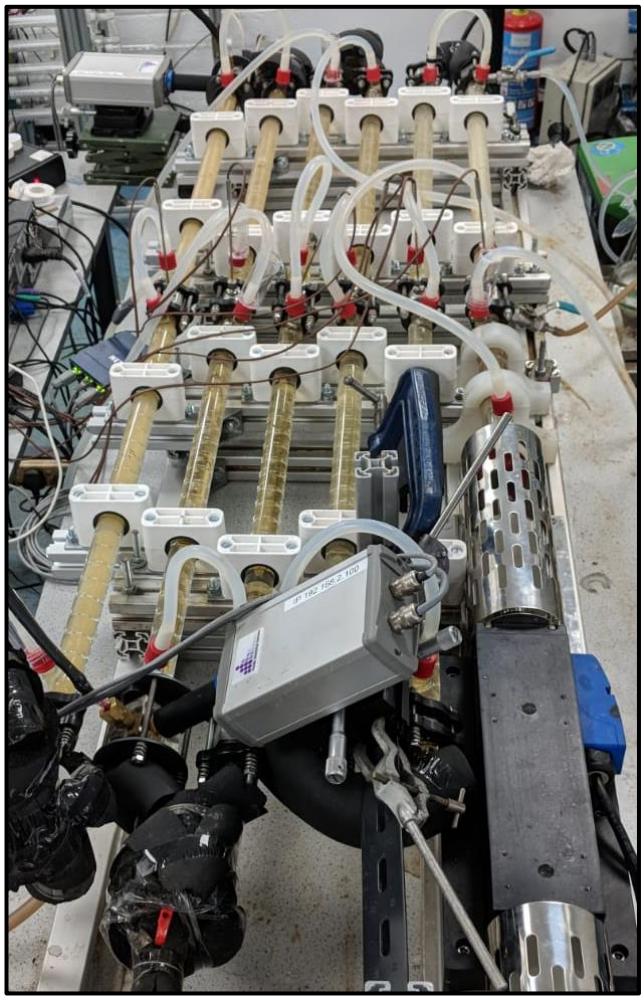

Figure 6.1 A photo showing the set-up of COBR

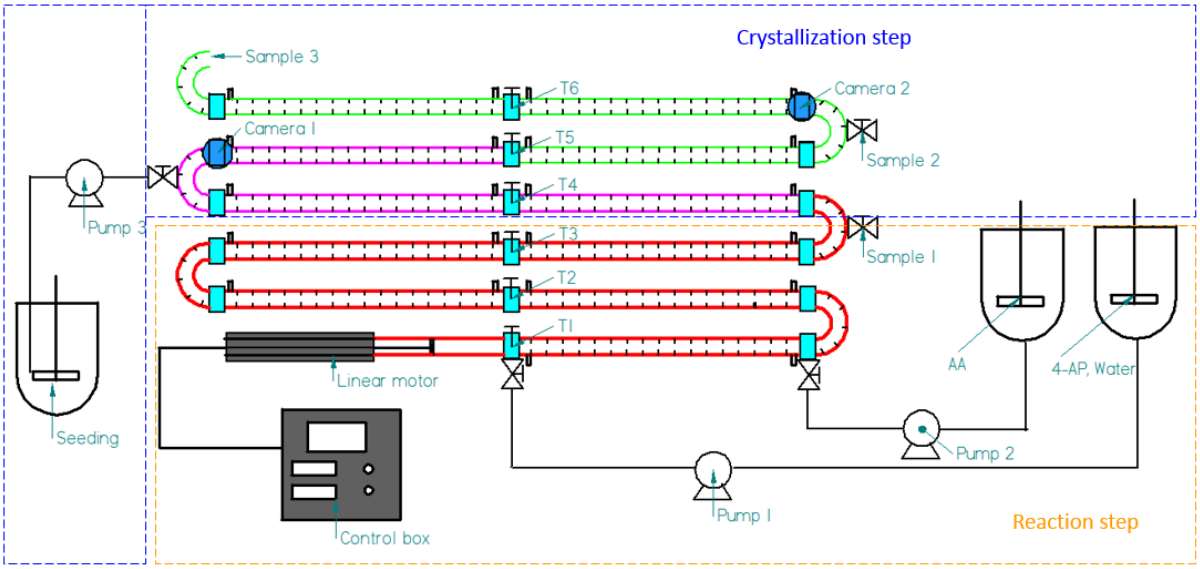

Figure 6.2 Schematic of the COBR platform for the reactive seeded cooling crystallization of paracetamol

As mentioned in Chapter 2.3.2, the mixing performance in COBR can be characterized by three dimensionless groups: the oscillatory Reynolds number (Re_0) , the Strouhal number (St) and the net flow Reynold number (Re_n) which are defined by the following equations[166, 245]:

$$Re_0 = \frac{x_0 \omega D}{\nu} \tag{6-1}$$

$$St = \frac{D}{4\pi x_0} \tag{6-2}$$

$$Re_n = \frac{\rho u D}{\mu} \tag{6-3}$$

where x_0 is the amplitude of oscillation from centre to peak (m), $\omega(=2\pi f)$ the angular frequency (rad s^{-1}), f the linear frequency (Hz), D diameter of column (m) and ν kinematic viscosity of the fluid (m^2 s^{-1}), ρ the fluid density (kg m^{-3}), μ dynamic viscosity of the fluid (Pa.s) and u the mean velocity (m s^{-1}). The oscillatory Reynolds number measures the

oscillation, and the Strouhal number represents the ratio of column diameter to oscillatory amplitude, which determines the length of eddy propagation.

6.2.3 Procedures

Paracetamol was produced by reacting 4-aminophenol and acetic anhydride, acetic acid was a side product when water reacted with the acetic anhydride in excess. At the start, the premixed 4-aminophenol and water from feed tank 1 was pumped through the COBR by pump 1 (Figure 6.2) at a high flow rate in order to get rid of any bubbles. Once degas has been done, the flow rate was reduced to an operational rate (Table 6.1) and oscillation was switched on, while the circulation continued. The purpose of circulating the mixture was to establish the three temperature zones shown in Figure 6.2. Once the temperature zones have successfully been set-up, acetic anhydride from feed tank 2 was introduced at a specific flow rate by pump 2 into the COBR where the temperature in this section of COBR was now at 75 °C. The reaction proceeded when the reactants were mixed and dissolved at the 1st bend and 2nd straight tube of COBR. Crystallization took place after the completion of the reaction, seed solution was fed into the COBR by pump 3 at a preset rate and at 50 ºC just before the reacted mixture has reached the seeding point. The outlet of the crystallization was collected in a product tank (not shown in Figure 6.2).

The shut-down procedures involve replacing the reactant feeds by water; stopping the seed pump before water has reached the seeding point; increasing the temperature of the whole COBR to 70 ºC that dissolves any residues in the system. After a certain time, the flow rate of water was increased and the temperature control switched off, COBR returned to room temperature and ready for next run. The operation conditions tested in this work are summarized in Table 6.1.

Table 6.1 COBR operation parameters

AA flow (g min^{-1})	**4-AP/H_2O flow (g min^{-1})**	**Main flow (g min^{-1})**	**Seed flow (g min^{-1})**	**Residence time (min)**
4	36	40	10	40

Sample preparation. Solution samples were taken at regular time intervals using a pipette with an accurate volume of 0.400 ml; and were quenched and diluted 100 times with the mobile phase solution (methanol:water = 1:3). Solid samples were collected by a syringe and immediately filtered and washed before drying in an oven at 40 ºC overnight. Dried particles were then moved to a desiccator to cool down and weighted until constant mass.

Seed preparation. Seeds were prepared using a blender and the mean size of seed crystals was measured by Mastersizer as 92.3 μm (Figure 6.3).

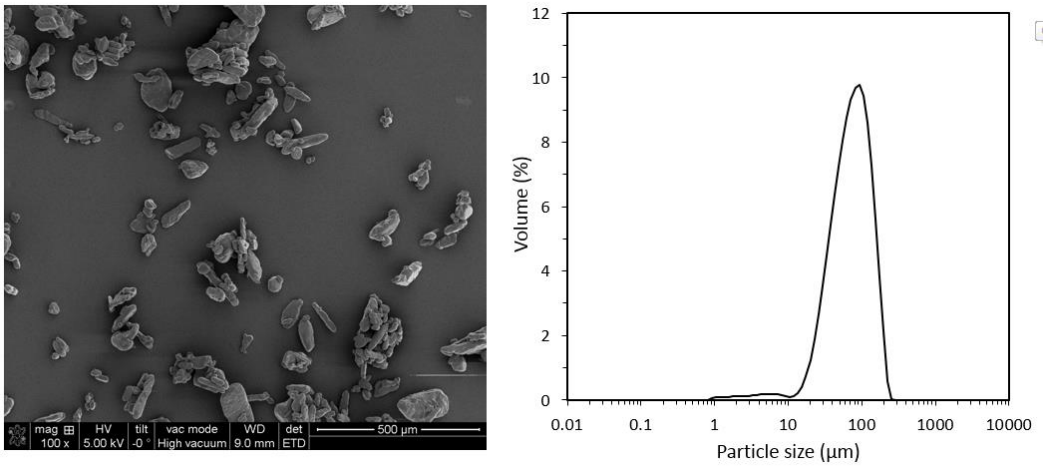

Figure 6.3 Particles size distribution of seed crystals

The determination of seed mass and the effect of seed mass on the sizes of final crystals are discussed later in details.

Supersaturation (S). In this work, the level of supersaturation is expressed in terms of the supersaturation ratio (S) defined as

$$S = \frac{c}{c^{\star}} \tag{6-4}$$

where c is paracetamol concentration in solution, $c^{\star}$ is equilibrium concentration in solution.

Operation conditions. A series of experiments were carried out in the COBR for the reactive seeded cooling crystallization of paracetamol. Table 6.2 summarizes the conditions.

Table 6.2 COBR operational conditions

Expt.	Runs	Frequency, f (Hz)	Amplitude, $2x_0$ (mm)	R_{eo}	R_{en}		S_t
					Reaction	Crystallization	
COBR-1	**1**	1	26	1225	57	71	0.09
	2	1	26	1225	57	71	0.09
	3	1	26	1225	57	71	0.09
COBR-2	**1**	1	30	1413	57	71	0.08
	2	1	30	1413	57	71	0.08
	3	1	30	1413	57	71	0.08
COBR-3	**1**	1	35	1649	57	71	0.07
	2	1	35	1649	57	71	0.07
	3	1	35	1649	57	71	0.07
COBR-4	**1**	0.7	30	989	57	71	0.08
	2	0.7	30	989	57	71	0.08
	3	0.7	30	989	57	71	0.08
COBR-5	**1**	1.2	30	1696	57	71	0.08
	2	1.2	30	1696	57	71	0.08
	3	1.2	30	1696	57	71	0.08
COBR-6	**1**	1.5	30	2120	57	71	0.08
	2	1.5	30	2120	57	71	0.08
	3	1.5	30	2120	57	71	0.08

6.3 Results and discussion

6.3.1 The reaction zone

The reaction was started once the two feeds of the reactants were met in the first straight tube as shown in Figure 6.2; was completed just before the sample point 1 where the temperature of the reaction zone (marked in thick red line in Figure 6.2) was maintained at 75 ºC. The solvent for the subsequent crystallization was a mixture of acetic acid and water with an Acid: H_2O ratio of 1:9. The amounts of reactants (4-AP and AA) required to deliver the above ratio were back calculated according to the reaction stoichiometry

and solubility profile[242]; their flow rates were subsequently determined to ensure a required residence time of 40 mins for both reaction and crystallization. More details on calculations of the concentrations of starting materials and flow rates can be found elsewhere[242] as well as in Appendix D2. HPLC analysis for samples taken at the sample point 1 have confirmed that the reaction was completed, the concentration of paracetamol was approximately stable (see Figure 6.7) where no peak for reactants was seen in the chromatogram, i.e. about 100% of conversion was obtained (see Appendix Figure E.5).

6.3.2 Effect of seed loading

For successful crystallizations in COBR, correct seeding structure is one of the most important and useful methods for preventing uncontrolled nucleation and the subsequent encrustation from taking place and for focusing growth on seed crystals[51, 110, 192]. Such a structure involves a correct combination of both seed size and seed loading. Seed size is fixed in this work, as shown earlier.

A great amount of work on seeding has been carried out in batch processes [103, 246, 247], the methodology of which could be applied to continuous crystallization. The seed loading, C_{seed} (%), is defined by Eq. (6-5) as the ratio of the mass of seed, W_{seed} (g), over the maximum theoretical yield, W_{theo} (g)[104, 247]:

$$C_{seed} = \frac{W_{seed}}{W_{theo}} \tag{6-5}$$

where W_{theo} can be calculated from the solubility data. For an un-agglomerated growth only model, nucleation is totally suppressed by seeds, there is neither agglomeration nor breakage in crystals, in addition crystal shape does not change during the entire process. Based on these assumptions, the number of seed crystals (N_s) can be assumed to be conserved and the crystal morphology (represented by the shape factor constant, F) does not change. Given crystals with a characteristic size of S_s (μm) for seeds and S_{ip} (μm) for the ideal product crystals, the ratio between the final mass of crystals and the mass of seeds becomes:

$$\frac{W_f}{W_{seed}} = \frac{FNs\rho_s S_{ip}^3}{FNs\rho_s S_s^3} = \left(\frac{S_{ip}}{S_s}\right)^3 \quad (6\text{-}6)$$

where ρ_s is the density of solid crystal (g ml^{-1}). The final mass of crystals produced, W_f (g), is a sum of the seed mass, W_{seed} (g), and the theoretical yield, W_{theo} (g) as:

$$W_f = W_{seed} + W_{theo} \quad (6\text{-}7)$$

Rearrangement and substitution of Eq. (6-5) and Eq. (6-7) into Eq. (6-6) yields:

$$\frac{W_f}{W_{seed}} = \frac{W_{theo}C_{seed}+W_{theo}}{W_{theo}C_{seed}} = \frac{1+C_{seed}}{C_{seed}} \quad (6\text{-}8)$$

By equating and rearranging equations (6-6) and (6-8), we have:

$$\frac{S_{ip}}{S_s} = \left(\frac{1+C_{seed}}{C_{seed}}\right)^{1/3} \quad (6\text{-}9)$$

As a result of Eq. (6-9), the ideal characteristic size of the product crystals, S_{ip} (μm) can be calculated when the mean size of seed crystals S_s (μm), and the seed loading, C_{seed} (%), are known. The relationship of the ideal normalized product size (S_{ip}/S_s) can graphically be represented as a function of the seed loading/mass, as shown in Figure 6.4.

The solid line in the seed response curve represents the effect of seed loading on the normalized product size; a decrease in the normalized product size is seen with increased seed loading. This is because the theoretical mass of crystals produced could consist of either numerous small crystals or fewer large ones, each seed crystal grows to a smaller final size than if there were fewer seeds at the same supersaturation, thus the increase of the seed loading in Figure 6.4 leads to the increase of the number of crystals. This trend was also reported for adipic acid – water systems[103], potassium alum – water

systems[247] and ammonium aluminium sulphate –water systems[246] in a batch stirred tank crystallizer (STC).

The seed response graph is also a very useful means for assessing seeding strategy, as the seed response curve itself represents the growth-dominated mechanism. Above the curve is associated with normalized product sizes being larger than the ideal values, in order to maintain such crystal growth this region is facilitated by non-encrustation; below the curve is the area where the final normalized product sizes are smaller than S_{ip}/S_s , two phenomena can contribute to this, either the occurrence of primary nucleation leads to massive small crystals without control or insufficient seed crystal surfaces for the solute material to grow on, solute molecules move to the reactor walls, leading to severe encrustation and blockage when seeds of larger sizes are combined with smaller seed loading[60]. To investigate the effect of seed loading on the final crystal products in this work, three seed loadings (10, 15 and 20 w/w %) were utilized in this work at a fixed seed size. The normalized actual product sizes (S_p/S_s) are the diamond symbols in Figure 6.4, where S_p refers to the actual size of final products (average of 5 measurements).

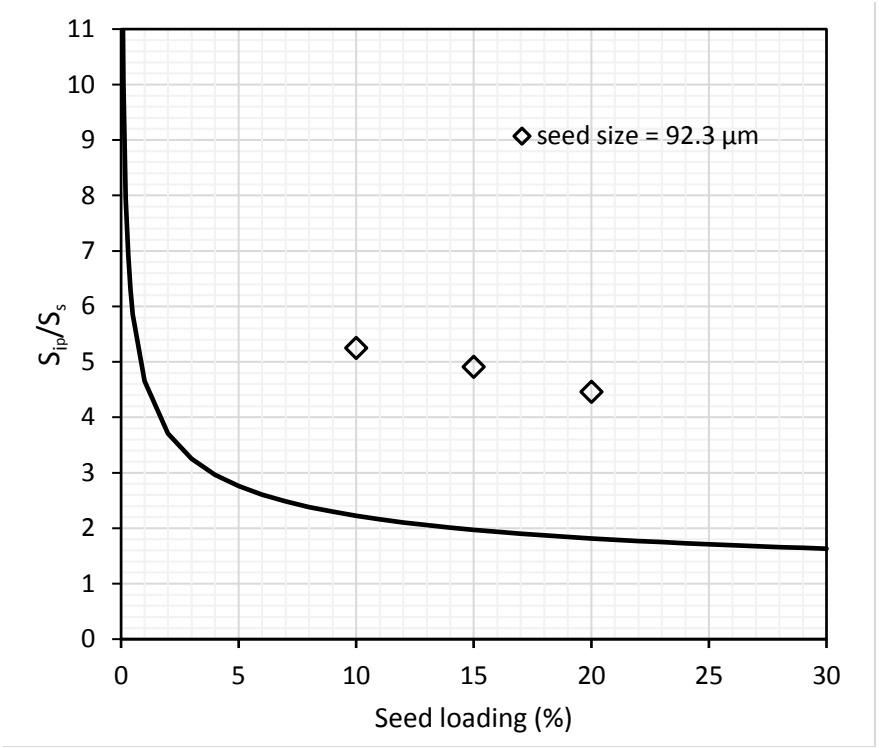

Figure 6.4 Seed response curve and actual product/seed ratios in COBR with a mean seed size of 92.3 µm

Blockages were dominant when the seed load was 0 % and 5 % in this work, the problem was solved by increasing the seeding load up to 10%, no encrustation was observed after running for 6 residence times (see Appendix Figure E.1B). Crystallizing slurry was mixed uniformly in tubes and the temperature/supersaturation control ensures sufficient crystal growth. Three regions along the COBR were set for the dissolution and mixing of reactants; the reaction region and the seeded cooling crystallization region (Figure E.1C). Product samples were collected at sample point 3 after 2 residence times: slurry samples were filtrated and washed before drying in the oven, whereas filtrates were analysed by HPLC measurement to track and confirm steady states.

When the seeding load increased from 10 % to 20 % in the continuous operation, the sizes of final products were 485, 453 and 412 μm respectively, giving the values of S_p/S_s of 5.25, 4.91.and 4.46, showing in the region above the seed response curve (Figure 6.4). Based on the above, seed loading of 15% was selected for experiments in this work. Accordingly, neither encrustation nor blockage was observed in the COBR for over 6 residence times that were the longest running time undertaken in this work.

The practical means of calculating seed mass is as follows. The theoretical solid mass concentration was 34.73 g kg^{-1} in this work when the temperature decreased from 75 ºC to 35 ºC, according to the solubility data[242]. Combining with the flow rate data in Table 6.1, the value of W_{theo} was calculated as 1.389 g min^{-1} by Eq. (6-10). Consequently, the solid concentration for seeding solution was 20.84 g kg^{-1}. To prepare this, 57.95 g paracetamol solid was added into 1 kg solvent (Acid: H_2O = 1:9 w/w) as the solubility of paracetamol was 37.11 g kg^{-1} at 50 ºC[242].

$$C_{seed} = \frac{\text{seed concentration} \times F_{seed}}{\text{crystal products mass concentraton} \times F_{main}} \times 100\ \% \qquad (6\text{-}10)$$

where F_{seed} (g min^{-1}) and F_{main} (g min^{-1}) are the flow rates of the seed suspension and the solution, respectively.

The fact that the actual product crystal sizes are larger than that predicted by the un-agglomerated growth model in Figure 6.4 suggests the existence of agglomeration, although the degree of agglomeration is difficult to estimate, as this would require data of breakage of crystals as well as crystal shape. Nevertheless, the agglomeration is

confirmed by macroscopic and SEM images in Figure 6.6 & 6.9. Briggs et al.[192] reported similar results in seeded crystallizations of β-L-glutamic acid in a COBR, indicating that the decrease of the number of seed crystals was caused by agglomeration among seed crystals.

6.3.3 Metastable zone width and operational path

Figure 6.5 shows the measured paracetamol concentrations at sample point 1 (after the reaction) and 3 (at the end of crystallization) superimposed with solubility and metastable zone width obtained previously[242, 248] . The concentrations of paracetamol at point 1 are almost the same, this is as expected due to the same ratios of starting materials and the same feeding flow rates in the reaction step. It can be seen that the solution was supersaturated post reaction at the sample point 1 at 75 ºC, the solution concentration decreased after the seeded crystallization, all within the metastable zone and close to the solubility curve. The three data points at each of the sampling locations were obtained at a fixed oscillation frequency, but different amplitudes. It is clear that the higher the oscillation amplitude, the lower the solution concentration, in turn the higher supersaturation for nucleation and crystal growth. This is expected as an increased mixing enhances energy dissipation and turbulence in the system[165, 171], a solution of which is closer to its solubility curve[51].

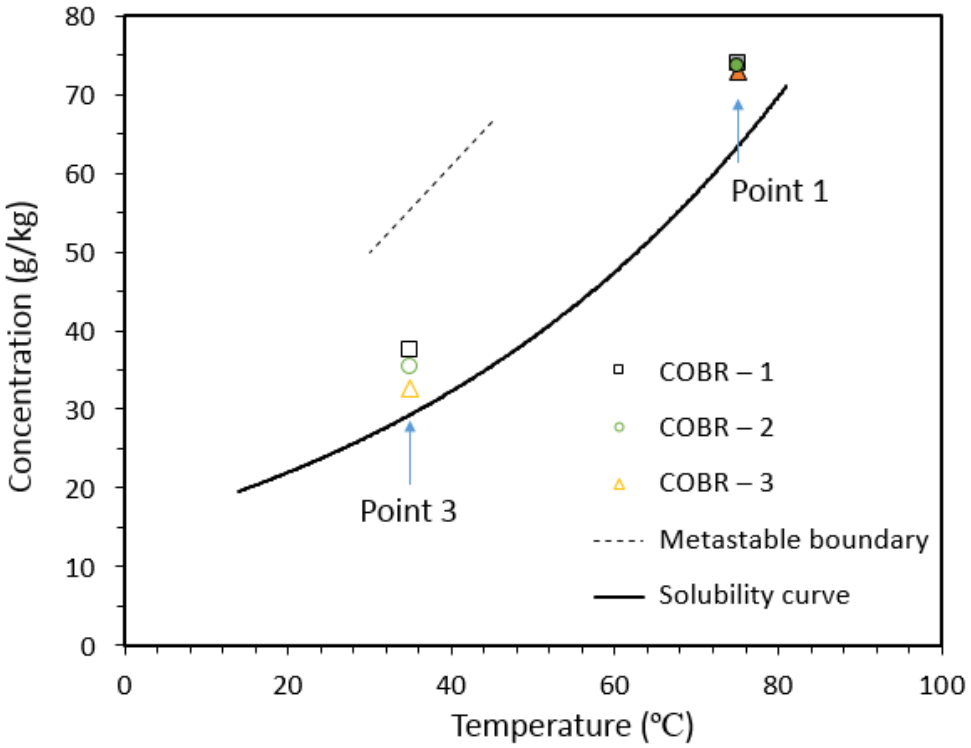

Figure 6.5 Solubility, metastable zone and crystallization path measurened gravimentrically in a solvent ratio of Acid : H_2O = 1:9[242, 248] Open symbols – concentrations after crystallization. Close symbols – concentrations just post reaction

The data of runs COBR 4 – 6 (Table 6.2) were obtained at a fixed oscillation amplitude but varying frequencies. Figure 6.6 shows the effect of oscillatory Reynolds number on the average size of crystal products; particle size decreased from 527 µm to about 364 µm for Re_0 from 989 to 2120. The trend of this work agrees with that by Lawton et al.[12] where oscillation frequency/amplitude had a similar effect on crystal size distributions. The shape of final crystals in this work were of column/plate like, the length of crystals was reducing with the mixing intensity. While agglomerates existed in all products, high mixing intensities can reduce the degree of agglomeration, which can affect the size measurements via Mastersizer. Moreover, attrition due to fragments of parent crystals was more likely to occur at higher mixing intensity during crystal growth. Multiple attrition mechanisms deduced in previous literature[249, 250] suggested that the fragments most likely formed by chipping and shattering could affect the whole size distribution. This can explain the slope change in the decreasing size with Re_0 (see Figure 6.6) showing the effect of mixing is more obvious at lower Re_0.

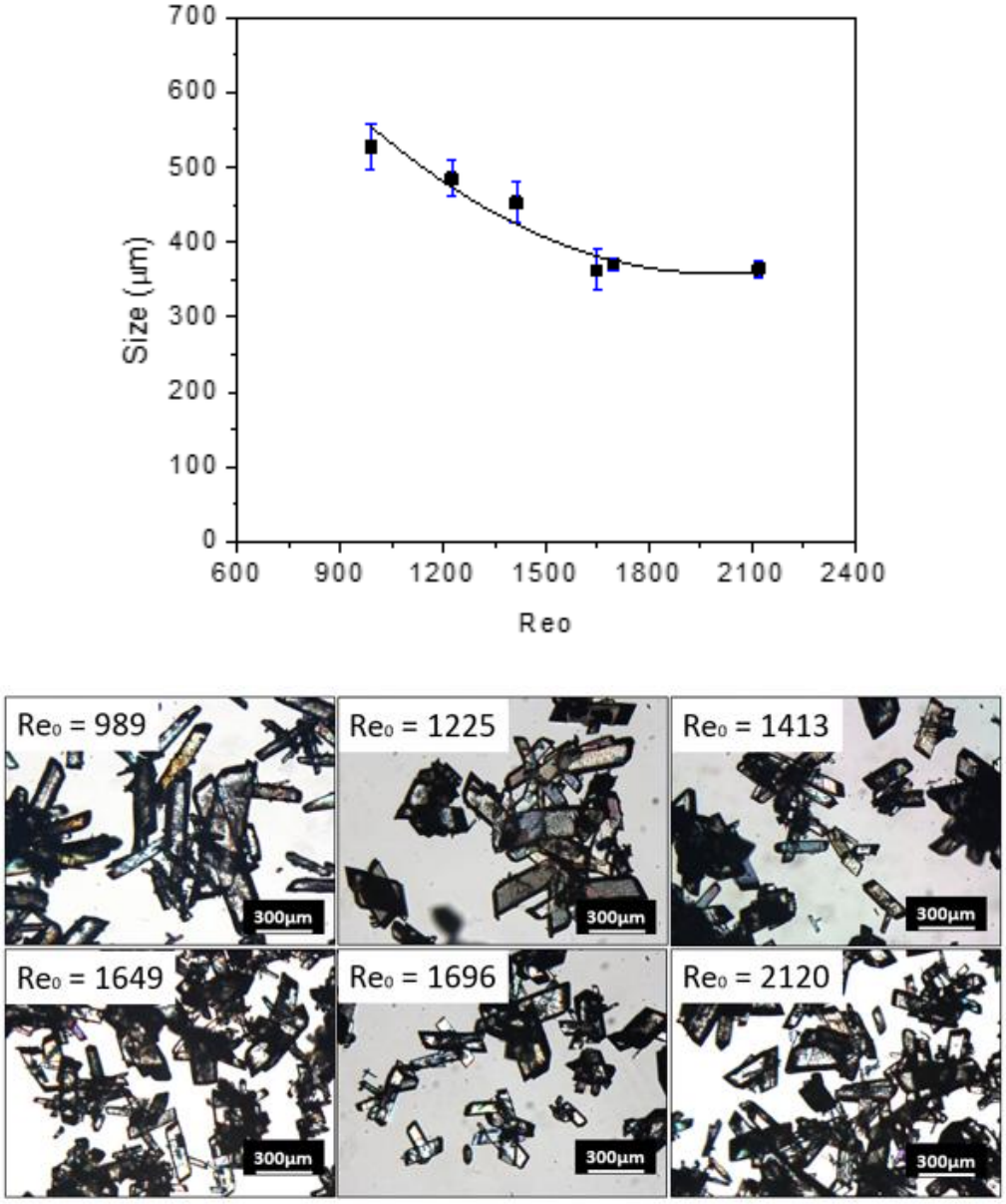

Figure 6.6 (up) the effect of oscillatory Reynolds number on crystals size; (down) images of crystal products under different mixing intensities

6.3.4 Steady state and crystal properties

For a batch crystallization process, the entire batch is cooled from a starting to an end temperature in a temporal domain. For a continuous process, however a very small fraction of solution is passing through pre-set temperature zones in a spatial domain; solution concentrations and crystal sizes measured at two different locations along the COBR enable the determination of spatial steady states, the rate of supersaturation consumption and local crystal growth rate. Solution concentrations and crystal sizes measured at different times in the same location in COBR allows the determination of

temporal steady states. In this work, samples were taken at three sampling points 1-3 along the COBR after 2 residence times as shown in Figure 6.2 and these concentration profiles as a function of time are displayed in Figure 6.7. Firstly, the concentration decreased from C1 to C3, verifying the correct operational path. Secondly the temporal steady states of concentration C1, C2 and C3 are clearly seen in Figure 6.7 where the difference in concentrations over different times is very small. Note that there is a tiny time delay at the start for C3 compared to C2 due to its location away from the feeding point. The spatial steady states of concentration can be assessed by the differences between C1 and C2, C1 and C3, C2 and C3, have also been achieved due to constant difference over time. This indicates that crystallization occurs when the reacted solution flows from sample point 1 to point 2, and paracetamol particles keep growing while moving from point 2 to 3.

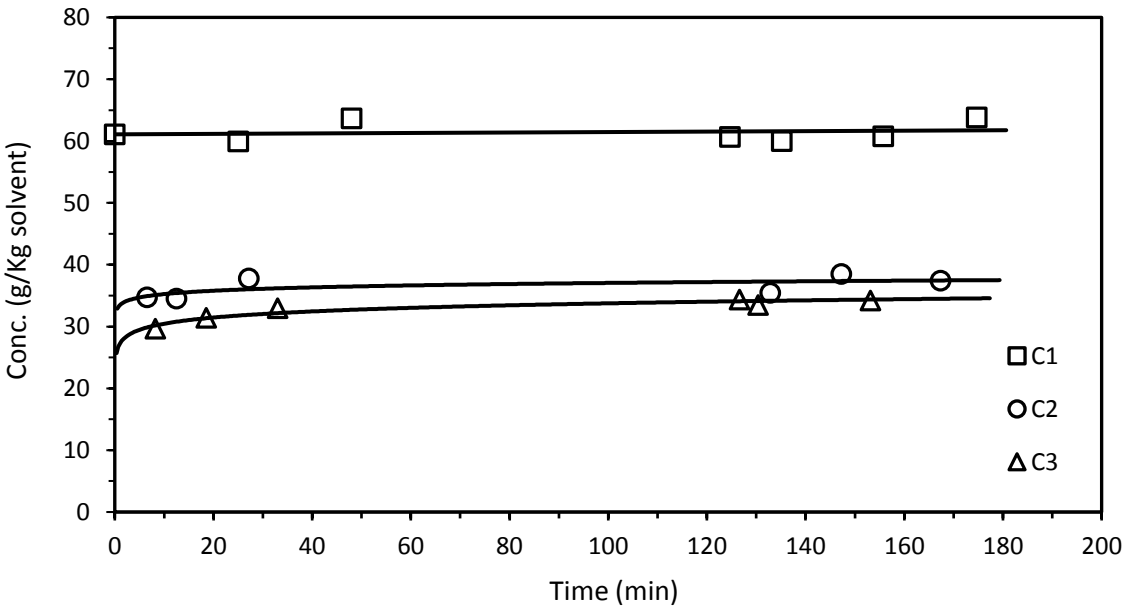

Figure 6.7 Concentration profile of C1-C3 in the COBR. Trend lines show the temporal steady state of solute concentration, constant distances between trend lines indicate the spatial steady state

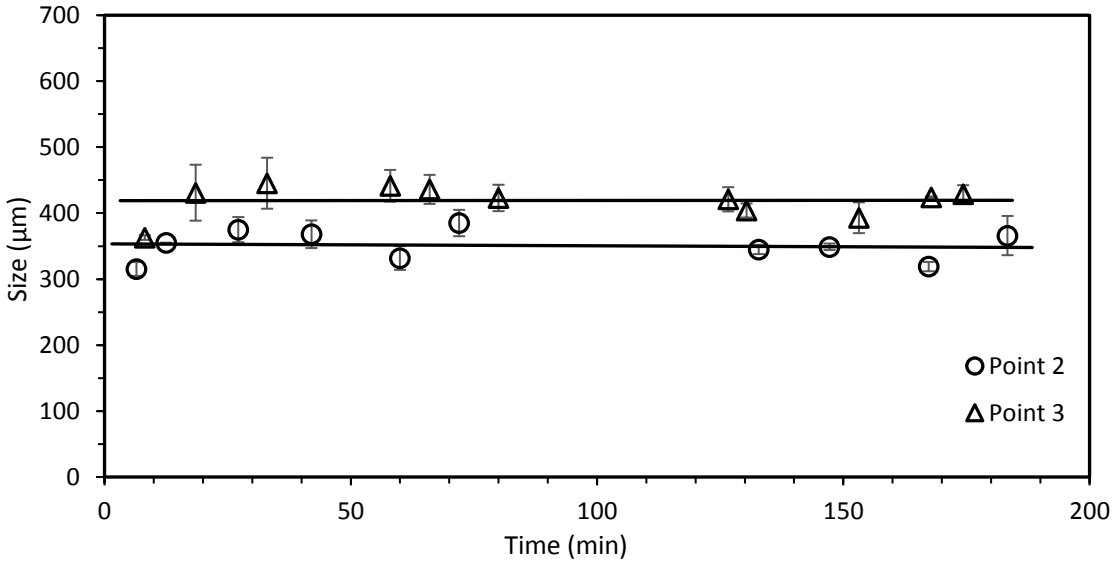

Figure 6.8 Size measurement for particles taken at sample point 2 and 3, trend lines show the temporal steady state of crystal size, constant distance between trend lines illustrates the spatial steady state.

Figure 6.8 shows the profile of mean particle sizes over time at sampling points 2 & 3. Crystal sizes increase from 350.95 µm at point 2 to 419.17 µm at point 3 extracted from SEM images in Figure 6.9. The temporal steady state was generally achieved with small fluctuations observed for particle sizes over time. Similarly, Brown et al.[14] reported both temporal and spatial steady states for solute concentrations in an anti-solvent crystallization of salicylic acid in a COBR, however, the temporal steady state for crystal size was unattainable due to the unstable flow rates, while spatial steady state in crystal size was obtained. It should be noted that, although Figure 6.9 shows crystal growth for individual paracetamol particles, agglomerates are found in most of solid products. In that case, both crystal growth and agglomeration have contributed to the increase of particle sizes shown in Figure 6.8.

The constant increase in crystals size between the two locations denotes that the spatial steady state was attained. Given a fixed distance of 1.7 m and the flow rate of 50 g min^{-1}, the local crystal growth rate between the two locations is calculated as 1.89 × 10^{-7} m s^{-1} for the supersaturation ratio of 1.10. This is comparable with previous literatures on paracetamol growth kinetics [84, 86, 143, 236]. If we assume a linear relationship between supersaturation and crystal growth[51], the overall growth rate would be 3.14 ×

10^{-7} m s^{-1} for the global supersaturation of 1.82 in this work. Although the level of supersaturation is a bit higher than previous studies, the growth rate is comparable with results of Mitchell et al.[84] and Worlitschek [238] of paracetamol in ethanol. The crystal growth rate for a reactive unseeded cooling crystallization of paracetamol in a batch OBR was 4.30×10^{-7} m s^{-1} under a similar supersaturation (S=1.91)[248], the higher value for the unseeded process indicates less control over crystal growth rates. An overall growth rate of 6.36×10^{-7} m s^{-1} was reported for antisolvent crystallization of paracetamol, which is also higher than our data of cooling crystallization[65].

By assuming that the local growth rate is fully fueled by the consumption of the driving force (supersaturation)[51], the growth rate constant, k, was evaluated as 5.74×10^{-5} kg m^{-2} s^{-1}, which is lower than 3.7×10^{-4} kg m^{-2} s^{-1} for the reactive unseeded crystallization of paracetamol in an OBR[248] . This is likely attributed to the utilization of seeds for controlling the growth rate.

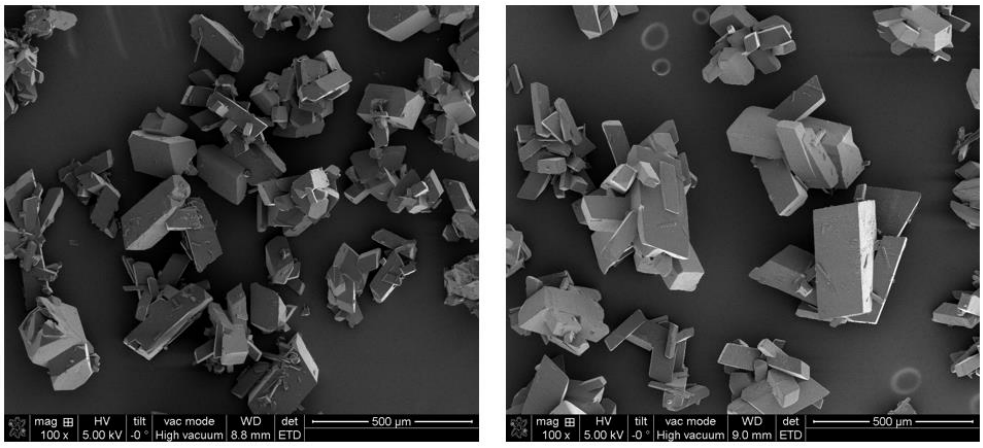

Figure 6.9 SEM images for particles taken at sample point 2 (left) and 3 (right), showing crystals growth along COBR

In general, SEM images of crystal products in the COBR in Figure 6.9 display elongated column shapes, which is the same as that in an OBR at the same solvent composition[248].

The XRD results for particle products are shown in Figure 6.10. It should be noted that different intensities (the vertical axis) are observed and compared with those of paracetamol products from OBR operations (see Figure 4.11). For paracetamol form I, there should be a peak with a high intensity (100) at about 24.37º and two peaks with intensities of 68 and 62 at 18.18 º and 23.48 º respectively[211, 251]. However, the latter two peaks are very small for the products made in the COBR (Figure 6.10 & Figure E.8). This indicates that the particles produced in COBR are either not of form I or a mixture of two polymorphs. Moreover, peak intensities at 12 º and 14 º are varying among different samples over time (see Appendix Figure E.8), highlighting the effects on crystals size and morphology. Research on paracetamol polymorph transformation in COBR can be an interesting topic for future study.

Crystals obtained from COBR were analyzed by HPLC, giving an average purity of 99.96% from 8 samples taken at sample point 3 (see Appendix Figure E.6).

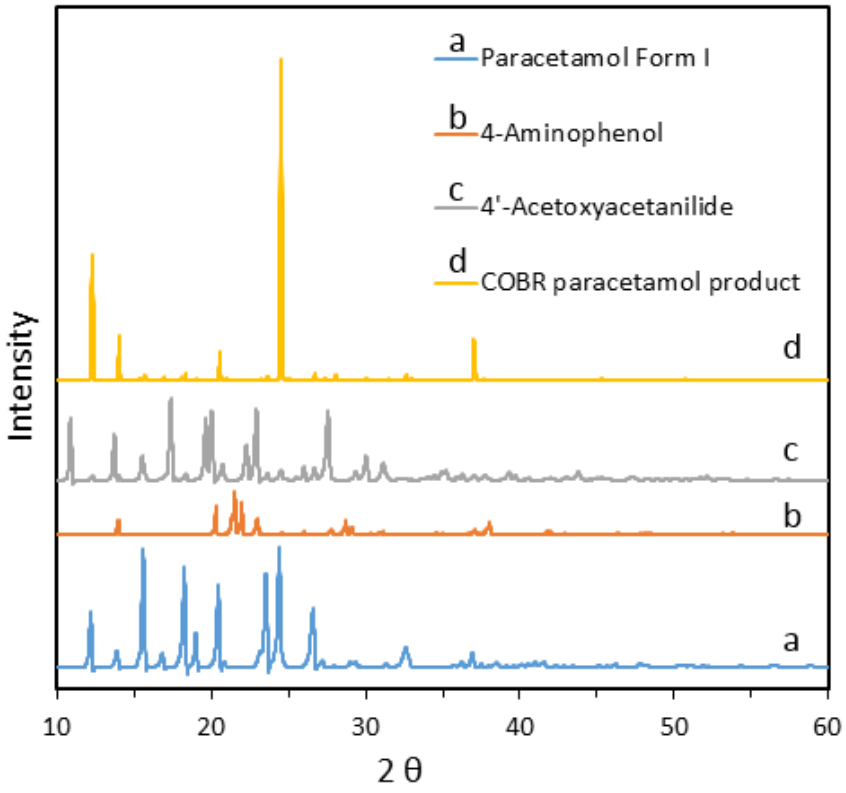

Figure 6.10 PXRD data for paracetamol particles produced in this work as well as purchased paracetamol (Form I) and possible impurities of 4-aminophenol and 4'-acetoxyacetanilide from previous study[242]

6.4 Conclusions

For the first time, a reactive seeded cooling crystallization of paracetamol was successfully carried out in a COBR. The seeding strategy of three seed masses (10, 15, and 20 %) at a fixed size was investigated in this work, enabling smooth and encrustation free runs with the crystallization path close to the solubility curve. Crystal agglomeration was also assessed by comparing the ideal to actual normalized product sizes. The effect of mixing intensity on crystal properties was discussed, crystals size reduced with the increase of R_{eo} number. By analyzing the concentrations and crystal sizes at two locations along the COBR, both temporal and spatial steady states in concentration and size were attained. The local growth rate was found to be 1.89×10^{-7} m s^{-1} when crystals flowed from point 2 to point 3, with the predicted overall growth rate as 3.73×10^{-7} m s^{-1} for a global supersaturation of 1.82. Crystals of polymorphic form I were continuously generated with an average purity of 99.96 %.

Chapter 7 – **Conclusions and recommendations for future work**

This chapter presents the summary of conclusions reached in previous chapters for this PhD work. Suggestions for future study are also put forward.

7.1 Conclusions

The reactive crystallization of paracetamol is considered as a single process for the purpose of continuous operation. The solubility for crystallization was optimized firstly, from which suitable reagent concentrations were determined. As in a single process, solubility for crystallization in the reactive crystallization of paracetamol is controlled by the solvent compositions that are directly produced in the reaction step.

The effects of reaction temperature and water content on reaction kinetics and mechanism as well as product quality were jointly investigated for the first time.

- Higher reaction rate constants for paracetamol synthesis are obtained for higher temperatures;

- Form I crystals with high purity are obtained in the presence of water, and 4'-acetoxyacetanilide without water. The presence of water can consume acetic anhydride, inducing the side reaction to the left hand direction. Thus more paracetamol can be formed instead of byproduct.

The dependency of nucleation orders and growth rates on solvent compositions was examined in an OBR:

- The nucleation orders for the three solvent systems used in this work are comparable, but higher than published data. A higher ratio of Acid: H_2O led to

a higher nucleation order; growth rates are comparable with previous recrystallization data;

- Both solvent compositions and reagent ratio are the means for influencing crystal morphology: crystals shapes change from column to needle-like with the increase of solvent compositions. At a fixed solvent, various supersaturation levels generated from different reagent ratios of AA: 4-AP also led to the similar changes to crystal morphologies.

It is demonstrated that the reagents and solvents from the reaction step are the means for controlling and delivering required crystal properties. Agglomerations are observed in the solvent of a low Acid: H_2O ratio and are likely influenced by the impurity PAA on crystal particles.

Finally, based on the above researches on reaction kinetics and crystallization kinetics under different conditions, this PhD work reports, for the first time, a reactive seeded cooling crystallization of paracetamol successfully carried out in a COBR. Effects of mixing intensity on crystal properties are discussed, crystals size reduces with the increase of R_{eo} number.

The seeding strategy was also investigated and a seeding map was established, with the correct combination of seed size (fixed in this work) and seed mass (10, 15, and 20 %), smooth and encrustation free runs are undertaken following the crystallization path close to the solubility curve.

Both temporal and spatial steady states in concentration and size are attained by analysing the concentrations and crystal sizes at two locations along the COBR. The local growth rate is found to be 1.89×10^{-7} m s^{-1} when particles flowed from point 2 to point 3, with the overall growth rate predicted to be 3.73×10^{-7} m s^{-1} under a global supersaturation of 1.82. Particle products are continuously generated in polymorphic form I with an average purity of 99.96 %.

7.2 Recommendations for future work

Based on this PhD research, some recommendations for future work are outlined below:

- Effects of solvent compositions and impurity on nucleation and growth kinetics could further be investigated combining the single crystal x-ray diffraction (SXRD) method. As known from this work that different reaction conditions generate different crystal morphologies, the growth rate for different crystal faces could be obtained and the information of interactions between solvent molecules or impurity on crystal surfaces can be collected. Thus the mechanism of adsorption of non-target molecule onto crystal lattice could more clearly be understood. Moreover, this can provide valuable information on polymorph transformations in such continuous system. For instance, Agnew et al.[243] produced paracetamol form II crystals in a COBR using a structure-related chemical, metasetamol, as a template molecule. The form II crystals give a block-like morphology which is different with previous literatures[209, 252] who reported that a block-like morphology was form I and a needle/elongated habit was form II. This illustrates that when the template forces the change of the polymorphic form, other crystal habits such as morphology will also be affected. Potential opportunities for other structure-related chemicals like PAA in this work should be investigated in conjunction with polymorph transformations.

- Reactive antisolvent crystallization is another area of research for future study. This requires solubility data of the product compound in both reaction solution and a proper anti-solvent. Similarly, reactive co-crystallisation could also be another research subject for investigation.

- The self-consistent Nývlt-like equation from Sangwal[126] provided a linear relationship between the intercept and initial saturated temperature T_0. For a specific solvent, the activation energy for crystals nucleation could be obtained from the slope by plotting intercept against different initial saturated temperatures. The value of T_0 in this work could be controlled by changing the ratio of AA/4-AP.

Thus more information on continuous reactive crystallization of paracetamol in COBR can be obtained.

- In this work, only one seed size was used, effects of seed size, seeding point or temperature on crystal properties should be investigated, leading to a more complete seed map.

  In addition, there are three temperature zones in total in the COBR research, only two of which are applied for the cooling crystallization step. More temperature zones can be setup to minimise any sudden temperature drop between reactor walls and the jacket, therefore to reduce any potential encrustation phenomena during crystallization.

- More in-situ process analytical technologies could be applied to the reactive crystallization process. While off-line HPLC and Mastersizer were employed in this research to monitoring solute concentrations and crystal size, errors might be induced in the sample preparation step. In-situ measurement could be more efficient and accurate for real-time operations, such as the focused beam reflectance measurement (FBRM) for tracking the changes of particle counts and online HPLC for measuring solute concentrations. In achieving that, a closed loop control system could possibly be established by using real time feedback from PATs, which in turn helps to control and monitor the operating conditions by gradually adjusting a few parameters such as cooling rate and mixing intensity.

- Paracetamol was chosen as a model compound in this work due to its significant application and simple operation requirements. From the comprehensive list of potential recipes in the Appendix (Table A.1 and Table A.2), other compounds of small as well as large molecules should be tested to enlarge the applicability, reliability and capability of the systems.

- The work conducted so far involved the reaction and crystallization steps, the final products were collected into a product tank without separation. In the future, the outlet of COBR can be connected to a continuous filtration/drying device where

crystal products are directly filtrated, washed and dried. These would enable more feedback of crystal properties, and in turn better control.

Furthermore, the recycling of mother liquor would enhance yield, would also allow monitoring of overall concentrations of both paracetamol and side product.

Appendix A-Potential chemicals for a reactive crystallization

Table A.1 List of pharmaceutical chemicals of small molecular weight for a reactive crystallization

Chemical[5, 6, 93, 95, 96, 129, 215, 253-257]	Molecular Weight (g/mol)	Application	Reaction	Reaction time	Reaction temperature	Solubility	Theoretically yield	Feasibility
Aspirin	180	Analgesic and antipyretic	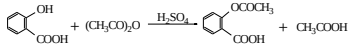	10-20 min	70-75°C	3.3g/L(20ºC), 10g/L(37ºC),	80%	√
Paracetamol	151	Analgesic and antipyretic	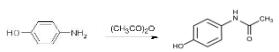	20-30 min	80°C	12.78g/L (20ºC), 14g/L (25ºC), 17.4g/L (30ºC), 50g/L (100ºC)	74.6%	√
Benzoic Acid	122	Expectorant, analgesic Treat fungal skin diseases	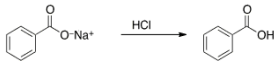	20 min	25°C	1.7 g/L (0 °C), 2.7 g/L (18 °C), 3.44 g/L (25 °C), 5.51 g/L (40 °C), 21.45 g/L (75 °C), 56.31 g/L (100 °C)	90%	√
L-glutamic Acid	147	Decrease or prevent nerve damage caused by anticancer drugs	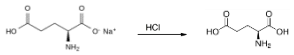	15min	80°C	7.2g/L (20 °C), 8.8g/L (25°C), 15.1g/L (40°C), 31.7g/L (60°C), 66.6g/L (80°C)	91%	√
Nicotinic Acid (Niacin)	123	treat niacin deficiency (pellagra) lower cholesterol and triglycerides and lower the risk of heart attack		ph=3-4	85°C	15g/l at 20°C, 16.67g/L(25°C), 150g/l at 100 °C		√
Coumarin-3-carboxylic acid	190	Anti-platelet aggregation Anti- blood clot	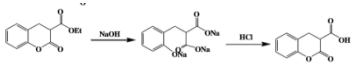	15-30min	70-80°C	13 g/L (37°C)	80%	√
4-methylacetanilide	149	Organic synthesis intermediate	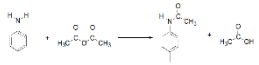	<60min	50°C	1 g/L (25 ºC)	86.30%	√
Vanisal sodium	256	Soap formulations	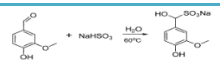	<30min	60°C	/	/	√
Salicylic acid	138	Anti-inflammatory	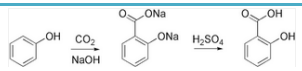	30min	30°C	1.24 g/L (0 °C)，2g/L(20 °C), 2.48g/L (25 °C), 4.14 g/L (40 °C) 17.41 g/L (75 °C), 77.79 g/L (100 °C)	88%	√

Sodium acetate	82	Food additive and pickling agent or a laboratory reagent	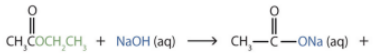			1190 g/L (0 °C), 1233 g/L (20 °C), 1255 g/L (30 °C),1372 g/L (60 °C), 1629 g/L (100 °C)	27%	×
Sodium salicylate	160	Analgesic and anti-inflammatory induces apoptosis in cancer cells		ph=5.4～5.8	70℃(60-85C)	107.9 g/100 mL (15 °C) 124.6 g/100 mL (25 °C) 141.8 g/100 mL (78.5 °C)	24%	×
Acetanilide	135	Analgesic and antipyretic	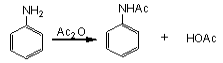	30-60min	40℃	4.6g/L（20℃)、5.6g/L（25℃）、8.4g/L（50℃）、55g/L（100℃）		×
4-Chloro-benzoic acid	157	An intermediate for manufacturing dyes, fungicides, pharmaceuticals	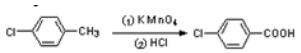	**4 hours**	70-90°C	/		×
DL-Mandelic acid	152	Antibacterial for urinary tract infections antibiotic	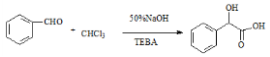	/	/	150 g/L (20 °C), 181g/L(25°C),		×
Sulfacetamide Sodium	236	An antibiotic to treat bacterial infections of the eyes	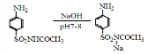	30min	90°C	/		×
Benzocaine	165	A local anesthetic a pain reliever	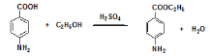	60min	95-98ºC	1.31g/l(25°C)	30-41%	×

Table A.2 List of pharmaceutical chemicals of large molecular weight for a reactive crystallization

Chemical[5, 6, 93, 95, 96, 129, 215, 253-257]	**Molecular Weight (g/mol)**	**Application**	**Reaction**	**Reaction time**	**Reaction temperature**
Clorprenaline Succinate	543	Relieve bronchospasm and palpitations	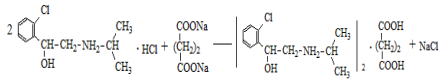	<60min	Room temperature
Phenytoin-Zn	568	Anti-epileptics	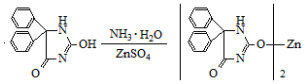	<60min	Room temperature
Sulfadiazine-Zn	564	Deal with burn wounds	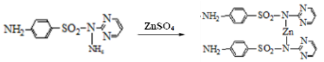	<60min	Room temperature
Piperazine Ferulate	475	Anticoagulants for cardiovascular and cerebrovascular diseases	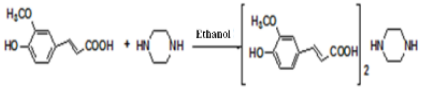	60min	60 ºC
Tetramethylpyrazine Ferulate	525	Anticoagulants for cardiovascular and cerebrovascular diseases	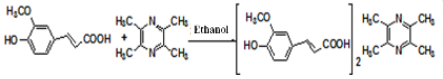	60min	60 ºC

Appendix B-Solubility of paracetamol

Table B. 1 Solubility of paracetamol in mixture of acetic acid and water with different ratios

Acetic acid: Water	0:10		3:7		5:5		7:3		8:2		10:0	
Temp. (ºC)	**Cs**	**SE**	**Cs**	**SE**	**Cs**	**SE**	**Cs**	**SE**	**Cs**	**SE**	**Cs**	**SE**
20	8.06	0.44	32.55	8.27	65.36	7.86	96.83	1.71	49.63	10.31	39.45	1.08
35	12.8	0.56	57.76	6.16	106.38	3.99	139.19	4.26	82.33	15.1	57.17	2.75
50	20.89	2.24	106.05	1.09	157.67	11.45	201.96	11.89	122.52	13.24	83.96	7.16
65	32.62	2.35	127.13	8.05	191.6	9.49	274.02	7.66	184.39	44.12	132.95	5.27
75	49.6	6.19	156.77	5.75	297.26	12.61	401.23	15.36	254.95	28.22	173.37	14.93

*Cs – Solubility of paracetamol (g kg^{-1} s_{olvent})
SE- standard error

Appendix C-Experimental procedures for reaction kinetic study

C1. Sample calculations for reactants contents according to the solubility data

The reactants for a 100ml scale synthesis at different temperatures are shown in Table C.1.

Table C. 1 Reactants dosages for synthesis crystallization at different temperatures

Temperature	*4-Aminophemol*	*Acetic Anhydride*	*Distilled Water*
75 °*C*	14.48 g	36.53 g	19.05 g
65 °*C*	9.89 g	34.38 g	19.43 g
50 °*C*	7.29 g	33.16 g	19.65 g

Taking the reactive crystallization at 75 °C as an example, according to the solubility data, with the solvent ratio at 7:3, solubility of paracetamol at 75°C is 401.23g $kg^{-1}_{solvent}$. The mass weight values of 4-aminophenol, acetic anhydride, paracetamol and acetic acid are 109.13 g mol^{-1}, 102.09 g mol^{-1}, 151.16 g mol^{-1} and 60.05 g mol^{-1} respectively. In order to produce 20.06g paracetamol in 50g of solvent, the weight of reactants and acetic acid were firstly calculated, as follows:

Weight of 4-aminophenol $=\frac{20.06\text{g}\times109.13\text{g mol}^{-1}}{151.16\text{g mol}^{-1}}$ = 14.48 g;

Weight of acetic anhydride = $\frac{20.06\text{g}\times102.09\text{g mol}^{-1}}{151.16\text{g mol}^{-1}}$ = 13.55 g;

Weight of acetic acid = $\frac{20.06\text{g}\times60.05\text{g mol}^{-1}}{151.16\text{g mol}^{-1}}$ = 7.97 g.

The paracetamol produced is required to be dissolved in a mixture solution of acetic acid and water with a ratio of 7:3. Hence, for 50g of solvent, the total amounts of water and acetic anhydride were determined by considering the hydrolysis reaction (See Figure 4.5 reaction (2)) as:

Weight of acetic acid = $0.7 \times 50\text{g} - 7.97\text{g} = 27.03\text{g}$;

Weight of acetic anhydride = $\frac{27.03\text{g} \times 102.09\text{g mol}^{-1}}{2 \times 60.05\text{g mol}^{-1}}$ +13.55g = 23g + 13.55g = 36.55g;

Weight of water = $\frac{27.03\text{g} \times 18.02\text{g mol}^{-1}}{2 \times 60.05\text{g mol}^{-1}}$ + 0.3×50g = 4.28g + 15g = 19.28g.

Therefore, the theoretical amounts of reactants required are: 4-Aminophenol 14.48g (0.13mol); Acetic anhydride 36.55g (0.36mol); Water 19.28g (1.07mol). In practice, however, the mass of crystals at the end of cooling is so large that the mixing condition is adversely affected. On balance, the content of 4-aminophenol was therefore reduced to 10g(0.09mol), so was the temperature to 70°C and acetic anhydride to 35g(0.34mol) accordingly, this gives the best controls in both good supersaturation and better mixing.

The procedure for the reactive crystallization of paracetamol involves the following steps:

1. Weight out 14.48g of 4-aminophenol and transfer it to the jacketed beaker;

2. Add 19.05g of distilled water and 36.53g of acetic anhydride;

3. Switch on the pre-heated water bath (T_{water}=75 ºC) and mix the solution using the magnetic stirrer (r_{mixing}=200 rpm) until the amine has dissolved;

4. Mix the solution for 30 minutes;

5. Chill the mixture solution to 20 ºC with a fixed cooling rate of 1.2 ºC min^{-1};

6. Perform a vacuum filtration of the mixture, washing the crystals with distilled water and drying these in the oven;

The steps 1-4 are related to the reaction, while steps 5-6 are associated with crystallization. 16 samples were taken at regular intervals at step 4 using a pipette with a fixed volume of 0.5ml. Although the total volume of samples exceeded 10% of the volume of the reaction solution, which may have affected the bulk mixing within the beaker, samples of less or equal to 10% of the total reaction volume were taken in experiments using OBR and COBR. All the samples were quenched by 1 ml of 2% concentration of sodium hydroxide solution in a series of 100 ml flasks, together with distilled water to dilute to the mark (i.e. the same volume) on each flask.

C2. Sample calculation for solvent composition after reaction

1) For the case with 20g water,

Weight of acetic acid from synthesis reaction = $\frac{10\text{g}\times 60.05\text{g mol}^{-1}}{109.13\text{g mol}^{-1}}$ = 5.50 g.

Weight of acetic anhydride in excess = 35g - $\frac{10\text{g}\times 102.09\text{g mol}^{-1}}{109.13\text{g mol}^{-1}}$ =35g – 9.35g = 25.65g

All the excess acetic anhydride reacts with water to produce acetic acid, then

Weight of water left = 20g - $\frac{25.65\text{g}\times 18.02\text{g mol}^{-1}}{102.09\text{g mol}^{-1}}$ = 20g – 4.53g = 15.47g.

Weight of acetic acid produced totally = 5.50g + $\frac{25.65\text{g}\times 2\times 60.05\text{g mol}^{-1}}{102.09\text{g mol}^{-1}}$

= 5.50 g + 30.17g = 35.67g.

The ratio of acetic acid to water = $\frac{35.67\text{g}}{15.47\text{g}}$ = 2.3 ≈ 7:3

The results may not be exactly the same because of the significant figures kept during the calculation.

2) For reaction without water,

The ratio of acetic acid to acetic anhydride = $\frac{0.092\ \text{mol} \times 60.05\ \text{g mol}^{-1}}{(0.34-0.092)\text{mol} \times 102.09\ \text{g mol}^{-1}} = \frac{5.52\text{g}}{25.32\text{g}} \approx 0.22$

= 2:9.

C3. Data acquisition system

In the set-up for reaction kinetic study, both the thermocouple and the turbidity probe were wired to the data acquisition system, i.e. NI Compact DAQ USB chassis (National Instruments Corp., NI cDAQ-9174), and controlled by the LabVIEW software (National Instruments Corp., NI LabVIEW^{TM} 2010, version 10.0). The signals can then be transferred to the computer via an analogue to a digital converter and constantly be recorded throughout the duration of a particular experiment. A simplified diagram was developed to acquire and monitor data, shown in Figure C.1, where the signals collected from the probes were displayed in temperature and voltage respectively, and were consequently written to a Measurement File located in C:\Desktop\test\lvm. An 'Elapsed Time' Boolean control was used to specify the duration of different experiments - when the 'Time has elapsed' turned to a 'True' argument, it indicated that the experiment was completed. A 'While loop' was applied to allow the execution of the LabVIEW diagram to be repeated until the 'Logical operator' received the 'Time has elapsed' command and the program was then terminated. An iteration operator ("i") provided a current state of the loop count, starting at 0 for the first runtime.

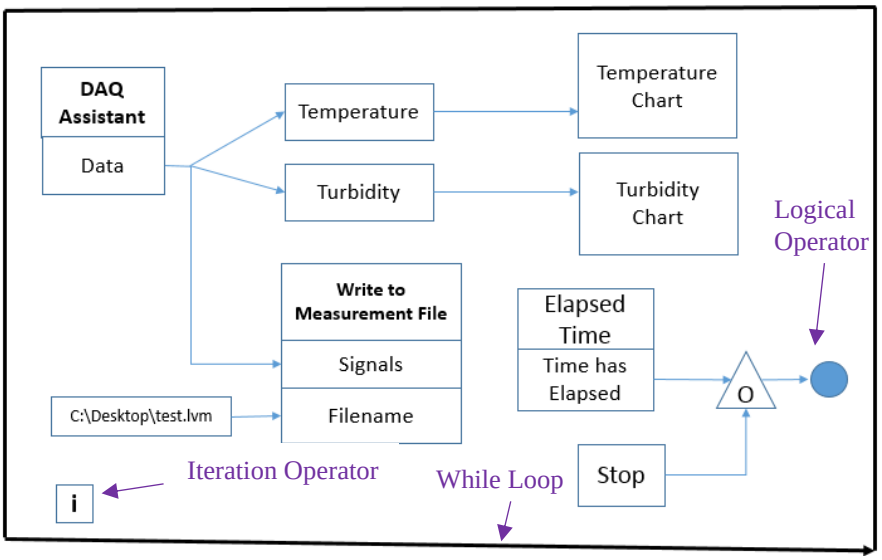

Figure C. 1 Simplified block diagram of LabVIEW program

C4. Reaction kinetics calculations

Figure C.2 shows the plot of the logarithm of the rate constant, ln k, versus the reciprocal of the absolute temperature, 1/T, with the correlation coefficient of 0.9993. This indicates that ln k' is directly depended on 1/T, whereas the activation energy E is constant in the same temperature range.

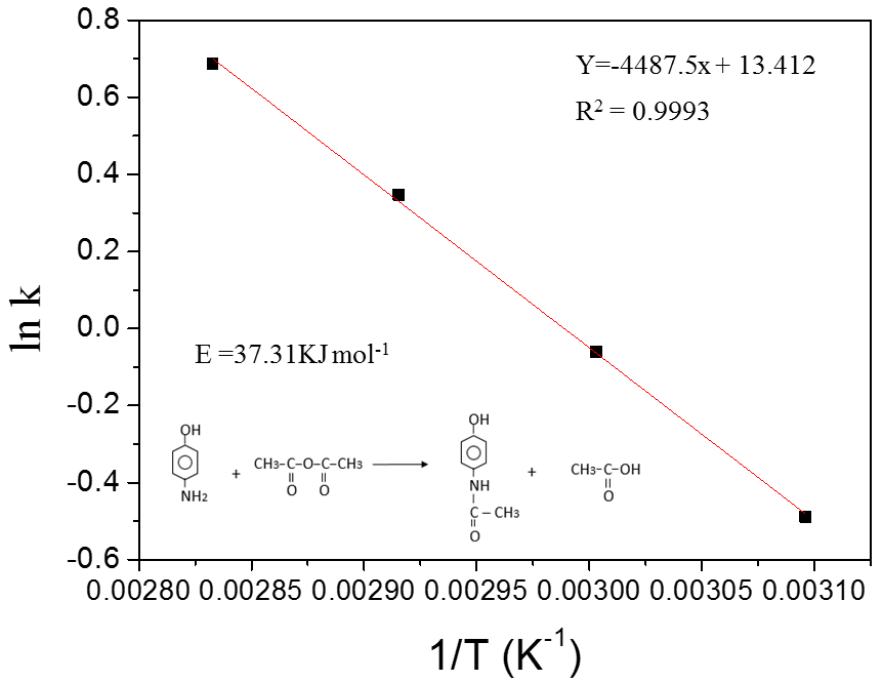

Figure C. 2 Plot of the logarithm of the rate constants (ln k) vs the reciprocal of absolute temperature (1/T, K^{-1})

According to the linear regression, ln k' = -4487.5 $\frac{E}{R}$ + 13.412, the activation energy was calculated to be 37.31KJ mol^{-1}.

C5. Synthesis mechanism

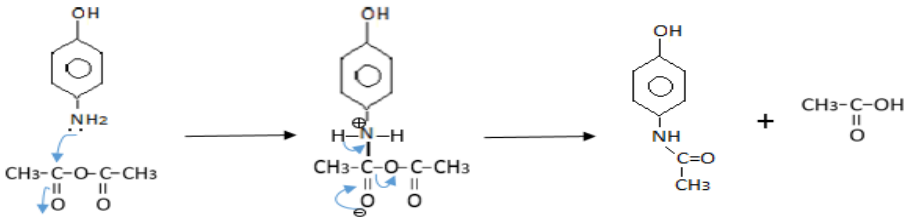

Figure C. 3 The reaction mechanism of paracetamol synthesis[219]

C6. Purity measurements

Table C. 2 HPLC data for components under different reaction conditions

No	Sample name	Paracetamol (%)	SE	4'-Acetoxyacetanilide (%)	SE
1	STD-Paracetamol	99.80	0.12	0.00	0.00
2	STD-4'-acetoxyacetanilide	1.59	0.20	99.00	1.87
3	Reaction at 50°C	100.36	0.63	0.00	0.00
4	Reaction at 60°C	101.01	0.29	0.00	0.00
5	Reaction at 70°C	99.63	0.17	0.00	0.00
6	Reaction at 80°C	98.60	1.45	0.00	0.00
7	reaction with 0g water	2.95	0.02	97.15	0.70
8	reaction with 5g water	96.00	0.86	3.87	1.03
9	reaction with 10g water	99.61	2.17	0.00	0.00
10	reaction with 20g water	99.05	0.13	0.00	0.00

- STD-Standard Sample, SE-Standard Error
- Purity values can be slightly more than 100% due to system and operation errors.

For reactions with 10g and 20g of water at different temperatures, paracetamol alone was detected by the HPLC measurement, whereas 4'-acetoxyacetanilide was identified in the samples from reactions without water and with only 5g (0.28mol) water.

This indicates that paracetamol particles can be obtained with a high purity (~99%) for reactive crystallization with enough water (≥ 10g, or 0.55mol). Note that the purities for the purchased paracetamol and 4'-acetoxyacetanilide are not 100% as shown in Figure C.6 & C.7, plus some of the 4'-acetoxyacetanilide solids were hydrolyzed in the mobile phase during the sample preparation process, these can explain the small amount of paracetamol measured in the STD 4'-acetoxyacetanilide solution and in sample 7.

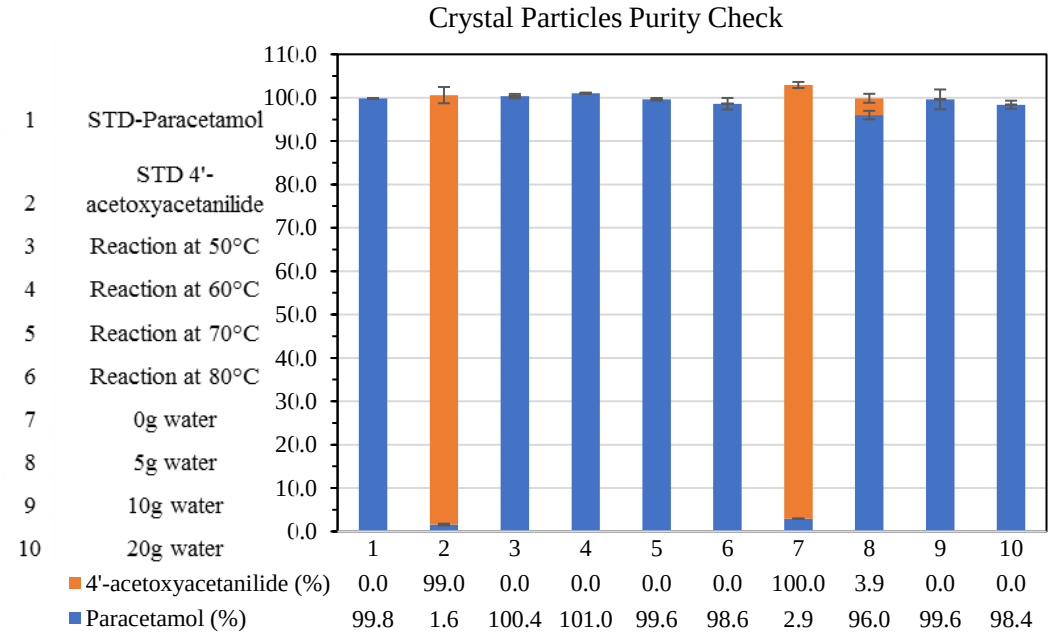

Figure C. 4 The purity results for paracetamol particles from reactive crystallizations under different reaction conditions

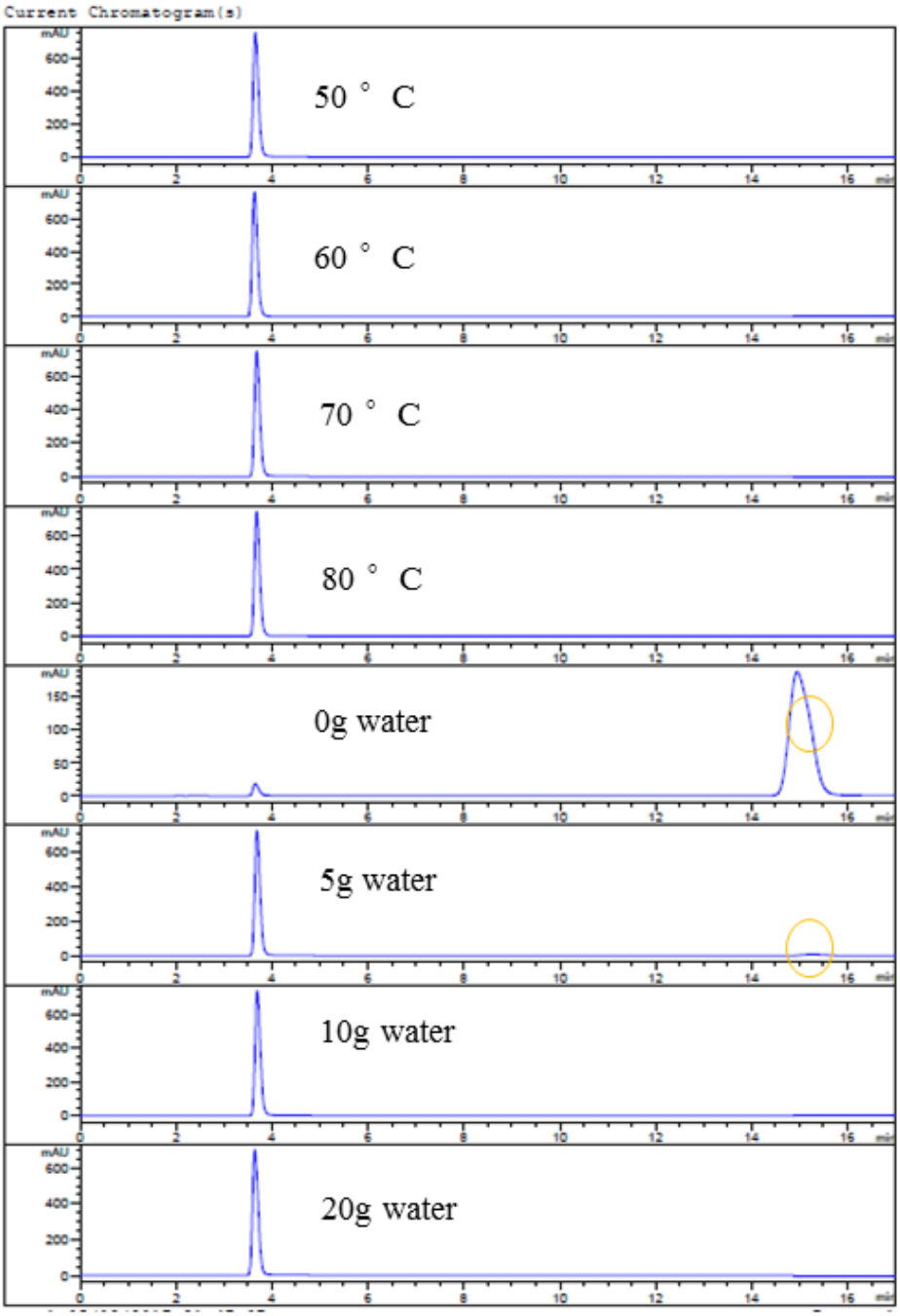

Figure C. 5 HPLC results for paracetamol purity measurement

C7. Image of paracetamol crystals

The images for the paracetamol particles produced from reactive crystallization are shown in Figure C.6.

Figure C. 6 Images of paracetamol particles after filtering (left) and drying (right) process

C8. Reactive crystallization in different solvents

There were 6 different solvents being used for the reactive crystallization, and paracetamol crystals were obtained in acetone, ethanol, isopropanol (IPA), acetic acid and acetic anhydride except dimethyl sulfoxide (DMSO). The operational methods and crystal properties are shown in Table C.3 and Figure C.7.

Table C. 3 The reactive crystallization of paracetamol in different solvents

Solvent	Acetone	IPA	Ethanol	Acetic acid	Acetic anhydride	DMSO
Method	Reaction + Cooling + Anti-solvent					Side reaction
Phenomena	✓White fine particles		Low yield	Bad filtration property		Dark solution
Crystal shapes	Rod-like	Enonged	Rectangle	Needle-like	Hexagon	No crystal
Purity	99%	99%	94%	98%	102%	

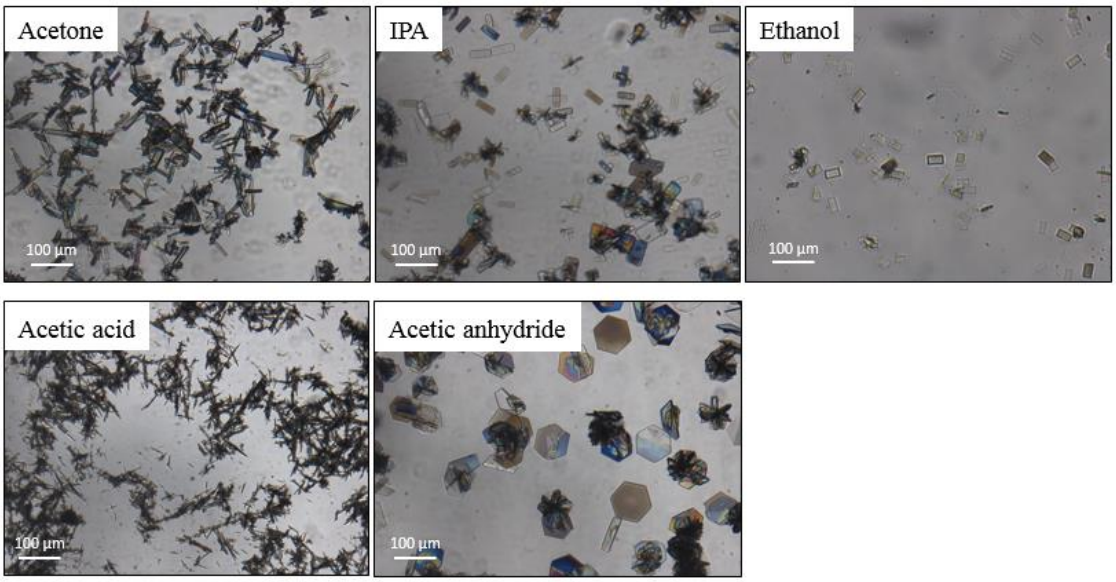

Figure C. 7 Microscopy images for crystal products from reactive crystallization of paracetamol in different solvents

Appendix D-Crystallization kinetics study in OBR

D1. Concentration vs time

HPLC method was applied to analyse the concentrations of compounds in the reactive crystallization process. The calibration curves for paracetamol (Figure D.1A) and 4-acetoxyacetanilide (Figure D.1B) are shown below.

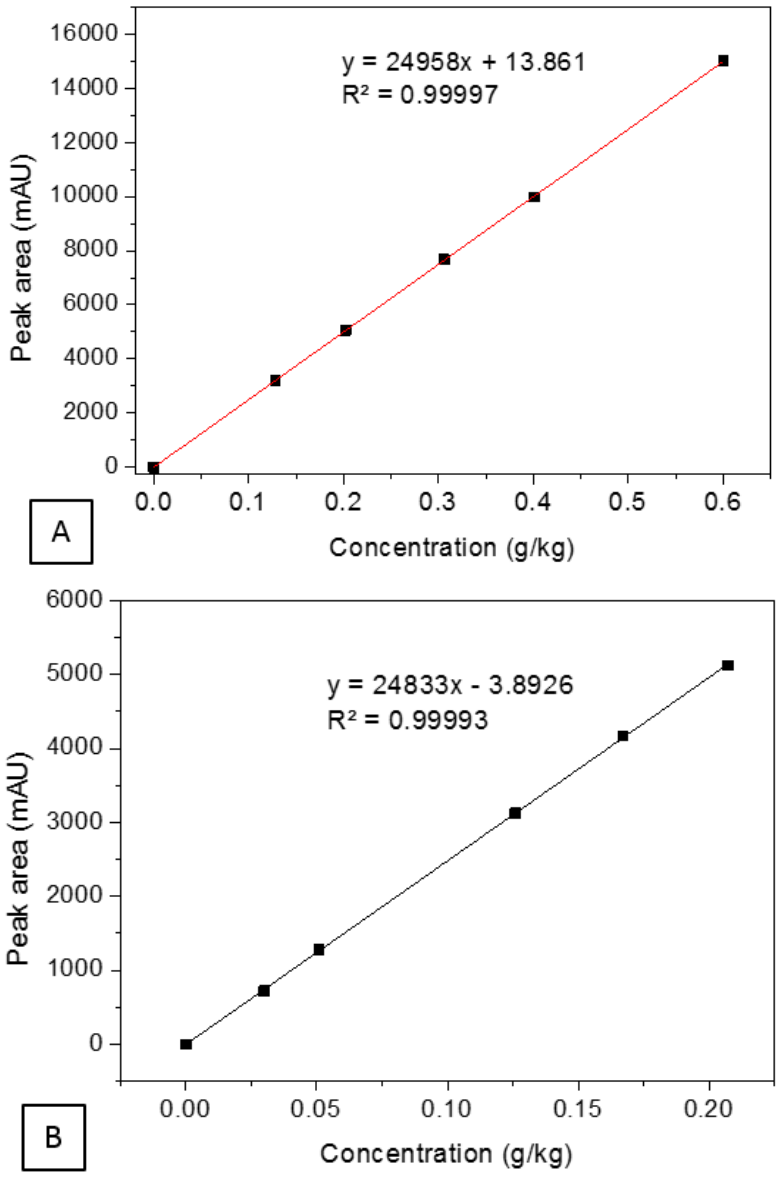

Figure D. 1 HPLC calibration curves for paracetamol (A) and 4- acetoxyacetanilide (B)

Although the chromatographic measurements gave a satisfactory resolution for 4-aminophenol and paracetamol, as illustrated in Figure D.2, the peak for 4-aminophenol is quite small and declines very fast at the beginning of the reaction. In fact, the concentration of 4-aminophenol decreased rapidly from sample 1 to sample 3 within about 5 minutes, which is too fast to obtain stable gradual changes. Instead, the concentrations of paracetamol and 4-acetoxyacetanilide after reaction were examined (see Figure D.3 A-C), in terms of the levels of supersaturation and impurity.

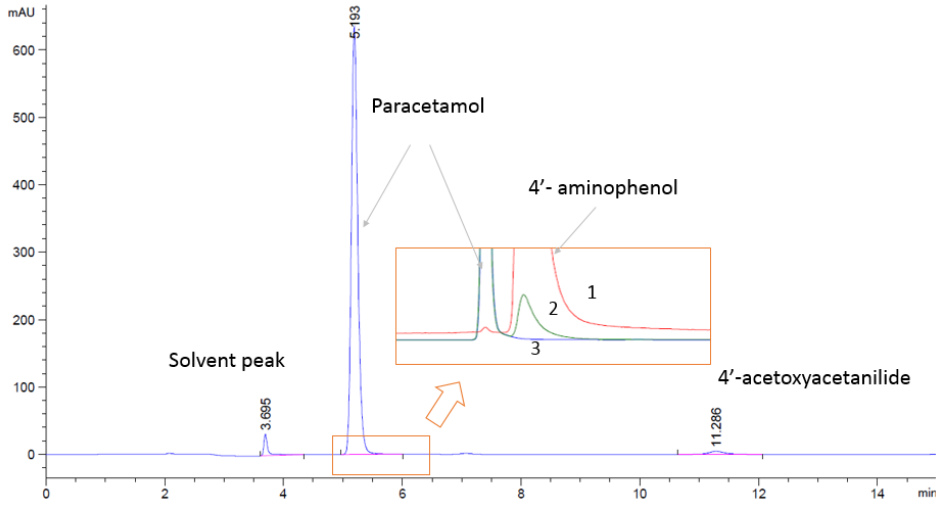

Figure D. 2 Chromatographic of solution samples taken from reaction crystallization system

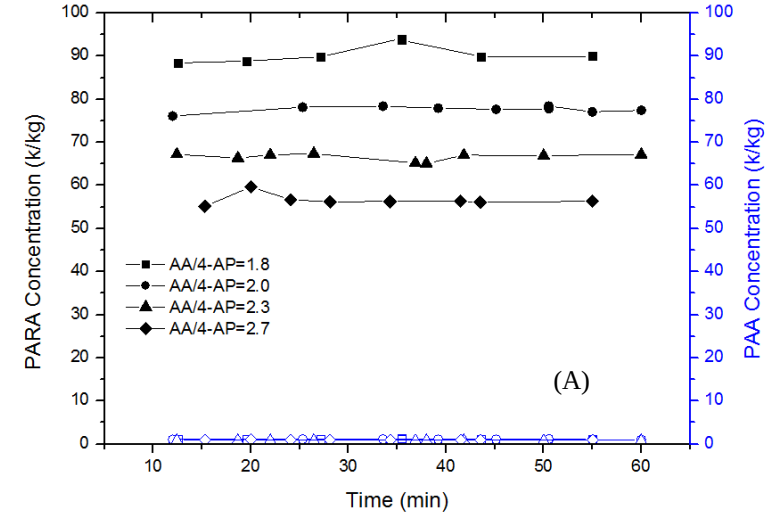

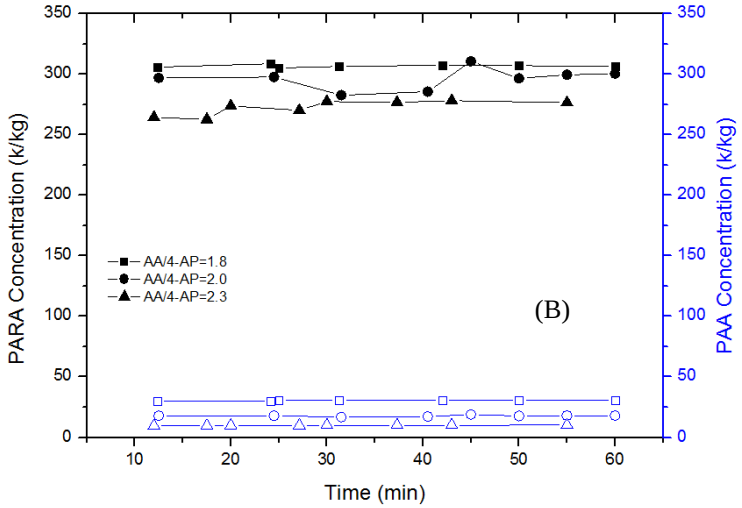

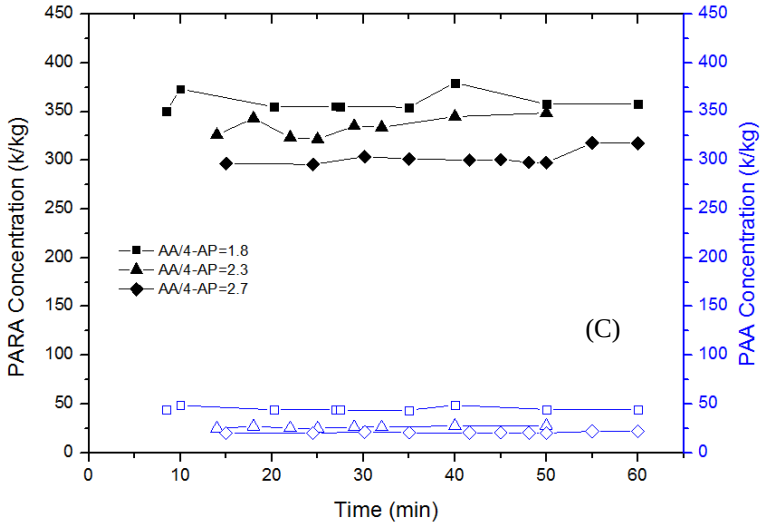

(A) Acetic acid: Water = 1:9

(B) Acetic acid: Water = 5:5

(C) Acetic acid: Water = 7:3

Figure D. 3 Concentration files for paracetamol (PARA) and 4- acetoxyacetanilide (PAA) for samples taken from different solvent conditions before crystallization process.

D2. Calculations of reactants and products

At the beginning of the reaction, we assume that there were x moles of 4-AP, y moles of water and *z* moles of acetic anhydride, the mass balance in *mol* for reaction 1 was then given below:

		Reaction 1			
Compound	**4-Aminophenol**	**Acetic anhydride**		**Paracetamol**	**Acetic acid**
MW(g/mol)	**109.14**	**102.09**		**151.163**	**60.05**
Amount (mol)	*x*	*z*		*x*	*x*

Because the amount of acetic anhydride was in excess, so there would be *(z-x)* moles left for reacting with water. As a result, the amounts of acetic acid produced would be doubled via reaction 2.

		Reaction 2			
Compound	**Acetic anhydride**	**Water**		**Acetic acid**	**Acetic acid**
MW(g/mol)	**102.09**	**18.015**		**60.05**	**60.05**
Amount (mol)	*z-x*	*y*		*z-x*	*z-x*

So at the end of reaction, the solvent composition would be:

Solvent composition		
Acetic acid (AC)	**Water (H_2O)**	**AC/H_2O**
60.05	**18.015**	
2(z-x)+x	*y-(z-x)*	*(60.05*2(z-x)+x)/18.015*(y-(z-x))*

For the reaction conditions consisting of solvent composition acid:water(w/w)=1:9, concentration of starting concentration 4-AP:water = 2.0, we get the above relationship based on a working volume of 1000 g:

$$\frac{(60.05*2(z-x)+x)}{18.015*(y-(z-x))}=0.11 \text{ (i.e.1:9)}$$

$$x/y = 2$$

$$109.14x+102.09z+18.015y = 1000$$

Therefore, we obtained the values of x, y and z as 0.53, 47.80, and 1.05 mol, respectively.

MOLECULE MASS (mol)		
4-Aminophenol	**Water**	**Acetic anhydride**
109.14	**18.015**	**102.09**
x	*y*	*z*
0.53	47.80	1.05

Similarly in terms of the mass:

4-Aminophenol	**Water**	**Acetic anhydride**
x	*y*	*z*
57.33 g	861.19 g	107.26 g

In this way, the masses of starting materials for different solvent compositions and supersaturations were obtained as below.

AC/H_2O	total amount (mol)		Amount (mol)		
		AA/4-AP	4-Aminophenol	Water	Acetic anhydride
	1000	z/x	*x*	*y*	*z*
1:9		0.61	47.30	1.09	0.61
		0.53	47.80	1.05	0.53
		0.44	48.28	1.02	0.44
		0.36	48.72	0.98	0.36
5:5		2.16	23.79	4.33	2.16
		1.87	24.89	4.30	1.87
		1.59	25.96	4.28	1.59
7:3		2.78	14.70	5.56	2.78
		2.43	15.68	5.60	2.43
		2.09	16.65	5.63	2.09

AC/H_2O	total mass (g)		Mass (g)		
		AA/4-AP	4-Aminophenol	Water	Acetic anhydride
	1000	z/x	*x*	*y*	*z*
1:9		1.8	67.07	852.06	111.04
		2.0	57.33	861.19	107.26
		2.3	48.21	869.76	103.72
		2.7	39.77	877.68	100.44
5:5		2.0	236.03	428.56	441.57
		2.3	204.21	448.30	439.34

		2.7	173.09	467.61	437.15
7:3		2.0	303.63	264.91	568.03
		2.3	265.60	282.46	571.41
		2.7	227.59	299.99	574.79

D3. Temperature & turbidity measurements

Figure D.4 shows one of the real time recordings for both temperature and turbidity measurements. The temperature profile (red line) started from left at about 75 ºC (the temperature at the end of reaction), then decreased to a final temperature of about 20 C, subject to a cooling rate. We heated it up after the end of crystallization to examine the dissolution profile. The turbidity profile (black line) shows the transmittance changing with time during crystallization. The initial drop in turbidity signal indicates the on-set nucleation.

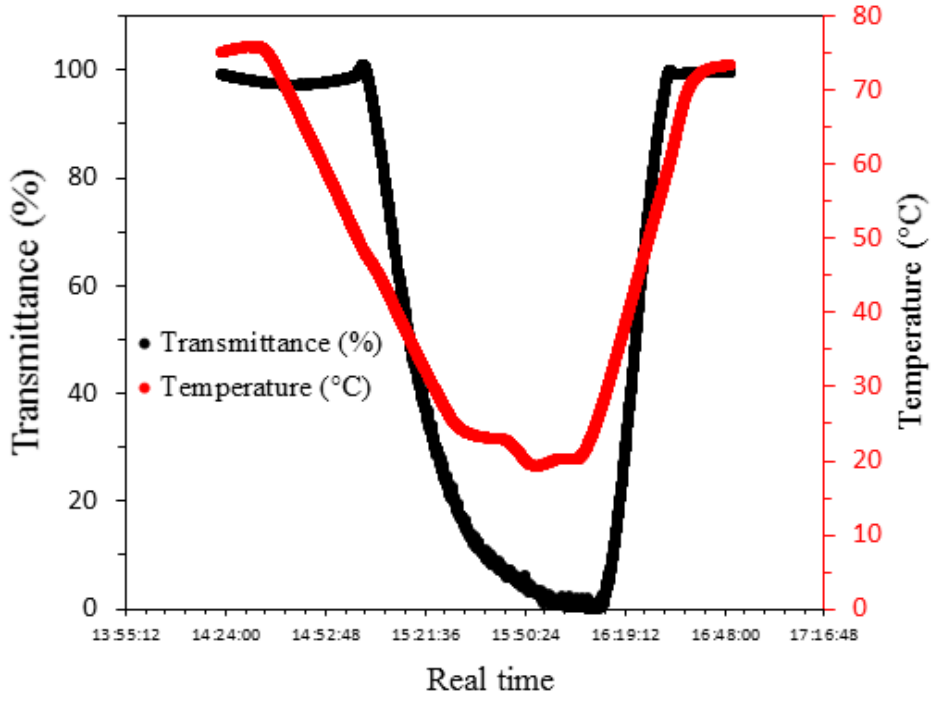

Figure D. 4 Results for temperature and turbidity measurements

D4. Images of the OBR set-up

Figure D. 5 Set up of an OBR

Three processes can be observed during the reactive crystallization experiment, which are dissolution of starting materials, paracetamol synthesis and crystallization, respectively. All of these steps occur in the same OBR vessel, as shown in Figure D.6. A light yellow solution was obtained after 4-AP had been dissolved in the mixture of acetic anhydride and water within 3 minutes at 50°C. At the same time, the temperature within the reactor was increased to 75 °C, the color of solution became darker due to dye impurities (formed from oxidation of the starting phenol) carried along with 4-AP solids and turned to purple as temperature increases. Although the minute impurity impacted the color of the mixture solution, paracetamol particles were well formed and shown as a white color.

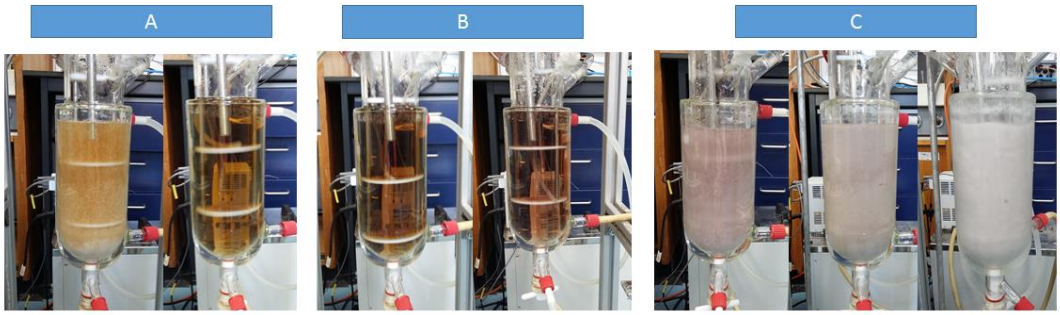

Figure D. 6 Dissolution, reaction and crystallization in an OBR. Photographs (A) show 4-AP dissolving in the starting solvents consisting of acetic anhydride and water. Photographs (B) show paracetamol synthesis solution at high temperature. Photographs (C) indicate the crystallization process directly following the reaction step under a controlled cooling rate.

D5. Effects of mixing on MSZW

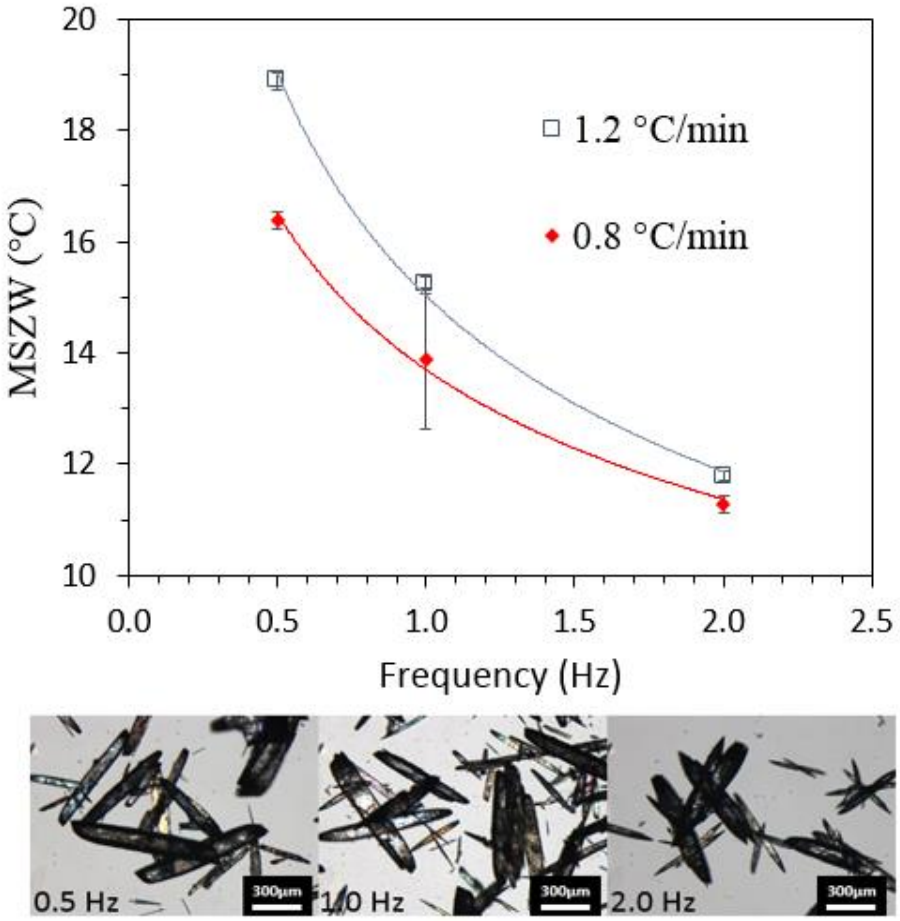

Figure D. 7 Effects of mixing on MSZW

D6. Effects of AA/4-AP on paracetamol concentration

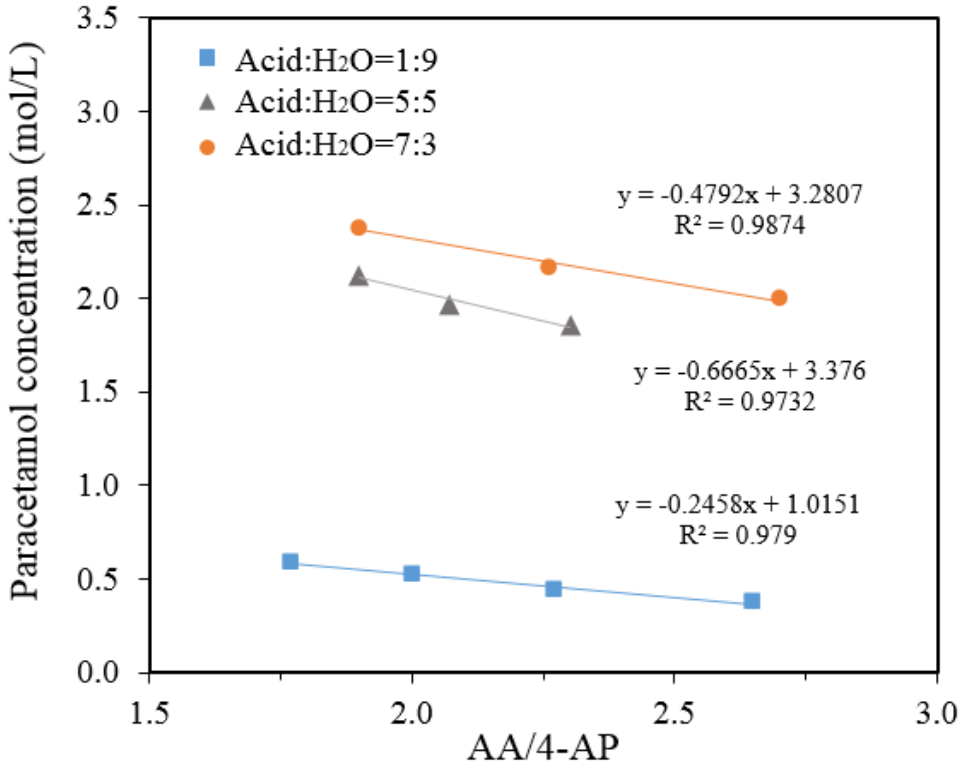

Figure D. 8 The relationship of paracetamol concentration and AA/4-AP in different solvent compositions

The concentration of paracetamol is influenced by the ratio of starting materials. This is due to the mass balance once the reaction reaches an equilibrium. For every targeted ratio of solvent, various reactant ratios of acetic acid (AA) and 4-aminophenol (4-AP)) can lead to different concentrations of paracetamol in the reaction solution. This then affects nucleation and crystal growth in the following crystallization step. Figure D.8 shows the linear relationship of paracetamol concentration as a function of AA/4-AP value in each solvent composition. Due to the solubility limitation, higher ratios of Acid/H_2O yield a solution of higher concentration, which is as expected. For a certain ratio of solvent, the concentration of paracetamol decreases as the AA/4-AP value increases. This suggests that beside of Acid/H_2O value, to obtain a specific solution for

crystallization, the ratio of AA/4-AP should also be controlled from the solute supersaturation point of view. In addition, the linear function for each trend line in FigureD.8 was obtained from the average value of paracetamol concentration at the same AA/4-AP ratio.

D7. Effects of supersaturation on crystal shapes for different solvent compositions

For different solvents, fine needle-shaped crystals were often produced in solutions of a higher ratio of acid (Figure D.9). Breakages of needle crystals were observed for solvents with a higher ratio of acid to water (Figure D.10).

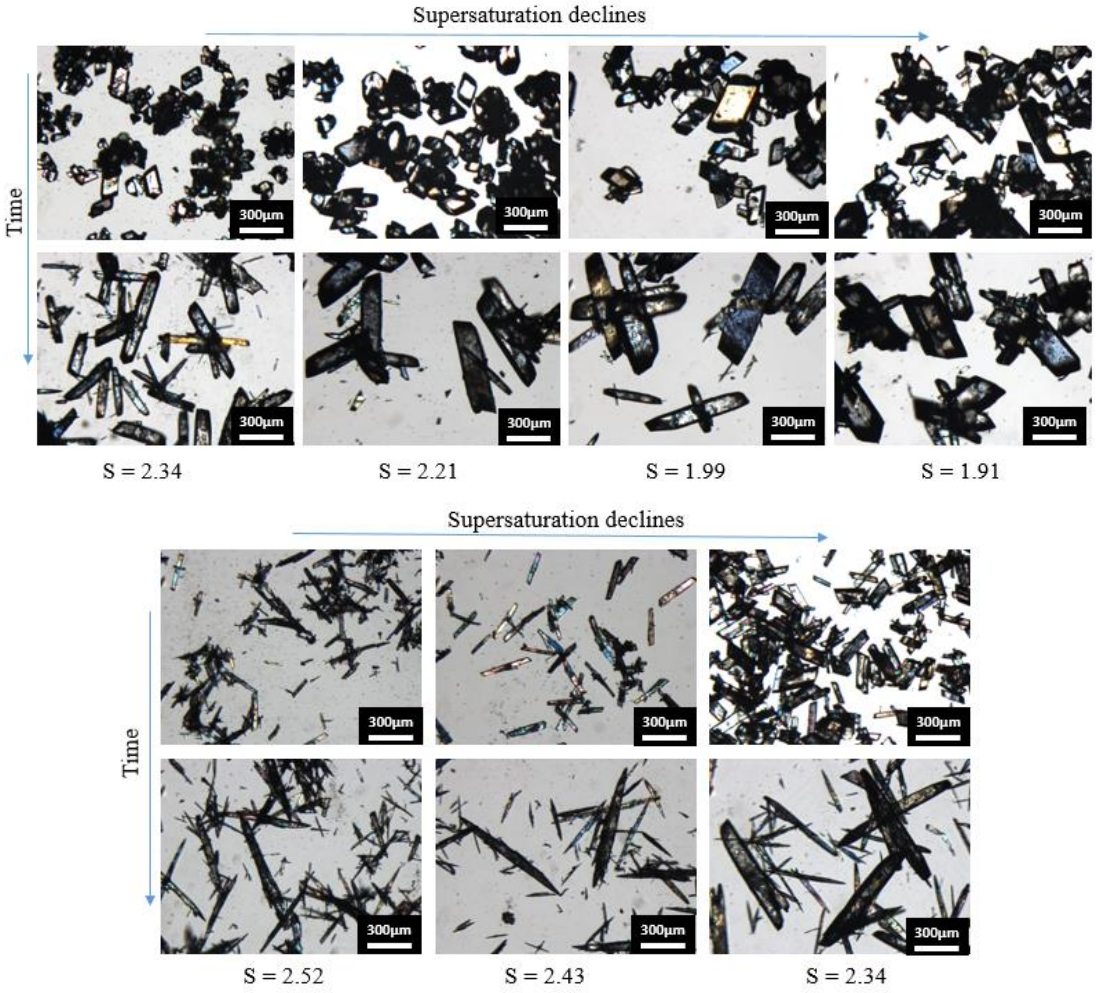

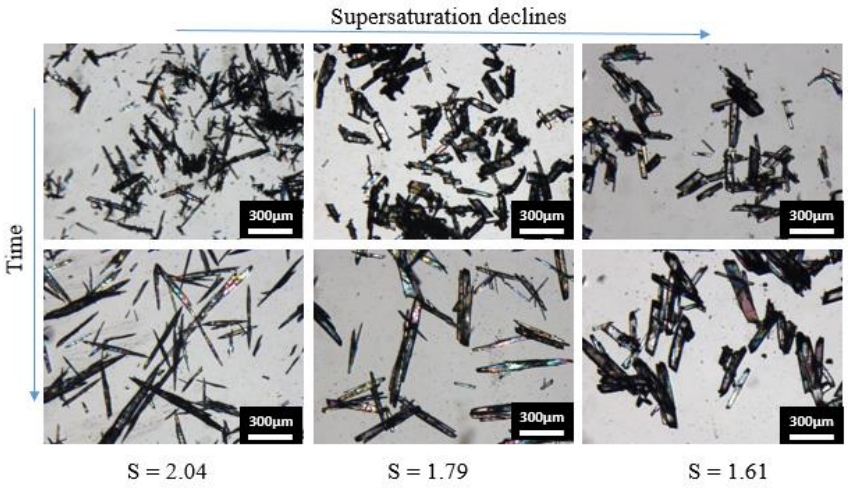

Figure D. 9 Microscope images of paracetamol crystallized at different supersaturation level under various solvent conditions: (up) acid/water = 1:9; (middle) acid/water = 5:5; (down) acid/water = 7:3

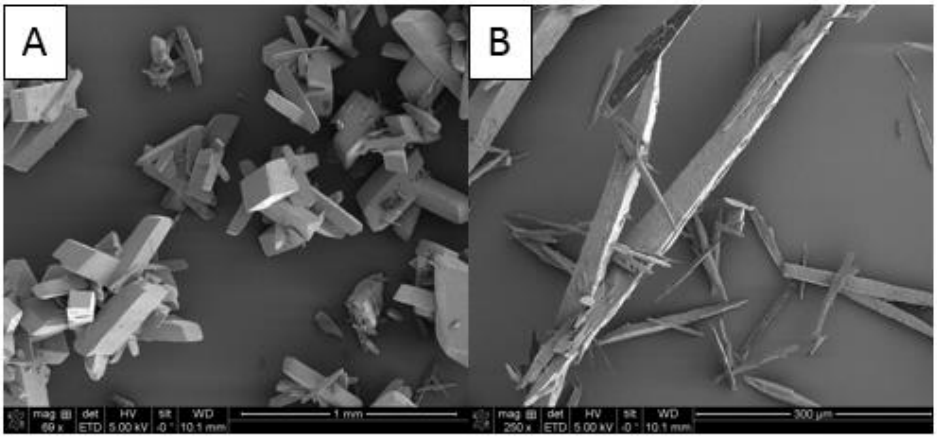

Figure D. 10 SEM images showing paracetamol crystals (A) agglomeration in low acid ratio solvent and (B) breakage at high acid ratio solvent during the reactive crystallization process

Appendix E– Reactive crystallization in COBR

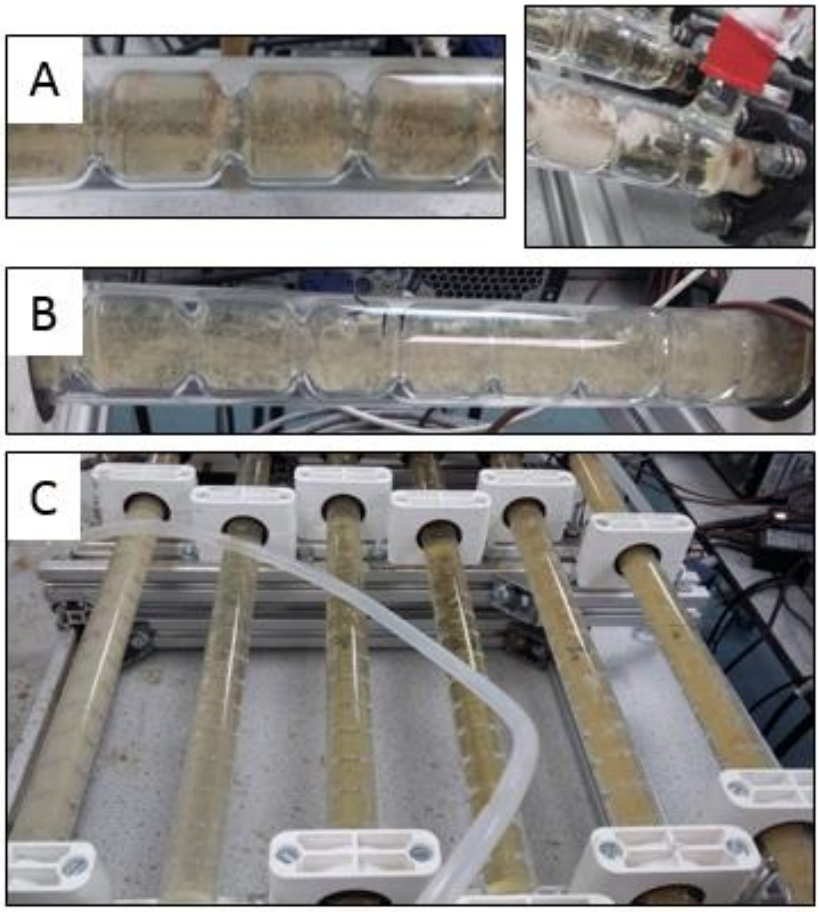

Figure E. 1 Reactive crystallization of paracetamol in a COBR. Photograph (A) shows encrustation (left) and blockages (right) during unseeded continuous operations. Photograph (B) shows uniformly mixed crystals flowing through a staight glass tube in a reactive crystallization process with 15% seeds loading. Photograph (C) illustrates the 3 steps during a reactive crystlalisation: dissolution, reaction, crystallization (from left to right).

E1. Cooling profiles

The higher the cooling rate, the higher the supersaturation level. COBR -8 experiment was carried out to compare with COBR- 2 to study the effect of cooling rate on seeded reactive crystallization of paracetamol. Figure E.2 shows the measured temperature

profile from 6 in-situ thermocouples along the COBR. The mean size of final products and the driving force for crystal growth are given in Table E.1.

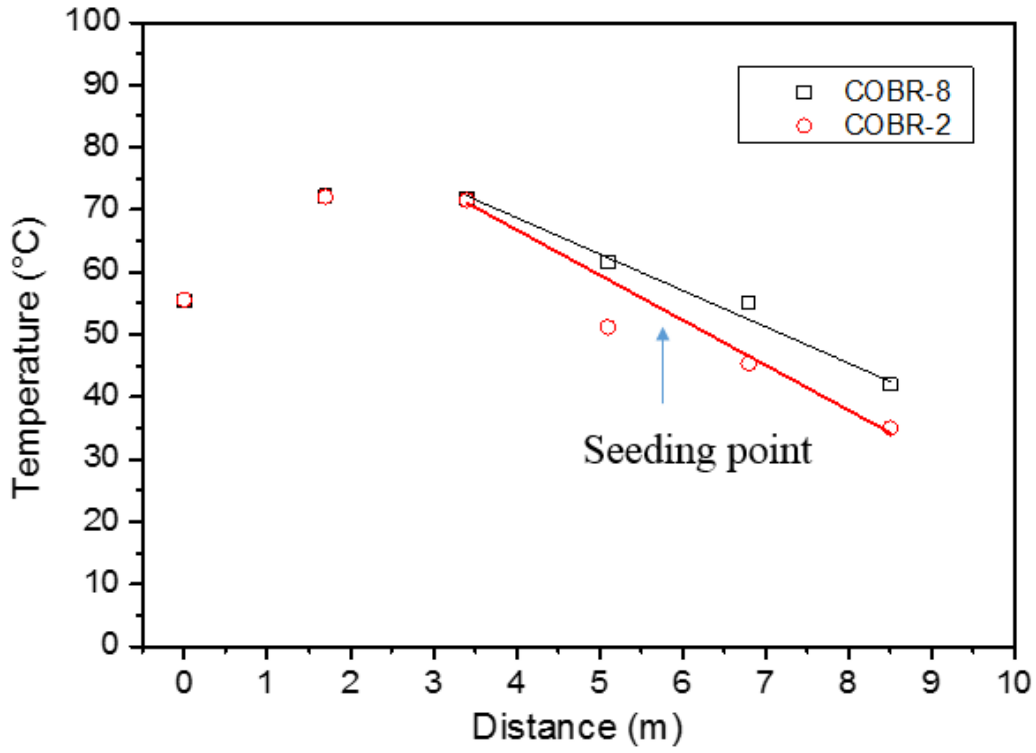

Figure E. 2 Cooling profiles for seeded reactive crystallization of paracetamol in a COBR. Plot showing measured temperatures from thermocouple 1 to 6 along distance during the COBR experiments.

Table E. 1 COBR operation conditions

	Seeds load (%)	Cooling rate (ºC min^{-1})	Products mean size (µm)	S	Operation mode
COBR-2	15	2.0	453	2.1	Continuous
COBR-8	15	1.6	522	1.5	Continuous

E2. PVM images

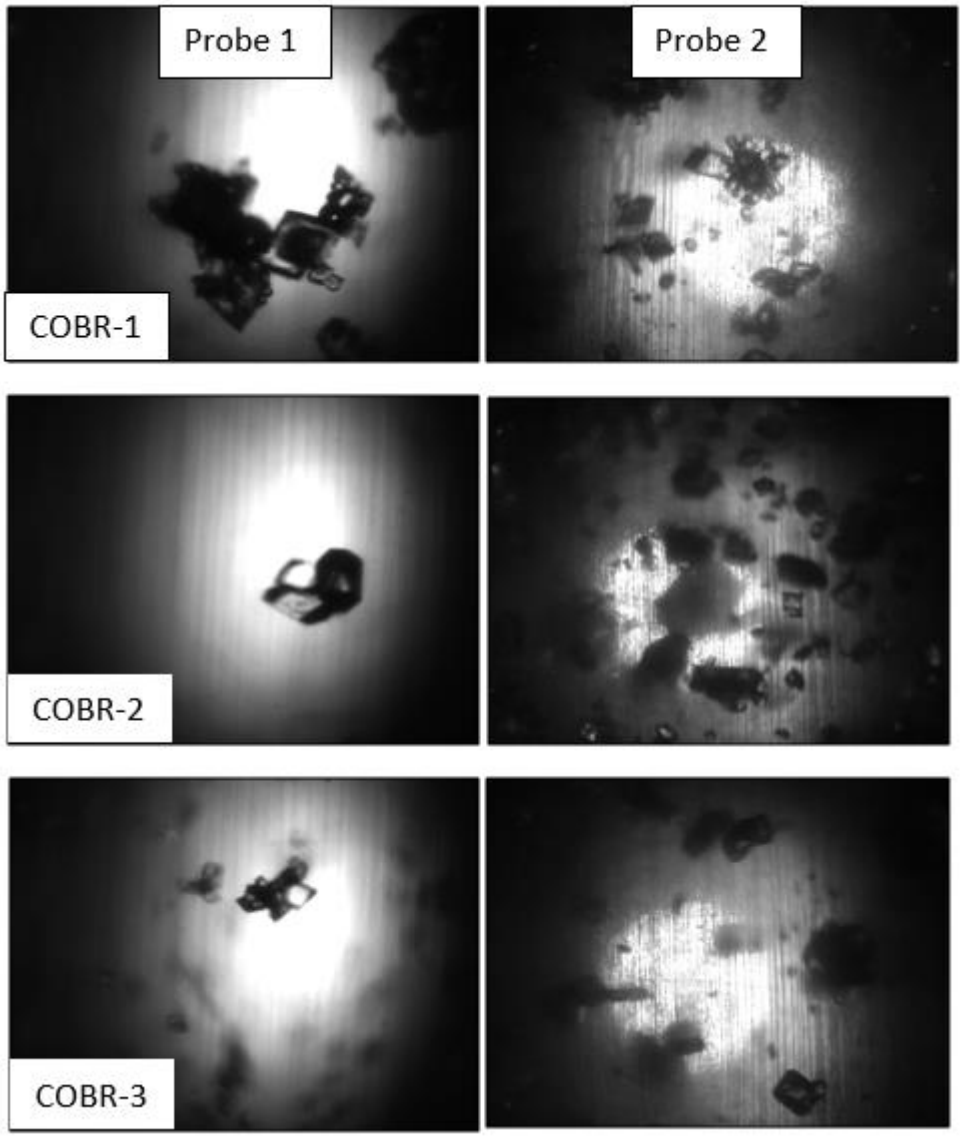

Figure E. 3 PVM images for reactive crystallization under the amplitude of 26 mm, 30 mm, and 36 mm at a fixed frequency of 1.0 Hz.

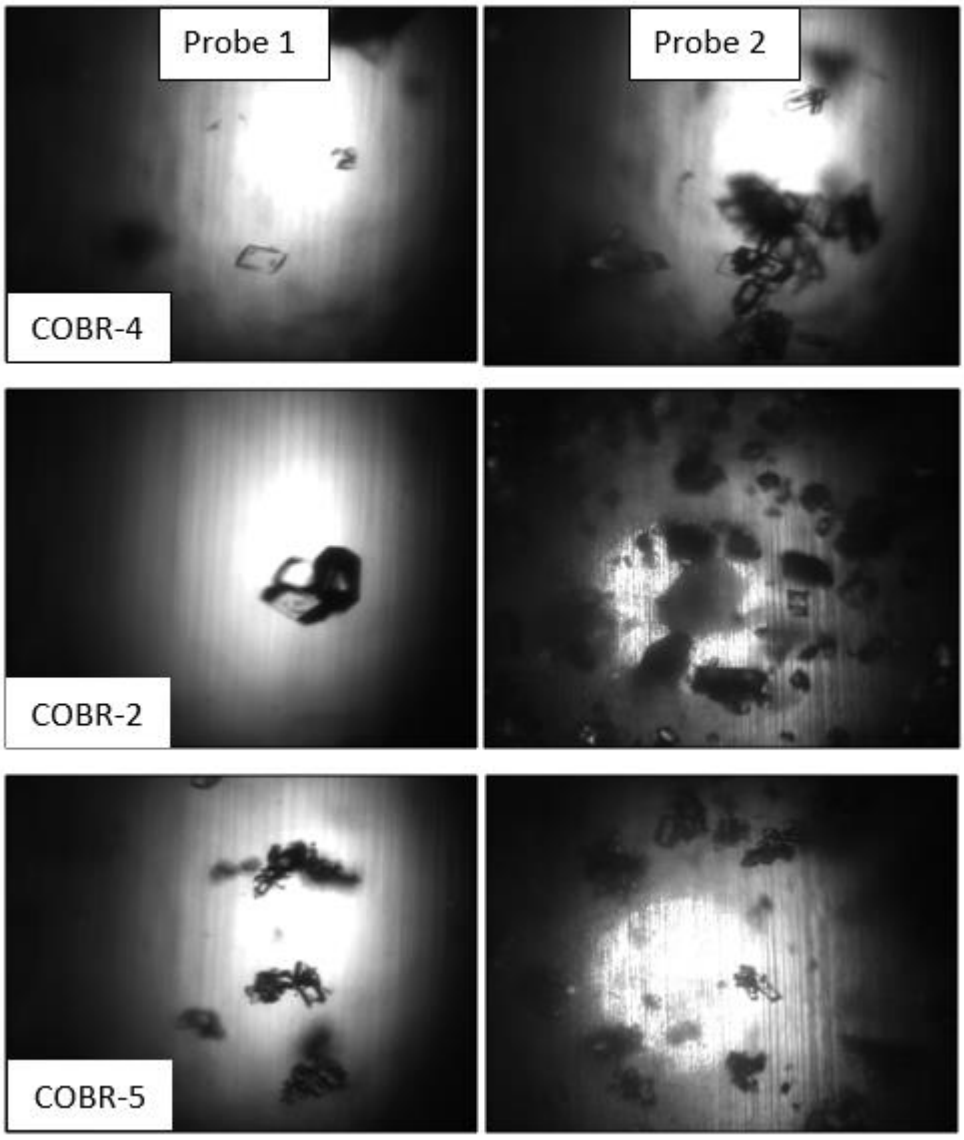

Figure E. 4 PVM images for reactive crystallization under the frequency of 0.5 Hz, 1.0 Hz, and 1.2 Hz with a fixed amplitude of 30 mm.

E3. HPLC chromatogram

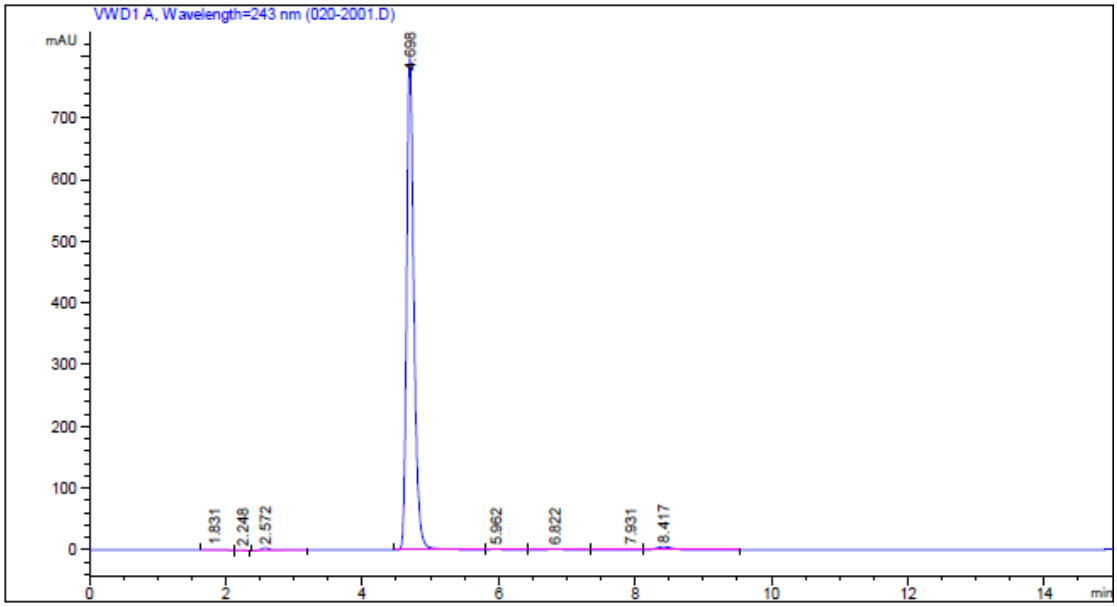

Figure E. 5 HPLC chromatogram for one of the samples taken at Sample Point 1

E4. Purity results

Particles obtained from COBR were analyzed using HPLC against the paracetamol samples provided by GlaxoSmithKline Pharmaceutical Company (purity of 99.8%). Results shown in Figure E.6 present a purity range of 99-101% for the paracetamol obtained in this work (mean of 99.96%).

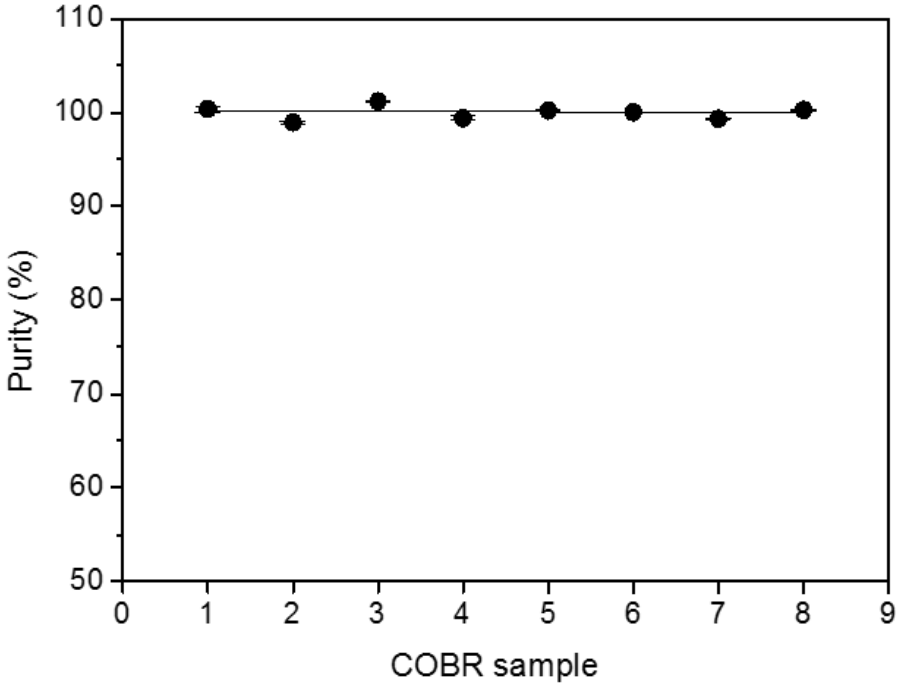

Figure E.6 Purity results for COBR products

E5. Feeding rates calculations

AC/H_2O	AA/4-AP	Flow rate (ml/min)	Feed 1 (mol/min)		Feed 2 (mol/min)
		Q	4-ap	H_2O	AA
1:9	2.7	40	0.01	1.92	0.04

AC/H_2O	AA/4-AP	Flow rate (g/min)	Feed 1 (g/min)		Feed 2 (g/min)
		Q	4-ap	H_2O	AA

1:9	2.7	40	1.59	34.62	4.01

Feed 1 (ml/min)	Feed 2 (ml/min)
	AA
36.11	3.72

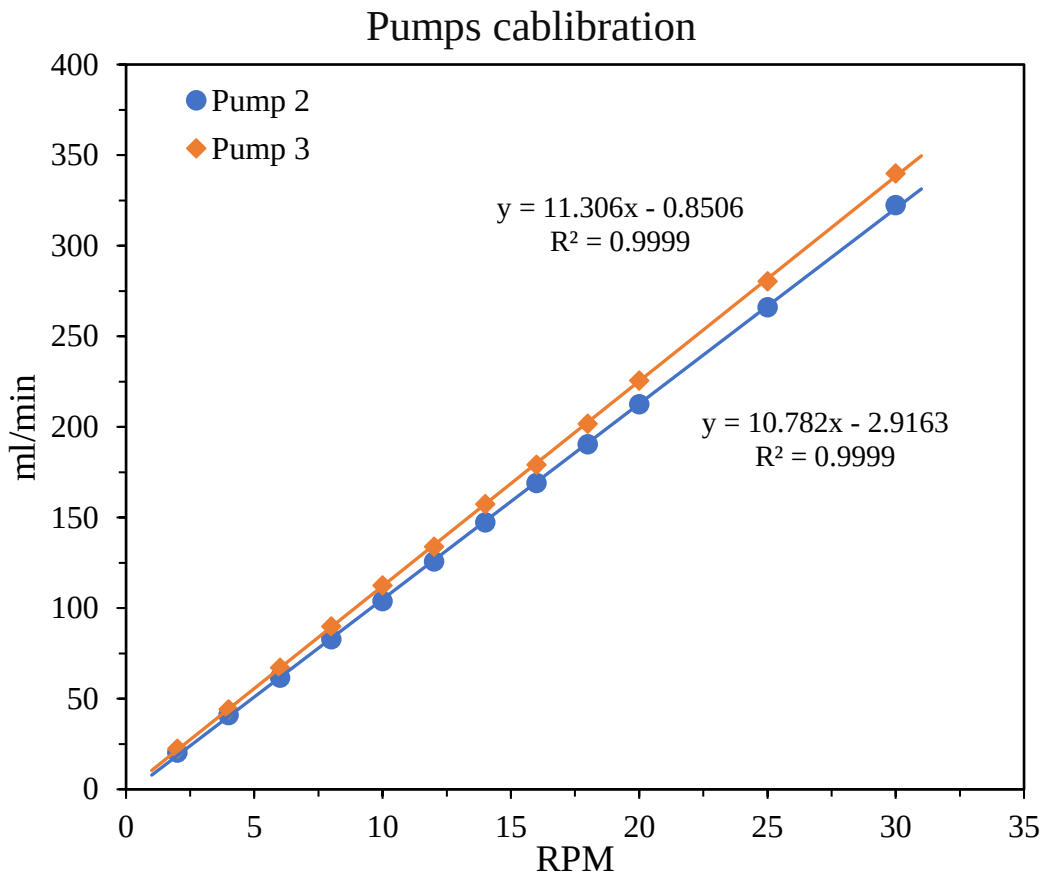

Figure E.7 Calibration results for pumps (pump 2- feed AA, pump 3-feed seeds)

E6. XRD results for COBR experiments

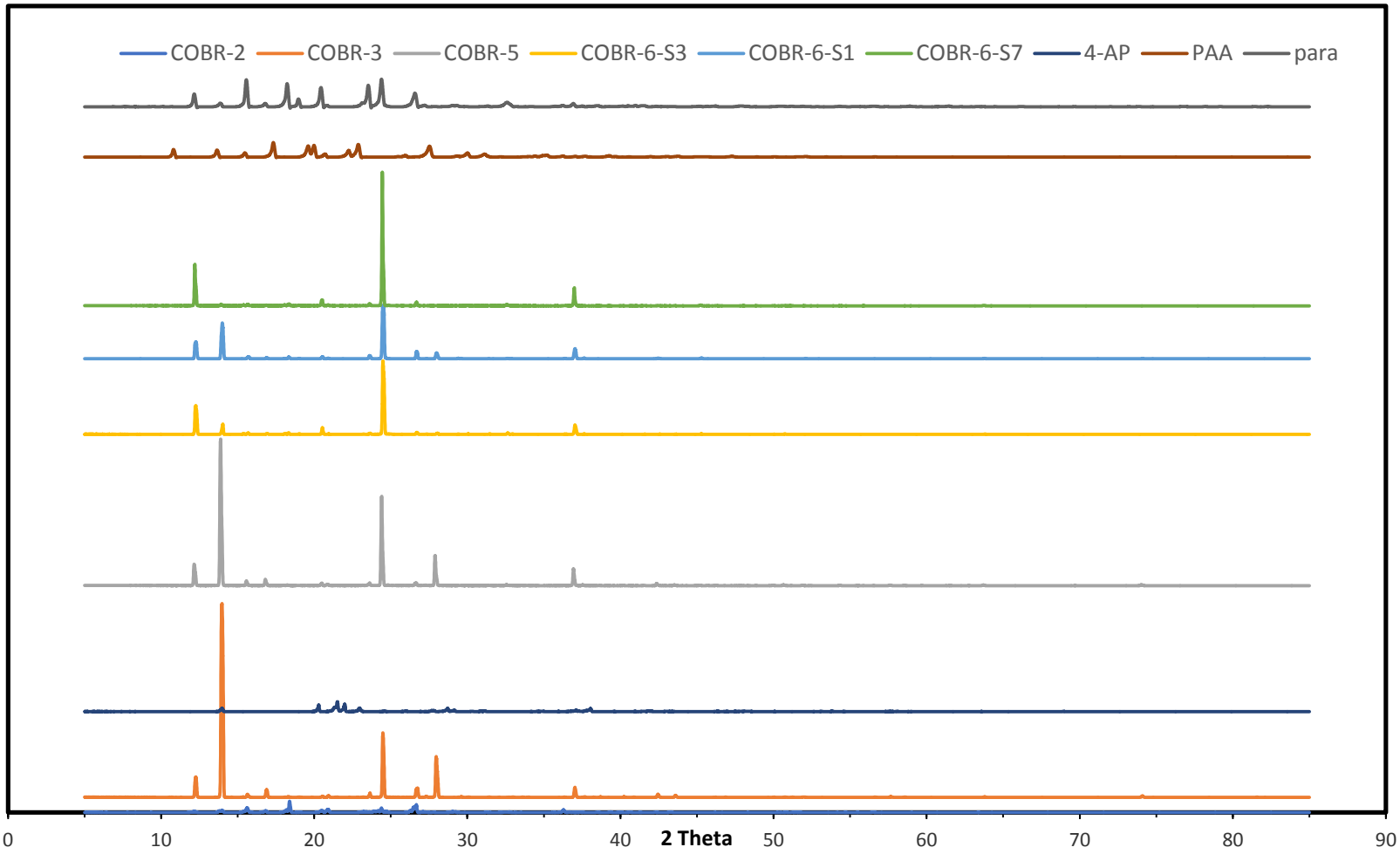

Figure E.8 XRD results for COBC crystal products

References

[1] D. W. Young, "Preparation of nu-acetyl-p-aminophenol," US Patent 3113150, 1963.

[2] F. A. Baron, H. L. Schulman, and A. E. Weinberg, "Preparation of N-acetyl-p-aminophenol," US Patent 3917695A, 1975.

[3] T. Lee, H. Y. Lin, and H. L. Lee, "Engineering reaction and crystallization and the impact on filtration, drying, and dissolution behaviors: the study of acetaminophen (paracetamol) by in-process controls," *Organic Process Research and Development,* vol. 17, no. 9, pp. 1168-1178, 2013.

[4] H. L. Lee, H. Y. Lin, and T. Lee, "Large-scale crystallization of a pure metastable polymorph by reaction coupling," *Organic Process Research and Development,* Article vol. 18, no. 4, pp. 539-545, 2014.

[5] J. A. Caro, M. Woldehaimanot, and Å. C. Rasmuson, "Semibatch reaction crystallization of salicylic acid," *Chemical Engineering Research and Design,* vol. 92, no. 3, pp. 522-533, 2014.

[6] M. Ståhl, B. L. Åslund, and Å. C. Rasmuson, "Reaction crystallization kinetics of benzoic acid," *AIChE journal,* vol. 47, no. 7, pp. 1544-1560, 2001.

[7] X. Ni and M. Mackley, "Chemical reaction in batch pulsatile flow and stirred tank reactors," *Chemical Engineering Journal,* vol. 52, no. 3, pp. 107-114, 1993.

[8] H. McLachlan and X.-W. Ni, "On the effect of added impurity on crystal purity of urea in an oscillatory baffled crystallizer and a stirred tank crystallizer," *Journal of Crystal Growth,* vol. 442, pp. 81-88, 2016.

[9] X. Ni and S. Gao, "Scale-up correlation for mass transfer coefficients in pulsed baffled reactors," *Chemical Engineering Journal and the Biochemical Engineering Journal,* vol. 63, no. 3, pp. 157-166, 1996.

[10] X. Ni, A. Fitch, and I. Laird, "Mixing apparatus and process," US Patent 9295955, 2016.

[11] N. Xiongwei, "Method and apparatus for phase separated synthesis," US Patent 6429268, 2002.

[12] S. Lawton, G. Steele, P. Shering, L. Zhao, I. Laird, and X. Ni, "Continuous crystallization of pharmaceuticals using a continuous oscillatory baffled crystallizer," *Organic Process Research and Development,* vol. 13, no. 6, pp. 1357-1363, 2009.

[13] S. Lawton, G. Steele, P. Shering, L. Zhao, I. Laird, and X.-W. Ni, "Continuous crystallization of pharmaceuticals using a continuous oscillatory baffled crystallizer," *Organic Process Research & Development,* vol. 13, no. 6, pp. 1357-1363, 2009.

[14] C. J. Brown, J. A. Adelakun, and X. Ni, "Characterization and modelling of antisolvent crystallization of salicylic acid in a continuous oscillatory baffled crystallizer," *Chemical Engineering and Processing,* vol. 97, pp. 180-186, 2015.

[15] L. Zhao, V. Raval, N. E. Briggs, R. M. Bhardwaj, T. McGlone, I. D. Oswald, A. J. Florence, "From discovery to scale-up: α-lipoic acid: nicotinamide co-crystals in a continuous oscillatory baffled crystalliser," *CrystEngComm,* vol. 16, no. 26, pp. 5769-5780, 2014.

[16] D. Zhang, S. Xu, S. Du, J. Wang, and J. Gong, "Progress of pharmaceutical continuous crystallization," *Engineering,* vol. 3, no. 3, pp. 354-364, 2017.

[17] T. McGlone, N. E. Briggs, C. A. Clark, C. J. Brown, J. Sefcik, and A. J. Florence, "Oscillatory flow reactors (OFRs) for continuous manufacturing and crystallization," *Organic Process Research and Development,* vol. 19, no. 9, pp. 1186-1202, 2015.

[18] T. Wang, H. Lu, J. Wang, Y. Xiao, Y. Zhou, Y. Bao, H. Hao, "Recent progress of continuous crystallization," *Industrial and Engineering Chemistry Research,* vol. 54, pp. 14-29, 2017.

[19] H. Morse, "Ueber eine neue Darstellungsmethode der Acetylamidophenole," *Berichte der deutschen chemischen Gesellschaft,* vol. 11, no. 1, pp. 232-233, 1878.

[20] K. G. Davenport and C. B. Hilton, "Process for producing N-acyl-hydroxy aromatic amines," US Patent 4524217, 1985.

[21] J. R. Fritch, O. S. Fruchey, T. Horlenko, "Production of acetaminophen," US Patent 4954652, 1990.

[22] M. Ghiaci, H. Aghaei , M. Oroojeni, "Synthesis of paracetamol by liquid phase Beckmann rearrangement of 4-hydroxyacetophenone oxime over H3PO4/Al-MCM-41," *Catalysis Communications*, vol. 10, no. 11, pp. 1486-1492, 2009.

[23] J. H. H. Bassford, "Manufacture of hydroxy amino compounds," US Patent 2132454, 1938.

[24] C. O. Henke and J. V. Vaughen, "Reduction of aryl nitro compounds," US Patent 2198249, 1940.

[25] S. Louis, "Manufacture of aromatic parahydroxyamines," US Patent 2765342, 1956.

[26] W. Godfrey and A. J. De, "Process of preparing nu-acetyl-p-amino phenol," US Patent 2998450, 1961.

[27] C. Rode, M. Vaidya, and R. Chaudhari, "Synthesis of p-aminophenol by catalytic hydrogenation of nitrobenzene," *Organic process research & development*, vol. 3, no. 6, pp. 465-470, 1999.

[28] J. B. Tingle and L. F. Williams, "Acyl, derivatives of ortho- and paraminophenol," *American Chemical Journal*, vol. 37, p. 51-71, 1907.

[29] B. F. Duesel and W. Godfrey, "Process for the preparation of n-acetyl-p-aminophenol (apap),"US Patent 3341587, 1967.

[30] J. H. Van Ness and J. B. Warner, "Preparation of N-acetyl-p-aminophenol," US Patent 4670589, 1987.

[31] R. G. Benner, "Process for preparing aminophenol," US Patent 3383416, 1968.

[32] P. Rylander, I. Karpenko, and G. Pond, "Process for preparing para-aminophenol," US Patent 3715397, 1973.

[33] D. C. Caskey and D. W. Chapman, "Process for preparing p-aminophenol and alkyl substituted p-aminophenol," US Patent 4571437, 1986.

[34] F. Morris, "Process for the preparation of acetylaminophenols," US Patent 3076030, 1963.

[35] D. C. Ruopp and M. A. Thorn, "Borate reduction of nitrophenols," US Patent 4264526, 1981.

[36] F. R. Bean, "Process for preparing aminophenols," US Patent 2446519, 1950.

[37] C. Henke and J. Vaughen, " Reduction of aryl nitro compounds" US Patent 2198249, 1940.

[38] F. Morris and R. M. Robinson, "Catalytic hydrogenation of nitrophenol," US Patent 3079435, 1963.

[39] S. Louis, "Process for the hydrogenation of nitro compounds," US Patent 3328465, 1967.

[40] M. N. Gilano, R. E. Beaupre, and M. A. Lipson, "Polymerization compositions and processes having polymeric binding agents," US Patent 3953309, 1976.

[41] H. Daunis and M. Gominet, "Process for the purification of p-aminophenol," US Patent 3658905, 1972.

[42] F. A. Baron, R. G. Benner, and A. E. Weinberg, "Purification of p-aminophenol," US Patent 3694508, 1972.

[43] F. A. Baron, "Purification of p-aminophenol," US Patent 3717680, 1972.

[44] K. Reid, "Purification of p-aminophenol," US Patent 3845129, 1974.

[45] M. J. Vaidya, S. M. Kulkarni, and R. V. Chaudhari, "Synthesis of p-aminophenol by catalytic hydrogenation of p-nitrophenol," *Organic process research & development,* vol. 7, no. 2, pp. 202-208, 2003.

[46] J. Huber Jr, "Stepwise reduction of p-nitrophenol," US Patent 4264525, 1981.

[47] R. Joncour, N. Duguet, E. Métay, A. Ferreira, and M. Lemaire, "Amidation of phenol derivatives: a direct synthesis of paracetamol (acetaminophen) from hydroquinone," *Green Chemistry,* vol. 16, no. 6, pp. 2997-3002, 2014.

[48] J. A. Foster, W. H. Mueller, D. A. Ryan, and H. Wiezer, "Process for preparing acyl aminophenols," US Patent 5648535, 1997.

[49] S. Ferguson *et al.,* "Use of continuous MSMPR crystallization with integrated nanofiltration membrane recycle for enhanced yield and purity in API crystallization," *Crystal Growth and Design,* vol. 14, no. 2, pp. 617-627, 2013.

[50] D. Acevedo and Z. K. Nagy, "Systematic classification of unseeded batch crystallization systems for achievable shape and size analysis," *Journal of Crystal Growth,* vol. 394, pp. 97-105, 2014.

[51] J. W. Mullin, *Crystallization*. Butterworth-Heinemann: Oxford, 2001.

[52] J. Ulrich and C. Strege, "Some aspects of the importance of metastable zone width and nucleation in industrial crystallizers," *Journal of crystal Growth,* vol. 237, pp. 2130-2135, 2002.

[53] A. Jawor-Baczynska and A. J. Florence, "Development of Continuous Crystallisation Processes of Pharmaceutical Compounds to Achieve Better Control Over Final Product Attributes," Available at http://ukmanufacturing2015.eng.cam.ac.uk/Conference%20Archive/Anna_JaworBaczynska__Presentation.pdf, 2014.

[54] T.T. C. Lai, S. Ferguson, L. Palmer, B. L. Trout, and A. S. Myerson, "Continuous Crystallization and Polymorph Dynamics in the l-Glutamic Acid System," *Organic Process Research and Development,* vol. 18, no. 11, pp. 1382-1390, 2014.

[55] S. Khan *et al.*, "In-process monitoring and control of supersaturation in seeded batch cooling crystallisation of l-glutamic acid: from laboratory to industrial pilot plant," *Organic Process Research & Development,* vol. 15, no. 3, pp. 540-555, 2011.

[56] M. Löffelmann and A. Mersmann, "How to Measure Supersaturation?," *Chemical Engineering Science,* vol. 57, pp. 4301-4310, 2002.

[57] C. Callahan and X. Ni, "Probing into Nucleation of Cooling Crystallisation in an Oscillatory Baffled Crystalliser," PhD Thesis, Heriot-Watt University, 2011.

[58] N. A. Mitchell and P. J. Frawley, "Nucleation kinetics of paracetamol–ethanol solutions from metastable zone widths," *Journal of Crystal Growth,* vol. 312, no. 19, pp. 2740-2746, 2010.

[59] A. Jones, S. Rigopoulos, and R. Zauner, "Crystallization and precipitation engineering," *Computers & chemical engineering,* vol. 29, no. 6, pp. 1159-1166, 2005.

[60] R. Davey and J. Garside, *From molecules to crystallizers*. Oxford University: New York, 2000.

[61] A. S. Myerson, *Handbook of Industrial Crystallisation*. Butterworth-Heinemann: Boston, 2002.

[62] Z. Nagy and E. Aamir, "Systematic design of supersaturation controlled crystallization processes for shaping the crystal size distribution using an analytical estimator," *Chemical Engineering Science,* vol. 84, pp. 656-670, 2012.

[63] S. Hodgen, "An Introduction to Crystallisation," Presentation. Glasgow.

[64] J. Mullin and O. Söhnel, "Expressions of supersaturation in crystallization studies," *Chemical Engineering Science,* vol. 32, no. 7, pp. 683-686, 1977.

[65] C. J. Brown and X. Ni, "Online evaluation of paracetamol antisolvent crystallization growth rate with video imaging in an oscillatory baffled crystallizer," *Crystal Growth and Design,* vol. 11, no. 3, pp. 719-725, 2011.

[66] J. Lu, Y. Li, J. Wang, G.-B. Ren, S. Rohani, and C.-B. Ching, "Crystallization of an active pharmaceutical ingredient that oils out," *Separation and Purification Technology,* vol. 96, pp. 1-6, 2012.

[67] N. Variankaval, A. S. Cote, and M. F. Doherty, "From form to function: crystallization of active pharmaceutical ingredients," *AIChE journal,* vol. 54, no. 7, pp. 1682-1688, 2008.

[68] F. Fusaro, J. Kluge, M. Mazzotti, and G. Muhrer, "Compressed CO 2 antisolvent precipitation of lysozyme," *The Journal of Supercritical Fluids,* vol. 49, no. 1, pp. 79-92, 2009.

[69] S. Kim, C. Wei, and S. Kiang, "Crystallization process development of an active pharmaceutical ingredient and particle engineering via the use of ultrasonics and temperature cycling," *Organic process research and development,* vol. 7, no. 6, pp. 997-1001, 2003.

[70] N. S. Tavare, *Industrial crystallization: process simulation analysis and design*. Springer Science & Business Media: Manchester, 2013.

[71] A. Jones, S. Rigopoulos, and R. Zauner, "Crystallization and precipitation engineering," *Computers & chemical engineering,* vol. 29, no. 6, pp. 1159-1166, 2015.

[72] B. O'Sullivan and B. Glennon, "Application of in situ FBRM and ATR-FTIR to the monitoring of the polymorphic transformation of D-mannitol," *Organic process research and development,* vol. 9, no. 6, pp. 884-889, 2005.

[73] A. Borissova *et al.*, "In situ measurement of solution concentration during the batch cooling crystallization of l-glutamic acid using ATR-FTIR spectroscopy

coupled with chemometrics," *Crystal Growth and Design,* vol. 9, no. 2, pp. 692-706, 2008.

[74] H. Hao, M. Barrett, Y. Hu, W.Su, S. Ferguson, B. Wood, and B. Glennon, "The Use of in Situ Tools To Monitor the Enantiotropic Transformation of p-Aminobenzoic Acid Polymorphs," *Organic Process Research and Development,* vol. 16, no. 1, pp. 35-41, 2011.

[75] D. Duffy, N. Cremin, M. Napier, S. Robinson, M. Barrett, H. Hao, B. Glennon, "In situ monitoring, control and optimization of a liquid–liquid phase separation crystallization," *Chemical Engineering Science,* vol. 77, pp. 112-121, 2012.

[76] H. Niinomi *et al.,* "Solubility measurement of a metastable achiral crystal of sodium chlorate in solution growth," *Journal of Crystal Growth*, vol. 394, pp. 106-111, 2014.

[77] K. A. Powell, A. N. Saleemi, C. D. Rielly, and Z. K. Nagy, "Periodic steady-state flow crystallization of a pharmaceutical drug using MSMPR operation," *Chemical Engineering and Processing,* vol. 97, pp. 195-212, 2015.

[78] H-H. Tung, E.L. Paul, M. Midler, J. A. McCauley, *Crystallization of Organic Compounds: An Industrial Perspective.* John Wiley & Sons: New York, pp.1-11, 2009.

[79] J. Mullin and J. Nývlt, "Programmed cooling of batch crystallizers," *Chemical Engineering Science,* vol. 26, no. 3, pp. 369-377, 1971.

[80] A. Mersmann, "Crystallization technology handbook," *Drying Technology*, vol. 13, no. 4, pp. 1037-1038, 1995.

[81] C. J. Brown and X. Ni, "Online evaluation of paracetamol antisolvent crystallization growth rate with video imaging in an oscillatory baffled crystallizer," *Crystal Growth & Design,* vol. 11, no. 3, pp. 719-725, 2011.

[82] Y. Cui, J. J. Jaramillo, T. Stelzer, and A. S. Myerson, "Statistical Design of Experiment on Contact Secondary Nucleation as a Means of Creating Seed Crystals for Continuous Tubular Crystallizers," *Organic Process Research and Development,* 2014.

[83] D. O'Grady, M. Barrett, E. Casey, and B. Glennon, "The effect of mixing on the metastable zone width and nucleation kinetics in the anti-solvent crystallization

of benzoic acid," *Chemical Engineering Research and Design,* vol. 85, no. 7, pp. 945-952, 2007.

[84] N. A. Mitchell, C. T. Ó'Ciardhá, and P. J. Frawley, "Estimation of the growth kinetics for the cooling crystallisation of paracetamol and ethanol solutions," *Journal of Crystal Growth,* vol. 328, no. 1, pp. 39-49, 2011.

[85] K. Kachrimanis and S. Malamataris, "Crystallization of Paracetamol from Ethanol-water Solutions in the Presence of Polymers," *Journal of pharmacy and pharmacology,* vol. 51, no. 11, pp. 1219-1227, 1999.

[86] R. A. Granberg, D. G. Bloch, and Å. C. Rasmuson, "Crystallization of paracetamol in acetone–water mixtures," *Journal of Crystal Growth,* vol. 198, pp. 1287-1293, 1999.

[87] R. A. Granberg and Å. C. Rasmuson, "Solubility of paracetamol in pure solvents," *Journal of Chemical & Engineering Data,* vol. 44, no. 6, pp. 1391-1395, 1999.

[88] C. J. Brown and X. Ni, "Evaluation of growth kinetics of antisolvent crystallization of paracetamol in an oscillatory baffled crystallizer utilizing video imaging," *Crystal Growth and Design,* vol. 11, no. 9, pp. 3994-4000, 2011.

[89] C. J. Brown and X. Ni, "Determination of metastable zone width, mean particle size and detectable number density using video imaging in an oscillatory baffled crystallizer," *CrystEngComm,* vol. 14, no. 8, pp. 2944-2949, 2012.

[90] M. Ståhl and Å. C. Rasmuson, "Towards predictive simulation of single feed semibatch reaction crystallization," *Chemical Engineering Science,* vol. 64, no. 7, pp. 1559-1576, 2009.

[91] K. Choong and R. Smith, "Optimization of semi-batch reactive crystallization processes," *Chemical engineering science,* vol. 59, no. 7, pp. 1529-1540, 2004.

[92] M. Torbacke and Å. C. Rasmuson, "Influence of different scales of mixing in reaction crystallization," *Chemical Engineering Science,* vol. 56, no. 7, pp. 2459-2473, 2001.

[93] B. L. Å. Slund and Å. K. C. Rasmuson, "Semibatch reaction crystallization of benzoic acid," *AIChE journal,* vol. 38, no. 3, pp. 328-342, 1992.

[94] J. Utomo, Y. Asakuma, N. Maynard, K. Maeda, K. Fukui, and M. O. Tadé, "Semi-batch reactive crystallisation of mono-ammonium phosphate: An experimental study," *Chemical Engineering Journal,* vol. 156, no. 3, pp. 594-600, 2010.

[95] H. W. Wang, Jeffrey, "Seeding and Optimization of Batch Reactive Crystallization," *Industrial & Engineering Chemistry Research,* 2015.

[96] H. Alatalo, H. Hatakka, J. Kohonen, S. p. Reinikainen, and M. Louhi-kultanen, "Process control and monitoring of reactive crystallization of L-glutamic acid," *AIChE journal,* vol. 56, no. 8, pp. 2063-2076, 2010.

[97] C. Ricardo and N. Xiongwei, "Evaluation and Establishment of a Cleaning Protocol for the Production of Vanisal Sodium and Aspirin Using a Continuous Oscillatory Baffled Reactor," *Organic Process Research and Development,* vol. 13, no. 6, pp. 1080-1087, 2009.

[98] C. He, J. Sun, C. Deng, T. Zhao, M. Deng, X. Chen, X. Jing, "Study of the synthesis, crystallization, and morphology of poly (ethylene glycol)-poly (ε-caprolactone) diblock copolymers," *Biomacromolecules,* vol. 5, no. 5, pp. 2042-2047, 2004.

[99] M. Volmer, "Kinetik der phasenbildung," 1939.

[100] A. Nienow, "The effect of agitation and scale-up on crystal growth rates and on secondary nucleation," *Trans. Inst. Chem. Eng.,* vol. 54, pp. 205-207, 1976.

[101] H. Powers, "Nucleation and early crystal growth," *Industrial Chemist,* vol. 39, pp. 351-355, 1963.

[102] C. Sung, J. Estrin, and G. Youngquist, "Secondary nucleation of magnesium sulfate by fluid shear," *AIChE Journal,* vol. 19, no. 5, pp. 957-962, 1973.

[103] O. Narducci, A. Jones, and E. Kougoulos, "Crystal product engineering in the seeded cooling crystallization of adipic acid from aqueous solution," *Organic Process Research and Development,* vol. 15, no. 5, pp. 974-980, 2011.

[104] W. Beckmann, "Seeding the desired polymorph: background, possibilities, limitations, and case studies," *Organic Process Research and Development,* vol. 4, no. 5, pp. 372-383, 2000.

[105] N. Al-Zoubi and S. Malamataris, "Effects of initial concentration and seeding procedure on crystallisation of orthorhombic paracetamol from ethanolic solution," *International journal of pharmaceutics,* vol. 260, no. 1, pp. 123-135, 2003.

[106] W. Beckmann, K. Nickisch, and U. Budde, "Development of a seeding technique for the crystallization of the metastable A modification of abecarnil," *Organic Process Research & Development*, vol. 2, no. 5, pp. 298-304, 1998.

[107] E. Aamir, Z. Nagy, and C. Rielly, "Evaluation of the effect of seed preparation method on the product crystal size distribution for batch cooling crystallization processes," *Crystal Growth & Design*, vol. 10, no. 11, pp. 4728-4740, 2010.

[108] K. J. Roberts, R. Docherty, and R. Tamura, *Engineering Crystallography: From Molecule to Crystal to Functional Form*. Springer, 2017.

[109] B. O'Sullivan, B. Smith, and G. Baramidze, "Recent advances for seeding a crystallization process," *Mettler Toledo Auto-Chem, Columbia Google Scholar*, 2012.

[110] R. Eder, E. Schmitt, J. Grill, S. Radl, H. Gruber-Woelfler, and J. Khinast, "Seed loading effects on the mean crystal size of acetylsalicylic acid in a continuous-flow crystallization device," *Crystal Research and Technology*, vol. 46, no. 3, pp. 227-237, 2011.

[111] R. J.P. Eder, E. K. Schmitt, J. Grill, S. Radl, H. Gruber-Woelfler, and J. Khinast, "Seed loading effects on the mean crystal size of acetylsalicylic acid in a continuous-flow crystallization device," *Crystal research and technology*, vol. 46, no. 3, pp. 227-237, 2011.

[112] S. Ferguson, G. Morris, H. Hao, M. Barrett, and B. Glennon, "Automated self seeding of batch crystallizations via plug flow seed generation," *Chemical Engineering Research and Design*, vol. 92, no. 11, pp. 2534-2541, 2014.

[113] C. J. Callahan and X.-W. Ni, "The influence of hydrodynamic environment on the nucleation mechanism of a chiral crystallization," Heriot-Watt University, 2014. http://spider.science.strath.ac.uk/cmac/files/media/Craig_Callahan_1.pdf.

[114] N. Al-Zoubi, I. Nikolakakis, and S. Malamataris, "Crystallization conditions and formation of orthorhombic paracetamol from ethanolic solution," *Journal of pharmacy and pharmacology*, vol. 54, no. 3, pp. 325-333, 2002.

[115] K. Mohammad, S. A. Rahim, and M. A. Bakar, "Effect of Seed Loading and Temperature of Seeding on Carbamazepine-Saccharin Co-Crystal," *Indian Journal of Science and Technology*, vol. 10, no. 6, 2017.

[116] A. Warstat and J. Ulrich, "Seeding during batch cooling crystallization–an initial approach to heuristic rules," *Chemical Engineering & Technology: Industrial Chemistry-Plant Equipment-Process Engineering-Biotechnology,* vol. 29, no. 2, pp. 187-190, 2006.

[117] P. J. Frawley, N. A. Mitchell, C. T. Ó'Ciardhá, and K. W. Hutton, "The effects of supersaturation, temperature, agitation and seed surface area on the secondary nucleation of paracetamol in ethanol solutions," *Chemical engineering science,* vol. 75, pp. 183-197, 2012.

[118] B. Long, H. Yang, and Y. Ding, "Impact of seed loading ratio on the growth kinetics of mono-ammonium phosphate under isothermal batch crystallization," *Korean journal of chemical engineering,* vol. 33, no. 2, pp. 623-628, 2016.

[119] T. Kleetz, R. Scheel, G. Schembecker, and K. Wohlgemuth, "Cooling Crystallization: Does Gassing Compete with Seeding?," *Crystal Growth & Design,* vol. 18, no. 9, pp. 4906-4910, 2018.

[120] X. Zhang, Z. Yang, J. Chai, J. Xu, L. Zhang, G. Qian, X. Zhou, "Nucleation kinetics of lovastatin in different solvents from metastable zone widths," *Chemical Engineering Science,* 2015.

[121] D. Erdemir, A. Y. Lee, and A. S. Myerson, "Nucleation of crystals from solution: classical and two-step models," *Accounts of chemical research,* vol. 42, no. 5, pp. 621-629, 2009.

[122] J. Nývlt, "Kinetics of nucleation in solutions," *Journal of Crystal Growth,* vol. 3, pp. 377-383, 1968.

[123] J. Nyvlt, O. Sohnel, and M. Matuchova, *The Kinetics of Industrial Crystallization.* Academia:Prague, 1985.

[124] Z. K. Nagy, M. Fujiwara, X. Y. Woo, and R. D. Braatz, "Determination of the kinetic parameters for the crystallization of paracetamol from water using metastable zone width experiments," *Industrial & Engineering Chemistry Research,* vol. 47, no. 4, pp. 1245-1252, 2008.

[125] C. J. Brown, Y. C. Lee, Z. K. Nagy, and X.-w. Ni, "Evaluation of crystallization kinetics of adipic acid in an oscillatory baffled crystallizer," *CrystEngComm,* vol. 16, no. 34, pp. 8008-8014, 2014.

[126] K. Sangwal, "A novel self-consistent Nývlt-like equation for metastable zone width determined by the polythermal method," *Crystal Research and Technology,* vol. 44, no. 3, pp. 231-247, 2009.

[127] K. Sangwal, "Novel approach to analyze metastable zone width determined by the polythermal method: physical interpretation of various parameters," *Crystal Growth and Design,* vol. 9, no. 2, pp. 942-950, 2009.

[128] K. Sangwal, "Recent developments in understanding of the metastable zone width of different solute− solvent systems," *Journal of Crystal Growth,* vol. 318, no. 1, pp. 103-109, 2011.

[129] K. Sangwal, "On the effect of impurities on the metastable zone width of phosphoric acid," *Journal of crystal growth,* vol. 312, no. 22, pp. 3316-3325, 2010.

[130] N. Kubota, "A new interpretation of metastable zone widths measured for unseeded solutions," *Journal of Crystal Growth,* vol. 310, no. 3, pp. 629-634, 2008.

[131] H. P. Wirges, "The Kinetics of Industrial Crystallization," *Chemie Ingenieur Technik,* vol. 58, no. 8, pp. 665-665, 1986.

[132] R. C. Reid, G. D. Botsaris, G. Margolis, D. J. Kirwan, E. G. Denk, G. S. Ersan, J. Tester, F. Wong, "Crystallization—Part I-Transport Phenomena of Nucleation and Crystal Growth," *Industrial & Engineering Chemistry,* vol. 62, no. 11, pp. 52-67, 1970.

[133] A. Myerson, *Handbook of industrial crystallization*. Butterworth-Heinemann, 2002.

[134] R. Mohan and A. S. Myerson, "Growth kinetics: a thermodynamic approach," *Chemical Engineering Science,* vol. 57, no. 20, pp. 4277-4285, 2002.

[135] F. Rosenberger, "Crystal growth kinetics," in *Interfacial Aspects of Phase Transformations*: Springer, 1982, pp. 315-364.

[136] A. A. Noyes and W. R. Whitney, "The rate of solution of solid substances in their own solutions," *Journal of the American Chemical Society,* vol. 19, no. 12, pp. 930-934, 1897.

[137] W. Nernst, "Theorie der Reaktionsgeschwindigkeit in heterogenen Systemen," *Zeitschrift für physikalische Chemie,* vol. 47, no. 1, pp. 52-55, 1904.

[138] A. Berthoud, "Théorie de la formation des faces d'un cristal," *Journal de Chimie Physique*, vol. 10, pp. 624-635, 1912.

[139] J. Valeton, "I. Wachstum und Auflösung der Kristalle. III," *Zeitschrift für Kristallographie-Crystalline Materials*, vol. 60, no. 1-6, pp. 1-38, 1924.

[140] J. David, "Effect of temperature on crystal growth and crystal properties of paracetamol," *Journal of the Chemical Society, Faraday Transactions*, vol. 92, no. 3, pp. 439-444, 1996.

[141] B. Y. Shekunov and D. J. Grant, "In situ optical interferometric studies of the growth and dissolution behavior of paracetamol (acetaminophen). 1. Growth kinetics," *The Journal of Physical Chemistry B*, vol. 101, no. 20, pp. 3973-3979, 1997.

[142] R. Ristic, S. Finnie, D. Sheen, and J. Sherwood, "Macro-and micromorphology of monoclinic paracetamol grown from pure aqueous solution," *The Journal of Physical Chemistry B*, vol. 105, no. 38, pp. 9057-9066, 2001.

[143] C. Ó'Ciardhá, N. Mitchell, K. Hutton, and P. Frawley, "Determination of the Crystal Growth Rate of Paracetamol As a function of solvent composition," *Industrial & Engineering Chemistry Research*, vol. 51, no. 12, pp. 4731-4740, 2012.

[144] R. A. Granberg and Å. C. Rasmuson, "Crystal growth rates of paracetamol in mixtures of water+ acetone+ toluene," *AIChE journal*, vol. 51, no. 9, pp. 2441-2456, 2005.

[145] B. Bellhouse, F. H. Bellhouse, C. M. Curl, T. I. MacMillan, A. J. Gunning, E. H. Spratt, S. B. MacMurray, and J. M. Nelems, "A high efficiency membrane oxygenator and pulsatile pumping system, and its application to animal trials," *ASAIO Journal*, vol. 19, no. 1, pp. 72-79, 1973.

[146] W. Van Dijck, "Tower with internal perforated plate suitable for extracting liquids by treatment with other liquids and for similar concurrent processes," US Patent 2011186, 1935.

[147] I. J. Sobey, "On flow through furrowed channels. Part 1. Calculated flow patterns," *Journal of Fluid Mechanics*, vol. 96, no. 1, pp. 1-26, 1980.

[148] K. Stephanoff, I. J. Sobey, and B. Bellhouse, "On flow through furrowed channels. Part 2. Observed flow patterns," *Journal of Fluid Mechanics,* vol. 96, no. 1, pp. 27-32, 1980.

[149] M. Mackley, "Usingocillatory flow to improve performance," *Chemical engineer,* no. 433, pp. 18-21, 1987.

[150] C. Brunold, J. Hunns, M. Mackley, and J. Thompson, "Experimental observations on flow patterns and energy losses for oscillatory flow in ducts containing sharp edges," *Chemical Engineering Science,* vol. 44, no. 5, pp. 1227-1244, 1989.

[151] A. Dickens, M. Mackley, and H. Williams, "Experimental residence time distribution measurements for unsteady flow in baffled tubes," *Chemical Engineering Science,* vol. 44, no. 7, pp. 1471-1479, 1989.

[152] X. Ni, S. Gao, R. Cumming, and D. Pritchard, "A comparative study of mass transfer in yeast for a batch pulsed baffled bioreactor and a stirred tank fermenter," *Chemical Engineering Science,* vol. 50, no. 13, pp. 2127-2136, 1995.

[153] P. Gough, X. Ni, and K. C. Symes, "Experimental flow visualisation in a modified pulsed baffled reactor," *Journal of Chemical Technology & Biotechnology: International Research in Process, Environmental AND Clean Technology,* vol. 69, no. 3, pp. 321-328, 1997.

[154] X. Ni and C. C. Stevenson, "On the effect of gap size between baffle outer diameter and tube inner diameter on the mixing characteristics in an oscillatory-baffled column," *Journal of Chemical Technology & Biotechnology,* vol. 74, no. 6, pp. 587-593, 1999.

[155] Y. Zhang, X. Ni, and I. Mustafa, "A study of oil–water dispersion in a pulsed baffled reactor," *Journal of Chemical Technology and Biotechnology: International Research in Process, Environmental AND Clean Technology,* vol. 66, no. 3, pp. 305-311, 1996.

[156] M. Mackley and P. Stonestreet, "Heat transfer and associated energy dissipation for oscillatory flow in baffled tubes," *Chemical Engineering Science,* vol. 50, no. 14, pp. 2211-2224, 1995.

[157] M. Mackley, G. Tweddle, and I. Wyatt, "Experimental heat transfer measurements for pulsatile flow in baffled tubes," *Chemical Engineering Science,* vol. 45, no. 5, pp. 1237-1242, 1990.

[158] G. Stephens and M. Mackley, "Heat transfer performance for batch oscillatory flow mixing," *Experimental Thermal and Fluid Science,* vol. 25, no. 8, pp. 583-594, 2002.

[159] M. Hewgill, M. Mackley, A. Pandit, and S. Pannu, "Enhancement of gas-liquid mass transfer using oscillatory flow in a baffled tube," *Chemical Engineering Science,* vol. 48, no. 4, pp. 799-809, 1993.

[160] X. Ni and S. Gao, "Mass transfer characteristics of a pilot pulsed baffled reactor," *Journal of Chemical Technology and Biotechnology,* vol. 65, no. 1, pp. 65-71, 1996.

[161] H. K. Gaidhani, B. McNeil, and X. W. Ni, "Production of pullulan using an oscillatory baffled bioreactor," *Journal of Chemical Technology & Biotechnology: International Research in Process, Environmental & Clean Technology,* vol. 78, no. 2-3, pp. 260-264, 2003.

[162] X. Ni, Y. S. De Gélicourt, M. H. Baird, and N. V. R. Rao, "Scale-up of single phase axial dispersion coefficients in batch and continuous oscillatory baffled tubes," *The Canadian Journal of Chemical Engineering,* vol. 79, no. 3, pp. 444-448, 2001.

[163] H. Jian and X. Ni, "A numerical study on the scale-up behaviour in oscillatory baffled columns," *Chemical Engineering Research and Design,* vol. 83, no. 10, pp. 1163-1170, 2005.

[164] M. Mackley and X. Ni, "Mixing and dispersion in a baffled tube for steady laminar and pulsatile flow," *Chemical Engineering Science,* vol. 46, no. 12, pp. 3139-3151, 1991.

[165] A. A. Hamzah, N. Hasan, M. S. Takriff, S. K. Kamarudin, J. Abdullah, I. M. Tan, W. K. Sern, "Effect of oscillation amplitude on velocity distributions in an oscillatory baffled column (OBC)," *Chemical Engineering Research and Design,* vol. 90, no. 8, pp. 1038-1044, 2012.

[166] P. Stonestreet and P. Van Der Veeken, "The effects of oscillatory flow and bulk flow components on residence time distribution in baffled tube reactors," *Chemical Engineering Research and Design,* vol. 77, no. 8, pp. 671-684, 1999.

[167] M. Abbott, A. Harvey, G. V. Perez, and M. Theodorou, "Biological processing in oscillatory baffled reactors: operation, advantages and potential," *Interface focus,* vol. 3, no. 1, p. 20120036, 2013.

[168] F. Castro, A. Ferreira, J. A. Teixeira, and F. Rocha, "Influence of mixing intensity on lysozyme crystallization in a meso oscillatory flow reactor," *Crystal Growth and Design,* vol. 18, no. 10, pp. 5940-5946, 2018.

[169] M. S. Abbott, G. V. Perez, A. P. Harvey, and M. K. Theodorou, "Reduced power consumption compared to a traditional stirred tank reactor (STR) for enzymatic saccharification of alpha-cellulose using oscillatory baffled reactor (OBR) technology," *Chemical Engineering Research and Design,* vol. 92, no. 10, pp. 1969-1975, 2014.

[170] X. Ni and A. Liao, "Effects of cooling rate and solution concentration on solution crystallization of L-glutamic acid in an oscillatory baffled crystallizer," *Crystal Growth and Design,* vol. 8, no. 8, pp. 2875-2881, 2008.

[171] X. Ni and A. Liao, "Effects of mixing, seeding, material of baffles and final temperature on solution crystallization of l-glutamic acid in an oscillatory baffled crystallizer," *Chemical Engineering Journal,* vol. 156, no. 1, pp. 226-233, 2010.

[172] A. W. Fitch, H. Jian, and X. Ni, "An investigation of the effect of viscosity on mixing in an oscillatory baffled column using digital particle image velocimetry and computational fluid dynamics simulation," *Chemical Engineering Journal,* vol. 112, no. 1, pp. 197-210, 2005.

[173] X. Ni, G. Brogan, A. Struthers, D. Bennett, and S. Wilson, "A systematic study of the effect of geometrical parameters on mixing time in oscillatory baffled columns," *Chemical Engineering Research and Design,* vol. 76, no. 5, pp. 635-642, 1998.

[174] X. Ni, Y. Zhang, and I. Mustafa, "An investigation of droplet size and size distribution in methylmethacrylate suspensions in a batch oscillatory-baffled reactor," *Chemical Engineering Science,* vol. 53, no. 16, pp. 2903-2919, 1998.

[175] S. M. Ahmed, A. N. Phan, and A. P. Harvey, "Mass transfer enhancement as a function of oscillatory baffled reactor design," *Chemical Engineering and Processing,* vol. 130, pp. 229-239, 2018.

[176] A. Mazubert, D. Fletcher, M. Poux, and J. Aubin, "Hydrodynamics and mixing in continuous oscillatory flow reactors—Part II: Characterisation methods," *Chemical Engineering and Processing*, vol. 102, pp. 102-116, 2016.

[177] A. Al-Abduly, P. Christensen, A. Harvey, and K. Zahng, "Characterization and optimization of an oscillatory baffled reactor (OBR) for ozone-water mass transfer," *Chemical Engineering and Processing: Process Intensification*, vol. 84, pp. 82-89, 2014.

[178] M. S. N. Oliveira, A. W. Fitch, and X. W. Ni, "A study of velocity and residence time of single bubbles in a gassed oscillatory baffled column: effect of oscillation amplitude," *Journal of Chemical Technology & Biotechnology: International Research in Process, Environmental & Clean Technology*, vol. 78, no. 2-3, pp. 220-226, 2003.

[179] X. Ni, D. Mignard, B. Saye, J. Johnstone, and N. Pereira, "On the evaluation of droplet breakage and coalescence rates in an oscillatory baffled reactor," *Chemical engineering science*, vol. 57, no. 11, pp. 2101-2114, 2002.

[180] D. Mignard, L. Amin, and X. W. Ni, "Population balance modelling of droplets in an oscillatory baffled reactor—using direct measurements of breakage rate constants," *Journal of Chemical Technology & Biotechnology: International Research in Process, Environmental & Clean Technology*, vol. 78, no. 2-3, pp. 364-369, 2003.

[181] R. Law, S. M. Ahmed, N. Tang, A. N. Phan, and A. P. Harvey, "Development of a more robust correlation for predicting heat transfer performance in oscillatory baffled reactors," *Chemical Engineering and Processing*, vol. 125, pp. 133-138, 2018.

[182] R. Kacker, S. I. Regensburg, and H. J. Kramer, "Residence time distribution of dispersed liquid and solid phase in a continuous oscillatory flow baffled crystallizer," *Chemical Engineering Journal*, vol. 317, pp. 413-423, 2017.

[183] M.-H.-l. Baird and P. Stonestreet, "Energy-dissipation in oscillatory flow within a baffled tube," *Chemical engineering research and design*, vol. 73, no. 5, pp. 503-511, 1995.

[184] A.T. Liao, "Characterisation of crystallisation of L-glutamic acid in a batch oscillatory baffled crystalliser," PhD thesis, Heriot-Watt University, 2008.

[185] G. Nelson, "Scale-up study of suspension polymerisation in an oscillatory baffled reactor," PhD thesis, Heriot-Watt University, 2001.

[186] G. Jimeno, Y. C. Lee, and X. Ni, "On the evaluation of power density models for oscillatory baffled reactors using CFD," *Chemical Engineering and Processing-Process Intensification,* vol. 134, pp. 153-162, 2018.

[187] X. Ni and N. E. Pereira, "Parameters affecting fluid dispersion in a continuous oscillatory baffled tube," *AIChE journal,* vol. 46, no. 1, pp. 37-45, 2000.

[188] X. Ni, A. Valentine, A. Liao, S. B. Sermage, G. B. Thomson, and K. J. Roberts, "On the crystal polymorphic forms of L-glutamic acid following temperature programmed crystallization in a batch oscillatory baffled crystallizer," *Crystal growth and design,* vol. 4, no. 6, pp. 1129-1135, 2004.

[189] P. Barrett, B. Smith, J. Worlitschek, V. Bracken, B. O'Sullivan, and D. O'Grady, "A review of the use of process analytical technology for the understanding and optimization of production batch crystallization processes," *Organic Process Research and Development,* vol. 9, no. 3, pp. 348-355, 2005.

[190] L. L. Simon, E. Simone, and K. A. Oucherif, "Crystallization process monitoring and control using process analytical technology," *Computer Aided Chemical Engineering,* vol. 41, pp. 215-242, 2018.

[191] J. Chen, B. Sarma, J. M. Evans, and A. S. Myerson, "Pharmaceutical crystallization," *Crystal growth and design,* vol. 11, no. 4, pp. 887-895, 2011.

[192] N. E. Briggs, U. Schacht, V. Raval, T. McGlone, J. Sefcik, and A. J. Florence, "Seeded crystallization of β-L-glutamic acid in a continuous oscillatory baffled crystallizer," *Organic Process Research and Development,* vol. 19, no. 12, pp. 1903-1911, 2015.

[193] R. Peña, J. A. Oliva, C. L. Burcham, D. J. Jarmer, and Z. K. Nagy, "Process Intensification through Continuous Spherical Crystallization Using an Oscillatory Flow Baffled Crystallizer," *Crystal Growth and Design,* vol. 17, no. 9, pp. 4776-4784, 2017.

[194] C. J. Brown, T. McGlone, S. Yerdelen, V. Srirambhatla, F. Mabbott, R. Gurung, M. L. Briuglia, B. Ahmed, H. Polyzois, J. McGinty, F. Perciballi, "Enabling precision manufacturing of active pharmaceutical ingredients: workflow for

seeded cooling continuous crystallisations," *Molecular Systems Design and Engineering*, 2018.

[195] A. J. Alvarez and A. S. Myerson, "Continuous plug flow crystallization of pharmaceutical compounds," *Crystal Growth & Design*, vol. 10, no. 5, pp. 2219-2228, 2010.

[196] J. Janson, E. R. Kraft, G. Kulp, and R. Malanchin, "Delivery of large molecular weight biologically active substances," ed: Google Patents, 2011.

[197] R. Bishop, *Modern Physical Metallurgy and Materials Engineering: Science, Process, Applications*. Elsevier Science & Technology, 1999.

[198] M. A. Mallah, S. T. H. Sherazi, M. I. Bhanger, S. A. Mahesar, and M. A. Bajeer, "A rapid Fourier-transform infrared (FTIR) spectroscopic method for direct quantification of paracetamol content in solid pharmaceutical formulations," *Spectrochimica Acta Part A: Molecular and Biomolecular Spectroscopy*, vol. 141, pp. 64-70, 2015.

[199] A. R. Khaskheli, A. Shah, M. I. Bhanger, A. Niaz, and S. Mahesar, "Simpler spectrophotometric assay of paracetamol in tablets and urine samples," *Spectrochimica Acta Part A: Molecular and Biomolecular Spectroscopy*, vol. 68, no. 3, pp. 747-751, 2007.

[200] B. L. Joseph, H. Shurvell, D. Lightner, and R. Cooks, "Introduction to organic spectroscopy," ed: Macmillan Publishing Company, New York, 1987.

[201] H. Hojjati and S. Rohani, "Measurement and prediction of solubility of paracetamol in water-isopropanol solution. Part 1. Measurement and data analysis," *Organic process research and development*, vol. 10, no. 6, pp. 1101-1109, 2006.

[202] M. Fujiwara, P. S. Chow, D. L. Ma, and R. D. Braatz, "Paracetamol crystallization using laser backscattering and ATR-FTIR spectroscopy: metastability, agglomeration, and control," *Crystal Growth and Design*, vol. 2, no. 5, pp. 363-370, 2002.

[203] S. Narwade, "Qualitative and Quantitative Analysis of Paracetamol in Different Drug Samples by HPLC Technique," *IOSR Journal of Applide Chemistry*, vol. 7, no. 8, pp. 46-49, 2014.

[204] A. Burger, "Zur interpretation von polymorphie-untersuchungen," *Acta Pharm Technol*, vol. 28, pp. 1-20, 1982.

[205] J. C. Burley, M. J. Duer, R. S. Stein, and R. M. Vrcelj, "Enforcing Ostwald's rule of stages: Isolation of paracetamol forms III and II," *European journal of pharmaceutical sciences*, vol. 31, no. 5, pp. 271-276, 2007.

[206] J. Ledru, C. Imrie, C. Pulham, R. Céolin, and J. Hutchinson, "High pressure differential scanning calorimetry investigations on the pressure dependence of the melting of paracetamol polymorphs I and II," *Journal of pharmaceutical sciences*, vol. 96, no. 10, pp. 2784-2794, 2007.

[207] M. Sacchetti, "Thermodynamic analysis of DSC data for acetaminophen polymorphs," *Journal of thermal analysis and calorimetry*, vol. 63, no. 2, pp. 345-350, 2000.

[208] E. V. Boldyreva, V. Drebushchak, I. Paukov, Y. A. Kovalevskaya, and T. N. Drebushchak, "DSC and adiabatic calorimetry study of the polymorphs of paracetamol," *Journal of thermal analysis and calorimetry*, vol. 77, no. 2, pp. 607-623, 2004.

[209] J. R. Méndez del Río and R. W. Rousseau, "Batch and tubular-batch crystallization of paracetamol: Crystal size distribution and polymorph formation," *Crystal growth and design*, vol. 6, no. 6, pp. 1407-1414, 2006.

[210] Y. Mori, M. Maruyama, Y. Takahashi, K. Ikeda, S. Fukukita, H. Y. Yoshikawa, S. Okada, H. Adachi, S. Sugiyama, K. Takano, S. Murakami, "Selective crystallization of metastable phase of acetaminophen by ultrasonic irradiation," *Applied Physics Express*, vol. 8, no. 6, p. 065501, 2015.

[211] G. Nichols and C. S. Frampton, "Physicochemical characterization of the orthorhombic polymorph of paracetamol crystallized from solution," *Journal of pharmaceutical sciences*, vol. 87, no. 6, pp. 684-693, 1998.

[212] M. L. Myrick, M. Baranowski, and L. T. Profeta, "An experiment in physical chemistry: polymorphism and phase stability in acetaminophen (paracetamol)," *Journal of chemical education*, vol. 87, no. 8, pp. 842-844, 2010.

[213] S. Zalac, M. Z. I. Khan, V. Gabelica, M. Tudja, E. MEStrovic, and M. Romih, "Paracetamol-propyphenazone interaction and formulation difficulties associated

with eutectic formation in combination solid dosage forms," *Chemical and pharmaceutical bulletin,* vol. 47, no. 3, pp. 302-307, 1999.

[214] P. Di Martino, P. Conflant, M. Drache, J.-P. Huvenne, and A.-M. Guyot-Hermann, "Preparation and physical characterization of forms II and III of paracetamol," *Journal of thermal analysis,* vol. 48, no. 3, pp. 447-458, 1997.

[215] D. Lednicer, *The organic chemistry of drug synthesis*. John Wiley & Sons: New York, 2007.

[216] F. Ellis, *Paracetamol: a curriculum resource*. Royal Society of Chemistry, 2002.

[217] R. L. F. de Caldeira, "An assessment of cross-contamination issues in the context of chemical and pharmaceutical processes using a continuous oscillatory baffled reactor," Heriot-Watt University, 2010.

[218] C. Lindenberg, M. Krättli, J. Cornel, M. Mazzotti, and J. r. Brozio, "Design and optimization of a combined cooling/antisolvent crystallization process," *Crystal Growth and Design,* vol. 9, no. 2, pp. 1124-1136, 2008.

[219] M. Srabovic, M. Huremovic, B. Catovic, S. Muratovic, and A. Taletović, "Design synthesis and crystallization of acetaminophen," *Journal of Chemical, Biological and Physical Sciences,* vol. 777, pp. 218-230, 2017.

[220] C. Sudha and K. Srinivasan, "Understanding the effect of solvent polarity on the habit modification of monoclinic paracetamol in terms of molecular recognition at the solvent crystal/interface," *Crystal Research and Technology,* vol. 49, no. 11, pp. 865-872, 2014.

[221] K. V. Prasad, R. I. Ristic, D. B. Sheen, and J. N. Sherwood, "Crystallization of paracetamol from solution in the presence and absence of impurity," *International journal of pharmaceutics,* vol. 215, no. 1-2, pp. 29-44, 2001.

[222] J. Li and M. F. Doherty, "Steady state morphologies of paracetamol crystal from different solvents," *Crystal Growth & Design,* vol. 17, no. 2, pp. 659-670, 2017.

[223] Z. B. Kuvadia and M. F. Doherty, "Effect of structurally similar additives on crystal habit of organic molecular crystals at low supersaturation," *Crystal Growth & Design,* vol. 13, no. 4, pp. 1412-1428, 2013.

[224] A.L. Chow, P. Chow, W. Zhongshan, and D. Grant, "Modification of acetaminophen crystals: influence of growth in aqueous solutions containing p-

acetoxyacetanilide on crystal properties," *International journal of pharmaceutics,* vol. 24, no. 2-3, pp. 239-258, 1985.

[225] E. M. Ålander and Å. C. Rasmuson, "Mechanisms of crystal agglomeration of paracetamol in acetone− water mixtures," *Industrial & engineering chemistry research,* vol. 44, no. 15, pp. 5788-5794, 2005.

[226] E. M. Ålander, M. S. Uusi-Penttilä, and Å. C. Rasmuson, "Agglomeration of paracetamol during crystallization in pure and mixed solvents," *Industrial & engineering chemistry research,* vol. 43, no. 2, pp. 629-637, 2004.

[227] N. M. Reis, Z. K. Liu, C. M. Reis, and M. R. Mackley, "Hydroxypropyl methylcellulose as a novel tool for isothermal solution crystallization of micronized paracetamol," *Crystal Growth & Design,* vol. 14, no. 7, pp. 3191-3198, 2014.

[228] D. Acevedo, Y. Tandy, and Z. K. Nagy, "Multiobjective optimization of an unseeded batch cooling crystallizer for shape and size manipulation," *Industrial & Engineering Chemistry Research,* vol. 54, no. 7, pp. 2156-2166, 2015.

[229] F. Fusaro, M. Mazzotti, and G. Muhrer, "Gas antisolvent recrystallization of paracetamol from acetone using compressed carbon dioxide as antisolvent," *Crystal growth & design,* vol. 4, no. 5, pp. 881-889, 2004.

[230] Z. Q. Yu, P. S. Chow, and R. B. Tan, "Seeding and constant-supersaturation control by ATR-FTIR in anti-solvent crystallization," *Organic Process Research & Development,* vol. 10, no. 4, pp. 717-722, 2006.

[231] M. W. Hermanto, P. S. Chow, and R. B. Tan, "Operating strategy to produce consistent CSD in combined antisolvent-cooling crystallization using FBRM," *Industrial & Engineering Chemistry Research,* vol. 51, no. 42, pp. 13773-13783, 2012.

[232] S. Finnie, R. Ristic, J. Sherwood, and A. Zikic, "Morphological and growth rate distributions of small self-nucleated paracetamol crystals grown from pure aqueous solutions," *Journal of crystal growth,* vol. 207, no. 4, pp. 308-318, 1999.

[233] R. A. Granberg, C. Ducreux, S. Gracin, and Å. C. Rasmuson, "Primary nucleation of paracetamol in acetone–water mixtures," *Chemical Engineering Science,* vol. 56, no. 7, pp. 2305-2313, 2001.

[234] C. T. Ó'Ciardhá, P. J. Frawley, and N. A. Mitchell, "Estimation of the nucleation kinetics for the anti-solvent crystallisation of paracetamol in methanol/water solutions," *Journal of Crystal Growth,* vol. 328, no. 1, pp. 50-57, 2011.

[235] R. Davey, "Solvent effects in crystallization processes," *Current topics in materials science,* vol. 8, pp. 429-479, 1982.

[236] J. Worlitschek and M. Mazzotti, "Model-based optimization of particle size distribution in batch-cooling crystallization of paracetamol," *Crystal Growth & Design,* vol. 4, no. 5, pp. 891-903, 2004.

[237] J. Bourne, "The influence of solvent on crystal growth kinetics," in *AIChE Symposium Series*, 1980, vol. 193, no. 76, pp. 59-64.

[238] M. Lahav and L. Leiserowitz, "The effect of solvent on crystal growth and morphology," *Chemical Engineering Science,* vol. 56, no. 7, pp. 2245-2253, 2001.

[239] R. Davey, "The role of the solvent in crystal growth from solution," *Journal of Crystal Growth,* vol. 76, no. 3, pp. 637-644, 1986.

[240] D. Woodruff, "How does your crystal grow? A commentary on Burton, Cabrera and Frank (1951)'The growth of crystals and the equilibrium structure of their surfaces'," *Phil. Trans. R. Soc. A,* vol. 373, no. 2039, p. 20140230, 2015.

[241] B. Y. Shekunov, D. J. Grant, R. J. Latham, and J. N. Sherwood, "In situ optical interferometric studies of the growth and dissolution behavior of paracetamol (acetaminophen) crystals. 3. Influence of growth in the presence of p-acetoxyacetanilide," *The Journal of Physical Chemistry B,* vol. 101, no. 44, pp. 9107-9112, 1997.

[242] M. Jiang and X. Ni, "Effects of water and temperature on reaction mechanism and crystal properties in a reactive crystallization of paracetamol," *Chemical Engineering and Processing,* vol. 131, pp. 20-26, 2018.

[243] L. R. Agnew, T. McGlone, H. P. Wheatcroft, A. Robertson, A. R. Parsons, and C. C. Wilson, "Continuous Crystallization of Paracetamol (Acetaminophen) Form II: Selective Access to a Metastable Solid Form," *Crystal Growth and Design,* vol. 17, no. 5, pp. 2418-2427, 2017.

[244] L. R. Agnew, D. L. Cruickshank, T. McGlone, and C. C. Wilson, "Controlled production of the elusive metastable form II of acetaminophen (paracetamol): a

fully scalable templating approach in a cooling environment," *Chemical Communications,* vol. 52, no. 46, pp. 7368-7371, 2016.

[245] X. Ni and P. Gough, "On the discussion of the dimensionless groups governing oscillatory flow in a baffled tube," *Chemical Engineering Science,* vol. 52, no. 18, pp. 3209-3212, 1997.

[246] N. Kubota and M. Onosawa, "Seeded batch crystallization of ammonium aluminum sulfate from aqueous solution," *Journal of Crystal Growth,* vol. 311, no. 20, pp. 4525-4529, 2009.

[247] N. Doki, N. Kubota, A. Sato, M. Yokota, O. Hamada, and F. Masumi, "Scaleup experiments on seeded batch cooling crystallization of potassium alum," *AIChE journal,* vol. 45, no. 12, pp. 2527-2533, 1999.

[248] M. Jiang and X. Ni, "Effects of solvents and impurity on crystallization kinetics and crystal properties in a reactive crystallization," O*rganic Process Research & Development,* Accepted, 2019.

[249] B. Biscans, P. Guiraud, C. Laguerie, A. Massarelli, and B. Mazzarotta, "Abrasion and breakage phenomena in mechanically stirred crystallizers," *Chemical Engineering Journal and the Biochemical Engineering Journal,* vol. 63, no. 2, pp. 85-91, 1996.

[250] S. Agrawal, A. Balandier, A. Paterson, and J. Jones, "Study on lactose attrition inside the mixing cell of a laser diffraction particle sizer using a novel attrition index," *Powder technology,* vol. 208, no. 3, pp. 669-675, 2011.

[251] I.C. Wang, M.J. Lee, D.Y. Seo, H.E. Lee, Y. Choi, W.S. Kim, C.S. Kim, M.Y. Jeong, G.J. Choi, "Polymorph transformation in paracetamol monitored by in-line NIR spectroscopy during a cooling crystallization process," *AAPS PharmSciTech,* vol. 12, no. 2, pp. 764-770, 2011.

[252] S. C. Barthe, M. A. Grover, and R. W. Rousseau, "Observation of polymorphic change through analysis of FBRM data: transformation of paracetamol from form II to form I," *Crystal Growth and Design,* vol. 8, no. 9, pp. 3316-3322, 2008.

[253] R. Vardanyan and V. Hruby, *Synthesis of essential drugs*. Elsevier, 2006.

[254] A. Ahmed and N. B. Chowdhury, "Esterification of Ethanol and Acetic Acid in a Batch Reactor in Presence of Sulfuric Acid Catalyst," *Global Engineering Science and Technology Conference*, Dhaka, 2016. (

http://www.communityresearch.org.nz/wp-content/uploads/formidable/Esterification-of-Ethanol-and-Acetic-Acid-in-a-Batch-Reactor-in-Presence-of-Sulfuric-Acid-Catalyst.pdf)

[255] M. Zhang, X. Cui, X. Chen, L. Wang, J. Li, Y. Wu, L. Hou, Y. Wu, "Facile synthesis of aryl (het) cyclopropane catalyzed by palladacycle," *Tetrahedron,* vol. 68, no. 3, pp. 900-905, 2012.

[256] C. Mauger and G. Mignani, "The Synthesis of Important Pharmaceutical Building Blocks by Palladium-Catalyzed Coupling Reaction: Access to Various Arylhydrazines," *Advanced synthesis & catalysis,* vol. 347, no. 6, pp. 773-782, 2005.

[257] H. Gruber-Woelfler, P. Radaschitz, P. Feenstra, W. Haas, and J. Khinast, "Synthesis, catalytic activity, and leaching studies of a heterogeneous Pd-catalyst including an immobilized bis (oxazoline) ligand," *Journal of catalysis,* vol. 286, pp. 30-40, 2012.